Numerical and Experimental Study of Electroadhesion to Enable Manufacturing Automation

By

Jianglong Guo

A Doctoral Thesis

Submitted in partial fulfillment of the requirements for the award of

Doctor of Philosophy of Loughborough University

April 2016

Acknowledgement

Writing this thesis has been a rewarding and challenging journey, which would not have been possible without the encouragement and guidance of my first supervisor, Dr. Laura Justham. My deepest gratitude goes first to her for her patience and precious time during our numerous meetings and discussions.

My heartfelt thanks should also go to Prof. Robert Parkin who introduced me to IA-CIM when I was in China. As my second year first supervisor, I am grateful for his encouragement and trust.

I would also like to thank my second supervisor Prof. Mike Jackson who has been encouraging and supporting me to conduct the first ‘wild’ or ‘blue-sky’ project in the center. I am very grateful for the PhD studentship funded by the center starting from 7th November 2012, the first day I arrived at Loughborough. In addition, the professional and systematic working environment created by the management team in the center has been very helpful.

During this PhD journey, I appreciate the priceless comments, suggestions, and help from my colleagues, Mr. Thomas Bamber, Dr. Matthew Chamberlain, and Dr. Mitul Tailor. Also, I thank the invaluable help and time from technicians, Mr. Richard Greenhough and Mr. Jagpal Singh.

Last but not the least, I would like to dedicate this thesis to my parents, Mrs. Xiaoping Zeng (曾小平) and Mr. Jiankang Guo (郭健康), and my younger brother, Mr. Jiaolong Guo (郭蛟龙), who have been supporting me steadfastly on this incredible PhD journey, and without whom this thesis would not have been possible.

Abstract

Robotics and autonomous systems (RAS) have great potential to propel the world to future growth. Electroadhesion is a promising and potentially revolutionising material handling technology for manufacturing automation applications. There is, however, a lack of an in-depth understanding of this electrostatic adhesion phenomenon based on a confident electroadhesive pad design, manufacture, and testing platform and procedure.

This PhD research endeavours to obtain a more comprehensive understanding of electroadhesion based on an extensive literature review, theoretical modelling, electrostatic simulation, and experimental validation based on a repeatable pad design, manufacture, and testing platform and procedure. The theoretical results show that: 1) it is inappropriate to derive the normal electroadhesive forces by the division of the measured shear forces and friction coefficients; and 2) there is an optimum electrode width of 1.8 mm for pads to achieve the maximum forces on insulating substrates when the space between electrodes is fixed at 1 mm. The simulation results show that the optimum electrode width is significantly affected by the existence of the air gap and substrate thickness variation on insulating substrates, although there is an optimum electrode width, around 2 mm, when the space between electrodes is fixed as 1 mm. The experimental results show that: 1) it is of great importance to control the environment when testing the pads to validate the models as the environmental factors can significantly influence the forces; 2) there is indeed an optimum electrode width of approximately 1.9 mm when the space between electrodes is fixed as 1 mm; 3) the direction of the surface texture plays an important role in achieving the electroadhesive forces; and 4) the pad design can significantly influence the forces and should be tailored to specific applications.

The results are useful for optimising the design of electroadheives. The identification of the need of the investigation into environmentally stable

electroadhesives is useful for both understanding electroadhesion and promoting the commercial application of electroadhesion. In addition, the simplified 3D electrostatic simulation method will save a significant amount of time and money for investigating different pad designs and optimising the pad design without pad manufacture and testing. Furthermore, the identification of the need for adaptive and intelligent electroadhesion and the proof of the concept may lead to a paradigm shift towards a revolutionising material handling technology for manufacturing automation.

Publications arising from this work

The following publications have been generated from this work:

J. Guo, M. Tailor, T. Bamber, M. Chamberlain, L. Justham, and M. Jackson, “Investigation of relationship between interfacial electroadhesive force and surface texture,” *J. Phys. D. Appl. Phys.*, vol. 49, no. 3, p. 35303(9pp), 2016.

J. Guo, L. Justham, M. Jackson, and R. Parkin, “A concept selection method for designing climbing robots,” *Key Eng. Mater.*, vol. 649, pp. 22 - 29, 2015.

J. Guo, T. Bamber, M. Chamberlain, L. Justham, and M. Jackson, “The influence of environmental factors on the electroadhesive forces obtainable during experimental testing,” in *2015 IOP Early Career Researchers Colloquium*.

T. Bamber, **J. Guo**, M. Chamberlain, L. Justham, and M. Jackson, “Relationship between applied voltage and obtainable electroadhesive forces,” in *2015 IOP Early Career Researchers Colloquium*.

J. Guo, T. Bamber, M. Chamberlain, L. Justham, and M. Jackson, “Simplified optimization modelling of coplanar interdigital electroadhesives and experimental verification,” *J. Phys. D. Appl. Phys.* (**under review**), 2016.

J. Guo, T. Bamber, T. Hovell, M. Chamberlain, L. Justham, and M. Jackson, “Geometric optimisation of electroadhesive actuators based on 3D electrostatic simulation and its experimental verification,” in *MECHATRONICS 2016* (**accepted**).

Electroadhesive gripper, UK Patent No. 1608729.8 (**inventor**, filed on 18th May 2016).

List of Contents

1 Introduction

1.1 Why electroadhesion?

Electroadhesion [1], or electrostatic adhesion, is an electrostatic attractive effect between two objects, i.e., the electroadhesive pad and the substrate to which the pad is to be attached onto, when subjected to strong electrical fields that are usually in kilovolts per milimetre ($kVmm^{-1}$) range. Electroadhesion is an advanced controllable and reversible adhesion technology. A cross-section view of an electroadhesive system, as can be seen in Figure 1-1. The electroadhesive system usually contains four essential components:

● the electroadhesive pad (1), made of conductive electrodes (1a) and dielectric materials (1b), where the conductive electrodes are embedded into or attached onto;

● the wall substrate (2), where the electroadhesive pad can adhere on;

● high voltage power sources (3), which are connected with electrodes and usually in kV range;

● and the control system to control the on and off of the electroadhesion system.

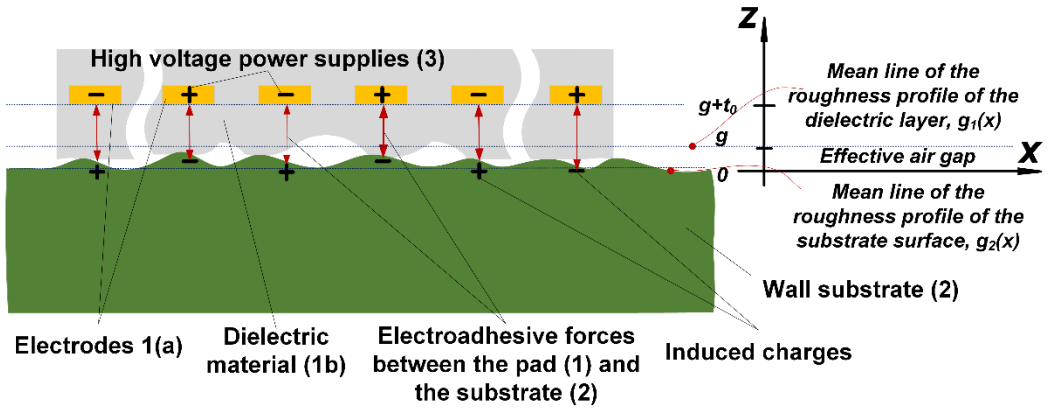

Figure 1-1 A cross-section view of an electroadhesive system (Note that the surface texture of the contacting surface has been exaggerated for clarity)

Electroadhesion has been extensively used for many applications. This includes:

electrostatic fixtures to hold workpieces [2], an adhesive method for space missions such as material handling [3] and controllable earth orbit grappling applications [4], electrostatic chucks for material handling and grasping in semiconductor industries [5], end effectors for gripping advanced composites and fibrous materials such as cloth [6] and carbon fibres [7][8], an adhesion mechanism for robots [9][10][11] and material handling units for manufacturing automation, and warehouse automation [12]. This is because, compared with other adhesion mechanisms [13], electroadhesion has four distinctive benefits.

Electroadhesion has an enhanced adaptability as it adheres to both conductive and insulating materials such as smooth aluminium and rough concrete surfaces [14]. In addition, it can be applied in vacuum, and therefore, space environments. Vacuum environments are also increasingly desirable for chip manufacturers [15].

Electroadhesive grasping is a gentle material handling method as it can be applied without contact with the substrates [16], so it is non-damaging or less-damaging to the substrate surface, which is desirable for some high value material handling tasks such as pick-and-place of silicon wafers in the semiconductor industries [15].

Furthermore, electroadhesion can bring lightweight and reduced complexity systems as it can help reduce the weight and complexity of a system in terms of control and the mechanical structure as it enables electrically controllable clamping and unclamping, which means pumps or motors are not required.

Last but not the least, electroadhesion is an ultra-low energy consumption adhesion method, usually in the microwatt (μW) to milliwatt (mW) range, as a very small current in the microampere (μA) to milliampere (mA) range runs through the electroadhesive pad [17]. This feature helps to reduce the energy consumed in pick-and-place applications by up to three orders of magnitude [12][18].

1.2 Research motivations

Although electroadhesion is a promising and potentially revolutionising material handling technology [12] due to its distinctive advantages as aforementioned, the applicability of this technology is currently constrained as there is a lack of an in-depth understanding of electroadhesion, both theoretically and experimentally. In addition, there is a lack of an effective, efficient, and confident research methodology and platform aiding the electroadhesive pad design, manufacture, and testing. Specifically, the following major challenges for electroadhesion have been identified.

1.2.1 Advanced modelling of electroadhesion

Little work has been done on a comprehensive understanding of how many variables influencing the electroadhesive forces obtainable as it takes time and money to investigate the relationship between all those factors and the electroadhesive forces. Because of this, there is no empirical model that can predict the performance of electroadhesives. Also, there is no experimentally validated theoretical model on electroadhesion. In addition, few simulation models have been experimentally validated. Furthermore, the understanding of the principle of electroadhesion was only hypothesised although it has to be noted that it is difficult to verify it experimentally.

1.2.2 Novel and confident pad design, manufacture, and testing

One limitation of electroadhesion is, compared with other adhesion methods such as magnetic adhesion [13], relatively weaker forces, such as 0.1 newton per centimetre square (Ncm^{-2}), can be observed. The electroadhesion phenomenon is often associated with complicated polarisations/depolarisations. The residual charge problem cannot be ignored and should be addressed as fast clamp and unclamp are desirable for any electroadhesive system. Great care must also be taken with regard to the dielectric material selection and optimisation for each specific electroadhesive application [19]. It is therefore

challenging to optimise the dielectric design and selection. Poor dielectric material selection and generation of the electroadhesive pad may easily cause electrical discharges such as corona discharges [20], electrical breakdowns, and electrical aging that may induce the failure or reduced life cycles of the electroadhesion system. Here, the failure of electroadhesion can be defined as a sudden change or drop of the electroadhesive forces. The failure of electroadhesion is usually caused by air bubbles trapped in dielectric materials, sharp edges along electrodes, and the change of environmental factors. There is a lack of systematic, robust, and novel pad design and manufacture techniques to address the above mentioned limitations and challenges. In order to quantify the performance of the electroadhesive pad with confidence, a repeatable force testing platform is needed. There is a lack of an advanced investigation into a repeatable force testing platform and measurement procedure to produce confident data for pad performance checking.

1.2.3 Enhanced adaptive and intelligent electroadhesion

An adaptive and intelligent electroadhesion system has been defined as an electrostatic adhesion system that is substrate surface texture adaptive, substrate shape adaptive, environmentally stable and adaptive, and substrate surface material adaptive with quick clamp/unclamp speed, lower power consumption, longer life cycles, and greater safety.

Although electroadhesion can be adaptable to different surfaces, the level of its adaptability is limited to flat and smooth surfaces if only a flat and rigid electroadhesive pad is used. It is therefore necessary to design and implement enhanced adaptive and intelligent electroadhesive solutions to increase the adaptability and intelligent level of electroadhesive systems. There is a lack of a comprehensive identification of the need for enhanced adaptive and intelligent electroadhesion.

Due to the research gaps identified above, it is therefore necessary, and this PhD

research endeavours, to obtain a more comprehensive understanding of the electroadhesion phenomenon based on an extensive literature review, simplified theoretical optimisation modelling, two-dimensional (2D) and three-dimensional (3D) electrostatic simulation, and experimental validation based on a systematic approach using a carefully designed electroadhesive pad design, manufacture, and testing platform and procedure.

1.3 Research aim and objectives

In order to address the research gaps identified above, the major research aim of this PhD research is to provide research solutions and directions for adaptive and autonomous robotic applications for manufacturing based on an in-depth understanding of the electroadhesion phenomenon in EPSRC Centre for Innovative Manufacturing in Intelligent Automation at Loughborough University (LU). To fulfil the aim, the identified research objectives are:

● To identify the factors influencing the electroadhesive forces.

● To conduct theoretical modelling of the electroadhesive force between the pad and the substrate based on the principle of electroadhesion published in the literature.

● To conduct 2D and 3D electrostatic simulation modelling of the electroadhesive system based on COMSOL.

● To develop a simplified optimisation model of coplanar interdigital electroadhesives and conduct its experimental verification based on a repeatable pad design, manufacture, testing platform and procedure.

● To investigate the relationship between the electroadhesive force and surface texture.

● To investigate the relationship between the electroadhesive force and pad geometry.

● To identify the need for adaptive and intelligent electroadhesion and design a demonstrable platform after the proof of the proposed concept.

1.4 Research contributions and novelties

In this PhD research, the contributions to the knowledge, to fulfil the research aim and objectives identified in section 1.3, are summarised as:

● The summarisation of a comprehensive literature review on electroadhesion technologies containing basics on understanding the electroadhesion phenomenon, electroadhesive pad design, pad manufacture, pad testing, modelling of electroadhesion, and electroadhesive applications.

This contribution contains no novelty. The comprehensiveness of this literature review, however, is unique and should be useful for future researchers as this literature review has identified why people have obtained different results from their theoretical and simulation models.

● The identification of the inappropriateness to derive the normal electroadhesive force by the division of the measured shear forces and friction coefficients.

This contribution is novel and highlights that only the measured normal electroadhesive forces are reasonable to validate the models.

● The identification of the need for controlling the environment to validate the models and investigate other influencing factors.

This contribution is novel and also highlights the need for the investigation into environmentally stable electroadhesives for commercial electroadhesive applications.

● The development of a simplified optimisation modelling of coplanar interdigital electroadhesives and its experimental validation.

This contribution is novel. The results are useful for optimised designs for

coplanar interdigital electroadhesives.

● The development of a systematic research methodology to investigate the relationship between the electroadhesive force and surface texture and the unique results obtained from the investigation.

This contribution is novel. The results not only highlight the need to control the surface texture in order to investigate the relationship between the electroadhesive forces and other influencing factors but also identify the need for the investigation into surface texture adaptive electroadhesives.

● The development of a systematic research methodology to investigate the relationship between the electroadhesive force and pad geometry based on a simplified 3D electrostatic simulation and its experimental validation.

This contribution is novel. The results are useful for optimised electroadhesive designs. Also the proposed methodology will save a significant amount of time and money for investigating different pad designs and optimising the pad design without pad manufacture and testing.

● The design and implementation of a mechatronic and demonstrable platform to prove the mentioned concept.

This contribution is novel. The proposed concept is aiming to promote the advancement of electroadhesive material handling applications for manufacturing automation.

1.5 Thesis structure

This thesis has been divided into 8 Chapters based upon the objectives identified in section 1.3. The remainder content of this thesis is outlined as follows.

Chapter 2: The fundamentals and basic principles of electrostatics and dielectrics for understanding electroadhesion are summarised. The principle of the electroadhesion phenomenon is also summarised. The reason why the

electroadhesive force measured in shear is greater than in normal is demonstrated. Basic theoretical models for deriving the electroadhesive force between the pad and substrate are summarised.

Chapter 3: A comprehensive literature review of the existing work on electroadhesion is presented by a chronological review of the research groups around the world. In addition, a detailed overview of electroadhesion in terms of electroadhesive pad design, manufacturing, testing, modelling of electroadhesion and electroadhesive applications is reported. Furthermore, a comprehensive summary and discussion of variables influencing the obtainable electroadhesive forces are illustrated.

Chapter 4: The need for the optimisation modelling of coplanar interdigitated electroadhesives is identified. A simplified and novel theoretical optimisation modelling of coplanar interdigitated electroadhesives is described. Also, a 2D electrostatic simulation to further support the theoretical analysis is carried out. Experimental validation of the theoretical analysis and simulation are presented based on a repeatable pad design, manufacture, and testing platform and procedure.

Chapter 5: The need for a systematic investigation into the relationship between the electroadhesive forces and different surface textures is identified. The unique experimental results from this investigation are described based on the proposed research method, including surface texture generation, surface texture characterization, pad design, manufacture, and testing, and correlation between the force obtained and the surface texture parameter.

Chapter 6: The need for a systematic investigation into the relationship between the electroadhesive forces obtainable and different pad geometries is identified. A 3D electrostatic simulation of nine pad geometries is carried out. The design of a customised mechatronic electroadhesive grasping platform is introduced for the experimental validation. An initial experimental validation of the simulation is

also carried out.

Chapter 7: The need for adaptive and intelligent electroadhesion is identified. A new and detailed definition of adaptive and intelligent electroadhesion is proposed thereafter. A mobile and autonomous electroadhesive grasping platform is designed after the proof of concept and for future demonstration.

Chapter 8: Conclusions are summarised in this Chapter. Possible future work are identified and summarised.

This PhD research contains both numerical and experimental study of the electroadhesion phenomenon. The results and findings obtained from Chapter 3 to Chapter 6 are identified as strong needs for adaptive and intelligent electroadhesion proposed in Chapter 7. The thesis structure diagram is demonstrated in Figure 1-2.

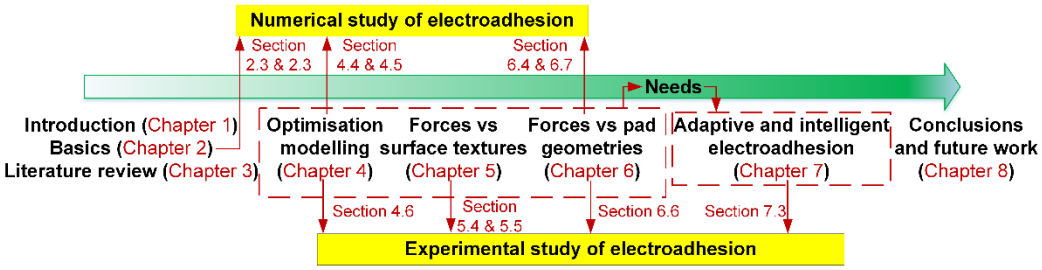

Figure 1-2 Overview of thesis structure

2 Basics of Electroadhesion

2.1 Introduction

Electroadhesion is a multidisciplinary, complicated, and dynamic electrostatic attraction phenomenon with over thirty-three variables influencing the obtainable electroadhesive forces between the electroadhesive pad and the substrate based on the literature survey [21]. These influencing factors include: 1) environmental factors such as ambient temperature, humidity, ambient pressure, contaminates, and the air pressure between the pad and substrate after applying the voltage, 2) electrode parameters such as electrode pattern, electrode width, space between electrodes, electrode thickness, electrode length, electrode thickness, conductivity, and effective electrode area, 3) pad dielectric parameters such as dielectric resistivity, dielectric permittivity, dielectric strength, dielectric surface texture, dissipation factor, dielectric molecular structure, weight, and polarizability, crystallinity, electronegativity, and electropositivity, 4) substrate parameters such as substrate resistivity, permittivity, dielectric strength, thickness, surface texture, molecular structure, weight, and polarizability, crystallinity, electronegativity, and electropositivity, and 5) electrical parameters such as voltage polarity (positive/negative/zero), voltage magnitude, and voltage type (direct/alternating current) [21]. In Chapter 2, the fundamentals of electrostatics and dielectrics for understanding electroadhesion, including electrostatic fundamentals, the principle of the electrostatic induction, classification of electric polarisations, introduction of dielectric relaxation, possible reasons causing the failure of electroadhesion, and safety consideration are all presented. After this, the basic principles with regard to how the electroadhesive forces are generated on conductive, semi-conductive, and non-conductive substrates are presented.

2.1 Fundamentals of electrostatics and dielectrics

In order to understand electroadhesion, an electrostatic application, it is necessary to understand voltage (electric field), charge (current), capacitance, and resistance (dielectric phenomenon). These are fundamental quantities in most electrostatic applications. Electrostatics is a vast and ongoing subject although it has been studied since around 600 before common era (B.C.E) [22]. The following contents in this section were interpreted and summarised from references [23][24][25][26], where more detailed contents can be seen.

2.1.1 Electrostatic fundamentals

2.1.1.1 Coulomb's law

Electrostatics is primarily based on the fact that like charges repel and unlike charges attract. Coulomb's law or Coulomb's inverse-square law states that the magnitude of the electrostatic force of interaction between two point charges is directly proportional to the scalar multiplication of the magnitudes of charges and inversely proportional to the square of the distance between them. The electric field generated by a point charge, q_0, in vacuum can be expressed as:

$$\overrightarrow{E_0} = \frac{q_0}{4\pi\varepsilon_0 \overrightarrow{r_0^2}} \quad (2\text{-}1)$$

where r_0 is the distance (in metres) from the charge and ε_0 is the permittivity of the free space or vacuum permittivity and has the value of 8.854 x 10^{-12} farad per meter (Fm^{-1} = 8.854 picofarad per meter, pFm^{-1}).

The force expression between two point charges, q_1 and q_2, in vacuum is:

$$\overrightarrow{F_0} = \frac{q_1 q_2}{4\pi\varepsilon_0 \overrightarrow{r^2}} \quad (2\text{-}2)$$

where r is the distance (in metres) between the charges (in coulombs).

Permittivity, ε, is a material property related to a material's ability to resist an electric field and the dielectric's ability to store electric energy. It is a measure of how an electric field affects and is affected by a dielectric medium thus affecting the Coulomb force between two point charges.

Permittivity is directly related to electric susceptibility, χ, which is a measure of how easily a dielectric polarises in response to an electric field. This relationship can be expressed as:

$$\varepsilon = \varepsilon_0 \varepsilon_r = \varepsilon_0 (1 + \chi) \quad \text{(2-3)}$$

where ε_r is the static and zero-frequency relative permittivity or dielectric constant of the material and $\chi = \varepsilon_r - 1$ is the electric susceptibility.

The relative permittivity is the ratio of the permittivity of the dielectric (ε_r) to vacuum permittivity (ε_0). In case of vacuum, the electric susceptibility is therefore 0. Also, dielectric constant is a measure of the charge retention capacity of a dielectric medium. The larger the dielectric constant, the greater the polarisation developed by a dielectric material in an external field will be. In an anisotropic material, the relative permittivity may be a tensor, causing birefringence. In metals, the permittivity is quite large but not infinite. The dielectric constant of most materials changes with the time-varying electric field over a certain critical range (which is material dependent). Also, it depends on the structure and impurities in the material, as well as environmental parameters such as temperature, humidity and pressure. This section only deals with dielectric materials that are homogeneous, isotropic, nondispersive, and linear under a step-function external field, expressed as:

$$\vec{E} = \begin{cases} 0, & t = 0 \\ \vec{E}, & t > 0 \end{cases} \quad \text{(2-4)}$$

Free charge cannot flow in a perfect dielectric insulator. A charge redistribution process in the dielectric however will occur if an external electric field is applied. The degree to which the dielectric material polarises is called polarisability, α . The polarisability of an atom, α_i , is defined by the equation:

$$\vec{p_i} = \alpha_i \vec{E_{loc}} \quad \text{(2-5)}$$

where p_i is the dipole moment of the atom and E_{loc} is the local electric field of the molecule.

The polarisation or polarisation density, P , of a slab of dielectric is the induced dipole moment per unit volume of the material, i.e.

$$\vec{P} = n\vec{p_i} \quad \text{(2-6)}$$

where n is the number of molecules per unit volume.

P can also be defined as the additional surface charge density produced when an electric field is applied to a slab of dielectric. The charge per unit area induced on the surface of a dielectric in an electric field is defined to be the displacement D , i.e.

$$\vec{P} = \vec{D_r} - \vec{D_0} = \varepsilon_r \varepsilon_0 \vec{E} - \varepsilon_0 \vec{E} = \chi \varepsilon_0 \vec{E} \quad \text{(2-7)}$$

where D_r is the displacement within a dielectric of relative permittivity ε_r and D_0 is the displacement in the absence of a dielectric.

The electrostatic force on a single charge, q_0 , in an external electric field, E , is given by the monopole force expression:

$$\vec{F_q} = q_0 \vec{E} \quad \text{(2-8)}$$

For bulk dielectric materials, the volume force density is:

$$f = \rho\vec{E} = (\nabla \bullet \vec{D})\vec{E} = \sum_{j=1}^{3} \frac{\partial T_{ij}}{\partial x_j} \quad (2\text{-}9)$$

Then the Maxwell stress tensor can be used to describe the electrostatic forces on entire dielectric bodies without the need to know the charge distribution. This is expressed as:

$$\overrightarrow{T_{ij}} = \varepsilon \overrightarrow{E_i}\overrightarrow{E_j} - \frac{1}{2}\varepsilon \overrightarrow{E_{ij}^2}\delta_{ij} \quad (2\text{-}10)$$

where $\delta_{ij} = \begin{cases} 1, & i = j \\ 0, & i \neq j \end{cases}$ is the Kronecker delta.

The net electrostatic forces on a closed volume is:

$$\overrightarrow{F_i} = \oiint (\sum_{i=1}^{3} \overrightarrow{T_{ij}} n_j) dS \quad (2\text{-}11)$$

The electrostatic forces can also be derived from the following equation:

$$F = \frac{\partial W}{\partial x} \quad (2\text{-}12)$$

where $W = \frac{1}{2} C U^2$ is the electric energy and C is the capacitance, and U is the electric potential.

The electrostatic forces can then be derived as:

$$F = U^2 \frac{\partial C}{\partial x} \quad (2\text{-}13)$$

Please note that in order to use the stress tensor, the electric filed should be calculated for which the charge distribution or the potentials should be derived.

2.1.1.2 Gauss's law

Also known as Gauss's flux theorem, Gauss's law relates to the distribution of electric charges to the resulting electric field and states that the net electric flux through any closed surface is equal to $\frac{1}{\varepsilon}$ times the net electric charge enclosed

within that closed surface. It can be expressed as the integral form:

$$\Phi_E = \frac{Q_0}{\varepsilon_0} \quad \text{(2-14)}$$

where $\Phi_E = \oiint_S \vec{E} \bullet d\vec{A}$ is the electric flux, the measure of the flow of the electric field through a given area, and defined as a surface integral of the electric field, through a closed surface, S, enclosing any volume. Q_0 is the total charge enclosed within the surface. $\bullet$ represents the dot product of the two vectors.

The integral form of Gauss's law can also be written to the differential form based on the divergence theorem:

$d\Phi_E = \vec{E} \bullet d\vec{A}$, then $\nabla \bullet \vec{E} = \frac{\rho_0}{\varepsilon_0}$ or $\nabla \bullet \vec{D} = \rho_0$ (2-15)

where $\nabla \bullet \vec{E}$ is the divergence of the electric field, ρ_0 is the free charge per unit volume or total electric charge density and $\vec{D} = \varepsilon \vec{E}$ is the electric displacement or the electric flux density.

$\vec{D}$, the "instantaneous" response to changes in electric field, represents how an electric field influences the organisation of electric charges in a dielectric medium, including charge migration and electric dipole reorientation.

2.1.1.3 Poisson's equation and Laplace equation

The electric field is the negative gradient of the electric potential or electric potential energy per unit charge, U, and can be expressed as:

$$\vec{E} = -\nabla U \quad \text{(2-16)}$$

The quantity U is used for the electric potential at any point. The electric field therefore depends both on the geometry of the electrodes and the magnitude of the electric potential.

Based on Gauss's law and the electric potential we have:

$$\nabla \bullet \vec{D} = -\nabla \bullet (\varepsilon \nabla U) = \rho \quad \text{(2-17)}$$

Poisson's equation that gives the potential in terms of volume charge density can then be derived as:

$$\nabla^2 U = -\frac{\rho}{\varepsilon} \quad \text{(2-18)}$$

In regions where there is no net charge density or no free charge, the Laplace equation can then be obtained as:

$$\nabla^2 U = 0 \quad \text{(2-19)}$$

where $\nabla^2 = \Delta$ is the Laplace operator.

The Laplace equation is most often used as the equation to derive electric fields as they can be computed directly from taking the gradient of the scalar potential.

2.1.1.4 Capacitance

The capacitance of a parallel capacitor can be expressed as:

$$C = \frac{\varepsilon S}{d} \quad \text{(2-20)}$$

where d is the distance between the two plates and S is the area of the plate.

The total charge on in the capacitor is given as:

$$Q = CU \quad \text{(2-21)}$$

2.1.1.5 Ohm's law

The current running through a conductor under the electric potential of U is given by:

$$I = \frac{U}{R} \quad \text{(2-22)}$$

where $R = \frac{\rho_R l}{A} = \frac{l}{\sigma_R A}$ is the resistance. In this case, $\sigma_R = \frac{1}{\rho_R}$ is the

conductivity, ρ_R is the electrical resistivity of the material measured in ohm-metres (Ω·m), l is the length of the conductor measured in metres (m), and A is the cross-sectional area of the conductor measured in square metres (m²).

2.1.2 Electric polarisation

In dielectric materials, the charges of positively and negatively charged particles at atomic and molecule level will balance each other. If an external electric field is applied, the neutral particles will be polarised, shifting the charges in the particles towards the direction of the field (i.e. positive charges go one way and negative the other). During the charge or electric dipoles redistribution process, energy or dielectric loss is involved. Charge flow or potential energy is therefore needed. This may be one of the reasons why fluctuating or dynamic electroadhesive forces over time will be observed. Also, the completion of the polarisation process is not instant and requires time.

Dielectric materials are grouped into ferroelectric and non-ferroelectric or normal dielectric or paraelectric materials. Normal dielectric materials are classified into three categories: 1) non-polar materials, elemental materials consisting of a single kind of atom, 2) polar materials, materials consisting more than one kind of atom without permanent dipole moments, and 3) dipolar materials whose molecules possess permanent dipole moments.

An electric dipole consists of two charges of the same magnitude, q, but opposite polarity, separated by a small distance, r. The dipole moment is defined as:

$$\vec{m} = q\vec{r} \quad \text{(2-23)}$$

The difference between the dipole moments before and after the application of an external field, E, is called the induced dipole moment:

$$\vec{M} = \alpha\vec{E} \quad \text{(2-24)}$$

The induced dipole moment of an atomic or molecule may arise from one or a number of sources which can be divided into six types of polarisations.

Electronic polarisation arises from the displacement of electrons in an atom relative to the positive nucleus. The electric field modifies the electron density quite quickly. This polarization is always present in atoms or molecules in most of materials. In non-polar materials, however, only the electronic polarisation exists.

Atomic or ionic polarisation is due to the relative displacement of atoms or ions of opposite polarity within a solid. In polar materials, both the electronic and ionic polarisation exist.

Although both the electronic and ionic polarisation are due mainly to the elastic displacement of electron clouds and lattice distortion within the atoms or molecules, their interaction is an intramolecular phenomenon that is relatively insensitive to temperature. The time involved in the electronic polarisation is of the order of 10^{-15} seconds whereas it is a 10^{-13} second for the ionic polarisation simply due to the fact that the ions are heavier than electrons by more than 10^3 times.

Orientational polarisation or dipolar polarisation results from the rotation of molecules that have permanent dipole moments. This rotational process encounters not only the resistance but also the mechanical friction due to the inertia resistance of the surrounding molecules. This process only occurs in solid polar materials possessing permanent dipoles. The interaction is therefore an intermolecular phenomenon which is strongly temperature dependent. In dipolar materials, electronic, ionic, and orientational polarisation will occur. In solid materials, the rotation of dipoles will be limited to a few discrete orientations due to the crystalline field determined by the interaction of the dipole with neighbouring ones.

The space charge polarisation, associated with mobile and trapped charges, occurs mainly in amorphous or polycrystalline solids or in materials consisting of traps. Charge carriers such as electrons, holes or ions may be trapped in the bulk or at the interfaces or may be impeded such that they are discharged or replaced at the electrical contacts, forming the space charges that will distort the field distribution and then affect the average dielectric constant. This polarisation contains two classes: the hopping polarisation and the interfacial polarisation.

The spontaneous polarisation arises from a phase transition at a critical temperature without the help of the external electric field in single crystals or crystallites in polycrystalline materials with a non-centrosymmetic structure such as ferroelectric materials. Reversible electric dipole moments spontaneously orient themselves parallel to the dipole moment of neighboring cells. The external electric field then aligns the randomly distributed dipole domains. This polarisation does not varnish but remains in the material after the removal of the field.

It is difficult to measure and differentiate the two types of the space charge polarization. For simplicity, the hopping and space charge polarisation are usually ignored, giving the total polarisation of an arbitrary normal dielectric system as:

$$\overrightarrow{P_{sum}} = \overrightarrow{P_e} + \overrightarrow{P_i} + \overrightarrow{P_o} \quad \text{(2-25)}$$

The response time for electronic and ionic polarization is so short that they can be considered to follow the excitation field instantaneously without a time lag. It is therefore P_o that has a time lag with the applied field, which is presented in the right corner in Figure 2-1. A finite but different polarisation time, for each mechanism, is needed before each of these dipoles is fully formed under the external electric field. The approximate time required for polarisation under the aforementioned step function electric field is shown in Figure 2-1.

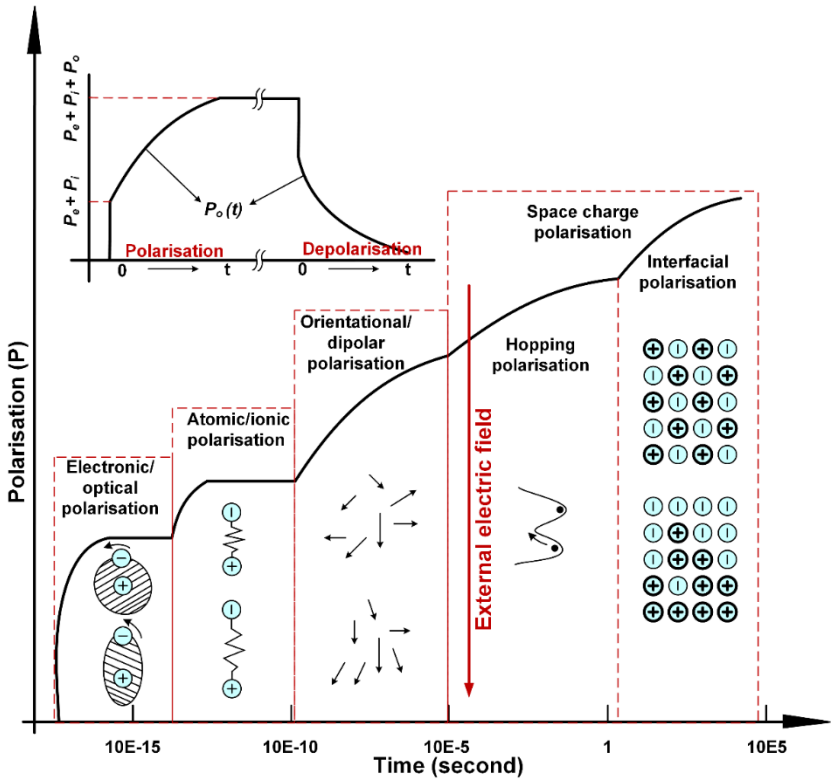

Figure 2-1 Polarisation of normal dielectric materials under a step-function electric field

Polymeric materials have been widely used as dielectric materials for insulation purposes due to them being lightweight, their flexibility to be tailor made for specific applications and better resistance to chemical attack. Non-polar materials can be made polar by introducing a small amount of impurities [26]. Non-polar polymeric films such as polystyrene (PS), polypropylene (PP), polyethylene (PE) and polytetrafluoroethylene (PTFE) showed a larger amount of electric charge accumulation but longer saturation time. Polar polymeric films such as polycarbonate (PC), polyethylene-naphthalate (PEN), polyimide (PI), and polyethylene-terephthalate (PET) however showed a shorter saturation time but smaller amount of electric charge accumulation [27].

Insulating substrates are different and need to be considered separately. They are also quite complex, due to the lack of free electrons moving through the solid, so a single positive electrode from an electroadhesive pad has been used as an example within this section. The polarisation process of the dielectric material between the electrode and the substrate surface can be seen in Figure 2-2,

where the applied external field, E_0, is decreased due to the opposite electric polarisation field, E_{p1}. This results in a reduced electric field $\left|\overrightarrow{E_1}\right| = \left|\overrightarrow{E_0}\right| - \left|\overrightarrow{E_{p1}}\right|$. The charge distribution of both polar dielectrics and nonpolar dielectrics can be approximately regarded as two equivalent areas of bound charges, $\pm Q_e$, which can be seen in the middle part of the Figure 2-2. The number of bound charges on the dielectric surfaces corresponds to the electric polarisation (P) capability of dielectrics under external electric fields.

Non-polar dielectrics (to the RHS of in Figure 2-2), such as rubber, do not have permanent electric dipole moments. Induced electric dipole moments will be generated by the electric field E_0, resulting a small E_{p1}. Polar dielectrics (to the left hand side of Figure 2-2), such as polyethylene, have permanent electric dipole moments, so a random orientation of polar molecules will be shown when no external electric field is applied. The molecules will be aligned with E_0, but not completely because of random molecule thermal motion. A small E_{p1} is then generated by these aligned molecules. This process is also called relaxsation polarisation because of the longer build and elimination time.

Based on the Gauss theorem, we have the electric polarisation:

$$\vec{P} = \chi_e \varepsilon_0 \vec{E} \quad \text{(2-26)}$$

and the relationship between the electric displacement, D, and electric field strength is given as:

$$\vec{D} = \varepsilon_0 \vec{E} + \vec{P} = \varepsilon_0 (1 + \chi_e) \vec{E} = \varepsilon \vec{E} \quad \text{(2-27)}$$

where E is the electric field in the dielectrics, ε_r is the relative permittivity, $\chi_e = \varepsilon_r - 1$ is the electric susceptibility, and ε is the dielectric permittivity.

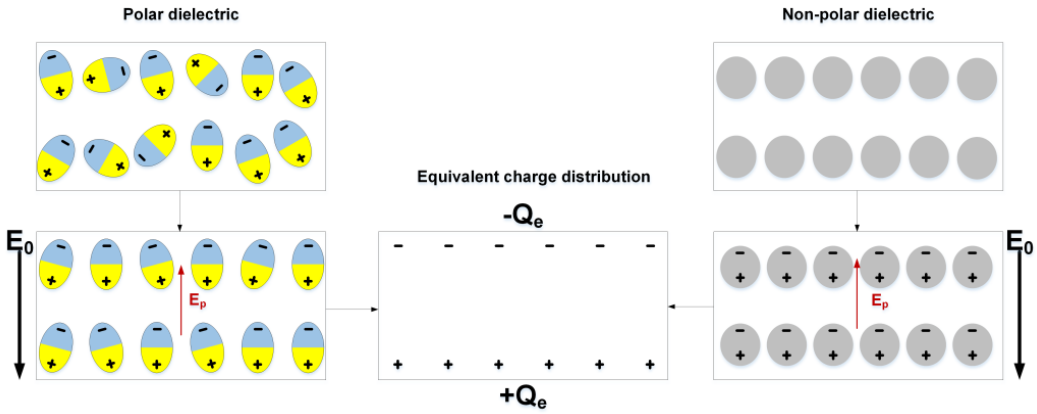

Figure 2-2 Polarisation process of the dielectric material

With regard to the dielectric material with relative permittivity of ε_{r1} , we have:

$$\overrightarrow{E_{p1}} = \frac{\vec{P}}{2\varepsilon_0} = \frac{1}{2}\chi_{e1}\vec{E} \quad (2\text{-}28)$$

and

$$\vec{E} = \overrightarrow{E_0} - \overrightarrow{E_{p1}} \quad (2\text{-}29)$$

By rearranging equation (2-28) with equation (2-29), we know:

$$\overrightarrow{E_{p1}} = \frac{\chi_{e1}\overrightarrow{E_0}}{2+\chi_{e1}} = \frac{\overrightarrow{E_0}(\varepsilon_{r1}-1)}{\varepsilon_{r1}+1} \quad (2\text{-}30)$$

where $\chi_{e1} = \varepsilon_{r1} - 1$ is the electric susceptibility the dielectric material.

A similar polarisation process will occur in the air gap between the dielectric and the substrate surface (E_{p2}) and on the surface of any wall substrates (E_{p3}), giving:

$$\overrightarrow{E_{p2}} = \frac{2\overrightarrow{E_0}\chi_{e2}}{(2+\chi_{e1})(2+\chi_{e2})} = 0 \quad (2\text{-}31)$$

and

$$\overrightarrow{E_{p3}} = \frac{2\overrightarrow{E_0}\chi_{e3}}{(2+\chi_{e1})(2+\chi_{e2})(2+\chi_{e3})} = \frac{2\overrightarrow{E_0}(\varepsilon_{r2}-1)}{(\varepsilon_{r1}+1)(\varepsilon_{r2}+1)} \quad (2\text{-}32)$$

where χ_{e2} is the electric susceptibility of the air, χ_{e3} is the electric susceptibility of substrate material, and ε_{r2} is the relative permittivity of the wall substrate.

Induced charges are then presented. These induced charges are opposite to the polarity of the electrodes. They cannot transfer from one atom to another as in a conductor, making large rotations and displacements impossible; thus no neutralisation will occur between these charges. However, a torque will be experienced when negative charges and positive charges are trying to move closer to each other. The combination of these forces leads to the electrostatic attractive force between the pads and the substrates.

Let σ_1 be the charge density of the upper surface of the selected electrode surface, σ_2 be the charge density of the down surface of the selected electrode surface. Therefore, based on the Gauss theorem, we have:

$$\overrightarrow{\sigma_1} + \overrightarrow{\sigma_2} = \vec{\sigma} = \overrightarrow{E_0}\varepsilon_0 \quad (2\text{-}33)$$

where $\sigma_1 = \varepsilon_0 E_1$ and $\sigma_2 = E_2\varepsilon_0$.

2.1.3 Electrostatic induction

The electrostatic induction phenomenon, discovered by John Canton in 1753 and Johan Carl Wilcke in 1762 [28], is a process where the formation of negative charges on one side and positive charges on the opposite side of a conductor are induced by an external electrostatic field produced by a charged insulator. This phenomenon is explained shown in Figure 2-3 (a), where A is the charged insulator and B is the uncharged conductor. The internal electric field inside B, produced by the induced negative and positive charges in B, cancels the field

generated by A, resulting a zero electric field in B. The negative charges on B are called bound induced charges while the positive ones are free induced charges. The result after grounding the conductor B can be seen in Figure 2-3 (b). In order to maintain the electric field inside B as zero, both the magnitude and distribution of the negative bound charges will change depending on the geometric shape of the conductor B. The charge distribution in the charged insulator A will not be affected as the charges in A cannot freely move. This is maybe one the reasons why there is a difference in obtainable electroadhesive forces between the pads and grounded and non-grounded conductive substrates as the charge density on the substrate surfaces is different.

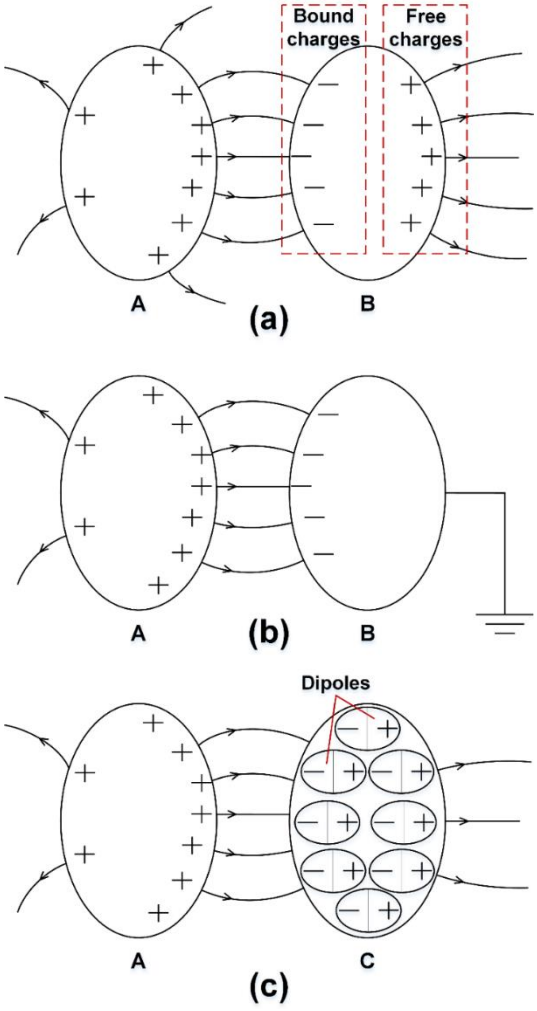

Figure 2-3 The example for the electrostatic induction phenomenon [24], where + denotes positive free charges

The electrostatic induction phenomenon prevails in conducting materials as conducting materials generally refer to materials consisting of a large amount mobile free charge carriers. For instance, in a metal, the concentration of free electrons (mobile charge carriers) is of the same order as that of the number of atoms, i.e. about 10^{22} to 10^{23} cm^{-3}. In semiconductors and dielectric materials, however, the number of mobile free charge carriers is far less than the number of atoms. Although an electric field would cause the movement of mobile charge carriers to produce space charge polarisation in a manner similar to electrostatic induction, space charge polarisation usually plays an insignificant role because it involves only a small number of mobile charge carriers, as compared to electric polarisation, which involves all atoms.

If the conductor B is replaced by an insulator, C, see Figure 2-3 (c), the field generated by A will not induce charges in C. Polarisation of C will occur by shifting slightly the normally symmetrical distribution of electron clouds of atoms and by orienting dipolar molecules toward the direction of the applied field to form dipoles. A big dipole is thus produced by the multiple tiny dipoles contributed by each atom or molecule. Dielectric relaxation and depolarisation will occur due to thermal agitation after removing C.

2.1.4 Dielectric relaxation

As can be seen from Figure 2-1, the polarisation time involved in the orientational, hopping and interfacial polarisation process is quite long and varies depending on the dielectric systems. The depolarisation process, which is defined as the time taking to bring the excited system back to its original equilibrium state, can be referred to as dielectric relaxation. After switching off the voltage connected with the electrodes, i.e., removing the external electric field, the charge density decays with time and can be expressed as:

$$\sigma_s(t) = \sigma_s(0)e^{-t/\tau_d} \quad (2\text{-}34)$$

where $\tau_d = \rho_R \varepsilon$ is the dielectric relaxation time and is the time needed for the originally induced charge to decay to 36.7% of its original value.

τ_d can be very large for some insulating materials. For instance, for a dielectric film, $\varepsilon = 3.1\varepsilon_0$ and $\rho_R = 1.7 \times 10^{17}$ (Ω−cm), resulting $\tau_d = 4.7 \times 10^4$ seconds or 13 hours. This means several days may be needed for charges to be completely neutralised. For example, as published by Yatsuzuka et al., the residual forces maintained the same level with the forces measured for more than 12 hours [15]. It is therefore not recommended to touch the electroadhesive pad, especially the bare electrode areas, even if the pad has been depolarised for some time as some charges may still remain on the electrodes.

2.1.5 Clamping and unclamping

Understanding the dielectric relaxation of materials used in electroadhesive systems is extremely useful for efficient and quick clamp and unclamp. A simple polarity reversal will not cause object release but will simply maintain the retention forces [7]. Although a short circuit of the electrodes will immediately neutralise the charges on the electrodes, the polarised particles in dielectric materials, especially those involved with the orientation of permanent dipoles or the migration of charge carriers, still requires time to be completely depolarised. It was recommended to increase the degree of cross-linking structure in dielectric materials to reduce dielectric loses and the dielectric relaxation time [19]. Also, increasing the temperature and reducing the impurities in materials may help reduce the dielectric relaxation time [29]. The application of AC voltage to electrodes in the electrodadhesive pads enabled nearly zero residual charge [15] however at the expense of larger current and higher power consumption. An increased voltage may also bring faster release speed [30]. Mechanical release mechanisms such as the use of the passage of pegs or air jets [7] were also employed for quick unclamping.

2.1.6 Possible reasons for the failure of electroadhesion

The macroscopic currents in a dielectric are mainly due to the displacement current, given by:

$$\vec{J} = \sigma_s \vec{E} + \frac{\partial \vec{D}}{\partial t} \quad \text{(2-35)}$$

A dielectric may suddenly loose its property of non-conduction, permanently or temporarily, when the electric field is high enough. This results in an electrical breakdown that consists of an abrupt rise of electrical current under the effect of an electric field. **The failure of electroadhesion is defined in this thesis as a sudden change or drop of the electroadhesive forces**. It is detrimental to have the failure of the electroadhesive end effectors when tasked to pick objects.

There are many factors which can cause the failure of electroadhesion such as pressure, space between electrodes, electrode materials, type and cleanness of insulating materials, and type and amplitude of the electric field. Additional considerations such as direct or indirect mechanical failures such as tearing off the pad due to large shear forces and fault operations such as putting the pad into extremely high temperature environments (such as over 150 ^{o}C for some polymers) are not included here. Possible reasons why these failures occur are summarised as below.

Reason 1: air gaps between the electrodes

It is necessary to fill dielectric materials in between the electrodes to deal with high voltages. However, if air is trapped in the material, the performance may be even worse than having no dielectric material at all. If the space between the parallel plates is filled with a dielectric material, the electric field strength in the material can be described as:

$$E = -\frac{U}{s} \quad \text{(2-36)}$$

where s is the space between the electrodes and U is the applied voltage.

If an air gap is located in the dielectric material, the electric field strength is expressed as:

$$E = -\frac{\varepsilon_r}{1+(\varepsilon_r - 1)(t_{air}/s)}\frac{U}{s} \quad (2\text{-}37)$$

where t_{air} is the thickness of the air gap and ε_r is the dielectric constant of the dielectric material.

The dielectric material not only has a higher dielectric breakdown strength but also a higher dielectric constant than the air. The dielectric materials screen out the electric fields. This leaves most of the voltage drop across the air, resulting in a higher electric field strength in the air gap which is less able to withstand it. Dielectric breakdown then occurs at a lower voltage than before. Due to this, care must be taken to eliminate the air and all other gases.

Note that the air gap in the dielectric material may also cause internal discharges as mentioned below. Injection of charges into the surface of the air gap will occur after the breakdown. This homocharge will reduce the electroadhesive forces and may accumulate significantly if the resistivity of the dielectric is very high [19].

Reason 2: sharp edges along the electrode surface

It can be seen from Figure 2-4 (a) that sharp electrode edges are produced by the unprofessional etching, compared with the professional etching shown in Figure 2-4 (b), which can cause a serious dielectric breakdown and generated a conductive region. This is because charge concentrations were generated at sharp points. The sharp edges may bring asymmetric electrode configurations, causing corona discharges (mentioned below) when the electric field is high enough to ionise the surrounding air. This leads to lower voltages that the unprofessional etched pad can bear with, thus bringing smaller electroadhesive

forces.

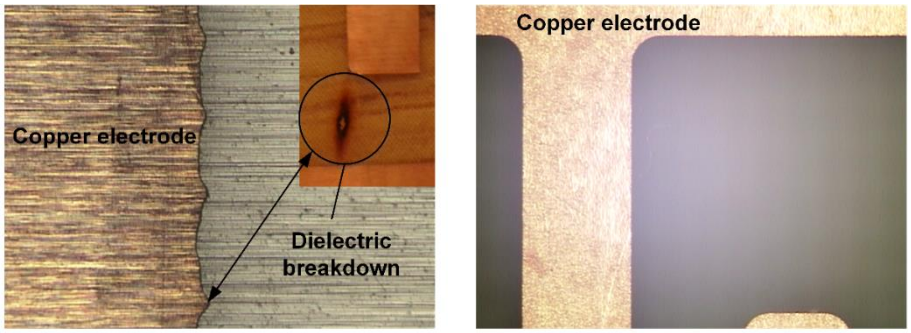

Figure 2-4 An example of sharp edges produced by etching

Reason 3: electrical aging

When the electroadhesive pad is tasked to conduct jobs continuously, the materials in the pad will be in a nonequilibrium state and its properties will change with time. Electrical aging, which relates to the lifecycle or lifetime of the material, is a gradual degradation process. This can lead to destructive breakdown of the material, thus causing the failure of electroadhesion.

Reason 4: electrical discharges

Electrical discharges involve processes by which atoms or molecules become electrically charged due to ionisation by avalanches of hot charge carriers. Electrical discharges usually start in the medium of gas state and cause air ionisation. In electroadhesive applications, partial discharges are usually the case as there will be no bridge of the electrodes or any pair of electrical contacts. Partial discharges contains four classes: corona discharges, surface discharges, internal discharges, and electrical treeing.

Corona discharges are arcs with rather short duration and high power density. They usually occur near a sharp point or edge of a metallic contact, or near a conducting particle whose surrounding fields are extremely high due to divergent or inhomogeneous local field distributions. Both positive (uniformly distributed bluish-white cloud) and negative (reddish spots of current pulses) voltages can

induce corona discharges if an asymmetric electrode configuration and a high voltage are applied. The corona discharges in the air depend on ambient humidity and contaminants. Surface discharges usually occur on the surface of a dielectric material. Internal discharges usually occur in inclusions or cavities existing in a dielectric material or in low density domains or channels created due to electrical stressing at high electric fields. Electrical treeing may be regarded as a combination of corona and internal discharges. For electroadhesive applications, corona discharges, surface discharges and internal discharges may be three main reasons for the failure of electroadhesion.

Reason 5: electrical breakdown in solids

There are two main electrical breakdowns in solid dielectric materials: 1) the thermal breakdown caused by continuously joule heating and thermal instability aroused by electrical conduction and polarisation, and 2) the electrical breakdown due to electronic processes other than thermal excitation such as hot carriers in high-mobility states. The breakdown permanently modifies the material properties of along the failing path.

2.2 Principles of electroadhesion

2.2.1 Principles of electroadhesive force generation

As can be seen in Figure 1-1, the conductive electrodes embedded within the dielectric materials are connected with high voltages in the range of kilovolts. Strong electric fields are then generated and induce image charges (opposite to the charged electrodes) in the substrates. The electrostatic adhesive forces are thus formed between the pad and the substrate. As previously described, the polarity of electrodes can be single polar using only one electrode and one high voltage converter or bipolar electrodes using at least two electrodes and two high voltage converters or tripolar which is introduced in section 3.3.1. The insulating materials covering the electrodes serve as dielectric buffers, preventing the charge neutralisation and dielectric breakdown between electrodes. The

dielectric material filled in between the electrodes and on the top of the electrodes can be the same or different based on existing laboratory techniques. The principles of electroadhesive force generation on conductive and insulating substrate materials are different.

For conductive substrates, such as metals, the electroadhesive forces are generated by electrostatic induction. As aforementioned, conducting materials such as copper have a large amount of electrons that are able to rearrange themselves quickly and easily. Equal and opposite charges are induced on the surface of conductive substrates after the application of the high voltage, and electroadhesive forces between the conductive electrodes and the conductive substrates are formed. It was found by Monkman that a permanent earth or negatively charged solution is suggested to clamping conductive substrates [17]. A special electrode configuration, as shown in Figure 2-5 (c), has been implemented by Monkman et al. [31] to avoid the inconvenient design shown in Figure 2-5 (b) where a permanent earth bond is required during lift and transportation which is not practical. Care must be taken to ensure the initial lifting force is enough when lifting conductive substrates which have been grounded.

When the aluminium base plate shown in Figure 2-5 (a) is removed (i.e. the object to be grasped is not grounded), different magnitude and types of forces were obtained [17]. Some materials, even with high dielectric constants, such as the rubber/polyester shown in Figure 2-5 (a) and (b), were found to exhibit nearly no electroadhesive force. For insulating substrates, the principle of electroadhesive force is therefore different from electrostatic induction. It was concluded by Monkman et al. that electric polarisations, especially the orientational polarisation and interfacial polarisation, account for the electroadhesive forces [29]. This was based on the fact that the electroadhesive pad was in contact with the substrate to be picked up.

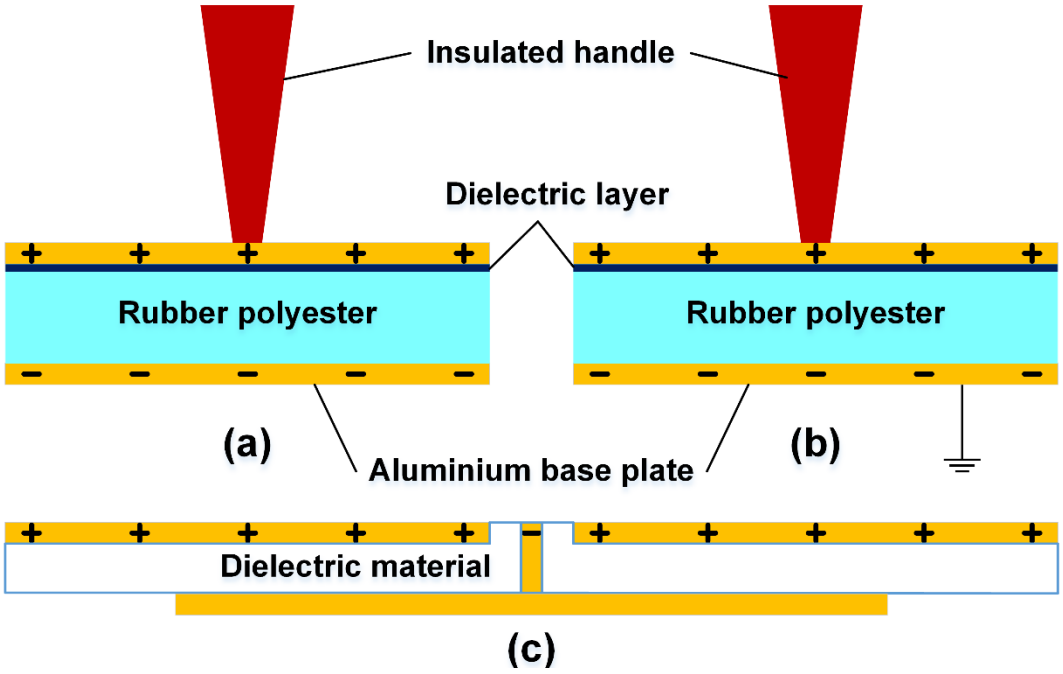

Figure 2-5 Monkman's electroadhesive end effector design [31]

Also, they concluded that the electroadhesive forces only exist at a dielectric interface. During the separation of two fabric materials, they found that:

● If the two fabric materials are totally different, both were picked up.

● If the two fabric materials have the same dielectric constants but different electroadhesion properties such as molecule structures, both were picked up if the one with better electroadhesion properties was placed at the bottom. Otherwise, both were not able to be lifted.

● If the two fabric materials have the same electroadhesion properties but with different dielectric constants, only the one placed on the top will be picked up.

Based on the third result, they concluded that the electroadhesive forces are proportional to the difference in charge densities at a dielectric interface. The electroadhesive gripping force is generated between charges on the electrodes in the pad and the net charges at the dielectric interface produced by the polarisation process. Because the charge density of a stack of the same material (such as carbon fibre sheets) is the same, the electroadhesive force between layers of the material is therefore zero [17]. Based on this assumption, a

theoretical model describing the dynamic force generation and removal processes in a single pole electroadhesive device was proposed by Zhang et al. [8] and the electroadhesive force per unit area was expressed as:

$$\overrightarrow{P_{ea}} = \vec{E}\sigma \quad \text{(2-38)}$$

where E is the applied electric field strength, $\sigma = \frac{\sigma_{R2}\varepsilon_0\varepsilon_{r1} - \sigma_{R1}\varepsilon_0\varepsilon_{r2}}{\sigma_{R1}t_0 + \sigma_{R2}t_1} U \exp(\frac{\sigma_{R1}t_0 + \sigma_{R2}t_1}{\varepsilon_0\varepsilon_{r1}t_1 - \varepsilon_0\varepsilon_{r2}t_0})$ is the charge density accumulated at the dielectric interface and σ_{R1} is the conductivity of the dielectric layer, σ_{R2} is the conductivity of the substrate, ε_{r1} is the relative permittivity of the dielectric layer, ε_{r2} is the relative permittivity of the substrate, t_0 is the thickness of the substrate and t_1 is the thickness of the dielectric layer.

It was found by the author that electroadhesive pads with bare electrodes facing the dielectric substrate (see Figure 2-6 (a)) are able to exhibit good electroadhesion properties. In this case, the orientational polarisation may play a major role in achieving the electroadhesive force obtainable. People used a novel control method to grasp the same fabric place in stack [32]. This should be a supplementary finding to Monkman's results.

The electroadhesion phenomenon can also be contactless both on conductive substrates such as an aluminium disks [33] and insulating substrates such as glass [16]. It was concluded by Jeon et al. that the atomic and electric polarisation account for the generation of the electroadhesive forces. In summary, for insulating substrates, the electroadhesive forces are generated by polarisation. Also, due to the dynamic characteristic of the electroadhesive forces obtained from dielectric materials, it takes time to reach the maximum forces, be it one minute or tens of minutes. In this thesis, only the contact based electroadhesion is considered.

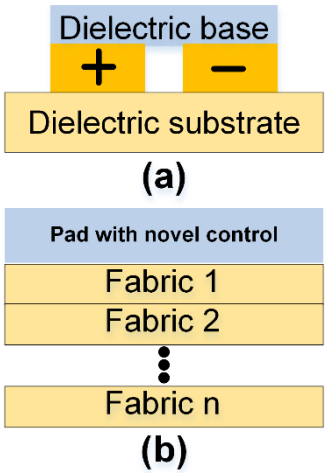

Figure 2-6 Supplementary results to Monkman's finding: (a) bare electrode pad and (b) pad with novel control [32]

2.2.2 Why the force in shear is greater than in normal

All the experimental results in the literature showed that the shear electroadhesive forces were larger than that of in normal. It is therefore inappropriate to derive the shear forces by the product of friction coefficients and normal forces although this has been used by some researchers [10][11][20]. Also, all the recorded normal electroadhesive forces did not claim the inclusion of suction forces (if not tested in vacuum environment), Van Der Waals forces and possible surface tension forces after the application of high voltages. The inclusion of suction forces, due to the air gap, and Van Der Waals forces due to the intimate contact, aroused by point polarisation (instant dipoles) [34], is shown in Figure 2-7 (a).

The recorded normal electroadhesive forces can be expressed as:

$$\overrightarrow{F_{normal}} = \overrightarrow{F_{ea}} + \overrightarrow{F_{suction}} + \overrightarrow{F_{van}} \quad (2\text{-}39)$$

where F_{ea} is the normal electroadhesive forces, $F_{suction}$ is the suction forces between the pad and the substrate and F_{van} is the Van Der Waals forces.

When a shear force is applied on the pad, restriction forces occur, as shown in

Figure 2-7 (b) [16], which may be the main reason that the recorded shear forces are stronger than the normal forces. Assuming that there is an angle, θ, as seen in Figure 2-7 (b), between the forces in normal and the restriction forces, the recorded shear electroadhesive forces can then be expressed as:

$$F_{shear} = \mu(F_{ea} + F_{suction} + F_{van} + F_{restriction}\cos\theta) + F_{restriction}\sin\theta \quad (2\text{-}40)$$

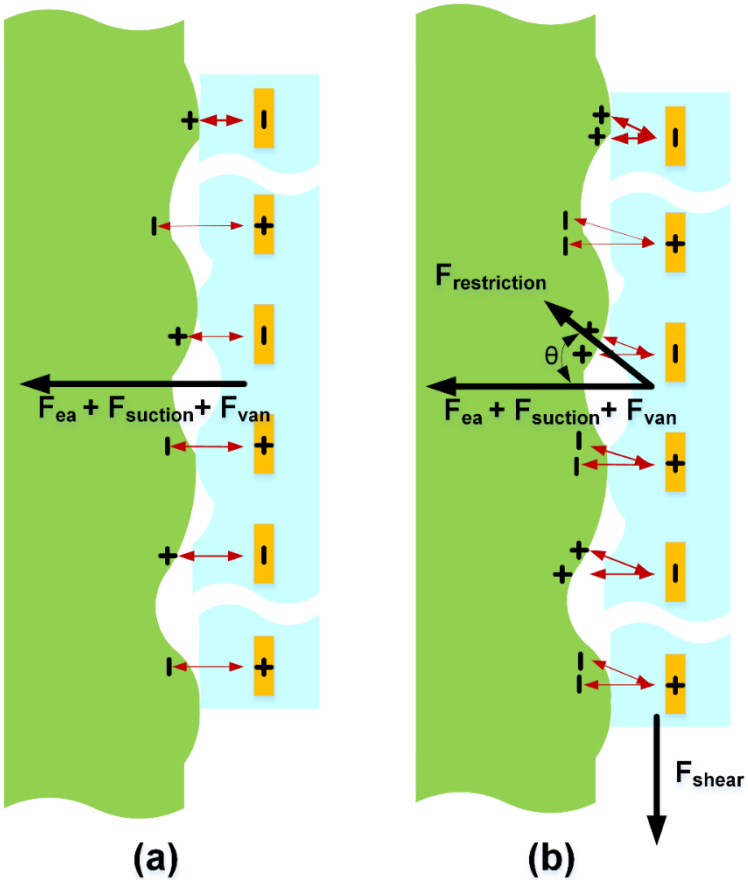

Figure 2-7 The electroadhesive forces based on the inclusion of the suction forces and Van der Waals forces

2.3 Development of basic theoretical models for understanding electroadhesion

A standardised and cost-effective procedure to investigate a research problem or phenomenon such as electroadhesion with several influencing variables contains two main steps [1]: 1) theoretical/mathematical modelling or

computational simulation, 2) followed by physical experiments to validate/support the theoretical analysis.

There are **at least thirty-three variables** (see section 3.8 in Chapter 3) affecting the electroadhesive forces generated between the electro-adhesive pads and adhering wall substrates [21]. The theoretical analysis of electroadhesion is, therefore, useful for understanding the phenomenon in a comprehensive way. In addition, this analysis will help us to:

● optimise parameters of the electroadhesive pads to generate larger attractive forces,

● set correct boundary conditions in electrostatic simulation of the electro-adhesion,

● design, set-up, and conduct comprehensive verification experimentation.

Although it is difficult to accurately quantify the electroadhesive forces, some approximate modelling and calculations can be carried out. This will provide an idea of the scale of the electroadhesive forces involved, and also help guide us to conduct the electrodhesive pad design, manufacture and experimental testing properly as mentioned above. A comprehensive approximation modelling diagram of the electroadhesion, summarised from the extensive literature survey (see Chapter 3) and analysis, can be seen in Figure 2-8. Please note that all the following equations are based on one-dimensional system for simplicity.

It should be noted that the dielectric strength of dielectric materials will change when the space between electrodes is smaller than 1mm, and no longer hold the rule [29], denoted by:

$$s_{\min} = \frac{U_{\max}}{\gamma} \quad (2\text{-}41)$$

where γ is the dielectric strength or field strength of the air and $U_{\max}$ is the

maximum voltage can be applied based on the minimum space between electrodes, $s_{\min}$.

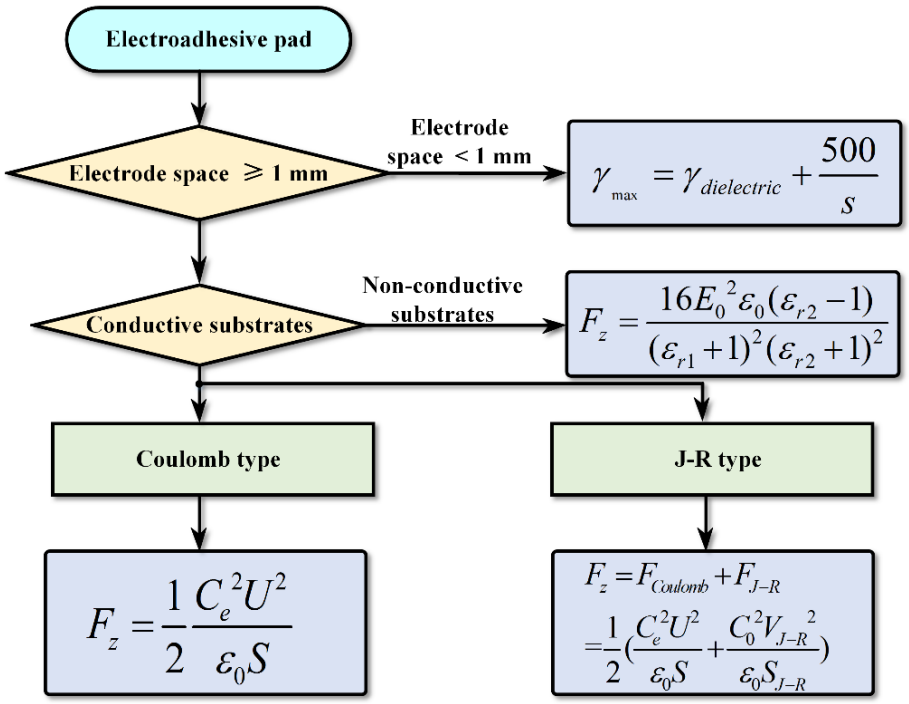

Figure 2-8 A comprehensive approximation modelling diagram of electroadhesion

For example, the dielectric strength of air is γ_{air} = 3000 (voltage per millimetre, Vmm^{-1}) when the scale of space between electrodes is greater than 1 mm; for $s_{\min}$ = 1 mm, the maximum voltage can be applied is $U_{\max}$ = 3000 V. However, this will not occur when space between electrodes is smaller than 1mm and the maximum dielectric strength of air will change to:

$$\gamma_{(air)\max} = \gamma_{air} + \frac{500}{s} \quad (2\text{-}42)$$

This corresponds to other dielectrics. As such, we may have the maximum dielectric strength of dielectrics, described by:

$$\gamma_{\max} = \gamma_{dielectric} + \frac{500}{s} \quad (2\text{-}43)$$

where $\gamma_{dielectric}$ is dielectric strength of the dielectric material and s is the space

between electrodes.

The difficulties of accurately modelling the electrostatic attractive forces between pads and substrates include:

● inhomogenous dielectric materials with unpredictable crystal structure polarisability and inhomogeneous electric fields always exist in nature;

● it is difficult to model the surface texture of all substrates accurately;

● some flexible/compliant electro-adhesive pads easily conform to surface irregularities, making the effective contact areas difficult to predict.

In order to conduct the approximation analysis, assumptions such as the ones mentioned in section 2.2.1 have to be made to simplify the theoretical analysis process.

2.3.1 Basic theoretical models on conductive substrates

When facing conductive substrate materials, dielectric materials with different properties such as volume resistivity will cause different mechanisms of generating the electroadhesive forces. Volume resistivity over 10^{14} Ω-cm (or resistivity larger than 10^{16} Ω) results in the Coulomb type electroadhesive pads, whilst volume resistivity between 10^{10} and 10^{12} Ω-cm (or resistivity between 10^{8} and 10^{13} Ω) results in Johnsen-Rahbek (J-R) type pads. Both the Coulomb force and J-R effect will exist, to some degree, in all electroadhesive pads, but the Coulomb force will dominate when the volume resistivity of dielectrics is over 10^{14} Ω-cm [35].

2.3.1.1 The Coulomb type electroadhesion

For the Coulomb type electroadhesion, the electroadhesive forces between the pad and the substrate can be derived from as a capacitor having dielectrics in series, or a series of parallel connections of two or several capacitors if using double-electrode or multi-electrodes respectively. The equivalent circuit of two

adjacent electrodes in series from the multi-electrode and bi-polar electroadhesive during the electroadhesion operation can be seen in Figure 2-9 (left), where g is the gap between the pad and the substrate, t_1 is the dielectric thickness, C_{1i} denotes the ith capacitance of the dielectric material and C_{0i} denotes the ith capacitance of the air between the dielectric and the substrate surface.

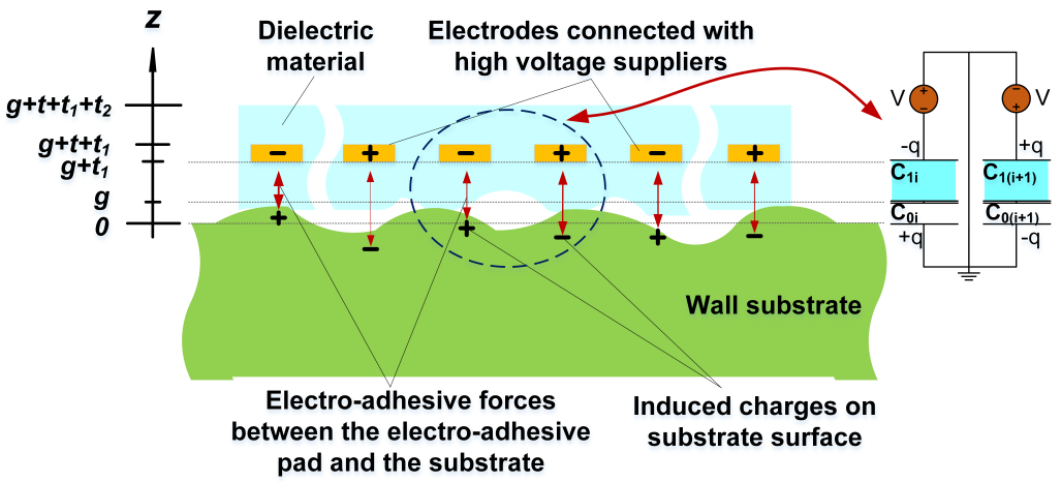

Figure 2-9 The Coulomb type electroadhesive

We assume the dielectric material is homogenous, linear, and isotropic. Charges are, therefore, uniformly distributed on the electrode surfaces and substrate surfaces. Since $g+t_1$ is far less than the size of the electro-adhesive pad, the fringing effect can therefore be ignored, making the problem an idealised planar capacitor. Therefore, no current leakage occurs in coulomb type electroadhesives, resulting significantly lower power consumptions, compared with the J-R type electroadhesion.

The total capacitance between the pad and substrate is, therefore, given as:

$$C_e = \sum_{i=1}^{n} \frac{C_{0i}C_{1i}}{C_{0i}+C_{1i}} = \frac{\varepsilon_0 \varepsilon_{r1} S}{\varepsilon_{r1} g + t_1} \quad (2\text{-}44)$$

where n is the total number of capacitors in series, S is the electro-adhesive

pad area, ε_0 is the permittivity of the air and ε_{r1} is the relative permittivity of the dielectrics.

The attractive forces between the pad and the substrate can be obtained from the Maxwell stress tensor method or the virtual work method from the perspective of deriving the energy stored in a capacitor:

$$W = \frac{1}{2}\int D \times E_0 \quad \text{(2-45)}$$

where W is the total energy stored in the capacitor, D is the electric displacement and E_0 is the applied electric field.

For the purpose of this work, the simpler virtual work method is used. Therefore, we have:

$$F_z dz + dW = 0 \quad \text{(2-46)}$$

where F_z is the applied force and dz is the displacement.

Since

$$dW = d(\frac{1}{2}C_e U^2) = \frac{1}{2}\frac{Q^2}{\varepsilon_0 \varepsilon_{r1} S} d(\varepsilon_{r1} z + t_1) \quad \text{(2-47)}$$

Hence, after substituting equation (2-47) into equation (2-46), the attractive force within the capacitor can be given as:

$$F_z = -\frac{1}{2}\frac{Q^2}{\varepsilon_0 S} = -\frac{1}{2}\frac{C_e{}^2 U^2}{\varepsilon_0 S} \quad \text{(2-48)}$$

where the negative sign corresponds to the attractive electroadhesive forces between the pad and the substrate.

Based on equation (2-48), the attraction force per unit area can be given as:

$$f_z = \frac{F_z}{S} = -\frac{1}{2}\frac{C_e^{\,2}U^2}{\varepsilon_0 S^2} \quad \text{(2-49)}$$

2.3.1.2 The J-R type electroadhesion

The J-R effect [36], firstly investigated by Johnsen and Rahbek, occurs when attaching the electroadhesive pads, covered by imperfect dielectrics with finite volume resistivity such as semi-conductive materials, onto metal substrates. Current leakage or charge transfer will occur through the contacting points between the pads and the substrates. However, a strong electrostatic attractive force can be generated by the interfaces accumulated by charges between the noncontact areas (see Figure 2-10). The comparably small gap between these non-contact areas, caused by surface irregularities of both surfaces in nature, contributes to the strong adhesion forces. Hence, for the J-R type electroadhesion, it is the potential difference applied across the interfaces mentioned above, rather than that applied through the dielectric layer and the air gap, which leads to the attractive forces. In this case, the J-R electrostatic attractive forces are independent from the dielectric material between the pad and the substrate [37], giving the J-R force as:

$$F_{J-R} = \frac{1}{2}\frac{C_0^{\,2}V_{J-R}^{\,2}}{\varepsilon_0 S_{J-R}} \quad \text{(2-50)}$$

where C_0 is the capacitance of the non-contact areas, V_{J-R} is the potential difference across the interfaces, and S_{J-R} is the effective J-R non-contacting areas (usually assume this to be the same as S). S_{J-R} is significantly influenced by the surface texture of the pad and substrate and the level of attractive forces.

Based on the equivalent circuit of the J-R type electroadhesive as can be seen in Figure 2-11, the potential difference across the interfaces can be given as [38]:

$$V_{J-R} = \frac{R_c}{R_c + R_d} U \quad (2\text{-}51)$$

where R_d is the volume resistivity of the dielectric material and R_c (usually much larger than R_d) is the contact resistance. R_d is related to surface texture, the properties of the dielectric material and contacting areas, forming a major component of the total resistance in the J-R type electroadhesive system.

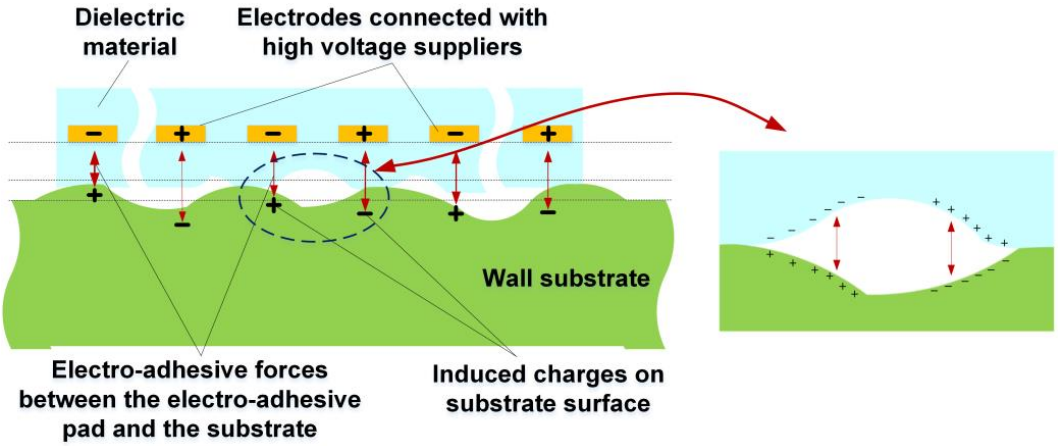

Figure 2-10 The J-R type electroadhesive

The capacitance of the non-contact areas can be given as:

$$C_0 = \frac{\varepsilon_0 S_{J-R}}{g} \quad (2\text{-}52)$$

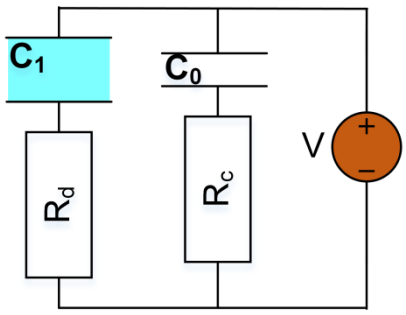

Figure 2-11 Equivalent circuit of the J-R type electro-adhesive

Apart from the J-R electroadhesive forces, the conventional Coulomb forces will also be generated between the electrodes and the substrates, giving the total

normal force:

$$F_z = F_{Coulomb} + F_{J-R} \quad (2\text{-}53)$$

The attractive force generated by the J-R type electroadhesive can therefore be given as:

$$F_z = \frac{1}{2}\left(\frac{C_e{}^2 U^2}{\varepsilon_0 S} + \frac{C_0{}^2 V_{J-R}{}^2}{\varepsilon_0 S_{J-R}}\right) \quad (2\text{-}54)$$

However, $F_{Coulomb}$ is much smaller than F_{J-R} based on a given applied voltage as the gap between the interfaces is much smaller than the thickness of the dielectric material, making $F_{Coulomb}$ almost negligible.

2.3.1.3 Comparison between Coulomb and the J-R type electroadhesion

The J-R type electroadhesion has stronger attractive forces than the Coulomb type as aforementioned. However, a much shorter detachment time can be seen in Coulomb type electroadhesion [35]. Residual charges or forces will remain and the dielectric's natural relaxation time will be observed after switching off the power supply of the electroadhesive pad. These residual charges may come from the dielectric polarisation, free mobile charges inside the dielectrics or, more commonly, from charges trapped in the dielectric materials. An RC time constant τ , can be used to characterise the charging/discharging times and this corresponds to the attaching/detaching times. With regard to Coulomb type electroadhesion, the equivalent circuit can be seen in Figure 2-12.

When the switch S1 is on and S2 is off, the capacitance of the electro-adhesive pad, C_e , is filled with a charge, Q , resulting in the attachment between the pad and the substrate. When the switch S1 is off and S2 is on ($t = 0$), an exponentially decaying current will be demonstrated, described by [35]:

$$I(t) = \frac{U}{R_0}\exp(\frac{-t}{\tau}) \quad (2\text{-}55)$$

where $\tau = C_e R_0$ and R_0 is the equivalent external resistance of the electro-adhesive system.

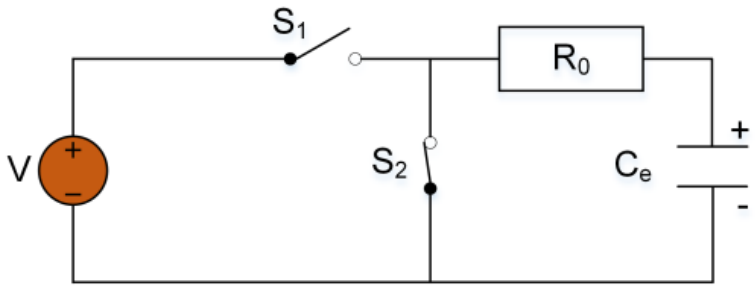

Figure 2-12 Equivalent circuit of the Coulomb type electro-adhesive

However, equation (2-55) no longer applies in J-R type electroadhesives. A non-exponentially decaying current will be shown, with a much longer decrease time which is several orders of magnitude longer depending the dielectric material property. It is, therefore, important to balance the attraction forces and detachment time, tailoring to specific requirements. It should also be noted that the time to remove those residual forces can be expedited both electrically and mechanically, if required. Incorporating an additional resistance in parallel with the electro-adhesive pad may reduce the time constant to some extent, though at the expense of increased power consumption, which may result in a lower efficiency. The incorporation of AC high voltage, rather than DC high voltage, can also significantly reduce the residual charges, though at the expense of decreased attractive forces and larger power consumption.

2.3.2 Basic theoretical models on insulating substrates

For the whole selected small element as configured in the left hand side of in Figure 2-13, we have:

$$E_2 - E_1 = E_{p1} + E_{p2} + E_{p3} = E_{p1} + E_{p3} \quad (2\text{-}56)$$

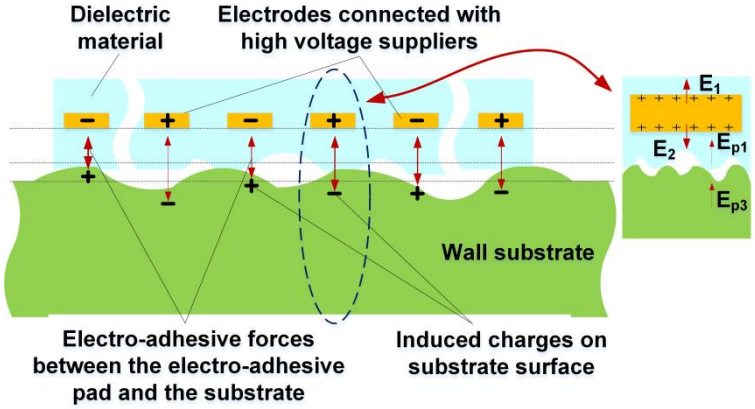

Figure 2-13 Electric field distribution after the polarisation

Clearly, the unequal charge density of the upwards and downwards surface of the selected electrode surface is aroused by the insulating materials. As such, based on the equation (2-55) and equation (2-56), we have:

$$\sigma_2 = \sigma[1 - \frac{2}{\varepsilon_{r1}+1} + \frac{4}{(\varepsilon_{r1}+1)(\varepsilon_{r2}+1)}] \quad (2\text{-}57)$$

The polarisation forces can be given as:

$$F_z = PE = \varepsilon_0 \chi_{e3} E^2 \quad (2\text{-}58)$$

Based on equations derived in section 2.1.2, we have:

$$E = E_0 - E_{p1} - E_{p2} - E_{p3} = E_0 - \frac{E_0(\varepsilon_{r1}-1)}{\varepsilon_{r1}+1} - \frac{2E_0(\varepsilon_{r2}-1)}{(\varepsilon_{r1}+1)(\varepsilon_{r2}+1)} = \frac{4E_0}{(\varepsilon_{r1}+1)(\varepsilon_{r2}+1)} \quad (2\text{-}59)$$

Then we have:

$$F_z = \frac{16{E_0}^2 \varepsilon_0(\varepsilon_{r2}-1)}{(\varepsilon_{r1}+1)^2(\varepsilon_{r2}+1)^2} \quad (2\text{-}60)$$

In reality, the electro-adhesive forces are difficult to calculate mathematically for many reasons. This includes factors such as 1) inhomogenous dielectric materials with unpredictable crystal structure polarisabilities, 2) four types of electrical polarisation mentioned above occur simultaneously, and 3)

inhomogeneous electric fields always exist in nature. These factors result in the equation (2-60) no longer applicable. However, the equation (2-60) can offer the scale of the attractive forces obtained, which is good.

2.4 Summary

This Chapter has demonstrated by far the most comprehensive understanding of electroadhesion, to the best of the author's knowledge, compared with other papers already published, in terms of introducing fundamentals of electrostatics and dielectrics for understanding electroadhesion, a detailed summarisation of the principles of electroadhesive force generation, and development of basic theoretical models. The key findings from this are:

● Optimised dielectric selection for different electroadhesive applications is the key for better electroadhesion properties.

● Possible reasons lead to the failure of the electroadhesion phenomenon include: air gaps between the electrodes, sharp edges along the electrode surface, electrical aging, electrical discharges, and electrical breakdown in solids. Safety considerations are therefore necessitated.

● The electroadhesion phenomenon can be both contact and contactless based. For conductive substrates, the electroadhesive forces are principally generated by electrostatic induction. For insulating substrates, the electroadhesive forces are generated by polarisation. The contact based electroadhesion is mostly due to the orientational polarisation and interfacial polarisation whereas the contactless electroadhesion is due to, mostly, the atomic and electric polarisation.

● It is inappropriate to derive the normal electroadhesive forces, by the division of the measured shear forces and friction coefficients. The inclusion of suction forces, Van der Waals forces, and possible surface tension forces after the application of high voltages, must be considered. The measured normal forces are therefore only useful for validating the models.

3 Literature Review

3.1 Introduction

In this Chapter, a comprehensive literature review of the basics and existing work on electroadhesion is conducted. Also, insights from other research fields relevant for the better understanding of electroadhesion are summarised. In section 3.2, a review of research groups who are and have been studying electroadhesion around the world is presented. In section 3.3 - 3.6, a detailed overview of electroadhesion is demonstrated in terms of electroadhesive pad design, manufacturing, testing, modelling of electroadhesion and electroadhesive applications. Finally, a summary and discussion about how the thirty three variables (Figure 3-1) influence the electroadhesive forces obtainable is presented, before the conclusions are shown for this Chapter.

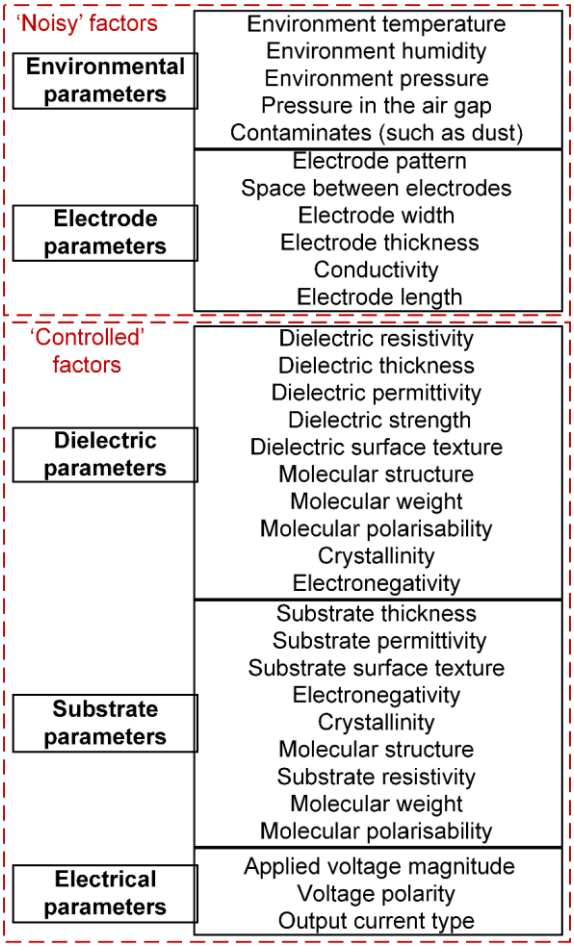

Figure 3-1 Variables influencing the obtainable electroadhesive forces

In this research, all the tests have been managed to maintain the dielectric parameters, substrate parameters, and electrical parameters. The environmental parameters and electrode parameters have been managed to minimise the noises by applying a controlled environment chamber and professional pad manufacturing process.

3.2 A chronological review of electroadhesion

Electroadhesion is a multidisciplinary research area involving: mechatronics such as flexible printed circuit boards and high voltage converters, system integration, Physics such as electric fields and polarisations, and materials such as dielectric material design and selection.

The development of modern electroadhesive theory stems from the discovery of the Johnsen-Rahbek effect in 1923 [36], and later the discovery by Balakrishnan in 1950 that the use of appropriate semiconductive materials in electrostatic grippers could lead to greater forces [39]. Based on this, Warning employed electrostatic grippers to hold work-pieces in 1960 [2]. In this thesis, the starting point of electroadhesion technology is attributed to Balakrishnan.

Since 1967, Krape and Beasley et al. from the Langley Research Center at NASA have published 1 NASA contract report [1] and 1 conference paper [3] on electroadhesion. The main contributions of this research group are 1) the understanding of factors influencing the obtainable electroadhesive forces including environmental factors and surface roughness based the world's first advanced electroadhesive force testing platform [1] and 2) electroadhesive grippers for material handling for space applications [3]. In 2015, Tom and Leung et al. from the NASA Marshall Space Flight Center published 2 conference papers [4][40] on electroadhesion. The main contributions of this group are 1) validation of electroadhesion as a docking method for spacecraft and satellite servicing [4] and 2) an advanced force testing rig that can measure normal, shear, peeling, and twisting electroadhesive forces [40].

In 1973, Wardly from IBM proposed the use of electrostatic chucks for handling silicon wafers [5]. Since then, there has been ongoing studies on modelling, designing, optimising, testing, and the application of electrostatic chucks for material handling in semiconductor industry, mainly in Japan and the US. Since 1996, Hatakeyama, Yatsuzuka and Asano from Yamagata University have studied electrostatic chunks in a fundamental way [41]. They have designed and implemented advanced setups for pad design, manufacture, and testing [41]. Also, they successfully addressed the residual charge problem by applying AC voltages [41]. Since 2006, Saito et al. from Tokyo Institute of Technology have published 2 journal papers [42][43] and 1 conference paper [34] on the modelling, design and implementation of gecko inspired compliant electrostatic chucks for rough surfaces. Other research groups working on electrostatic chucks also include TOTO ltd. [44], Yonsei University [45], Micron Technology Inc. [38], FM Industries, Inc. [46], SEMCO [47], and Tsinghua University [48].

Since 1986, Monkman et al. from the University of Hull have published 5 key journal papers [6][7][31][49][50]. The main contributions of Monkman et al. include 1) the investigation and basic modelling of the principle of electroadhesion on fabric materials, 2) the design and implementation of various electroadhesive grippers and conveyer belts for handling clothing and fibrous materials and 3) compliant shape adaptive electroadhesive grippers.

Since 1992, Chen and Chestney et al. from Brunel University have published 1 journal paper [51] and 1 conference paper [19] on electroadhesion. Zhang collaborated with electroadhesive researchers from Brunel University and University of Liverpool [8][52]. The main contributions include 1) the investigation and theoretical modelling of the dynamic characteristics of the charging/discharging process [52] and 2) the design and implementation of robotic systems for handling non-rigid materials based on a modular cell electrostatic gripping device [8][51].

Since 1994, Jeon and Yamamoto et al. from the Higuchi Lab led by Prof. Toshiro Higuchi (changed to Yamamoto Lab led by Prof. Akio Yamamoto since March 2015) have been publishing journal papers and conferences papers on electroadhesion [53]. The main contributions of this research group include 1) the modelling, design and implementation of electrostatic levitation or contactless electroadhesive suspension [16], 2) the application of contactless electroadhesion into the semiconductor industry for the handling of silicon wafers, hard disks, and glass panels based on advanced robotic systems [15], 3) the design and implementation of an advanced electroadhesive force testing platform [16], and 4) the world's first electroadhesive climbing robot [10].

Since 2007, Karagozler et al. from Carnegie Mellon University have published 1 conference paper on electroadhesion [54]. The main contribution of this research group is the application of electroadhesion for inter-module adhesion, power transfer, and communication in modular robots [54].

In 2011, Grabit Inc. was founded [12]. Grabit is a SRI International spin-off company and the world's first commercial material handling company based on electroadhesion. Five other companies also joined the commercialisation of electroadhesive grippers including Trumpf Werkzeugmaschinen GmbH [55], the Boeing company [56], J. Schmalz GmbH [57], ElectroGrip Co. [40][58], and Fraunhofer IPT [59].

Since 2011, Téllez and Jeffrey et al. from the Menrva Research Group at the Simon Fraser University led by Prof. Carlo Menon have published 3 journal papers [60][61][62] and 2 conference papers [63][64] on electroadhesion. The main contributions of this research group include 1) the invention of electro-dry-adhesion, the combination of elecgtroadhesive and gecko inspired dry adhesive [60] and 2) the comparison of different pad geometries for electroadhesives [63]. In 2014, Savioli et al. from the University of Padova started a collaboration with the Menrva Research Group on surface adaptive morphing

electroadhesives [64], the combination of shape memory polymers and electroadhesion.

Since 2011, Koh et al. from the Monash University Malaysia led by Prof. S. G. Ponnambalam have published 3 journal papers [20][65][66] and 3 conferences papers [67][68][69] on electroadhesion. The research is a collaboration between the Monash University Malaysia and Indian Institute of Information Technology. The main contributions of this research group are 1) empirical modelling of electroadhesive forces [68], 2) extended experimental investigations into the relationship between applied voltages and forces obtainable [20] and 3) the application of a novel hybrid electrostatic and elastomer adhesion mechanism for wall climbing robot [66].

Since 2011, Griffiths et al. from Bristol Robotics Laboratory and Heath et al. from the Advanced Composites Centre for Innovation and Science at Bristol University have published 2 conference papers [70][71] on electroadhesion. The main contributions are 1) invesitigation various dielectric and conductive materials for electroadhesion [70] and 2) identification of limitations in conformal coating for electroadhesive pads [71].

Since 2012, Ruffatto et al. from the Robotics Lab at Illinois Institute of Technology led by Prof. Matthew Spenko have published 2 journal papers [14][72] and 4 conference papers [73][74][75][76] on electroadhesion. The main contributions of this research group are 1) experimental validation of the feasibility of using a finite element method based electrostatic simulation for optimising electroadhesives [73], 2) the design and implementation of an advanced and reconfigurable electroadhesive force testing platform [14][72], 3) two novel electroadhesive pad manufacturing methods [14][73], and 4) electro dry adhesives [72].

Since 2012, Germann and Shintake et al. from the Microsystems for space technologies laboratory at EPFL led by Prof Dario Floreano have published 2

journal papers [77][78] and 2 conference papers [79][80] on electroadhesion. The main contributions of this research group are 1) the application of electroadhesion in modular soft robots based on a novel pad pattern [77], 2) stretchable electroadhesion based on a novel pad manufacturing process and an advanced electroadhesive force testing platform [79], and 3) a lightweight 2-finger soft electroadhesive gripper for grasping curved objects [78].

Since 2012, Chen et al. from the Robotics Institute at BeiHang University led by Prof. Rong Liu have published 1 journal paper [81] and 4 conference papers [82][83][84][85] on electroadhesion. The main contributions of this research group include 1) dynamic theoretical modelling of electroadhesion during the charging process [83] and 2) design and implementation of a double-tracked [81] and gecko inspired legged [84] electroadhesive climbing robots.

Since 2012, Guo et al. from Zhengzhou University of Light Industry have published 4 journal papers [86][87][88][89] and 1 conference paper [90] on electroadhesion. The main contributions of this research group are 1) the combination of electrorheological gel with electroadhesive pads for improving adhesive forces [86], 2) simulation modelling of tri-polar electroadhesives [88], and 3) a new type of electrode array model (sieve bottom) [89].

Since 2013, Ryan Etkins from Micro Robotics Lab at the University of Maryland has one poster [91] on electroadhesion published online. A. Simpson Chen, now a PhD candidate in this lab, is now also working on electroadhesion. The main contribution of this research group is the generation of the largest electroadhesive force per unit area (to date), 7.5 Ncm^{-2}, based on a pad made of two cPDMS electrodes coated with parylene-C on a wall substrate (note that it is not mentioned specifically in his publication).

Since 2013, Kiran et al. from the Creative Machines Lab at Cornell University have posted their work online. They have been investigating an electroadhesion based pick-and-place device [92].

Since 2014, Tong et al. from the Newcastle University (UK & Australia) have published 1 conference paper on electroadhesion [93]. The main contributions of this research group are 1) implementation of an in-house double layer electroadhesive pad manufacturing method [93] and 2) the design and implementation of an electroadhesive climbing robot that can conduct floor to vertical wall transition [93].

Since 2014, Mao et al. from Chongqing University have published 2 journal papers [94][95] and 1 conference paper [96] on electroadhesion. The main contribution of this research group is theoretical modelling of electroadhesives based on the Maxwell stress tensor method [94][95].

Since 2014, Takada et al. from Shibaura Institute of Technology have published 1 conference paper on electroadhesion [97]. The main contribution of this research group is the design and implementation of an advanced electroadhesive force testing platform for the evaluation of pillar arrays based electro dry adhesives [97].

Recently, a collaboration has been conducted between the Australian National University, Duke University, Tsinghua University, Wuhan University and Monash University (Australia). The main contribution of this collaboration is a novel simulation model for interdigitated electroadhesives considering multiple dielectric layers and surface roughnesses [98].

Other research universities working on electroadhesion does include Keio University (since 2012) [99], Tarbiat Moda University [100], VIT University [101], University of Engineering and Technology Taxila and University of East London [102], Harbin Institute of Technology [103], Harbin Engineering University [104], and South China University of Technology [105].

It has to be noted that **all the research groups did not address the research gaps identified in section 1.2**. This chronological review tends to only

summarise the contributions of all the research groups. Critical discussions and reviews of their work are demonstrated in section 3.3 - 3.8.

3.3 On electroadhesive pad design

The electroadhesive pad is an essential part of an electroadhesive system (see Figure 1-1). Electroadhesive pads, either flexible ones [14][71] or rigid ones [3][5], are the result of pad design and manufacture. Pad design is the first step towards the realisation of an electroadhesive system. Pad design involves the design of electrode configurations, electrode materials, and dielectric materials. In section 3.3.1 - 3.3.3, these three elements are considered in detail.

3.3.1 Electrode configuration

The polarity of the electroadhesive pad can be uni-polar, bi-polar, and tri-polar [106], see Figure 3-2. All the existing pads were based these three designs.

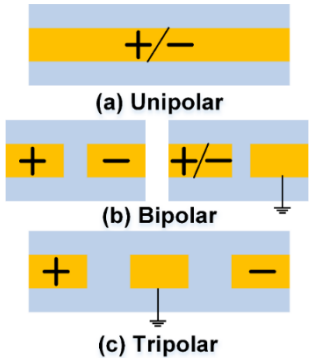

Figure 3-2 Pad polarity design

The uni-polar or single pole design requires only one high voltage source, either positive or negative. It is more common for grasping conductive or semi-conductive materials due to its simplicity and reduced risk of dielectric breakdown. Also, higher forces are observed. However, it is difficult to grasp dielectric materials as the polarisation/depolarisation time takes a long time [19]. The bi-polar or dual pole design requires both the positive and negative voltage source. This requires a higher voltage [8] than the single pole design to achieve the same level of either normal or shear forces, however, it has a quicker clamp/unclamp

characteristic for grasping non-conductive materials [15][41]. This design facilitates contactless electroadhesion unless the dielectric covering the electrodes is a Johnsen-Rahbek type [106], see section 2.3.1. The tripolar design requires positive, grounded or 0 V and negative voltage sources [87]. Few people have experimentally tested this design for electroadhesive applications.

The configuration of the electrodes can be non-coplanar [93], see Figure 3-3 (a). Most designs published within the literature review make the electrodes coplanar [3][5][14][71].

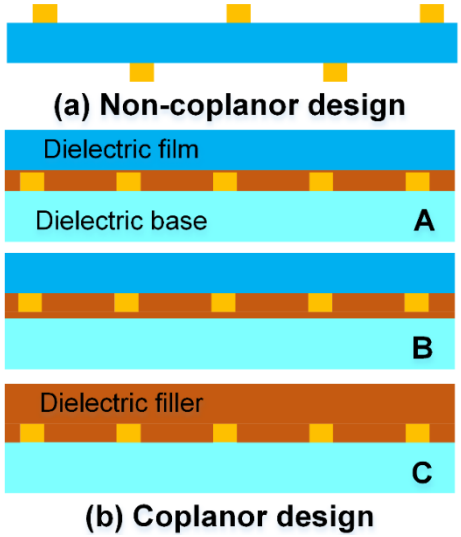

Figure 3-3 Pad configuration design

For coplanar designs, the dielectric materials between the electrodes and covering the electrodes can be different such as insulating sealants and dielectric films [15] or the same such as silicone sealant [15] and Electrolube DCA silicon by conformal coating [71] depending on the pad manufacturing methods. There are therefore three different configurations [15] as shown in Figure 3-3 (b). There is little work on investigating the difference between the coplanar and non-coplanar design. This will be introduced in Chapter 6.

Different electroadhesive pad geometries have been used, including one-electrode designs, double-electrode designs, interdigitated shape designs, spiral shape designs, concentric designs, and other designs. One-electrode design

involves with only one electrode and is the simplest design [19]. Double-electrode designs include double-electrode designs in square configurations [41][63] and in oblong configurations [63]. Interdigitated shape designs, a series of double-electrode designs, include normal rectangular comb shape designs with [10][64] and without arc transitions [81], square comb shape designs [77], round comb shape designs [84] and a sinusoidal comb design [107]. Different comb designs used in the semiconductor industry that can be implemented in electroadhesive pad designs include the serpentine-electrode shape design [108] and shaped comb designs such as the angled comb design [109], saw-tooth comb design [110], and novel jagged-edge comb design [111]. Spiral shape designs include rectangular, square spiral designs [41][77] with and without arc transitions, and round spiral shape designs [77]. Concentric designs [74] are similar to comb designs. Other designs include the Hilbert design and the chessboard design [74]. One-electrode design is good at producing larger forces when grasping conductive and semi-conductive materials, however, it is difficult for grasping insulating substrates. Comb designs, spiral designs, and concentric designs are good at grasping insulating substrates. Comb designs are difficult to produce uniform force distributions whereas spiral and concentric designs are able to produce uniform forces in all axis [77]. Although various designs have been investigated, there lacks a comprehensive comparison of different designs.

3.3.2 Electrode materials

Any conductive or semi-conductive material can be suitable for the electrode material although a material that can carry a higher charge density is preferable. Electrodes are required to be connected with high voltage sources for generating high electric fields.

One of the most preferable electrode materials used for electroadhesion is copper [16][15][81][71] primarily due to the easy of procurement and its cost-effectiveness. Aluminum [63][70], graphite such as conductive graphite E33 [77],

metal alloy such as copper-nickel [74], carbon mixed in other materials such as carbon black mixed with soft polyurethanes [112], carbon mixed with silver [90], carbon mixed with Ecoflex silicon [79] and carbon mixed with poly-dimethylsiloxane (PDMS) [97][60] have also been used. It is interesting to note that stretchable electrodes can be achieved by using conductive polymers made up of a mixture of silicon rubber and carbon black [79]. Although little difference in terms of forces achievable was found between the copper foil and the silver ink [70], there is no comprehensive direct comparison between different electrode materials available in the literature.

3.3.3 Dielectric materials

The dielectric materials serve as dielectric buffers, preventing the charge neutralisation and dielectric breakdown. Dielectric materials must have enough dielectric strengths to prevent dielectric breakdown under a given voltage and reasonably good dielectric constants (e.g. 4) to achieve enough forces. The selection of dielectric materials is extremely important depending upon the specific application. For example, it may be desirable to have dielectric materials that can produce higher electroadhesive forces under lower voltage for health and safety purposes. It may be also desirable to have materials that can have efficient and quick clamp/unclamp characteristics. Compliant dielectric materials, usually dielectric materials textured with special and micro-scale patterns, may help improve the contact between the pads and the substrates [49] as those patterns would help increase the contact areas.

Polymers have been extensively used in electroadhesive applications as they can be manufactured to be lightweight, thin, and flexible. Polymers which have been used in electroadhesion applications include cellulose acetate [19], polyurethane (PUC) [63][112], polyimide (PI) [81], polyethylene-terephthalate (PET) [15], polyethylene (PE) [15], PDMS [63], polypropylene (PP) [63], polyvinylchloride (PVC) [20], silicone oil and sealant [15], paper [70], glass-

epoxy resin [15] and epoxy resin [15]. Other dielectric materials may ceramics due to their high dielectric constants and short dielectric relaxation time [15].

3.4 On electroadhesive pad manufacturing

Electroadhesive pads can be made professionally from commercial PCB companies. Professionally made pads tend to bring better repeatability and quality but the purchases are limited in material selection, and they are usually more expensive than manufacturing in-house. Pads made in-house tend to be more cost-effective and bring more flexibility in material selection that can be used to produce greater forces. The pad manufacturing process involves the manufacture of both electrodes and dielectric materials. Electrode manufacturing methods can be classified into two main categories, i.e. additive manufacturing methods and subtractive or material removal methods. Additive manufacturing methods include 3D printing methods, ink-jet printing methods, screen printing methods, conductive painting methods, electroplating, and molding/deposition methods. Subtractive manufacturing methods include machining methods such as manual cutting, PCB milling, laser cutting and water jet cutting, and etching methods such as chemical etching. Dielectric manufacturing methods include attaching/gluing commercial dielectric films to the electrodes, conformal coating such as spraying, brushing and dip coating and spin coating.

3.4.1 Professional manufacturing methods

Based on the literature survey, the most commonly used [14][71] professional electroadhesive pad manufacturing method is based on flexible printed circuit board (FPCB) or PCB manufacturing methods. The operation procedures of this method can be summarised as:

1) Prepare clean and dry copper laminates (usually made by depositing copper on thin polymer films) based on the pad designs.

2) Transfer a patterned masking layer onto the copper laminates.

3) Etch the unwanted copper areas.

4) Remove the mask, leaving the patterned electrode.

5) Place dielectric materials on the top of the copper laminates after etching.

There are several ways that the wanted copper area can be protected during etching. These include laser direct image methods [21][113], ultraviolet light exposure methods [14][71] and heat transfer printing methods such as the press-n-peel method [114]. The press-n-peel method is cheap but takes time to transfer large size (such as A4 size) pad geometries onto the copper laminates. In addition, the copper laminates are no longer flat because of the cooling, contracting occurring after ironing, which is not good. The laser direct image methods are similar to ultraviolet light exposure methods based on light sensitive materials. Laser direct imaging is conducted after dry film lamination by photoresist laminators [113]. This method can bring thinner line widths with higher accuracy than conventional photolithography techniques [113]. Apart from etching, the other way of patterning metals based on pad designs is liftoff. Firstly, a sacrificial layer is deposited and patterned. The metal is then deposited by sputtering, or vaporisation or electroless deposition. Patterned electrode can be retained after removing the sacrificial layer [115].

Less commonly used professional electrode manufacturing methods include ink-jet printing, screen printing, PCB milling, laser cutting, and water jet cutting [116]. Professional ink-jet printing techniques are not good at generating large size pads as it will be extremely slow (e.g. at least 24 hours) to produce an A4 size pad unless multiple nozzles and advanced setup are used, which takes effort and money. Both ink-jet printing methods and screen printing methods are, however, relatively expensive, compared with etching methods, due to the cost of inks and printers. PCB milling is only applicable on rigid boards such as FR4 PCBs [116]. Metal electrodes may also be cut into desired geometries using laser cutters and water jet cutters [116] and then glued onto dielectric films. These two

methods can be alternatives for the coarse manual cutting method mentioned in section 3.4.2.

Professional dielectric manufacturing methods include coverlay methods [21] and conformal coating methods [71]. The coverlaying process involves using hot press coverlay film laminators to press dielectric films on top of the copper laminates after etching. This can be completed in ambient environments but preferably in a vacuum to minimise the potential air entrapped between copper laminates and dielectric films. One of the commonly used conformal coating methods in the PCB industry is silk screen printing of dielectric materials such as silicone, epoxy, acrylic, urethane, and paraxylene [117].

3.4.2 In-house manufacturing methods

Electroadhesive pads were commonly made in-house based on papers published. All the above professional manufacturing methods can be implemented in-house. Electrodes for electroadhesion can be manufactured manually such as manual painting of conductive materials and manual cutting of conductive sheets. They can be also manufactured by etching, printing such as inkjet printing and screen printing, and moulding.

The most straightforward and economic electrode manufacturing method is the manual cutting method [63]. The insulation of electrodes can be completed in three different ways. The easiest way is to glue another layer of dielectric film as the dielectric cover [63]. The second solution is to fill some dielectric materials in between electrodes and then glue dielectric films on the top [15]. Conformal coating of dielectric materials on top of the electrodes and in between electrodes is the third solution [71]. An example of the manual cutting method can be seen from the work completed by Koh et al. [20], where two aluminum foil electrodes were glued onto dielectric materials and both the electrodes and dielectric film were adhered on a PVC adhesive tape. Koh et al. also produced manual conductive silicon electrode generation process by applying a stencil. The

thickness of the dielectric layer was controlled by applying a blade coating process [66]. The manual cutting method is time-consuming if mass production of pads is needed. Also, this method is not good at producing repeatable and accurate electroadhesive pads.

Manual painting of conductive materials on dielectric films is another straightforward and fast electrode manufacturing method. Examples of this method include painting nickel electrodes on Mylar films using conductive pens [93] and painting conductive graphite e33 on PVC films using a paint brush [77]. This method however is difficult to generate even electrode thickness, smooth electrode edges and accurate electrode widths.

The most commonly used method used in electroadhesive pad manufacture in-house is the customised etching method [19][64]. A customised electroadhesive pad manufacturing method based on the combination of etching of alloy mesh and spin coating of silicon dielectrics can be seen in Figure 3-4. The procedures needed for this method include:

- Generate the base dielectric layer by spin coating.
- Prepare the copper laminates base on the pad geometry designs.
- Generate a protective layer on top of the copper laminates.
- Etch the unwanted copper areas (usually ferric chloride granules).
- Dry the copper laminates after cleaning the protective layer.
- Insulate the electrodes.
- De-gas and cure the pad.

The quickest way to generate electrodes for electroadhesive applications is inkjet printing of conductive inks that can be room cured quickly [118]. Only the research group from Stanford University has investigated using inkjet printing of

silver ink to manufacture electrodes for electroadhesion and has achieved the smallest electrode width (0.5 mm) and space between electrodes (0.5 mm) [119].

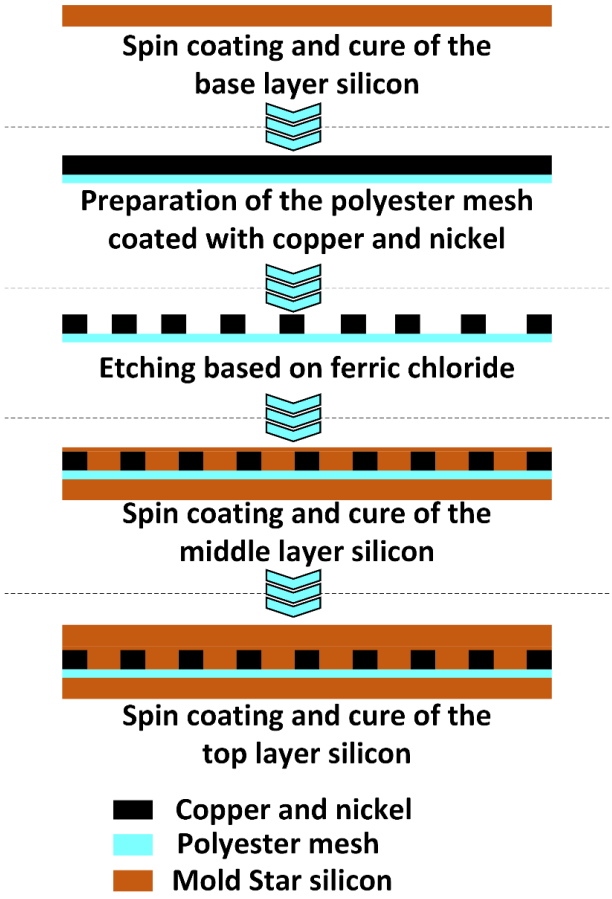

Figure 3-4 Pad manufacture by chemical etching and spin coating [19][64]

The molding method may also bring electrodes with smaller electrode widths and gaps [14][73][74]. An example of this method can be seen in Figure 3-5. The procedures needed for this method include:

- Prepare the mould cores base on the pad geometry designs.
- Fill conductive materials into the mould cores. Curing of the conductive materials should be considered if needed.
- Insulate the electrodes.
- De-gas and cure the pad.

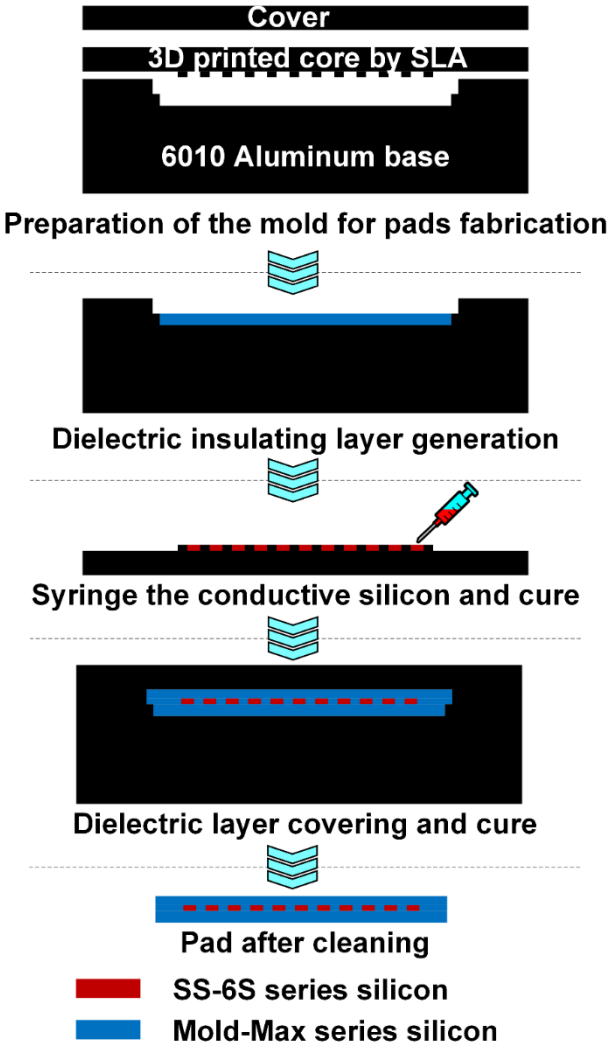

Figure 3-5 Pad manufacture by the molding method [14][73][74]

The molding method allows more complicated 3D pad surfaces and geometries to be manufactured. However, the generation of mold cores takes efforts and money for mass production of numbers of pads with different pad geometries and sizes. Instead of generating multiple mold cores for different pad designs, the screen printing methods require multiple screens.

Complex electroadhesive pads can also be manufactured by hybrid methods, such as the combination of 3D printing, shape deposition manufacturing (SDM), laser cutting and patterning, and a texturing technique, known as surface microsculpting [120]. The electroadhesive pad or gripper generated by Suresh et al. from Standord University was only 6 g and capable of grasping curved objects

weighing up to 11 N [120]. Hybrid manufacturing methods may be a positive solution to lightweight, flexible, and advanced adaptive electroadhesive pads or grippers.

3.5 On electroadhesive force testing

Electroadhesive forces are expected to be measured to quantify the performance of the electroadhesive pads manufactured. In principle, there are two measurement methods: 1) direct measurement or normal force measurement methods and 2) indirect measurement or shear force measurement methods [121]. Direct measurement methods can be achieved by pulling away the attached electroadhesive pad by a force applied normally or perpendicularly. Indirect measurement methods can be achieved by displacing the attached electroadhesive pad by tangential or shear forces.

3.5.1 Direct/normal electroadhesive force measurement methods

Direct electroadhesive force measurement methods can only be used for quantifying force performance of rigid electroadhesive pads or flexible pads attached onto rigid pad holders as, for flexible electroadhesive pads, direct force measurement methods are difficult or impossible to be implemented [81]. These methods can be classified into two categories: 1) normal/perpendicular to horizontal planes [15][21][79], see Figure 3-6 (a), and 2) normal/perpendicular to vertical planes [73], see Figure 3-6 (b). Load cells [15][97], strain gauges [122] and force/torque sensors [21][73] can be used to obtain the normal electroadhesive forces. These force sensors can be connected to both substrates, see Figure 3-6 (a), and pad holders, see Figure 3-6 (b). Advanced setups should consider enclosing the force testing platforms with vacuum chambers [4][122][45] and environmental chambers [1] that are capable of varying temperature and humidity levels to understand electroadhesion better. Also, advanced setups are preferable to be reconfigurable [14][21][73][97] so that the same setup can conduct normal and shear force measurements

simultaneously. Furthermore, the alignment issue of the direct measurement methods cannot be neglected. Advanced setup such as a tip-tilt alignment mechanism [123] is needed to reduce the tilt moment produced during the measurement.

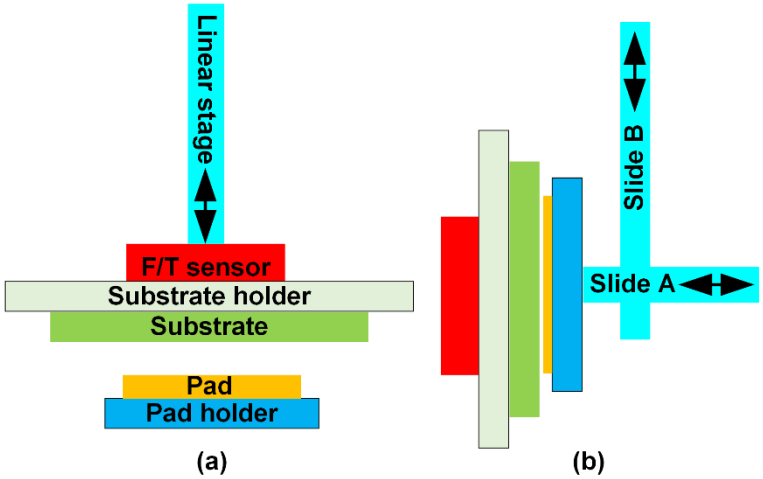

Figure 3-6 Normal electroadhesive force measurement methods: (a) vertical orientation and (b) horizontal orientation

3.5.2 Indirect/shear electroadhesive force measurement methods

Indirect force measurement methods measure forces in shear, which may not necessarily need to consider the alignment issue [121]. The most straightforward and easiest way is to attach known weights [70][85] or spring scales [60] or a force gauge [20][81][94] to the electroadhesive pads attached on the wall substrate, see Figure 3-7 (a). The shear force is then recorded when the pad is detached from the wall. It is difficult to align the known weights or spring scales with the pads. A mechanical pulley, see Figure 3-7 (b), can be used to make sure the force applied is parallel to the test substrate [20]. Also, it is difficult to manually drive the spring scales or force gauges at constant speeds. Finer, constant and accurate movement and force recording can be achieved by using load cells [61][64][71] or 6-axis force/torque sensors [73][79] assembled on linear stages, see Figure 3-7 (c). A vertical axis linear stage can be added to increase the level of confidence that the pad is in proper alignment with the force sensor,

see Figure 3-7 (d). Similar to direct force measurement methods, the force sensors can also be connected to the substrates [79].

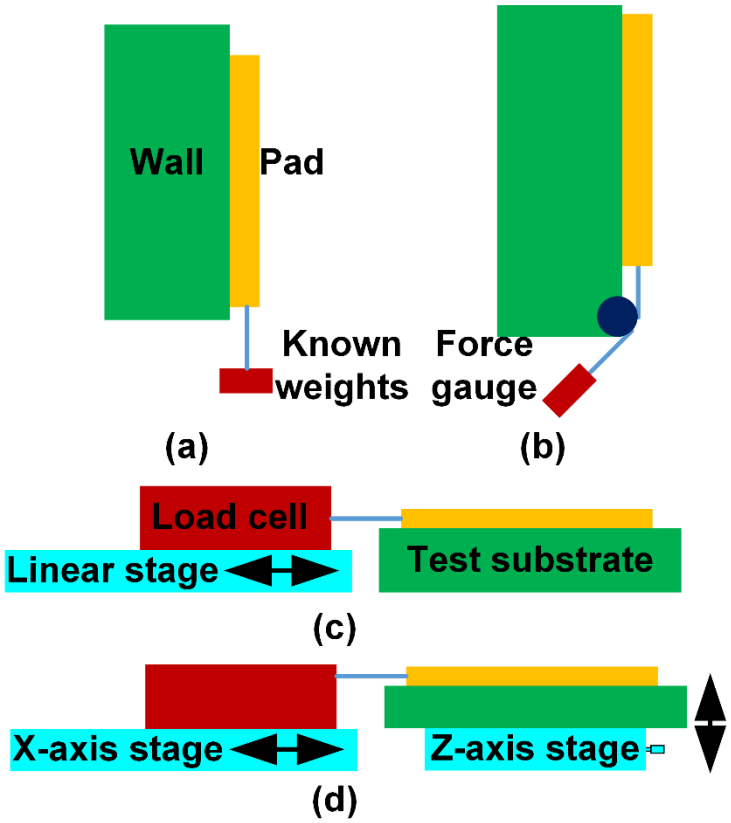

Figure 3-7 Shear electroadhesive force measurement methods: (a) vertical orientation using known weights, (b) vertical orientation using force gauge, (c) horizontal orientation using load cell, and (d) horizontal orientation using load cell with advanced adjustment

In order to increase the level of confidence in the data collected in the published literature, calibration measurements are suggested to be conducted when the pads are under no voltage [63][71]. Cleaning the dust and contaminates from the pads and substrate using acetone or masking tapes [73] is also suggested after several times of testing of the same pad if the testing is not in a dust-free environment. The most important thing that is suggested in the published literature that cannot be neglected for repeatable results is the consideration of residual charge dissipation process [21][60][73]. Although the current running through the pads is small, potential safety issues due to the high voltage should also be considered. Until now, only two research groups in the UK [17][21] have

considered using interlock systems in the electroadhesive force measurement platform to minimise the health and safety risks.

3.6 On electroadhesion modelling

Modelling of electroadhesion is important for understanding and designing electroadhesives. Theoretical modelling, electrostatic simulation, and empirical modelling have all been investigated and used to design electroadhesives. Theoretical modelling is based on physical principles and equations. Since the principle of electroadhesion is still under investigation due to the complexity in understanding the polarisation processes involved, theoretical models published so far are all based on ideal assumptions. Electrostatic simulation is also based on basic physical and mathematical equations. Computational methods such as finite element method are often adopted to solve analytic equations. Empirical modelling is often adopted when theoretical modelling is impossible or too difficult. Empirical models are based on experimental data after fitting. Relevant references will be demonstrated in the section 3.6.1 to 3.6.3.

3.6.1 Theoretical modelling

Theoretical normal electroadhesive forces are the multiplication of polarisations and electric fields [14][31]. They can generally be derived by the virtual work method [96] and Maxwell stress tensor method [81][94][98]. Simple theoretical models based on classic theories on parallel capacitors [29][63][77][79] have been used by most researchers. Four times' difference in forces that can be derived was found between these models [51][63]. Two times' difference was even found by the same research group [77][79]. The theoretical equation for calculating shear electroadhesion forces was derived simply by multiplying the friction coefficient with the normal forces [11][20][54][79]. These simple models however usually do not and cannot include enough geometric information of bipolar electroadhesives such as electrode widths and spaces between electrodes. Seven variables such as voltage magnitude, electrode width, space

between electrode, dielectric thickness, air gap thickness, dielectric constant of the dielectric layer, and substrate have been successfully considered in theoretical models based on the Maxwell stress tensor method. People stated in their references [81][94][98] that their future work is to optimise the geometry of the electroadhesives based on their theoretical model, however, no work has been published.

3.6.2 Electrostatic simulation modelling

Various finite element (FE) method based electrostatic simulations for understanding electroadhesion have been conducted. All the published simulation models were in 2D although 3D models are preferable as the results will be more accurate. 3D models however are more computationally intensive and may require advanced meshing techniques for accurate modelling.

Electrostatic simulations based FE software such as ANSYS [45], COMSOL Multiphysics [124], CoventorWare [125] have been extensively used for designing electrostatic chucks and interdigital sensors. The seminal work of using electrostatic simulations for optimising electroadhesives was completed by Ruffatto et al. from IIT. They used Autodesk Multiphysics FE software [73] and COMSOL Multiphysics [74] with MATLAB to simulate and optimise electroadhesive geometries for electroadhesive applications. However these models did not consider the existence of an air gap between the pads and substrates although the simulation results were experimentally validated. After this, Sabermand et al. used COMSOL Multiphysics and obtained different results [100] compared with the results from Ruffatto et al. Also, pseudo dynamic electroadhesion was considered by combing both the electrostatic physics and time dependent module from COMSOL [100]. Mao et al. used ANSYS [96] and Ansoft Maxwell simulation to support their theoretical models [94]. The most recent simulation model published by Cao et al. considered the air gap and surface roughness into their simulation model [98].

3.6.3 Empirical modelling

There are over thirty three variables influencing the electroadhesive forces obtainable [21]. Also, the understanding of the relationship between some variables such as applied voltage and electroadhesive forces is still unclear in terms of publication. It is therefore impossible to derive a theoretical model that considers all or most of the variables. In addition, from the published literature, the polarisation/depolarisation process of the electroadhesion is still not well-understood. Simulation software is based on classical theories and equations which are not necessarily accurate to describe the high voltage based polarisation/depolarisation process. Further, it will be too complicated to consider changing environmental factors, inhomogenous materials, and surface texture in simulation models. Empirical modelling based on experimental data may be a solution to an advanced model that can predict the pad performance and aid the pad design. Koh et al. employed an empirical comb capacitance calculation equation into the simple theoretical model based on parallel capacitor [68]. Also, they proposed empirical working models for the relationship between applied voltage and electroadhesive forces [68]. However, no specific equations but two envisioned trends were published.

3.7 On electroadhesive applications

Electroadhesive applications can be classified into two main categories: material handling and robotic climbing. These will be introduced, in turn, in the section 3.7.1 and 3.7.2.

3.7.1 Material handling

Electroadhesive pads or end effectors have been used as material handling units since their invention. To the best of the author's knowledge, the first electroadhesive application was carried out by Warning who employed electrostatic forces to hold work-pieces [2]. After this, Krape [1] and Beasley et al. [3] applied flexible electroadhesive grippers for handling of curved

objects and space material handling applications. Since the first application of electrostatic forces for wafer handling in the semiconductor industry proposed by Wardly [5], electrostatic chucks have been extensively designed and investigated especially by Japanese and US researchers [15][38][126]. In the UK, electroadhesive pads were used as end effectors for gripping advanced composites and fibrous materials such as cloth [6] and carbon fibres [7][8]. Electrostatic forces were also used for electrostatic levitation or contactless electroadhesion applications [16]. Recently, electroadhesive forces have been used as soft robotic end effectors to grasp complex parts such as the 2-finger 6 gram soft gripper implemented by Shintake et al. [80] and conveyor belts for material transmission [12][67].

It is interesting to note that, due to the technology development of electroadhesion, there are now six major patented electroadhesive based robotic grippers from commercial companies: Grabit Inc. [12], Trumpf Werkzeugmaschinen GmbH [55], the Boeing company [56], J. Schmalz GmbH [57], ElectroGrip Co. [58], and Fraunhofer IPT [59]. Grabit Inc. has successfully addressed challenges faced by manufacturers in handling objects that are porous, fragile or delicate, irregularly shaped, dusty or damp, and rough or smooth [12]. Similar to Grabit, Trumpf and Boeing have also investigated electroadhesive end effector based robotic solutions for automated pick-and-place applications [55][56]. J. Schmalz GmbH has been investigating alternative solutions such as electroadhesive grippers for grasping carbon fiber reinforced plastics (CFRP) [57]. Fraunhofer IPT has successfully implemented advanced automated electrostatic gripping systems for handling of non-rigid semi-finished textiles and carbon/glass fiber materials [127]. **However, these companies did not address the research gaps identified in section 1.2.**

3.7.2 Robotic climbing

To the author’s best knowledge, the first published tracked electroadhesive

climbing robot was implemented by Yamamoto et al. in 2007 [10]. The first compliant legged and tracked electroadhesive climbing robot was implemented by Prahlad et al. [11] in 2008, and the world's first electroadhesive climbing robot that can conduct wall transitions such as the ground to vertical wall transition has only conceptually been designed [11]. Electroadhesive climbing robots have been extensively designed and implemented in research institutes worldwide such as the work conducted by Chen et al. from Beihang University [81][84][85], the work by Griffiths et al. from Bristol University [70], the work by Longo et al. from the Universitat Politècnica de Catalunya [128], the work by Etkins from the University of Maryland [91], the work by Koh et al. from Monash University [66][68][69], the work by Tong et al. from Newcastle University [93], the work by Seitz et al. from Harvard and Stanford University [9], and the work by Guo et al. from Loughborough University [13].

Other electroadhesive applications also include soft modular robots [77], desktop clamping [129], material classification [12], and desktop cleaning [12].

3.8 Variables influencing the obtainable electroadhesive forces

As already illustrated, electroadhesion is a multidisciplinary, complicated, and dynamic electrostatic attraction phenomenon with thirty-three variables influencing the obtainable electroadhesive forces between the electroadhesive pad and the substrate [21] (see Figure 3-1). Other variables that may influence the electroadhesive forces obtainable should also be further investigated. For instance, if AC voltage is used, the frequency may influence the electroadhesive forces obtainable. Also, some dielectric properties such as the dissipation factor of the dielectric may influence the electroadhesive forces obtainable. As shown in Figure 3-1, the variables have been sub-divided into 5 categories and these will be considered in more detailed in the following 5 sections of this Chapter.

3.8.1 Environmental parameters

The environmental factors which affect the electroadhesive forces obtainable

include ambient temperature, humidity, ambient pressure, and contaminates and the air pressure between the pad and substrate after applying the voltage. Environmental factors affect and modify the dielectric properties of electroadhesive pads such as dielectric strength, permittivity, and resistivity. Also, they arouse electric discharges and dielectric degradation that causes the failure of the adhesion. Take the PET film as an example, temperature affects the dielectric constant, dielectric strength, and resistivity. The higher the temperature, the larger the dielectric constant, and the smaller, to some extent, the dielectric strength and resistivity. The dielectric strength will also decrease as the humidity increases [130].

To date, little evidence has been found to show any detailed attempts being made to systematically investigate the influence of environmental factors. The work by Monkman investigated the influence of environmental factors on the electroadhesive forces obtainable and he concluded that only temperature and humidity have a noticeable effect on the properties of the electrostatic attraction obtainable. However, many changeable factors exist in most industrial environments such as noise, temperature, pressure, humidity, and light level [17]. During Monkman's work, the temperature and humidity were not controlled in a sealed environment. The temperature and humidity were therefore not controlled simultaneously, which may bring inconclusive proof of the assertions made. It was found by Savioli et al. that different electroadhesive forces in shear were obtained on three different days based on the same pad and testing procedures. This was attributed to possible factors such as temperature and humidity [64]. However, no further founding was obtained on how each environmental factor influences the electroadhesive forces obtainable.

● Environment temperature

It was found that higher attractive forces can be achieved by elevating the temperature as high temperatures help increase the electrical conductivity and

accelerate particle movement within the insulating material. Conversely, the particles appear to move slower at lower temperatures, thus reducing the conductivity and the achievable attractive forces [29]. However, the temperature should be controlled within a workable range to enable the operation of electroadhesion as insulating materials will melt at high temperature (say 400 ^{o}C for the PET film), causing the failure of the electroadhesion.

The magnitude of the permanent dipole moment is proportional to temperature [17]. Also, the macromolecular or crystal structures of dielectric materials will be affected by temperature. Fabrics could be picked up properly in temperatures well beyond most industrial environments [17]. However, nearly no electroadhesive force was obtained on the nylon when the temperature increased beyond 40 °C whereas other fabric materials still functioned properly in excess of 60 °C [17]. This is perhaps due to the fact that molecular mobility increases when temperature increases, which results in a disorientation of dipole moments and hence a reduction in polarisation.

One limitation of electroadhesive grasping is the remained residual charges in dielectrics after switch off the voltage. This prevents fast unclamping the object being grasped. Higher temperatures may help increase the release speed as quicker particle movements and dielectric depolarisation can be achieved [17]. This may be due to the fact that, at the higher the temperature, the orientation polarisation is lower, and thus the decaying or depolarisation time is shorter.

● Environment humidity

Any traces of moisture trapped or absorbed in dielectric materials will dramatically alter the desired dielectric properties. However, a completely dry environment was also found not to be the best for electrostatic charge generation [17]. The obtainable electroadhesive forces increase with the presence of moisture and only decrease significantly at larger levels of humidity. Varying moisture content was introduced uniformly to a 10 cm x 10 cm section of

clothes (paper composite ‘J-Cloth’) after being fully dried and weighed. 0.25ml increments of distilled water were introduced by means of a calibrated syringe for testing. It was found that there was nearly no electroadhesive forces when the cloth was completely dry. The observed force improved significantly with the first 0.25 ml of water and only stopped increasing as saturation was approached [17].

● Environment pressure, air pressure between the pad and substrate, and contaminates (such as dust)

It was found that air pressure, together with the applied voltage and the dielectric material properties, determines the current density at the adhering interfaces [29]. However, how the pressure affects the electroadhesive forces is unknown. Dust particles are attached by electroadhesive pads during use and after use due to the inherent ability of an electrostatic charge to attract objects [131]. How dust and other contaminates such as oil affect the electroadhesive forces is also unknown.

3.8.2 Dielectric parameters

Usually, solid dielectrics are used for electroadhesion rather than liquids and gases. Solid dielectrics get permanently damaged when dielectric breakdown occurs whereas gases fully and liquids partly recover their dielectric strength. Also, there is no perfect insulator, especially at a high electric field. The dielectric parameters of the insulating layer covering the electrodes for electroadhesion includes dielectric thickness, dielectric surface texture, and dielectric material properties such as permittivity, dielectric resistivity, dielectric strength, molecular polarisability, crystallinity, electronegativity, molecular structure, and molecular weight.

The first study of optimising the selection of dielectric materials for electroadhesive end effectors was the work done by Chestney et al. They concluded that the dielectric materials used in such electroadhesive devices are

of paramount importance for effective and reliable operation [19]. The work summarised the rationales for the selection of dielectric material, and includes the requirements from the end effectors themselves. These are: 1) low cost, 2) lightweight (to minimise the mass and moment of inertia), 3) rapid operation, 4) easily configurable (to handle a variety of shapes), 5) reliable, 6) easy to maintain, 7) safe, and 8) contamination-free. Other requirements for the dielectric itself include: 1) high dielectric strength (to avoid dielectric breakdown), 2) toughness to improve reliability, 3) minimum conductivity (to avoid charge leakage), and (4) maximum dielectric permittivity (to maximise the electroadhesive forces obtainable) [19]. The work also concluded that cellulose acetate was a preferable material choice as it has the best compromise with a reasonably high dielectric permittivity and a conductivity close to the theoretical optimum. The work by Monkman found that the dielectric constant was not the only determining factor. He found that the properties of electroadhesion were determined by the polarisability of materials rather than the dielectric relative permittivity when the substrates were not being earthed. He concluded that, generally, low density, high crystallinity, large molecular weight and structure based dielectric materials were good choices for electroadhesion [131]. Also, the selection of the dielectric material and the charge polarity (if a single pole electroadhesive is used) should depend on the permanent dipole moment (if any) of the substrate materials to be lifted [131].

● Dielectric thickness

Both the simulation results [14][81][94][96][100][132] and experimental results [63] showed that the dielectric thickness should be at a minimum whilst avoiding dielectric breakdown. All the existing simulation results agreed well with the theoretical analysis. The experimental results obtained by Téllez et al. showed that the electroadhesive forces decreased nonlinearly with increasing the dielectric thickness, which matched well with the theoretical model. The results

were based on using pads that have an interdigitated electrode shape glued on polypropylene samples with different thicknesses ranging from 110 μm to 550 μm [63]. However, as aforementioned, the normal electroadhesive forces cannot be directly derived from the forces obtained in shear as a multiple by the friction coefficients. The match is therefore doubtful. For most dielectric materials, the thinner the thickness, the larger the achievable electroadhesive forces. The experimental results obtained by Kyoko et al. showed that the thinner the dielectric film, the larger the attractive forces obtainable based on three PE sheets with different thicknesses of 50 μm, 150 μm, and 250 μm and two epoxy resins with different thicknesses of 123 μm and 228 μm. Also the thicker the PE sheets, the higher the threshold voltage that results in force saturation observed [15]. However, thinner pads may easily get deformed and torn which could lead to the failure of electroadhesion. Also, some dielectric materials such as Buna-N rubber, disobeyed the relation mentioned above over a certain range of thickness [1], which requires further research and validation.

● Dielectric surface texture

The dielectric surface textures directly affect the air gap and contact area between the pad and the substrate. Simulation results showed that the force would decrease significantly with a small increase in the air gap [81][94][96][100]. The larger the contact area, the larger the electroadhesive forces obtained [69]. Increased electroadhesive forces can also be obtained by attaching specially designed and manufactured surface textures on the dielectric material such as dry adhesives [61][97]. The combination of electroadesion and directional dry adhesives is a promising solution moving forwards so that the pads can be more adaptable to rough surfaces and have greater adhesive forces thus enhancing their realibility and robustness in use.

● Dielectric constant

Dielectric constant, as aforementioned, is directly related to the polarisability of

the dielectric material. All the simulation results showed that the higher the dielectric constant the larger the electroadhesive forces can be obtained. The simulation results obtained by Sabermand et al. showed that the relationship between the dielectric constant and the electroadhesive force was linear [100] whereas other researchers obtained different nonlinear relationships [94][81]. The work by Téllez et al. tested four different insulating polymer materials: PP, PET, PDMS, and ST-3050, on the same flat, clean, horizontal melamine substrate. They used the same interdigitated electrode design and found that the ST-3050 polyurethane was the best due to its compliance [63]. However, no evidence showed that the thickness of the four dielectric materials were the same for this work. Also, although the work by Tazetdinov [121] tested three different dielectric materials that have different dielectric constants and confirmed that the lower the dielectric constant the lower the forces obtainable, no evidence showed that the surface texture of the three dielectric coatings was similar. The reason why there is little experimental data on investigating the relationship between the dielectric constant and the electroadhesive force obtainable may be due to the fact that it is difficult to procure different dielectric materials that have the same thickness and surface texture.

● Dielectric resistivity

Theoretically, a large resistivity will restrict the movement of charges and a small resistivity will cause significant current consumption and leakages. As stated in 2.3.1, the resistivity of the dielectric layer affects the type and magnitude of electroadhesive forces obtainable on conductive substrate materials. No work has been done on the investigation into how the resistivity of the dielectric layer affects the electroadhesive forces obtainable on non-conductive substrate materials.

● Dielectric strength

High dielectric strength was recommended by Chestney et al. to avoid dielectric

breakdown and to improve the reliability of the electroadhesive systems [19]. The stronger the dielectric strength, the smaller the space between electrodes, the thinner the dielectric layer, and the higher the voltage, the higher the electroadhesive forces obtainable. However, the space between electrodes and the thickness of the dielectric layer should not be too small to induce dielectric breakdown.

● Molecular structure, molecular weight, molecular polarisability, crystallinity, and electronegativity/electropositivity of the dielectric

The above factors are grouped together because they are correlated with each other. Different dielectric materials have different molecular polarisability and therefore different electroadhesion properties. The molar polarisability, according to the Clausius-Mossotti equation, can be expressed as:

$$P_{molar} = \frac{\varepsilon_r - 1}{\varepsilon_r - 2}\frac{M}{\rho} = \frac{N_A \alpha}{\varepsilon_0} \quad \text{(3-1)}$$

where M is the molecular weight, ρ is the charge density, and N_A is the Avogadro constant.

Little study has been found on optimising the dielectric material for electroadhesion by looking into its molecular structure, molecular weight, molecular polarisability, crystallinity, and electronegativity/electropositivity.

The dielectric material for electroadhesion should usually demonstrate characteristics such as low dielectric loss, high mechanical strength, be free from gaseous inclusions and moisture and resistant to thermal and chemical deterioration. Optimised dielectric material selection for specific applications is the key for better electroadhesion properties.

3.8.3 Substrate parameters

Very few substrate materials have been found to exhibit no electroadhesive force

if appropriate dielectric materials are chosen [131]. Substrate parameters which will have an effect on electroadhesion include substrate thickness, substrate surface texture, and substrate material properties such as permittivity, resistivity, molecular structure, molecular weight, molecular polarisability, crystallinity, and electronegativity/electropositivity. It should also be noted that residual charges, which may exist after applying the high voltage on the substrate, can influence the electroadhesive forces obtainable for the next experimental test. It is necessary dissipate the residual charges by grounding both the pad and the substrate each time after the test. However, to date, only a few researchers have considered the residual charges and measured the surface potential of the substrate and the pad to make sure that the residual charges do not affect the measured forces [20][60].

● Substrate thickness

The simulation results obtained by Mao et al. showed that the thickness of the wall substrate can be ignored [94], whereas the result found by Ruffatto et al. showed that the overall electric field strength decreased at larger substrate depths [73] and the highest shear pressure generated by the optimised electrode widths for the concentric circle pattern was found when the electric field was measured up to a depth of 3 mm [14]. Simulation results found by Cao et al. also strengthened that the substrate thickness has significant influence on the electroadhesive force obtainable, especially when the air gap is smaller [98]. Also, the force increases with wall thickness but reaches a limit when the wall thickness is larger than the distance between the centerline of two electrodes [98]. This difference of opinion maybe because Mao et al. only calculated the interfacial electroadhesive forces when changing the substrate thickness whereas Ruffatto et al. calculated the overall effect of the whole substrate thickness.

● Substrate surface texture

The surface texture of the substrates directly affect the air gap and contact area

between the pad and the substrate. Most researchers concluded that smoother surfaces would exhibit greater electroadhesive forces obtainable as a larger contact area and smaller air gap can be achieved [20][72]. However, for materials that are difficult to be polarized, such as polymethylmethacrylate (PMMA) and polycarbonate, only relatively small electroadhesive forces can be obtained even when the surface of the material is smooth [63]. Compliant and flexible pads help to increase the forces between the pad and the substrate. The consideration of the air gap and substrate surface textures is important to accurately derive the electroadhesive forces both in simulation and theoretical analysis [45]. However, more in-depth research is required. A further experimental investigation of how surface textures affect the electroadhesive forces is presented in chapter 5.

● Substrate permittivity

Monkman stated in his master thesis that there was no clear correlation between permittivity and electroadhesive forces [17]. All the simulation results showed a nonlinear increase of electroadhesive forces when increasing the dielectric constant of the substrate [81][94]. This is potentially because substrate materials with larger permittivity are easier to be polarised, thus more polarisation charges can be obtained, resulting in larger attractive forces. There is no trustable experimental result on the relationship between the electroadhesive forces obtainable and substrate dielectric constant as it is difficult to procure substrates with different dielectric constants but the same surface texture and dimensions. However, various experiments have been done on different substrate materials. For instance, the work done by Téllez et al. tested different substrate materials such as concrete, PMMA, glass, painted steel and both painted, and bare drywall (gypsum board) [63]. The work done by Ruffatto et al. tested a painted drywall, finished wood, glass, steel, carbon fibre sandwich panel, graphite M55J, thermal black paint on aluminium, copper-clad Rogers 4003, white beta cloth, reinforced Kapton, reinforced Kapton MLI film, and ceramic tiles [72][76]. The work by

Koh et al. tested an aluminium plate, brick, ceramic tiles, concrete slab, and glass panel. They found that the obtainable forces on the ceramics and glass panel were higher than a brick and concrete [20]. In all these cases, they did not mention that they carried out their experiments in a controlled environment.

● Substrate resistivity

As mentioned in section 2.3, the principle of electroadhesion changes when the resistivity of the substrate changes. This is because the resistivity of the substrate determines the substrate type, be it conductive, semi-conductive, and insulating substrates.

● Molecular structure, molecular weight, molecular polarisability, crystallinity and electronegativity/electropositivity of the substrate

Molecular polarisability was found to be the major factor which determines the electroadhesion properties [17]. Macromolecular polarisation or spontaneous polarisation and molecule structures also have a profound effect. For example, cotton and rayon are all basically polysaccharides, but each has its own solid configuration [17]. Also, Polythene and annealed polythene differ only in the thickness of their crystal structures [17]. However, completely different or totally opposite electroadhesion properties were however observed. Electronegativity describes the tendency of an atom or a functional group to attract electrons towards itself. It was found by Monkman that materials with an electronegativity of 2, being the neutral centre of the range, would not show good electroadhesion properties as they have little permanent dipole moment [17]. Carbon, however, has an electronegativity of 2.5, so it should not be expected to have as good an electroadhesion as metals that have a large amount of permanent dipole moment and high degree of crystallinity. However, it is a highly crystalline substrate and thus can exhibit good electroadheison properties [17].

3.8.4 Electrical parameters

The voltage parameters include voltage polarity, voltage magnitude, and output current of the high voltage source connected with the electrodes.

● Voltage polarity

It was found by Monkman that the applied voltage polarity should be different for electronegative and electropositive substrate materials. If a single pole is used, the charge polarity will also depend on the permanent dipole moment (if any) of the substrate materials to be grasped [131]. Koh et al. found that positive and negative polarity produced similar levels of output electroadhesive forces on glass and concluded that static charges would not discriminate the charge polarity for electroadhesive grasping [65].

● Applied voltage magnitude

All theoretical analysis, simulation and experimental results showed that the magnitude of the applied voltage has a strong influence on the electroadhesive forces obtainable. The results showed that there is a quadratic increase between the voltages applied and the electroadhesive forces obtainable [14][63][77][79] [81][94][96][100][132]. However, most of the experimental results showed that the relationship between the applied voltage and the electroadhesive force is not simply a quadratic relationship [15][20]. The quadratic relationship only occurred when the applied voltage was under 4 to 6 kV [15][20]. After this range, a saturation trend was observed and only a marginally increasing adhesive force could be obtained at the expense of a high supply current. This may be due to current leakage in dielectric materials and corona discharge in the air gap [20]. The work done by Koh et al. proposed that a square root, cubic root or logarithmic relation between the voltage magnitude and the electroadhesive force would occur at higher voltages. Based on this, second order and third order working models were proposed and concluded that there is a range of optimum higher voltages to remain electrically efficient for electroadhesive applications [20]. Koh

et al. also found that there was a ‘dropdown effect’ on most substrates after applying voltages around 10 kV. In addition, it was found by that increased voltage may bring faster release speed [30]. Since the tested maximum voltage difference between electrodes was only 20 kV [65][70], the investigation of the relationship between the applied voltage and the electroadhesive force is still incomplete and thus requiring further work.

● Output current magnitude and frequency

By turning off the operating voltage, the electrostatic forces typically drop. However, when using a DC voltage source a residual force remains. This effect can be compensated for by using an AC voltage source operated at low frequency [41]. It has been found that the limitation of the current input (from 0.5 A to 0.1 A) could help reduce the amount of discharges and short cuts.

3.8.5 Electrode parameters

The electrode geometric information includes electrode pattern, space between electrodes, electrode width, conductivity and electrode length.

● Electrode pattern

Various electrode patterns have been designed and tested for electroadhesive applications, as mentioned in section 3.3.1. Different electrode configurations showed different forces in the electroadhesive forces obtainable [63]. Téllez et al. have tested the jagged design, the double electrode rectangular design in a square configuration, the double electrode semi-circular design, the interdigitated design and the double electrode rectangular design in an oblong configuration [63]. They found that the interdigitated design performed the best on a glass substrate based on the same PP dielectric layer, electrode thickness, effective electrode area and the same clean and dust-free environment. Germann et al. have compared the comb design, rectangular spiral design and round spiral pattern design [77] based on the same electrode width (2 mm),

space between electrodes (2 mm) and effective pad area. They found that the comb design has very high shear forces in the direction perpendicular to the electrodes but very weak shear forces in the parallel direction. The rectangular spiral design has a similar level of shear forces in the horizontal and vertical directions but a very weak force in the diagonal direction. The round spiral pattern design has similar shear forces in all directions although the forces were the weakest among the three design. Comb, square spiral, Hilbert curve and concentric shapes were compared by Ruffatto et al. [74]. Both of their experimental and simulation results suggested that, overall, concentric shapes with varying electrode widths were preferable to achieve greater shear adhesive forces on drywall, wood, tile, glass, and steel. This may be due to the fact that concentric shapes have fewer sharp edges. However, the results were based on the fact that Van der Waals forces played a significant role in the forces obtained although they claimed a 500% increase compared with the preliminary reported results. Further investigation on this is presented in chapter 6.

● Space between electrodes

Most of the theoretical analysis and simulation results showed that a nonlinear and significant decrease in obtainable electroadhesive forces can be seen when increasing the space between electrodes [14][63][77][79][81][94][96][132]. However, the minimum space between electrodes should not induce dielectric breakdown. Results obtained by Mao et al. also showed that there was only a slight decrease when the distance was larger than 5 mm [94]. However, the simulation result from Ruffatto et al. showed a different trend, a nearly linear decrease, but their experimental result showed different nonlinear trends depending on the substrate materials [73]. Their results were based on a fixed electrode width of 3 mm and varying space between electrodes such as 0.6, 1, 2 and 4 mm. They concluded that for rough surfaces such as wood and drywall, it is beneficial to have slightly smaller spaces between electrodes, say 1-2 mm,

for greater forces [73]. They explained that smaller spaces between electrodes can bring stronger but highly locally concentrated electric fields whereas larger spaces may bring weaker but more uniform and dispersed electric fields. This may allow more uniform surface polarization, possibly providing higher adhesion forces for rough surfaces [73]. Also, Jeon et al. found that it is beneficial to have many boundaries to make the clamp and unclamp faster on non-conductive substrates such as glass [16]. For dielectrics which are slightly conductive, it is, however, advantageous to have less boundaries thus a larger effective electrode area [16]. Further experimental validation is therefore needed to further test and validate the results both on smooth and rough surfaces.

● Electrode width

There is a clear debate on whether the electrode width should be as small as possible or whether there should be an optimum value in terms of both simulation and experimental validation. An optimum ratio of 16 : 1 (electrode width: space between electrodes) was concluded based on the simulation results observed when the electrode width of was set to 8 mm and the space between the electrodes was set to 0.5mm by Koh et al. [67]. The simulation work by Ruffatto et al. found that an optimum electrode width of approximately 3 mm was found when electrode widths of 1, 2, 3, 4, and 6 mm and a fixed space between electrodes of 0.6 mm were used. The experimental results were found to have a similar trend with the simulation results but a different optimum electrode width was found on rough surfaces such as drywall. Also, the electric field strengths produced by electrode widths smaller than 3 mm decreased significantly whereas a smaller decrease was seen for electrode widths larger than 3 mm. They concluded that smaller electrode widths were found to be more desirable to achieve greater electric field strength whereas larger electrode widths are preferable for thicker substrate depths. Furthermore, the end electrodes were suggested to have reduced electrode widths to achieve higher overall electric

field strength [74]. The simulation result by Sabermand et al. found that the electrode width only affected the electroadhesive forces marginally by ignoring its effect on electrode number [100]. Also, an optimum value for electrode width of 0.6 mm was found compared with other values tested (0.4, 0.8, 1, and 1.4 mm). However, it was recommended that smaller electrode widths should be used for certain pad areas. It was stated by Jeon et al. that there exists an optimum ratio of the electrode width and space between electrodes [16]. This result however was not presented in their paper.

● Electrode thickness

The simulation results by Ruffatto et al. showed that the electrode thickness does not affect the electroadhesive forces obtained. A difference of less than 2% in field strength was found when changing the thickness of the electrodes from 1 mm to 5 mm [73]. This is reasonable as only the surface charge of the electrodes account for the electroadhesive forces obtainable. However, further experimental work to validate this is required.

● Conductivity

Various electrode materials have been tested such as copper, alunimum, copper nickel alloy, conductive graphite E33, carbon black, conductive polymers such as cPDMS, carbon filled silver, and silver ink, as mentioned in section 3.3.2. It was stated by Krahn et al. that an increased conductivity would allow a more even charge distribution and increased adhesion [60]. An experimental comparison between different electrode materials is needed.

● Electrode length

It was stated by Jeon et al. that the electroadhesive force is proportional to the area of the electrodes [16]. Longer electrode length means larger pad area, thus larger electroadhesive forces can be obtained. This was experimentally validated by Koh et al. [20]. The simulation results by Sabermand et al. showed that a

linear increase of forces would be obtained when increasing the electrode length [100]. Also Ruffatto et al. suggested that the relationship between the number of electrodes and the electric field strength is linear [74].

3.9 Summary

In this Chapter, a comprehensive literature review of electroadhesion is demonstrated in terms of electroadhesive pad design, manufacturing, testing, modelling of electroadhesion and electroadhesive applications. Also, a summarisation and review of the thirty three variables influencing the electroadhesive forces obtainable is shown. A brief summarisation of the findings from this review can be seen below:

● Electroadhesion is a multidisciplinary, complicated, and dynamic electrostatic attraction phenomenon with over thirty three variables influencing the obtainable electroadhesive forces between the electroadhesive pad and the substrate. Further theoretical and experimental work are required to fully understand influencing parameters such as the environmental factors, material properties of both the dielectric layer covering the electrodes and the substrate, and electrical paramaters such as the magnitude of the applied voltage.

● Pad design involves the design of electrode configurations, electrode materials, and dielectric materials. Although this research is not aiming to investigate the electrode and dielectric materials in detail, it is necessary to conduct a comprehensive experimental comparison of various electrode and dielectric materials mentioned in Chapter 2.

● Pad manufacturing involves the manufacture of both electrodes and dielectric materials. Pads can be made in-house or professionally made by commercial companies. A comprehensive experimental comparison of various pad manufacture methods mentioned in Chapter 2 is useful. It is also necessary to investigate novel electrode/dielectric materials that can help produce the

maximum electroadhesive force and achieve the fastest clamping and unclamping speed, especially on non-conductive substrates.

● Electroadhesive forces are expected to be measured to quantify the performance of the electroadhesive pads manufactured, either through normal force measurement methods or shear force measurement methods.

● Modelling of electroadhesion is important for understanding and designing electroadhesives. Theoretical modelling, electrostatic simulation, and empirical modelling have been investigated and used to design electroadhesives. However, there lacks an experimentally validated theoretical model. Also, few simulation models have been validated in a controlled environment. In addition, there is no advanced empirical model predicting the performance of electroadhesives.

● Material handling and robotic climbing are the two main electroadhesive applications.

The comprehensiveness of this literature review is unique and should be useful for future researchers. In a word, the understanding of electroadhesion is still incomplete. To investigate a research phenomenon like this, it is advisable to conduct a theoretical analysis first before spending time and money on the pad design and manufacture for the experiments. This is presented in Chapter 4.

4 Optimisation Modelling of Coplanar Interdigitated Electroadhesives

4.1 Introduction

Interdigital sensors and transducers have been widely used both in research and industrial applications [115]. Also, the interdigitated electrode shape has been one of the most popular geometries for electroadhesive applications due to the fact that interdigitated electroadhesives can generate larger electroadhesive forces with quicker response times. In this Chapter, the need for the optimisation modelling of coplanar interdigitated electroadhesives is identified. The research methodology is then proposed. After this, a detailed description and explanation of the proposed research methodology are conducted, including the development of a simplified and novel theoretical optimisation model of coplanar interdigitated electroadhesives, an example of a 2D electrostatic simulation, and experimental validation based on a confident testing platform and procedure.

4.2 The research need

It is impossible to derive accurate analytical and computational models due to inhomogenous materials and electric fields existing in nature. However, approximate or simplified modelling is still useful for understanding electroadhesion and the geometrical optimisation of the electroadhsive pad. As summarised in section 3.6.1, simple theoretical models [31][51][63][77][79] have been used by many researchers for understanding electroadhesion. Some researchers even used different equations in their published papers such as the case in [77] and [79]. A 4-fold can be seen in the applied simple theoretical models due to the attention which has been paid to the modelling and understanding of electroadhesion. These simple models do not include enough geometric information of the interdigital electroadhesives such as electrode widths and spaces between electrodes. They therefore cannot be used directly

to derive the optimisation model of the interdigitated electroadhesives. Various simulations and theoretical analysis have been conducted. Only the simulation models achieved by Ruffatto et al. based on a gradient decent optimisation algorithm coupled with COMSOL Multiphysics [73], the optimisation model achieved by Koh et al. based on an empirical comb capacitance equation [68] and the simulation model by Sabermand et al. [100] concluded that there is an optimum electrode width when the space between electrodes was fixed. Also, Ruffatto et al. have validated, to some extent, their simulation results. There is little work on the experimental validation of the theoretical optimisation modelling of interdigital electroadhesives on both conductive and non-conductive substrates.

Electroadhesive forces can generally be derived by the virtual work method [96] and Maxwell stress tensor method [83][94]. In this chapter, the simpler virtual work method is adopted. By using this method, the most important part is to derive the comb capacitance of an interdigitated electroadhesive. The interdigitated electrode geometry (see Figure 4-1 (a)) is a finger or comb like periodic symmetric pattern and is the most preferable electroadhesive geometry, as mentioned in section 2.2.2. For comb electroadhesive systems, detailed electric field lines exist and can be seen in Figure 4-1 (b) and (c). Since the length of the electrodes is much larger than their widths and thicknesses, and the electroadhesive pad area is much larger than the gap between the electrodes and the substrate surfaces, all the related fringing fields (edge/boundary effects), E_1, can be ignored. Although E_2 can induce relatively large attractive forces between the comb fingers, it is evident that these forces on both sides of comb electrodes will cancel each other. Also, due to E_2, the electrodes will not touch each other as they are deposited in dielectrics. In addition, all the effects between electric fields are assumed to be neglected. As a consequence of these considerations, only the fields between the electrodes and substrates, E_3, and

the fields between the electrodes, E_4 (which travels from the positive electrodes penetrating the dielectric materials and the substrates to the negative electrodes), lead to the attractive forces within the interdigitated electroadhesive system. E_3 is negligible compared with E_4. Therefore, only the half side closest to the wall substrate of E_4 contribute primarily to the attractive forces between the pad and the substrate.

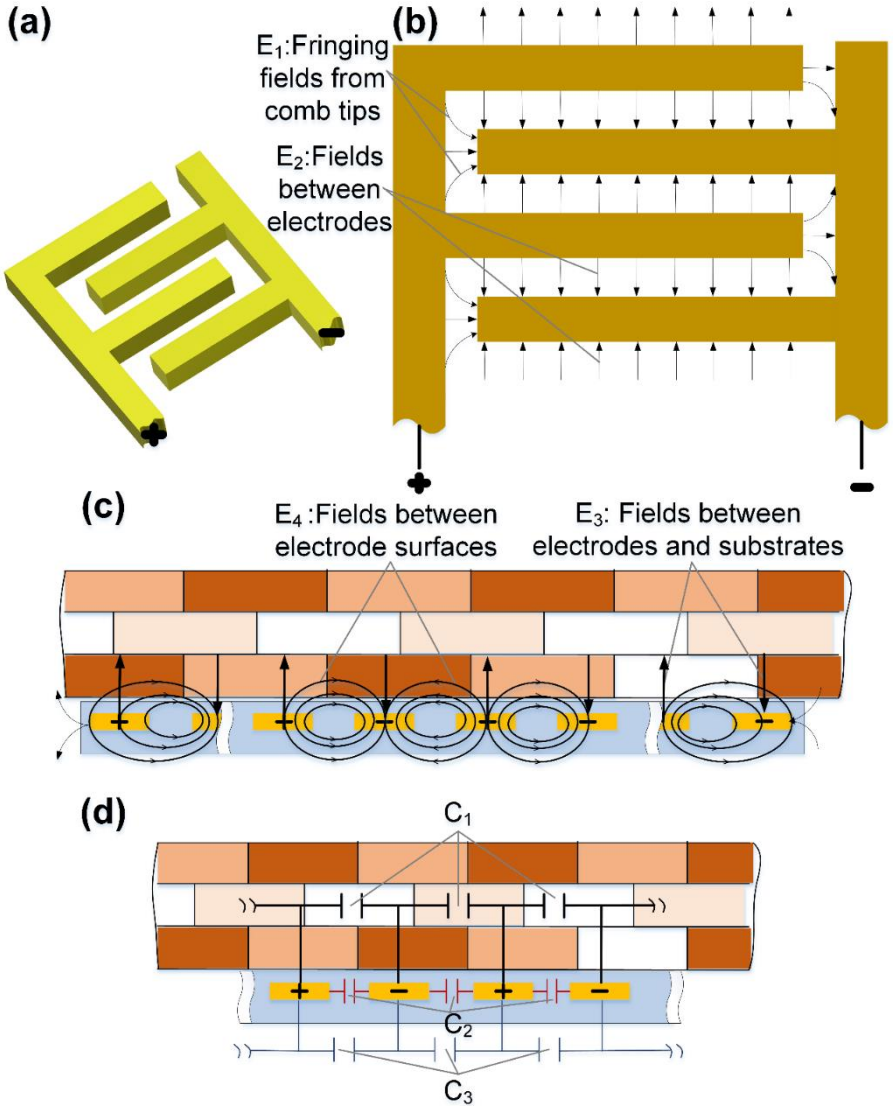

Figure 4-1 Electric fields and capacitances in the interdigitated electroadhesive system

Based on Figure 4-1 (a), (b) and (c), we can create the equivalent circuit for the

coplanar interdigitated capacitance presented in Figure 4-1 (d), where C_1 and C_3 are coplanar capacitances based on E_4, and C_2 can be regarded as the normal parallel capacitance between the electrodes because of E_2. However, the electro-adhesive forces between the pad and the substrate only depend on C_1, a parallel connection of pairs of coplanar capacitance unit.

Various methods have been used to compute the coplanar capacitance within the interdigitated electroadhesive system, including the continuum model, finite element calculations, non-dimensionalised plot of capacitances, approximating expressions, and conformal mapping methods [115][133]. The conformal mapping method (or the Schwartz-Christoffel transformation [134]) can transform a complex, coplanar geometry into a simple parallel circumstance, and has been one of the most frequently used methods [115][135][136].

The coplanar capacitance unit, boxed by the rectangle in Figure 4-2, is the capacitance from the half positive electrode to the half adjacent negative electrode.

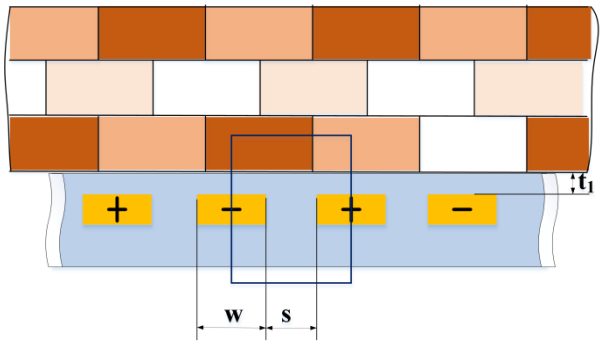

Figure 4-2 Selected cross-sectional view of the coplanar capacitance unit

Based on the conformal mapping method, we have the total effective capacitance of the interdigitated electroadhesive system without the consideration of the edge effects, described by [135]:

$$C_e = (2\text{N-1})\text{L}C_1 = \frac{2\text{N-1}}{2}\text{L}\varepsilon_0\varepsilon_{eff}\frac{K(k_0)}{K(k_0^{'})} \quad (4\text{-}1)$$

where N is the total number of comb finger pairs, L is the finger overlap length of the electrode, S is the space between electrodes, W is the width of electrodes, $K(k)$ is the complete elliptic integral of the first kind, k is the modulus of the elliptic integral function and

$$\varepsilon_{eff} = 1 + \frac{\varepsilon_{r1}-1}{2}q_1 + \frac{\varepsilon_{r2}-\varepsilon_{r1}}{2}q_2 \quad (4\text{-}2)$$

$$q_i = \frac{K(k_i)K(k_0)}{K(k_i^{'})K(k_0^{'})} \quad (4\text{-}3)$$

$$k_0 = \frac{w}{w+s} \quad (4\text{-}4)$$

$$k_i = \frac{\sinh(\frac{\pi s}{2h_i})}{\sinh(\frac{\pi(s+w)}{2h_i})}\sqrt{\frac{\cosh^2(\frac{\pi(s+w)}{2h_i}) + \sinh^2(\frac{\pi(s+w)}{2h_i})}{\cosh^2(\frac{\pi s}{2h_i}) + \sinh^2(\frac{\pi(s+w)}{2h_i})}} = \frac{\tanh(\frac{\pi s}{2h_i})}{\tanh(\frac{\pi(s+w)}{2h_i})} \quad (4\text{-}5)$$

$$k_i^{'} = \sqrt{1-k_i^2} \quad (i=1, 2) \quad (4\text{-}6)$$

When attaching the pad on conductive substrates, the effective permittivity can be given by

$$\varepsilon_{eff1} = 2(1 + \frac{\varepsilon_{r1}-1}{2}q_1) \quad (4\text{-}7)$$

where $h_1 = t_1$.

When attaching the pad on insulating substrates, the effective permittivity can be given by

$$\varepsilon_{eff2} = 1 + \frac{\varepsilon_{r1}-1}{2}q_2 + \frac{\varepsilon_{r1}-\varepsilon_{r2}}{2}q_1 \quad (4\text{-}8)$$

Assuming the thickness of the insulating substrates is far larger than the dimensions of the interdigitated electroadhesive system, then we have $q_2 = 1$. Therefore the equation (4. 8) can be approximated as:

$$\varepsilon_{eff\,2} = 1 + \frac{\varepsilon_{r1} - 1}{2} + \frac{\varepsilon_{r1} - \varepsilon_{r2}}{2} q_1 \quad \text{(4-9)}$$

Several other forms using the same conformal mapping methods have been also investigated. However, this requires further validation as no one applied then for electroadhesive force modelling.

For insulating substrates:

$$C_e = \text{(2N-1)L}\varepsilon_0(\varepsilon_{r1} + \varepsilon_{r2})\frac{K(k_0)}{K(k_0^{'})} \quad \text{(4-10)}$$

$$C_e = \frac{\text{(2N-1)L}[\varepsilon_0(\varepsilon_{r1} + \varepsilon_{r2}) + 1]}{2\pi^2}\frac{K(k_0)}{K(k_0^{'})} \quad \text{(4-11)}$$

In addition, several approximation methods have been used to simplify the computation of the conformal mapping method, including:

$$C_e = (2N-1)L\frac{4(\varepsilon_{r1} + \varepsilon_{r2})\varepsilon_0}{\pi}\sum_{n=1}^{\infty}\frac{1}{2n-1}J_0{}^2\left\{\frac{(2n-1)\pi s}{2(s+w)}\right\} \quad \text{(4-12)}$$ (for insulating substrates [137])

where J_0 denotes the zero order of Bessel function of the first kind.

$$C_e = (2N-1)L\frac{2\varepsilon_{r1}\varepsilon_0}{\pi}\ln[1 + \frac{2w}{s} + \sqrt{(1 + \frac{w}{2})^2 - 1}] \text{(4-13)}$$ (for insulating substrates [138])

where a direct contact between fluids and electrodes was considered and w/2s >>1 and l>>w.

and

$$C_e = \frac{(2N-1)L\pi\varepsilon_{\text{eff}}\varepsilon_0}{\ln(\frac{\pi s}{w+t_1}+1)} \quad (4\text{-}14)$$

where $\varepsilon_{\text{eff}} = \varepsilon_{\text{r1}}$ when s is far larger than t_1, whilst $\varepsilon_{\text{eff}} = \frac{\varepsilon_{\text{r1}} + \varepsilon_{\text{r2}}}{2}$ when s is similar to t_1.

A good approximation expression to compute $\frac{K(k_0)}{K(k_0')}$ can be given as:

$$\frac{K(k_0)}{K(k_0')} = \frac{\pi}{2\arccos h[\frac{1+k_0'}{k_0} + \frac{k_0(k_0')^{(-0.25)}}{4(1+k_0')}]} \quad (4\text{-}15)$$

All the existed models have not been experimentally validated yet. It is therefore desirable to have a theoretical model that is computationally easier and can be used for both conductive and non-conductive substrates. Since dielectric loss exists in inhomogenous and anisotropic materials, it is impossible to accurately compute the electroadhesive forces mathematically. In order to ease the theoretical approximation modelling process, the following assumptions were made:

● Direct current (DC) high voltage source with dual polarity is used;

● The pad is rigid and the contacting surface is completely flat, so no air gap exists between the pad and the substrate (infinite thickness);

● Both the dielectric materials and insulating substrates are homogenous, linear, and isotropic;

● No free charge exists in the electroadhesion system except on the electrodes;

● The length of electrodes is much larger than their widths, spaces, and thickness. They are therefore assumed to be negligible;

● The electroadhesive pad area is much larger than the gap between the electrodes and the substrate surfaces;

● The electroadhesive pad is placed in a vacuum and stable environment;

● An uniform electrode width distribution is used. This was verified by Raffatto et al. [74] that, for interdigitated pads, only the width of the end electrodes needs to be smaller.

● The charge distribution along the electrode is uniform thus the electric field distribution is uniform, although this cannot be the truth [139].

4.3 Research methodology

A recognised research procedure was presented in section 2.3 to study a phenomenon that has many influencing parameters. This forms the research methodology adopted in this Chapter as can be seen in Figure 4-3.

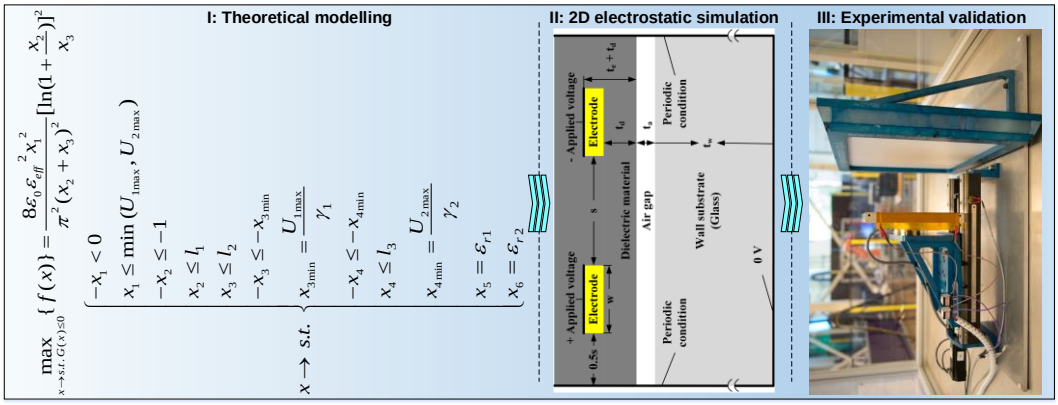

Figure 4-3 Research procedure

The first stage of this research includes a simplified and computationally easier theoretical model of the coplanar interdigitated electroadhesives. This is necessary and useful for the pad geometrical optimisation. After this, a 2D electrostatic simulation to further support the theoretical analysis by considering the effect of the air gap and the substrate thickness has been carried out. Finally, experimental validation are performed.

4.4 A simplified theoretical modelling of coplanar interdigital electroadhesives

Based on the assumptions mentioned above: the materials in the electroadhesive system are homogenous, linear, and isotropic, the Gauss theorem can be applied. Theoretically the electric field lines should be distributed elliptically. However, as aforementioned, it is difficult to conduct a curve integral of the ellipse mathematically. Here, I simplify the electric field ellipse lines into concentric lines. Also, I assume the electric fields are uniformly distributed along the electrode length direction, so the 3D problem can be transformed into a 2D one by taking the cross-section of the electrode panel into consideration, which can be seen in Figure 4-4. In this case, r is the radius of the concentric electric field, θ is the angle between the radius plane and electrode plane radius r, and U_0 is the applied voltage on the electrodes.

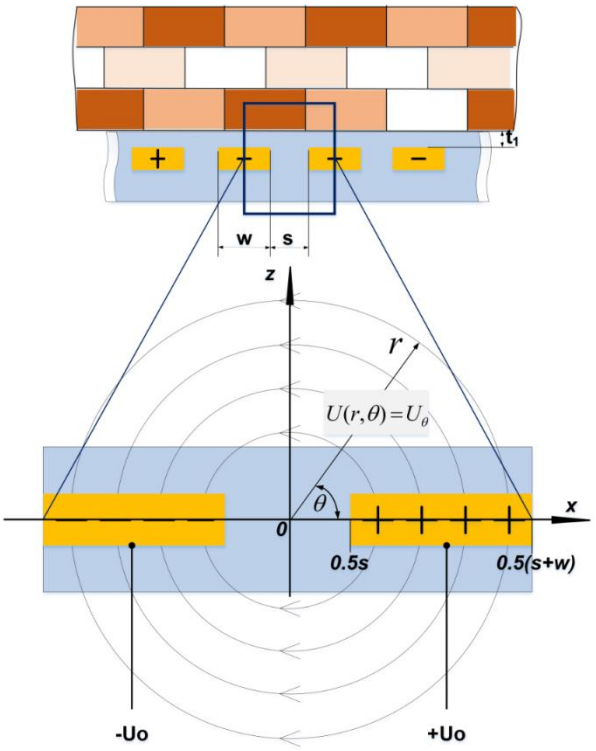

Figure 4-4 Simplified electric fields distribution with the selected coplanar electrodes

As it has been assumed that there is no free charge in the space except the

charges on the electrodes, the Laplace equation can then be applied. Therefore, under the polar coordinate condition:

$$\Delta U = \frac{\partial^2 U}{\partial r^2} + \frac{1}{r}\frac{\partial U}{\partial r} + \frac{1}{r^2}\frac{\partial^2 U}{\partial \theta^2} \quad (4\text{-}16)$$

Any radial planes that go through the center can be regarded as equipotential planes, and the electric field direction of every point on these planes is perpendicular to these equipotential planes. The electric potential of any points in this system, $U(r,\theta)$, is, therefore, a function of only θ, giving

$$\frac{\partial^2 U}{\partial r^2} = \frac{1}{r}\frac{\partial U}{\partial r} = 0 \quad (4\text{-}17)$$

Hence, by substituting the equation (4-16) into equation (4-17), we have:

$$\frac{1}{r^2}\frac{\partial^2 U}{\partial \theta^2} = 0 \quad (4\text{-}18)$$

Considering the initial conditions:

$$\begin{cases} U(\theta = 0) = U_0 \\ U(\theta = \pi) = -U_0 \end{cases} \quad (4\text{-}19)$$

We obtain:

$$U = U_0 - \frac{2U_0\theta}{\pi} \quad (4\text{-}20)$$

Based on the Maxwell Equation, the electric field is the gradient of the potential field:

$$E = -\nabla U = \frac{2U_0}{\pi r} \quad (4\text{-}21)$$

Based on Gauss' theorem, the charge density along the electrode surface is given as:

$$\sigma = \varepsilon_0 \varepsilon_{eff} E = \varepsilon_0 \varepsilon_{eff} \frac{2U_0}{\pi r} \quad (4\text{-}22)$$

When attaching the pad on conductive substrates, the effective permittivity can approximately be given by:

$$\varepsilon_{eff1} = \frac{\pi \varepsilon_{r1}(s + 0.5w)}{t_1} \quad (4\text{-}23)$$

When attaching the pad on insulating substrates, the effective permittivity can approximately be given by:

$$\varepsilon_{eff2} = \frac{\pi \varepsilon_{r1} \varepsilon_{r2}(s + 0.5w)}{4\varepsilon_{r2} t_1 + \varepsilon_{r1}[\pi(s + 0.5w) - 2t_1]} \quad (4\text{-}24)$$

The effective permittivity in the equation (4-23) and (4-24) was derived by simplifying the capacitors with changing distance between plates into a fixed value of $0.5\pi(s + 0.5w)$ (see Figure 4-5).

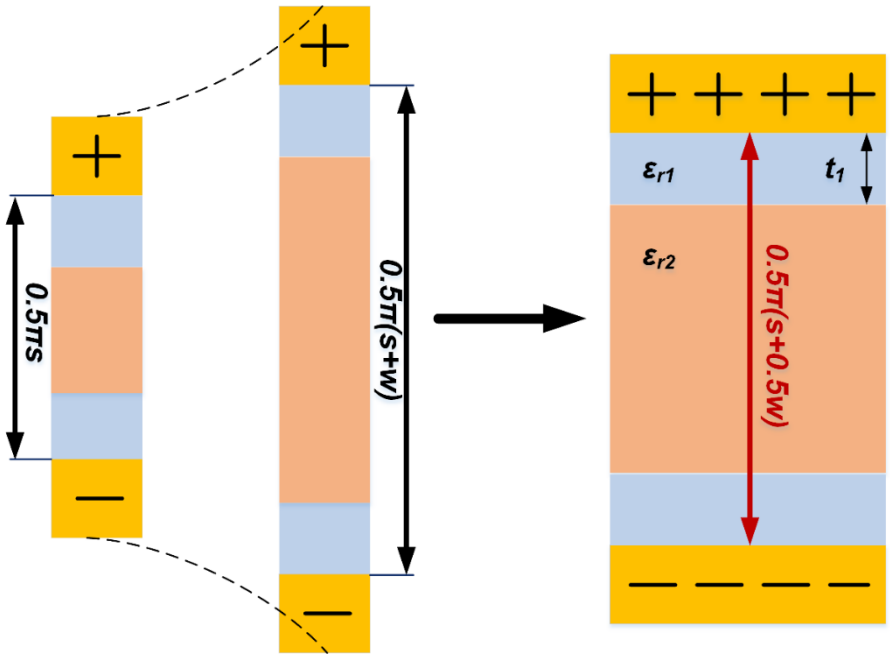

Figure 4-5 Simplified method for effective permittivity calculation

Since the thickness of the electrodes is negligible, all the charges are distributed

along the surface of the electrodes, i.e. the horizontal axis. It is then possible to obtain all the charges on the electrodes by integrating the charge density along the horizontal axis, giving:

$$Q = \int_{0.5s}^{0.5(w+s)} \sigma dS = \mathrm{L}\int_{0.5s}^{0.5(w+s)} \sigma dx = \frac{2LU_0\varepsilon_0\varepsilon_{eff}}{\pi}\ln(1+\frac{w}{s}) \quad (4\text{-}25)$$

According to the definition of capacitance, we have:

$$C_1 = \frac{Q}{U} = \frac{Q}{2U_0} = \frac{L\varepsilon_0\varepsilon_{eff}}{\pi}\ln(1+\frac{w}{s}) \quad (4\text{-}26)$$

Based on the equation (4-26), the total capacitance of an interdigitated electroadhesive pad with N pair of fingers is:

$$C_e = (2N-1)C_e = \frac{(2N-1)L\varepsilon_0\varepsilon_{eff}}{\pi}\ln(1+\frac{w}{s}) \quad (4\text{-}27)$$

Since the selected coplanar unit area of the interdigitated electroadhesive is $S = \frac{1}{2}L(w+s)$, by substituting the equation (4-26) into equation (2-43), based on the assumptions made above, the electrostatic attraction force per unit area corresponds to the following equation

$$f_z = -\frac{8\varepsilon_0\varepsilon_{eff}{}^2U_0{}^2}{\pi^2(w+s)^2}[\ln(1+\frac{w}{s})]^2 \quad (4\text{-}28)$$

4.4.1 Optimisation modelling of interdigitated electroadhesives on both conductive and non-conductive substrates

Based on the equation (4-28), the problem of obtaining the maximum attractive force per unit area can be converted to a variable-constrained non-linear optimisation problem, which can be solved in MATLAB using its optimisation toolbox. For the purpose if this research, the fminsearchbnd() function was used. The objective function and constraints of the proposed optmisation model were given as:

$$\max_{x \to s.t.\, G(x) \le 0} \{f(x)\} = \frac{8\varepsilon_0 \varepsilon_{eff}{}^2 x_1^2}{\pi^2 (x_2 + x_3)^2} [\ln(1 + \frac{x_2}{x_3})]^2$$

$$x \to s.t. \begin{cases} -x_1 < 0 \\ x_1 \le \min(U_{1\max}, U_{2\max}) \\ -x_2 \le -1 \\ x_2 \le l_1 \\ -x_3 \le -x_{3\min} \\ x_3 \le l_2 \\ x_{3\min} = \dfrac{x_1}{\gamma_1} \\ -x_4 \le -x_{4\min} \\ x_4 \le l_3 \\ x_{4\min} = \dfrac{x_1}{\gamma_2} \\ x_5 = \varepsilon_{r1} \\ x_6 = \varepsilon_{r2} \end{cases}$$

where x_1 is the applied voltage, x_2 is the width of electrodes and smaller than a designated value l_1, x_3 is the space between electrodes and smaller than a designated value l_2, x_4 is the thickness of the dielectric film and is smaller than a designated value l_3, x_5 is the permittivity of the dielectric film, x_6 is permittivity of the substrate, γ_i is the dielectric strength of the dielectrics between the electrodes (i=1) and covering the electrodes (i=2), and $U_{i\max}$ is the maximum voltage that can be applied (i=1, 2).

4.4.2 A worked example of the model

For non-conductive substrates, the following assumptions were made:

- $\gamma_1 = \gamma_2$ = 60000 Vmm^{-1};
- x_2 is greater than or equal to 1 but smaller than or equal to 10 mm;

- x_3 is greater than or equal to 1 but smaller than or equal to 10 mm;
- x_4 is greater than or equal to 0.1 but smaller than or equal to 10 mm;
- x_5 is greater than or equal to 2 but smaller than or equal to 10;
- x_6 is greater than or equal to 2 but smaller than or equal to 10; hence x_1 greater than or equal to 1 but smaller than or equal to $\min(U_{1\max}, U_{2\max})$=6000 V.

By using the fminsearchbnd() function in MATLAB, the maximum attraction force per unit area on non-conductive substrates is 0.0033 Nmm^{-2} or kPa under the condition of x_1 =6000, x_2 =1.79, x_3 =1, x_4 =0.1, x_5 =10 and x_6 =10. The relationship between f_z and x_1, x_2, x_3, x_4, x_5 and x_6 can be seen from Figure 4-6 to Figure 4-11 respectively.

From Figure 4-6, it can be concluded that the electroadhesive force increases quadratically with the applied voltage that is less than 6000 V. Also, it can be concluded from Figure 4-7 that there is an optimum electrode width to achieve the maximum attraction force per unit area when attaching the pad on non-conductive substrates when the space between electrodes was fixed at 1 mm. In addition, the smaller the space between electrodes (see Figure 4-8) and the dielectric thickness (see Figure 4-9), and the larger the permittivity of the dielectric film (see Figure 4-10) and the substrate (see Figure 4-11), the larger the attractive forces obtainable.

Please note that the results demonstrated from Figure 4-6 to Figure 4-11 were all based on the fact that only one variable was changed whilst others were maintained. The optimum electrode width/space between electrodes is about 1.8. When changing the space between electrodes, different optimum electrode widths are obtained, as shown in Figure 4-7.

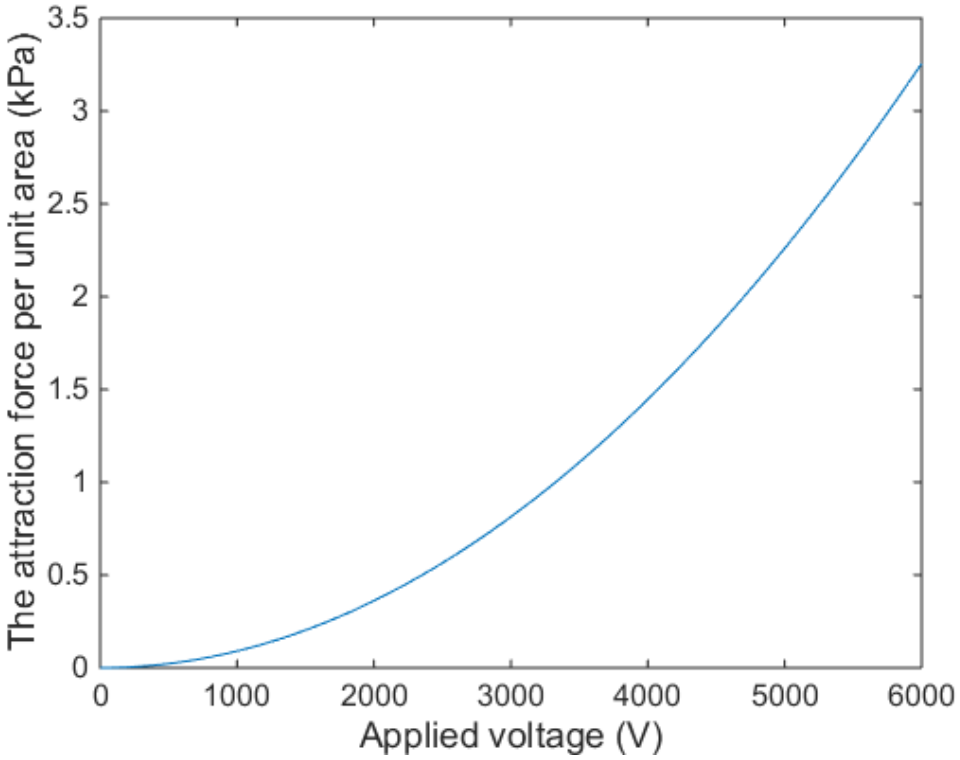

Figure 4-6 Relationship between the applied voltage and the force per unit area

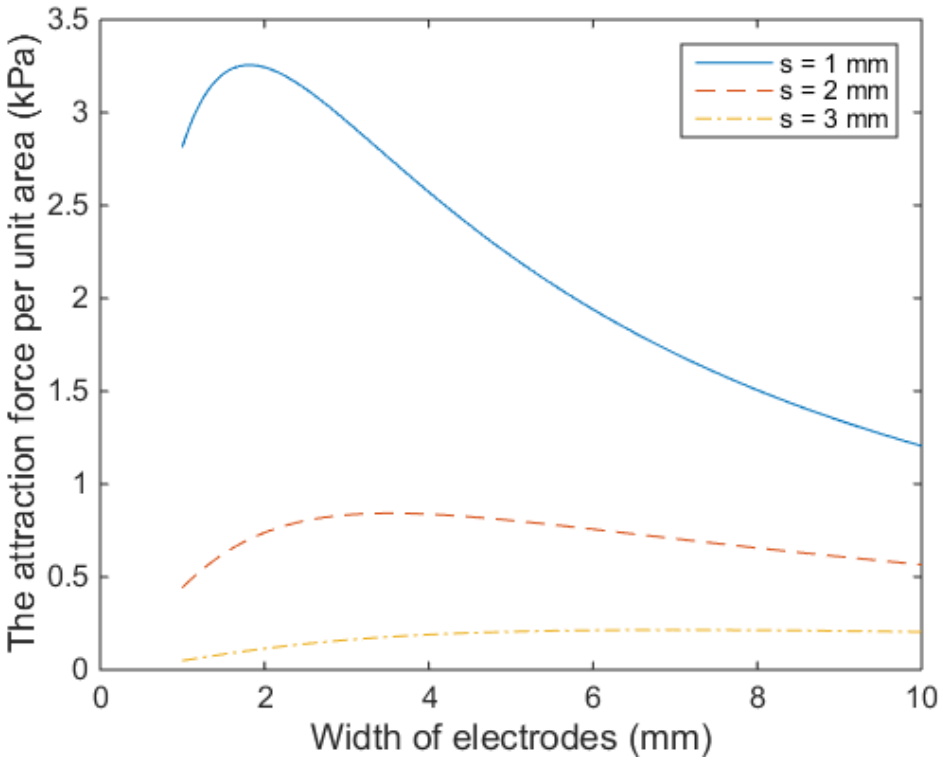

Figure 4-7 Relationship between the electrode width and the force per unit area

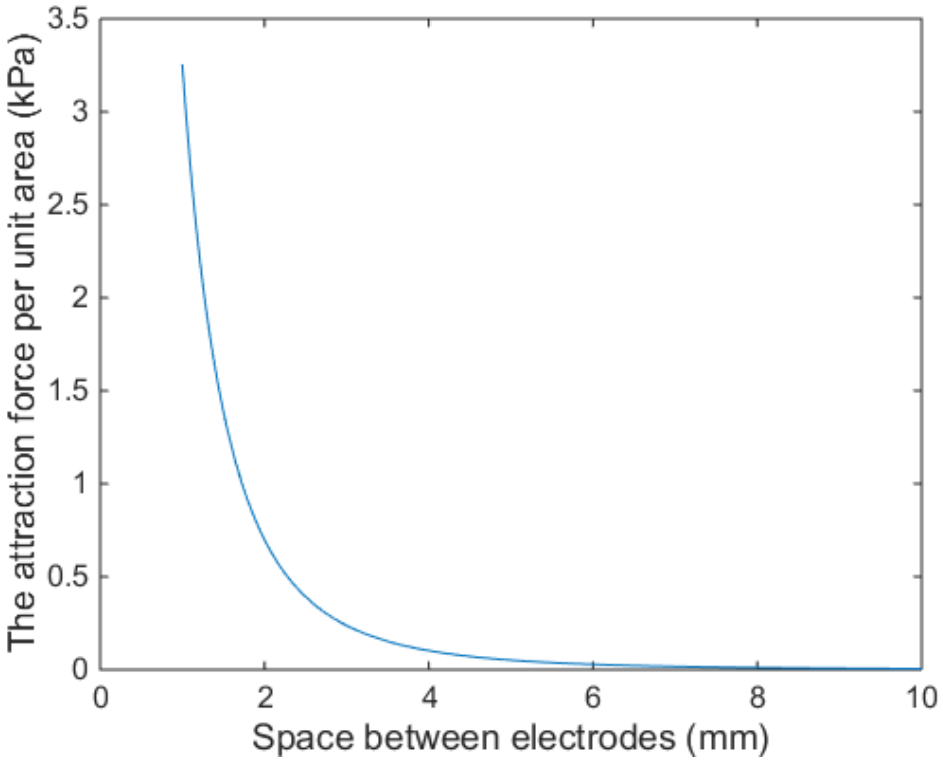

Figure 4-8 Relationship between the space between electrodes and the force per unit area

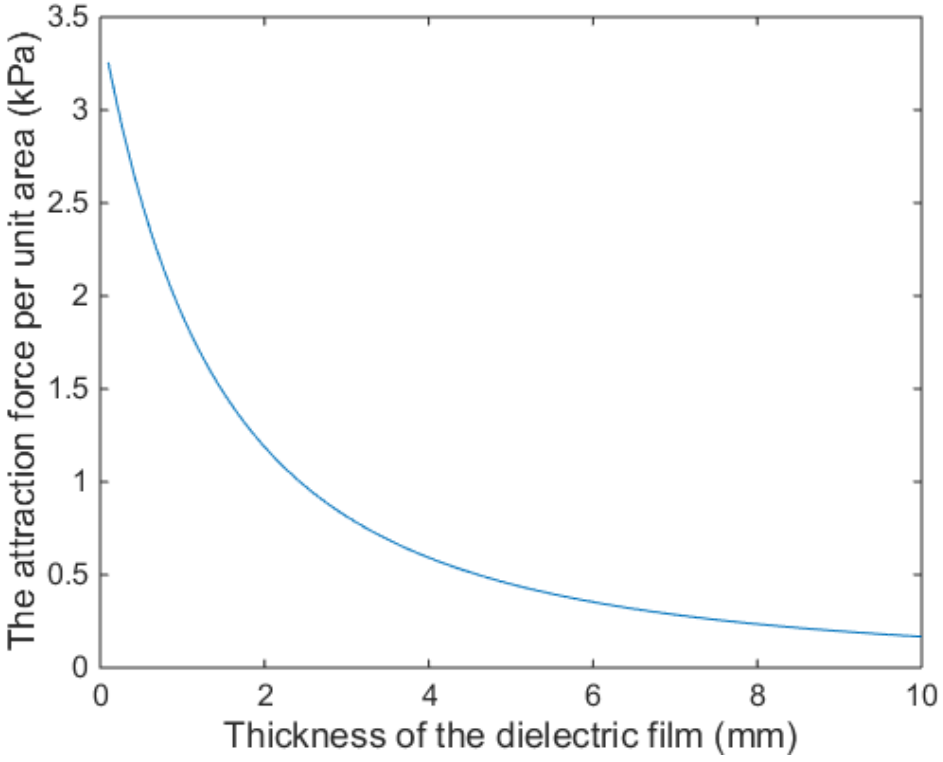

Figure 4-9 Relationship between the dielectric thickness and the force per unit area

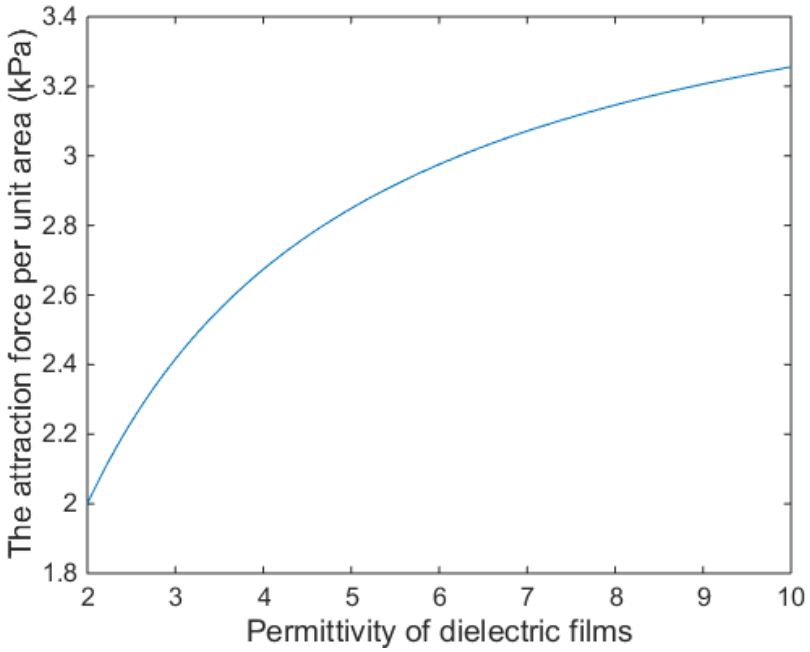

Figure 4-10 Relationship between the permittivity of dielectric films and the force per unit area

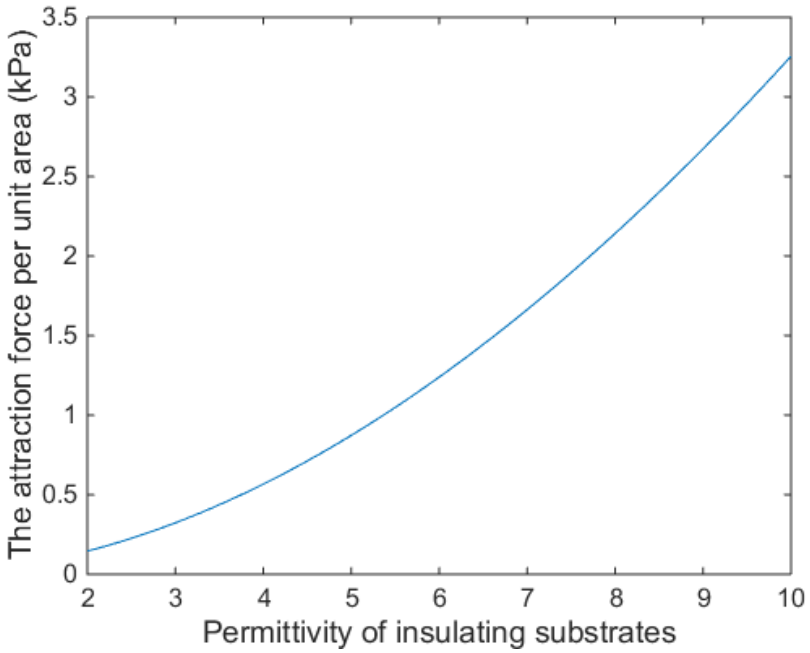

Figure 4-11 Relationship between the permittivity of insulating substrates and the force per unit area

For conductive substrates, I assume the same parameter range as per the non-conductive case. It can be concluded from Figure 4-12 and Figure 4-13 that the electrode width should be as large as possible and the space between electrodes

should be as small as possible to generate the maximum effective pad area. This agrees with the statement published by Schubert et al. that a double-electrode design would be better when facing conductive substrates [79].

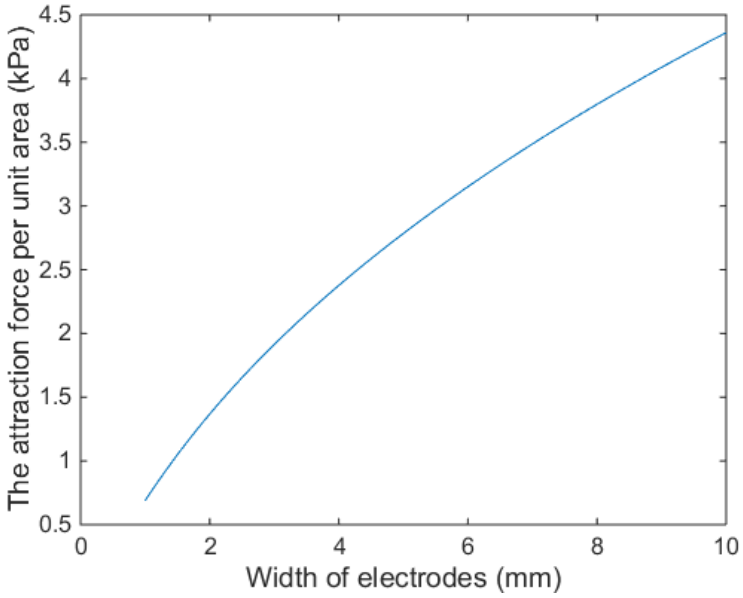

Figure 4-12 Relationship between the electrode width and the force per unit area on conductive substrates

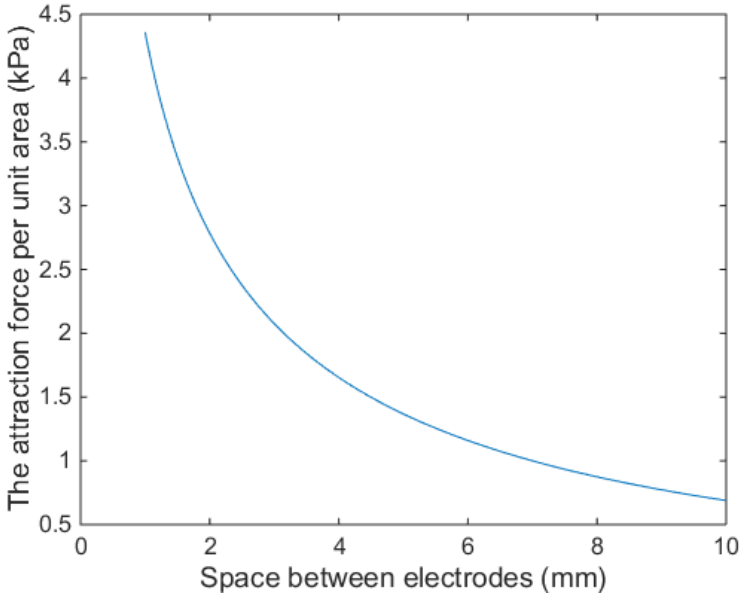

Figure 4-13 Relationship between the space between electrodes and the force per unit area on conductive substrates

4.5 2D electrostatic simulation using COMSOL

In order to further support the results from the theoretical analysis, a 2D electrostatic simulation using COMSOL was conducted. The diagram of the 2D model can be seen in Figure 4-14. This 2D model considers non-conductive substrate as a worked example.

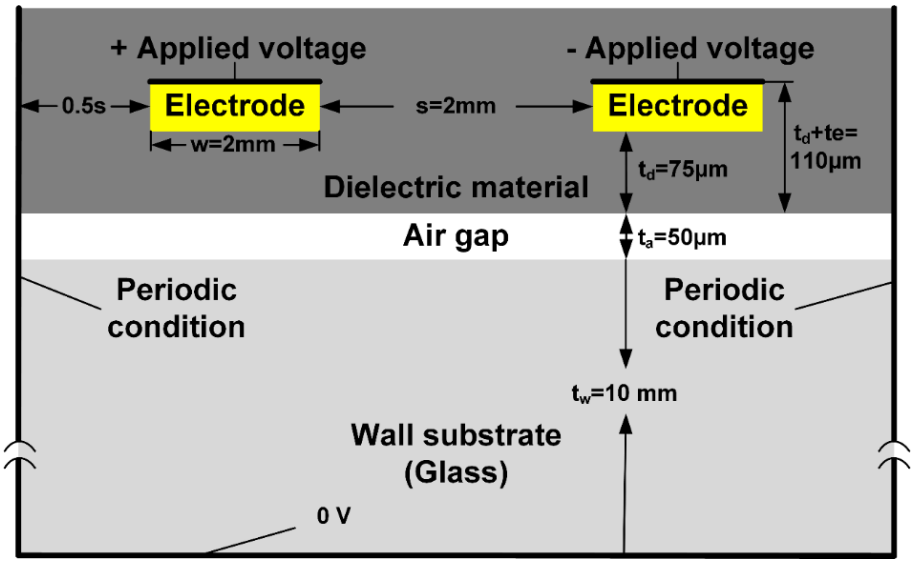

Figure 4-14 2D electrostatic model diagram

In the diagram, w denotes the electrode width (pre-set as 2 mm), s denotes the space between electrodes (pre-set as 2 mm), t_d denotes the thickness of the dielectric layer (pre-set as 0.075 mm), t_e denotes the thickness of the copper electrodes (pre-set as 0.035 mm), t_a denotes the thickness of the air gap layer (pre-set as 0.05 mm), t_w denotes the thickness of the glass substrate (pre-set as 10 mm). The dielectric constant of the dielectric material and glass substrate were pre-set as 11.7 and 4.2 respectively. The applied voltage was pre-set as 6000 V and applied on both electrodes. The bottom of the wall substrate was grounded and set to 0 V. Since interdigital electroadhesive pads usually have periodical electrode arrays, periodic conditions are applied.

It can be seen from Figure 4-15 that the electrode thickness has little effect on

the electroadhesive forces obtainable. This supports the aforementioned assumption that the thickness of electrodes is negligible was reasonable. It can be concluded from Figure 4-16 that the smaller the air gap the larger the forces obtainable.

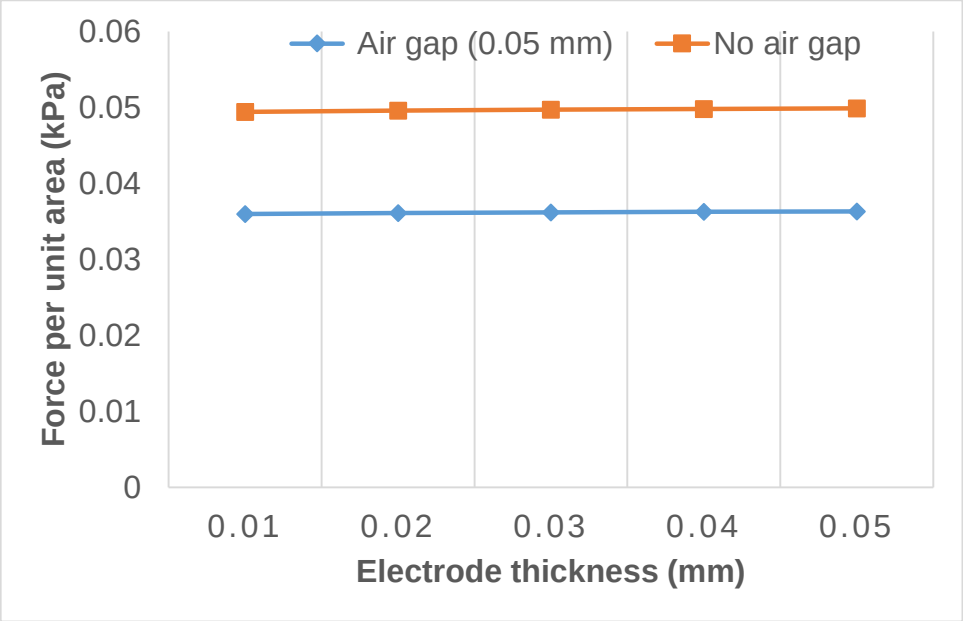

Figure 4-15 Electrode thickness vs electroadhesive force

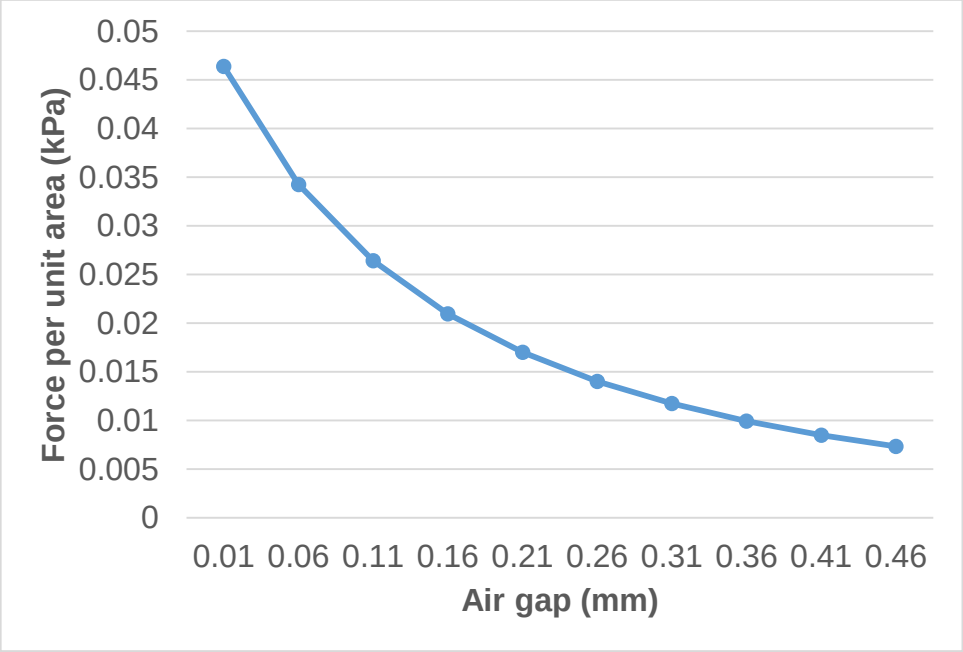

Figure 4-16 Air gap vs electroadhesive force

From Figure 4-17 to Figure 4-21, the result of the 2D model with an air gap and without has similar trends but the forces without an air gap are larger than with an air gap. It can be seen in Figure 4-17 that the force increases quadratically with the increase of the applied voltage, which is similar to the theoretical analysis. The dielectric thickness seems to have little effect on the electroadhesive forces obtainable when it changes from 0.01 mm to 0.1 mm, as can be seen in Figure 4-18. The space between electrodes should be as small as possible, similar to the theoretical result. It is interesting to note that, however, the electroadhesive force obtainable is almost the same with and without an air gap when the space is larger than 8 mm (see Figure 4-19). The dielectric constant of the dielectric layer seems to have less effect on the electroadhesive forces obtainable, as shown in Figure 4-20, compared with the theoretical results. The effect of the substrate dielectric constant on the force obtainable is slightly different with and without an air gap, as shown in Figure 4-21. It is important to note the different trend shown in Figure 4-22, where the maximum force is obtained at electrode width of 2 mm with an air gap, although, in general, the forces without an air gap are larger than with an air gap.

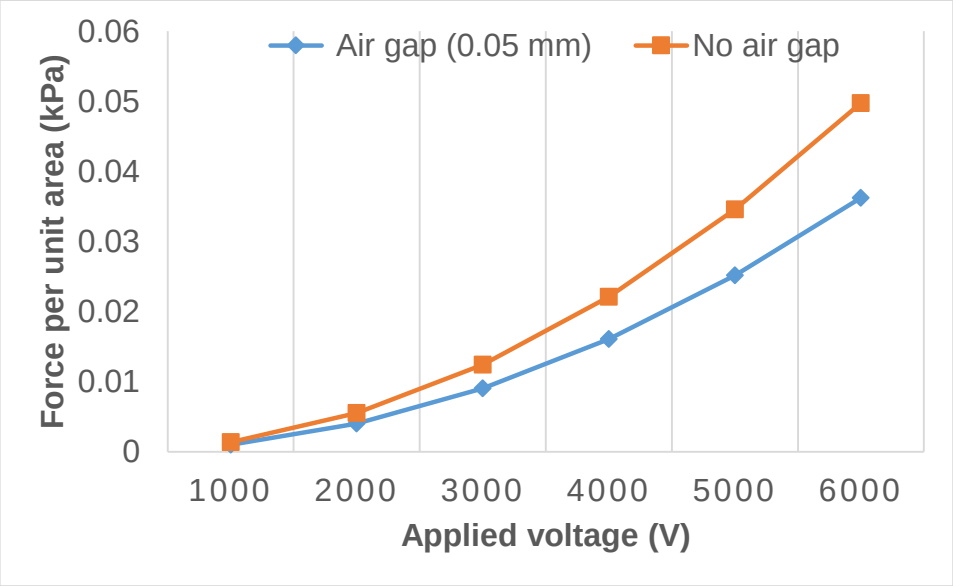

Figure 4-17 Applied voltage vs electroadhesive force

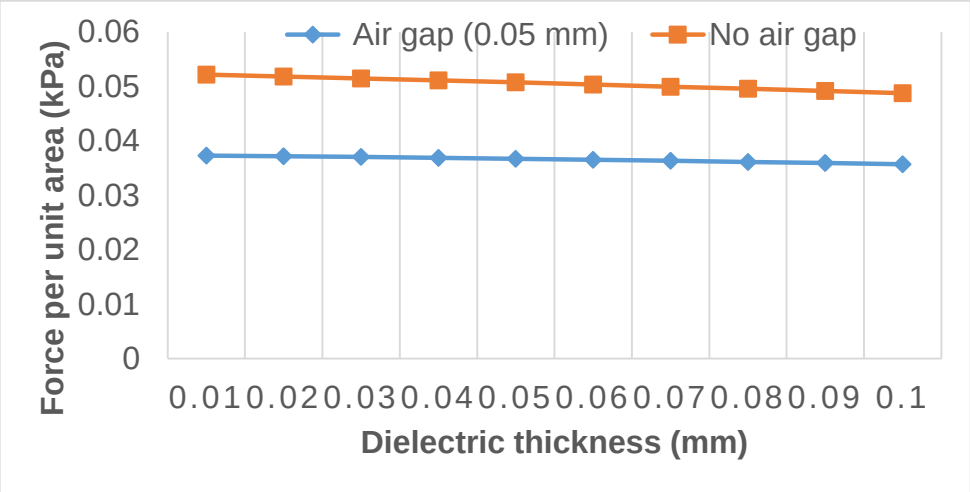

Figure 4-18 Dielectric thickness vs electroadhesive force

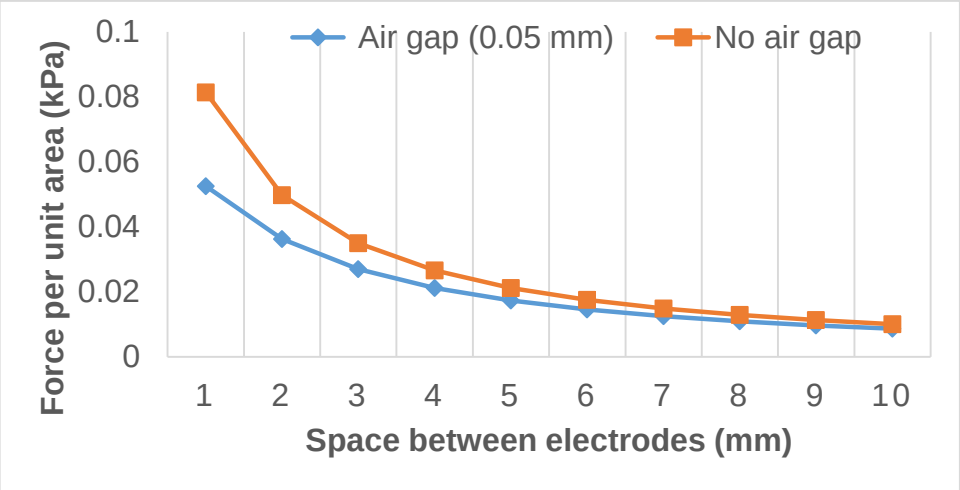

Figure 4-19 Space between electrodes vs electroadhesive force

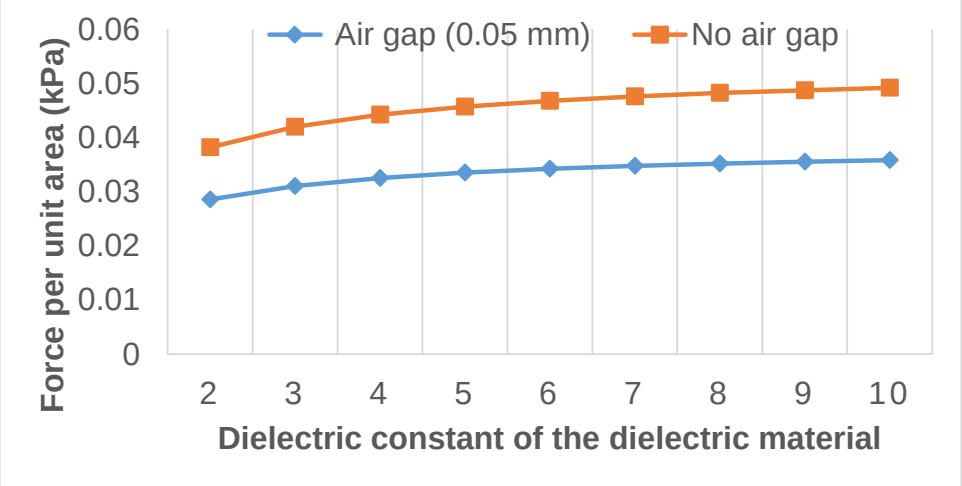

Figure 4-20 Dielectric constant of the dielectric material vs force

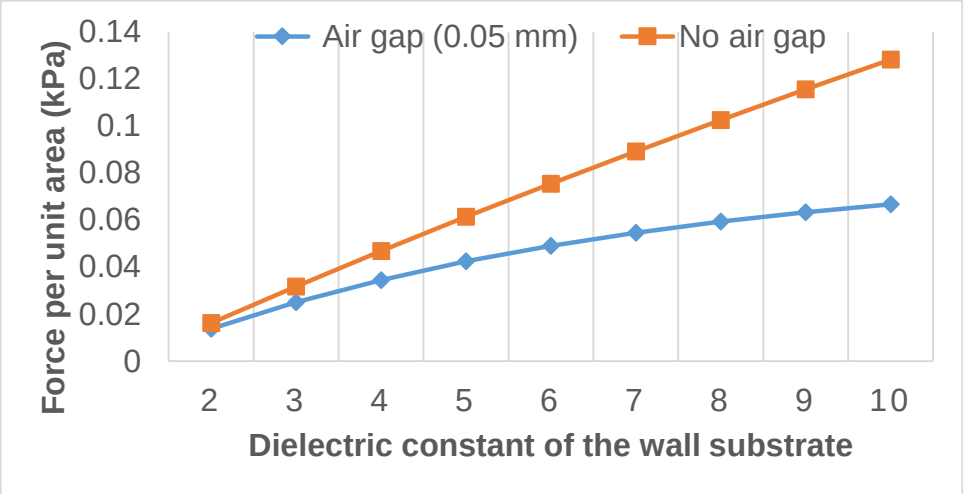

Figure 4-21 Dielectric constant of the wall substrate vs force

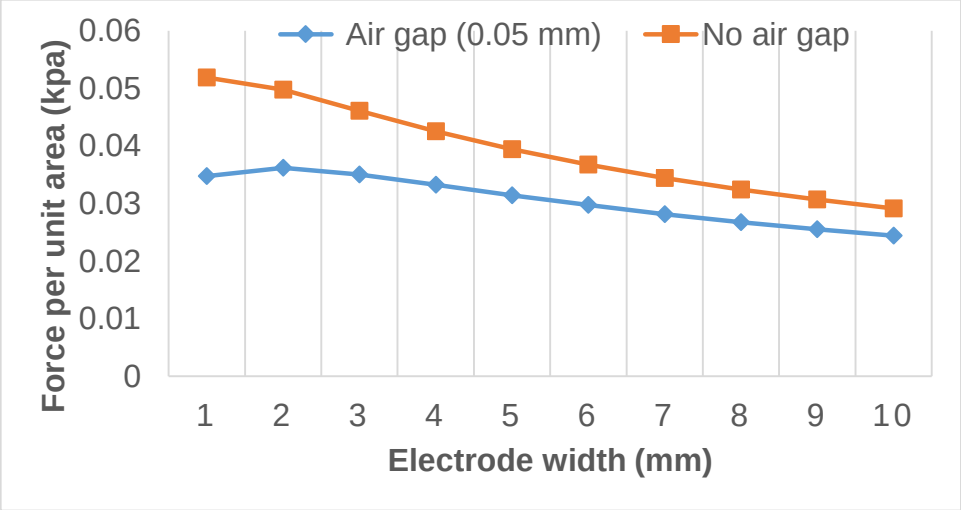

Figure 4-22 Electrode width vs electroadhesive force

For the 2D electrostatic simulation model without an air gap, it can be seen from Figure 4-23, Figure 4-24, and Figure 4-25 that:

● for thinner wall substrates, where the thickness is equal to or smaller than 1.7 mm, the larger the electrode width, the larger the forces obtainable;

● for thicker wall substrates, where the thickness is equal to or greater than 2.2 mm, the smaller the electrode width, the larger the forces obtainable;

● for thicker wall substrates, where the thickness is between 1.8 mm and 2.1 mm, the optimum electrode widths of approximately 2.7 mm, 2.3 mm, 1.6 mm and

1.9 mm can be found.

In addition, the difference in the electroadhesive forces obtainable is relatively small when changing the electrode width from 1 mm to 3 mm in all cases. On non-conductive materials, in order to have more boundaries, we usually choose smaller electrode widths. Please note that all the above results were based on a fixed space between the electrodes (1 mm).

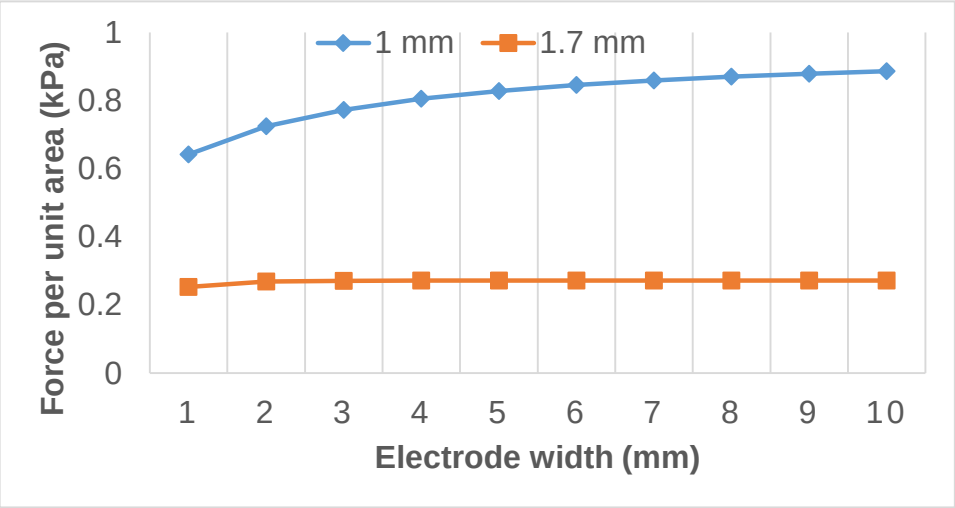

Figure 4-23 The relastionship between forces and electrode widths under no air gap and wall thicknesses of 1 mm and 1.7 mm

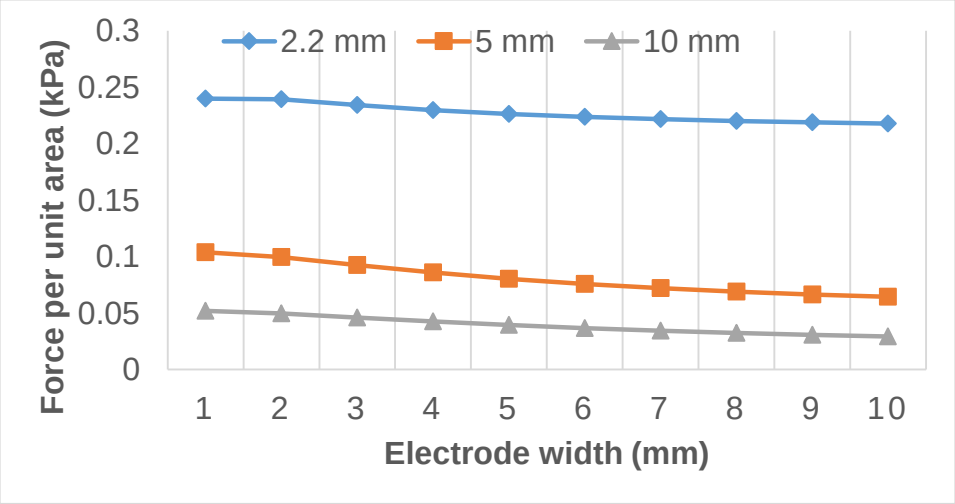

Figure 4-24 The relastionship between forces and electrode widths under no air gap and wall thicknesses of 2.2 mm, 5 mm, and 10 mm

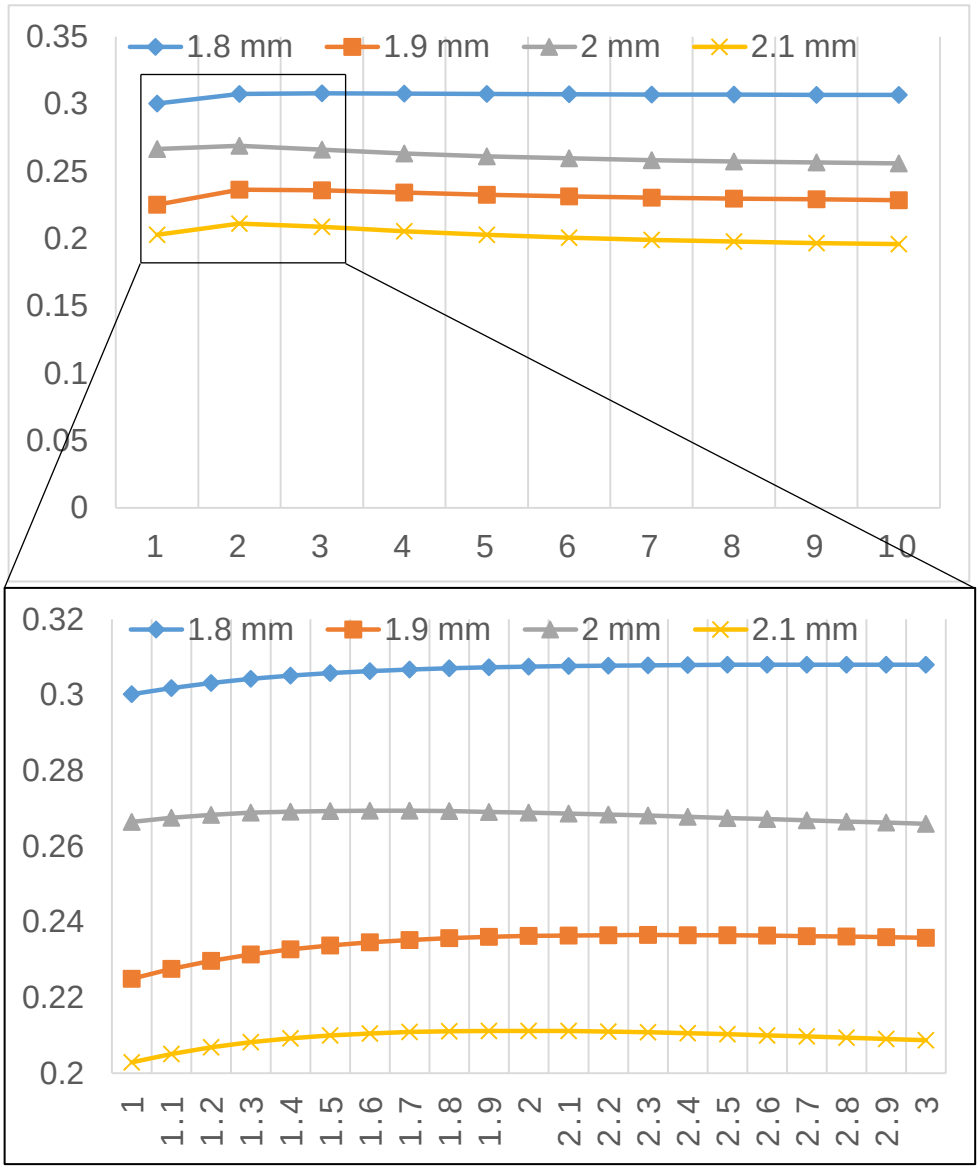

Figure 4-25 The relastionship between forces and electrode widths under no air gap and wall thicknesses of 1.8 mm, 1.9 mm, 2 mm, and 2.1 mm

For the 2D electrostatic simulation model with an air gap, it can be seen from Figure 4-26 and Figure 4-27 that:

● for thinner wall substrates, where the thickness is equal to or smaller than 2 mm, the larger the electrode width, the larger the forces obtainable;

● for thicker wall substrates, where the thickness is equal to or greater than 3 mm, an optimum electrode width of approximately 2 mm can be found.

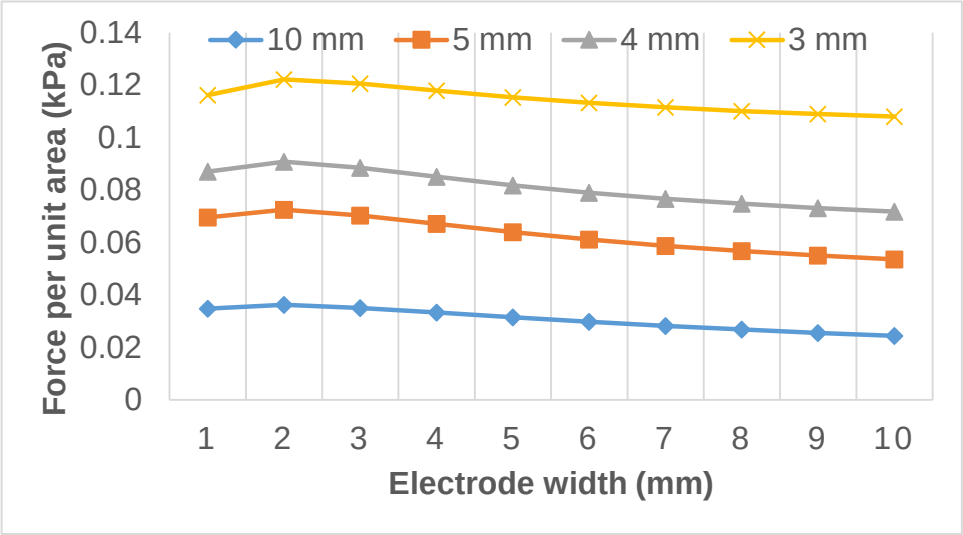

Figure 4-26 The relationship between forces and electrode widths under an air gap and wall thicknesses of 3 mm, 4 mm, 5 mm, and 10 mm

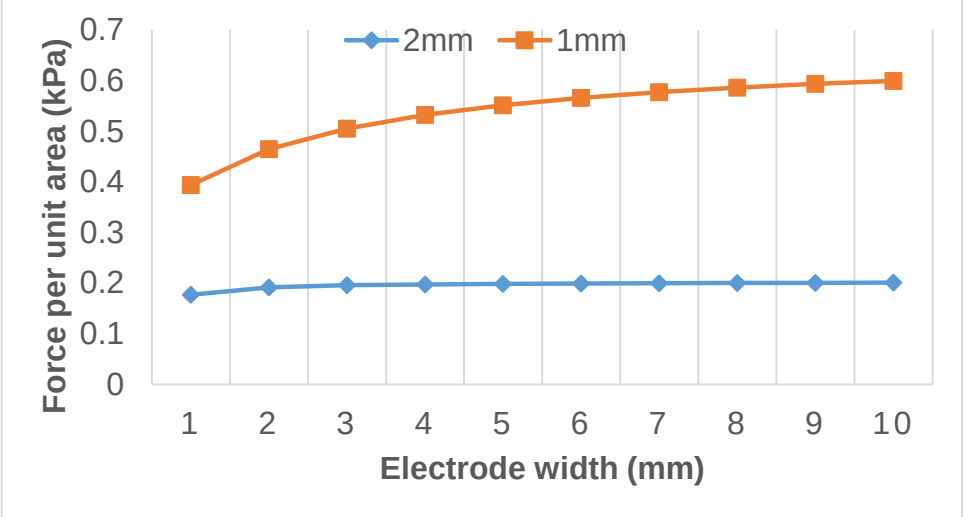

Figure 4-27 The relationship between forces and electrode widths under an air gap and wall thicknesses of 1 mm and 2 mm

It has to be noted that all the above simulation results were based on considering the polarisation of the whole substrate, i.e. the surface average of the whole substrate. If only the interfacial effect is considered, i.e. the line average of the contacting surface between the pad and the substrate, as shown in Figure 4-28, the results demonstrate that the smaller the electrode width the larger the forces obtainable regardless of the thickness of the wall substrate. The results

presented in Figure 4-28 was based on a wall thickness of 2 mm.

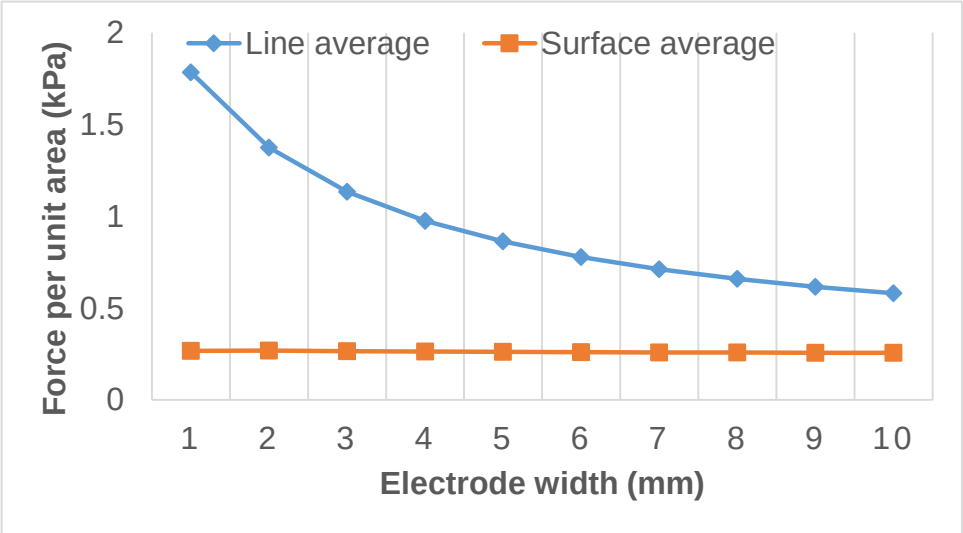

Figure 4-28 The difference between the line average method and the surface average method

4.6 Experimental validation

4.6.1 Experimental set-up and equipment

A repeatable electroadhesive pad design, manufacture, and testing platform (Figure 4-29) has been established and used for the fundamental research to understand the electroadhesion phenomenon in EPSRC Centre for Innovative Manufacturing in Intelligent Automation at LU. Pad designs were conducted in Solidworks. The rationale of the pad design is described in section 4.6.3. The pad manufacturing process was inspired by professional flexible printed circuit board techniques and based on a Xerox solid ink printer, ferric chloride granules and a chemical bubble etching tank, conformal coating, and dielectric degassing and curing based on a vacuum oven. The details of the pad manufacturing process are depicted in section 4.6.3, 5.4.4, and 6.6.1. The pad testing platform and procedure was based on a reconfigurable and mechatronic setup containing mainly a linear rail to enable vertical and horizontal movement and an ATI force/torque sensor to record the obtainable forces. The details of the pad testing platform and procedure are demonstrated in section 4.6.4, 5.4.4, and 6.6.2.

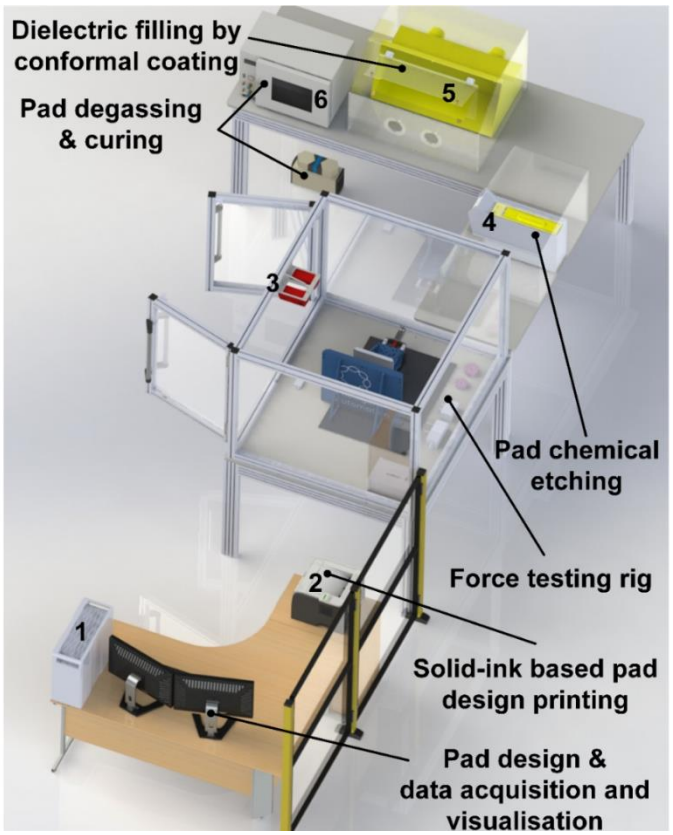

Figure 4-29 The electroadhesive pad design, manufacture, and testing platform at LU

4.6.2 Safety considerations

As stated in section 2.1.6, safety considerations are necessary before pad manufacture and testing due to the risks from the failure of the electroadhesion phenomenon. For a normal human body path, 10 mA is considered the maximum safe current (at 50 Hz). Although the current runs through the elelctroadhesive pad is in the range of μA to mA, an electrical safety interlock system or safety screens are still required [131]. Although safety considerations are nothing to do with academic research, great care has been taken in the electroadhesion research at LU, not only on pad manufacturing based on chemical etching and conformal coating but also on pad testing. Risk assessments are suggested to be completed before any electroadhesive pad manufacture and testing. This can be seen in Figure 4-29, where a glove box in enclosing two spray booths and an electrical safety interlock system have been used.

4.6.3 Electroadhesive pad design and manufacture

The pads were designed using Solidworks (see Figure 4-30) and based on the following two equations

$$L_1 = T + (2N - 1)(w + s) + w \quad (4\text{-}29)$$

and

$$L_2 = 2(G_1 + G_2) + L \quad (4\text{-}30)$$

where L_1 is the total effective length of the pad, L_2 is the total effective width of the pad, L is the electrode overlap length, G_1 is the width of electrode connection, G_2 is the space between connection line and comb fingers, w is the electrode width, s is the space between electrodes, N is the number of electrode pairs, and T is the tail that can be used for the connection to the high voltage supply.

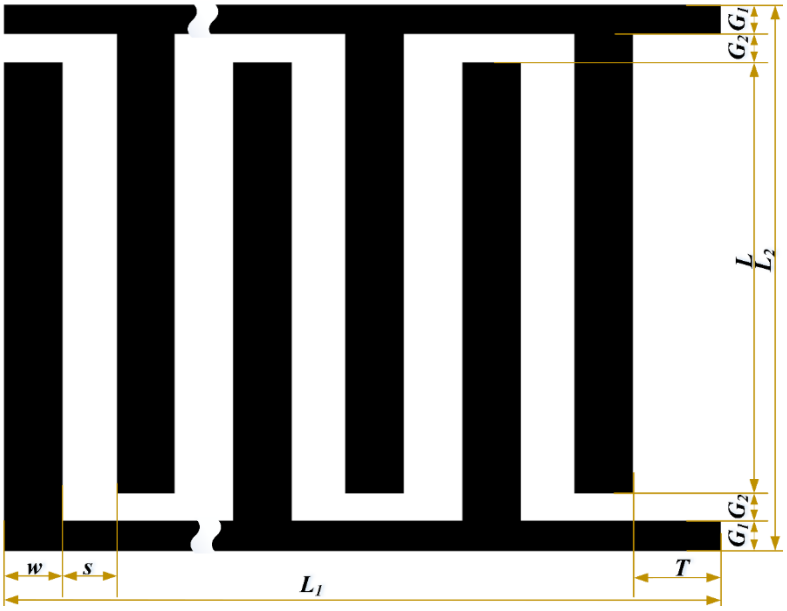

Figure 4-30 Interdigital coplanar electroadhesive pad design

Since it is clear that the dielectric thickness of the dielectric layer should be as small as possible, only the electrode width and space between electrodes was

varied. In order to make all the pad designs the same effective pad area, we therefore set T = 40 mm, L_1 = 270 mm, L_2 = 170 mm, L = 150 mm, and G_1 = G_2 = 5 mm. For the investigation into the relationship between electrode widths and obtainable electroadhesive force, all the other geometrical parameters were maintained (s = 1 mm). Five pads that have different electrode widths were selected. For the investigation into the relationship between the space between the electrode and the electroadhesive force obtainable, all the other geometrical parameters were maintained (w = 4 mm). Five pads that have different spaces between electrodes were selected. The geometric information of these ten pads can be seen in Table 4-1. The selection of the pads were based on the fact that the number of electrode pairs is integral and the difference range can be between 0 mm to 10 mm. The designed pads were then professionally manufactured using the procedures presented in Figure 4-31. The professional manufacturing method is envisioned to bring repeatable and high quality pads. The copper electrode thickness was set as 18 μm, the PI base (dielectric constant: 3.2) thickness was set to 12.5 μm including an unknown thickness of adhesive and the PI coverlay was a combination of a 12.5 μm PI (dielectric constant: 3.8) with a 15 μm adhesive.

Table 4-1 Geometric information of the pads for Chapter 4

Electrode width (mm)	Electrode space (mm)
0.9	1
1.9	1
3.8	1
5.3	1
9.6	1
4	9.3
4	6.8
4	5
4	3.8
4	2.9

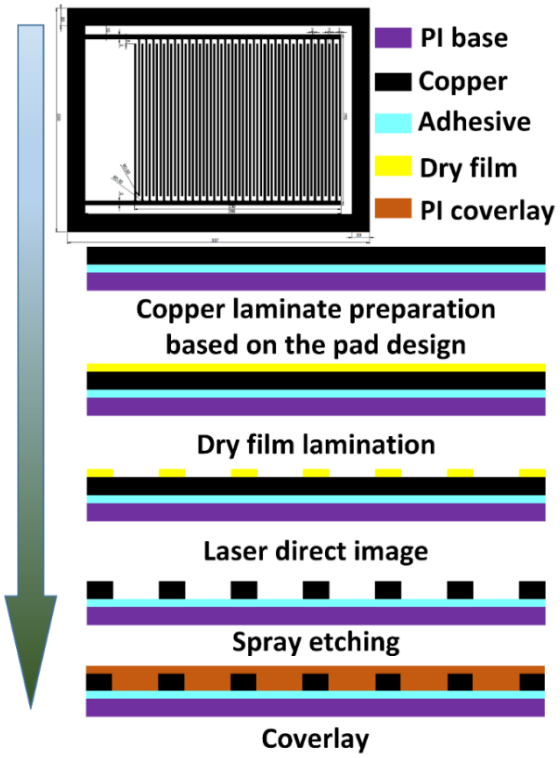

Figure 4-31 Pad manufacture procedure for Chapter 4

4.6.4 Electroadhesive force measurement

A bespoke mechatronic and reconfigurable electroadhesive force measurement platform was used to obtain the normal electroadhesive forces between the pad and substrates. The system diagram can be seen in Figure 4-32 (a), where a 6-axis ATI Gamma Force/Torque (F/T) sensor (resolution: +/- 0.05 N) was used to record the electroadhesive forces. The communication between the F/T sensor and the computer was through a netbox via an Ethernet cable and the data was selected to be sampled at 152 Hz. The reason why 152 Hz was selected was because the frequency was compatible to an IMU sensor worked together with the F/T sensor for another purpose. The reason why 152 Hz was selected was because the frequency was compatible to an IMU sensor worked together with the F/T sensor for another purpose. The linear rail can achieve vertical movement using a servo motor with encoder driven by a Kollmorgen motor driver connected with a CompactRio. This allows almost real time control of the linear rail via a Xilinx FPGA which is designed to communicate with the computer via Ethernet.

The smallest movement of the linear rail is approximately 0.8 μm. The pad was connected with two EMCO high voltage converters (HVC) with (±) 0 - 10 kV output and 0 - 5 V reference input. The reference input was from a direct current power supply unit, Instek GPD3303, which was designed to communicate with the computer through via a USB. The physical measurement platform can be seen in Figure 4-32 (b). A Labview interface was developed for interactive control of the movement of the linear rail, changing the supply voltage, recording, and saving the electroadhesive force data. Please note that electrical safety interlock system and safety screens were applied in this advanced measurement platform [140].

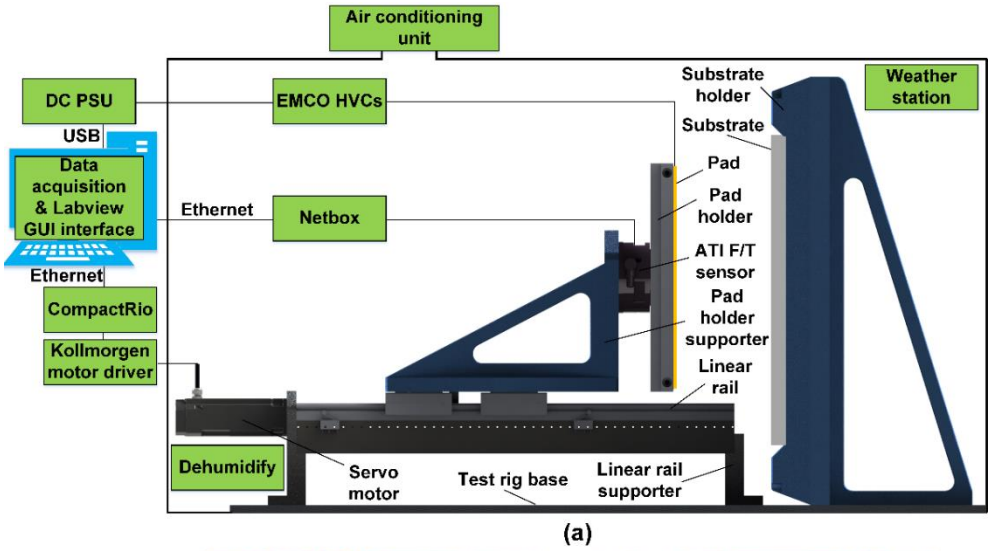

(a)

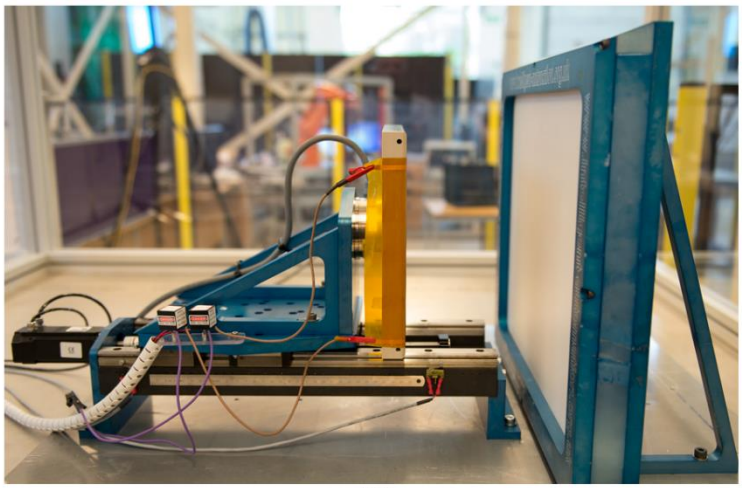

(b)

Figure 4-32 Electroadhesive force measurement platform: (a) system diagram and (b) physical set up

For each pad, the experiments were repeated 5 times. The electroadhesive force measurement procedures can be seen in Figure 4-33. The pad was initially attached on the pad holder. The substrates were fixed properly such that the position of the different substrates was guaranteed to be the same with respect to the pad. A 30 $\pm$ 1 N preload was then applied on the substrates. The recording of the electroadhesive force was then started by turning on the power supply, thus providing power to the pad. The pad was charged for 60 seconds. After this, the pad was pulled away by activating the servo motor. When the motor stopped, the data recording was completed and the data exported as text files. These files were further filtered and analysed in MATLAB. The next experiment was set to be conducted after 540 seconds of waiting. The start of this lag time was at the commencement of the pulling away of the pad.

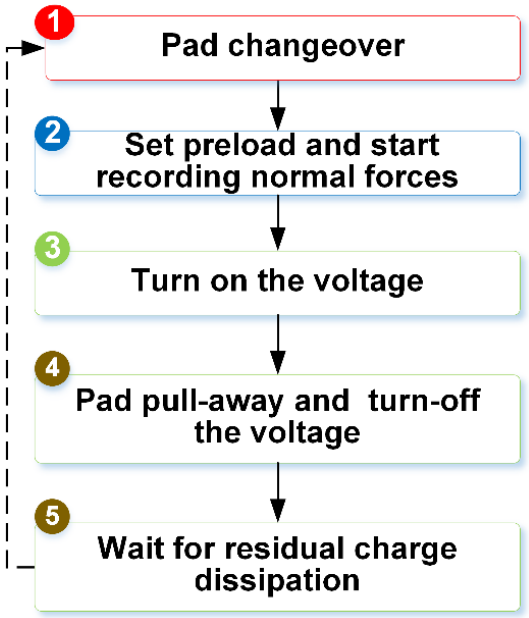

Figure 4-33 Electroadhesive force measurement procedures

The dwell time was useful for residual charge dissipation. During the residual charge dissipation process, the pad was grounded for 300 seconds after each test. Also, the aluminium (Al) substrate was grounded for 300 seconds each time before the pad was changed. An electrostatic fieldmeter, FMX-003, mounted on Kanya frames, was used to compare the surface charge value of the plate before

applying the voltage and after the grounding. 300 seconds were enough to obtain similar results with less than 5% difference. Also, each time after applying the preload, little difference was observed after 10 seconds' stabilising. A fixed experiment time of 10 minutes (540 seconds plus 60 seconds) for each test was therefore set for this investigation. The motor pull-off velocity (0.1 mms^{-1}) and pull-off acceleration (50 $revs^{-2}$), charge time (60 seconds) and discharge time (540 seconds) were maintained at constant values when conducting the experiments.

Within the research laboratory, where the fundamental research was undertaken, it has been recorded that the lab temperature changed from 17 °C to 28 °C, relative humidity changed from 28 % to 73 % and air pressure changed from 996.3 hPa to 1015.2 hPa between January and August 2015. Preliminary experimentation was carried out and results have been obtained over a three day period. All variables were controlled except the temperature (22.1 °C - 23.7 °C), relative humidity (44 % - 56 %) and air pressure (1002 hPa - 1009 hPa). A relative difference in force of almost 100% was observed, see Figure 4-34 (a).

A relative difference in force of nearly 200% (see Figure 4-34 (b)) was obtained by a further 5-day experiment based on a different pad design when the temperature (20.8 – 21.5 °C), relative humidity (43 – 64 %), and air pressure (993.8 – 1013 hPa) were not stable. I believe this is a reason that hinders the application of electroadhesive solutions in ambient industrial environments where unstable and unpredictable forces may be achieved. In addition, because of this, it is required to conduct the experiment in a stable environment. All the tests for the 10 pads were therefore performed in a custom built environmental chamber (made of insulating foams), where an air conditioning unit and a dehumidifier were employed to main the temperature and humidity. Due to the use of the environmental enclosure, the temperature was maintained at 25 °C ± 0.2 °C, humidity at 32 % ± 2 %, and pressure at 1013 hPa ± 1 hPa.

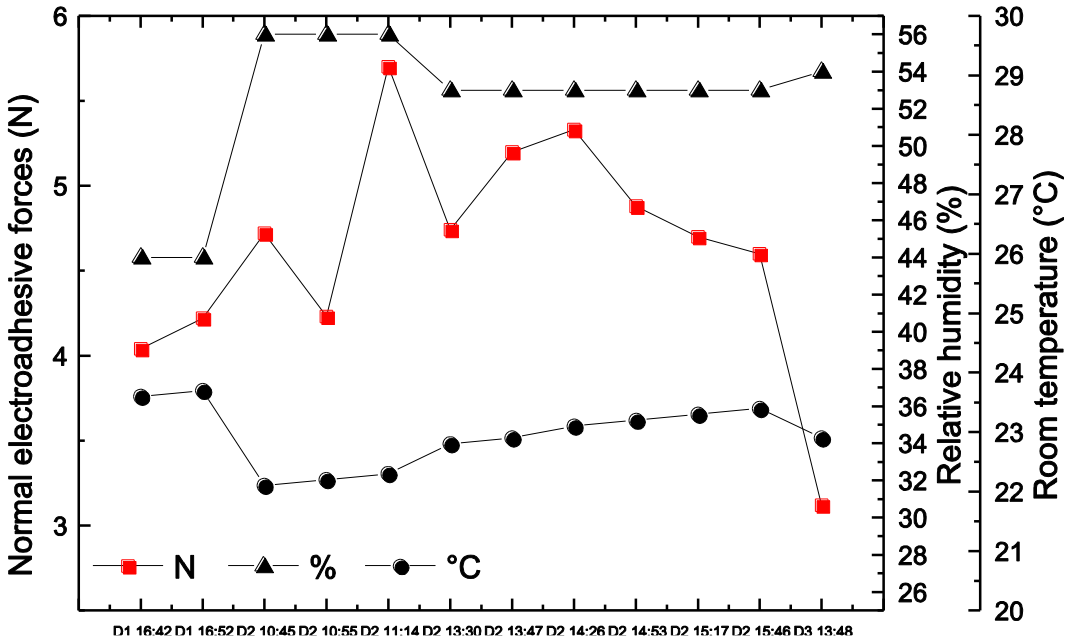

(a)

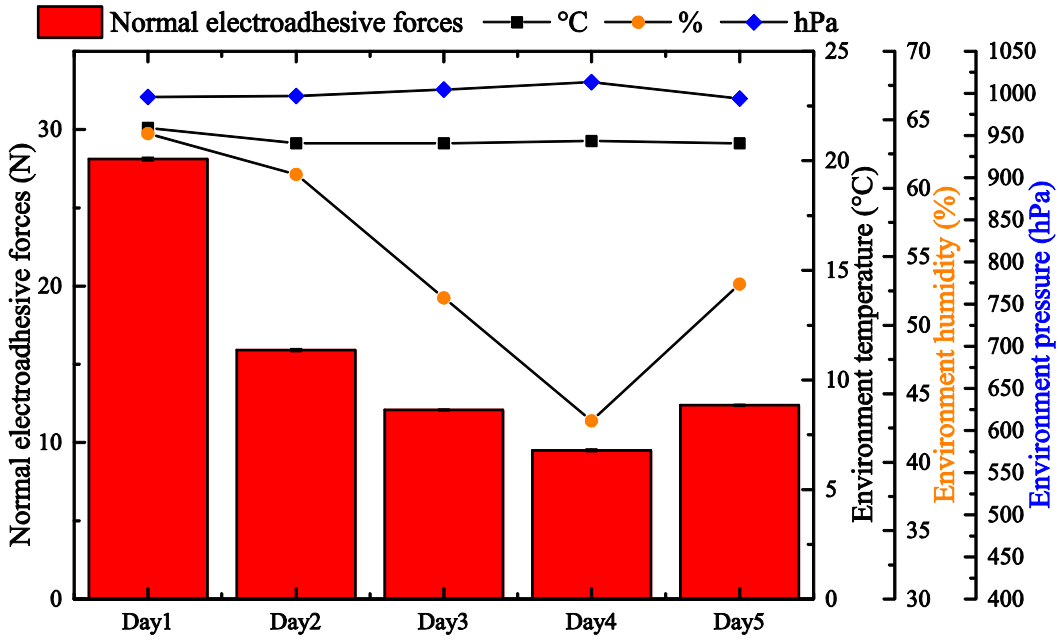

(b)

Figure 4-34 The electroadhesive forces obtained in different environmental conditions: (a) a 3-day and (b) a 5-day experiment

4.6.5 Results

The electroadhesive forces were recorded when the PI base side of the pads was facing the toughened glass and the aluminium (Al) plate. 2 kV was applied on the pads. Before each test, the force with no voltage applied was recorded to check the potential suction forces, Van der Waals forces, and surface tension

forces mentioned in section 2.2.2. Little normal forces (not more than 0.05 N for all the pads) were observed when no voltage was applied. This is thought to be due to the microscopic surface features of the contacting surfaces between the PI base side and the smooth glass and Al plate. This means the forces recorded under a voltage are predominately normal electroadhesive forces.

The experimental results manifesting the relationship between the electroadhesive forces obtainable and the spaces between electrodes can be seen in Figure 4-35. For both conductive substrates, such as the Al plate, and non-conductive substrates, such as the toughened glass plate, the smaller the space between electrodes, the larger the electroadhesive forces obtainable. The experimental results manifesting the relationship between the electroadhesive forces obtainable and the electrode widths can be seen in Figure 4-36. For non-conductive substrates, such as the toughened glass, there is indeed an optimum electrode width, approximately 1.9 mm, when the space between electrodes was fixed at 1 mm. For conductive substrates, such as the Al plate, the electrode width should be as large as possible to achieve larger force per unit area.

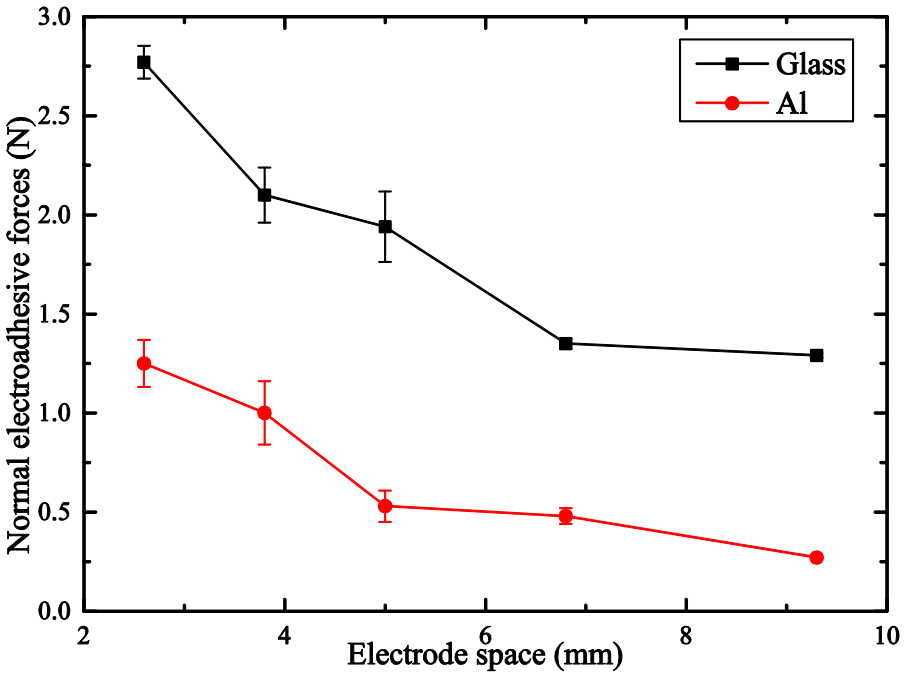

Figure 4-35 Experiment results on forces vs spaces between electrodes

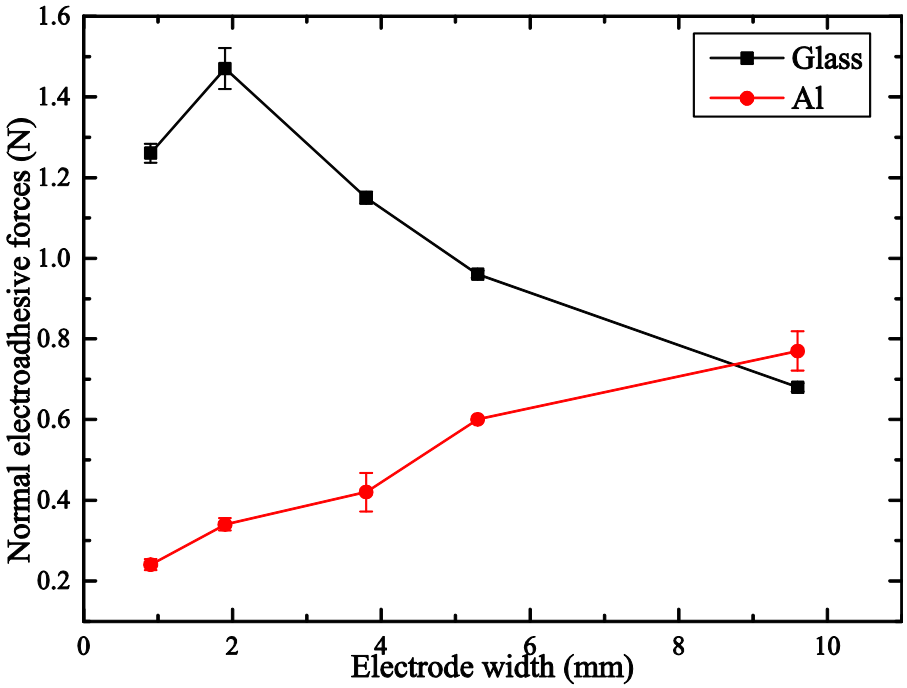

Figure 4-36 Experiment results on forces vs electrode widths

4.6.6 Discussion

Few researchers have experimentally validated their theoretical and simulation results. This is due to the fact that it takes quite a large amount of time and money to implement a confident pad design, manufacture, and testing platform and procedure, and conduct the experiments. The comparison between the theoretical and experimental results can be seen in Figure *4-37* and Figure 4-38. This is adapted from the results demonstrated in Figure 4-35 and Figure 4-8, and Figure 4-36 and Figure 4-7. The comparison results presented in Figure 4-37 and Figure 4-38 show that there is a good agreement between the theoretical and experimental results in terms of the general trend.

Although it has been experimentally and theoretically validated that there is an optimum ratio between the electrode width and the space between electrodes for the electroadhesive pad to achieve the maximum forces on insulating substrates, it has to be noted that there is a clear deviation between the experimental and theoretical results. This may due to the air layer between the pad and the substrate and system errors/noises during the experiment. Advanced theoretical

modelling considering the surface texture information of the pad and the substrate, and environmental factors requires further investigation. Also, the propose model is based on static analysis. The electroadhesion phenomenon, however, is dynamic, dynamic theoretical modelling of electroadhesives considering the dynamic polarisation and de-polarisation process, and the un-uniform electric field distribution in nature needs further investigation. In addition, a comparison of existing theoretical models is needed.

With regard to the electrostatic simulation modelling, as finite element method has an inherent drawback solving high-aspect ratio systems, novel methods should be investigated. There is little work on advanced simulation modelling considering the surface texture information of the pad and the substrate, material properties of the pad and substrate, and environmental factors. It is useful to conduct an advanced simulation to investigate the dynamic polarisation and de-polarisation process of the electroadhesive system before theoretical modelling.

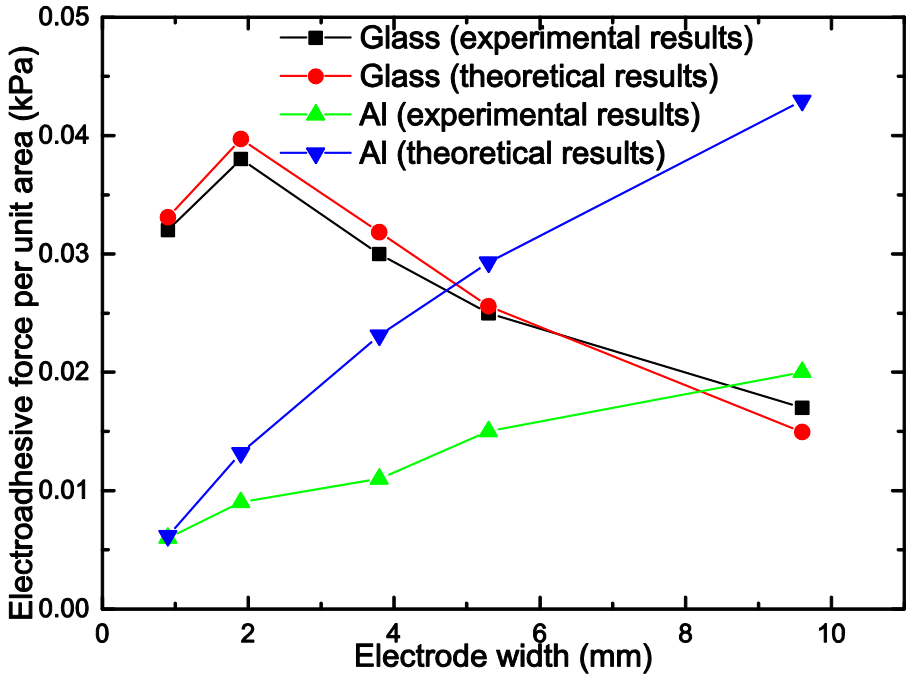

Figure 4-37 Comparison between the theoretical and experimental results on forces vs electrode widths

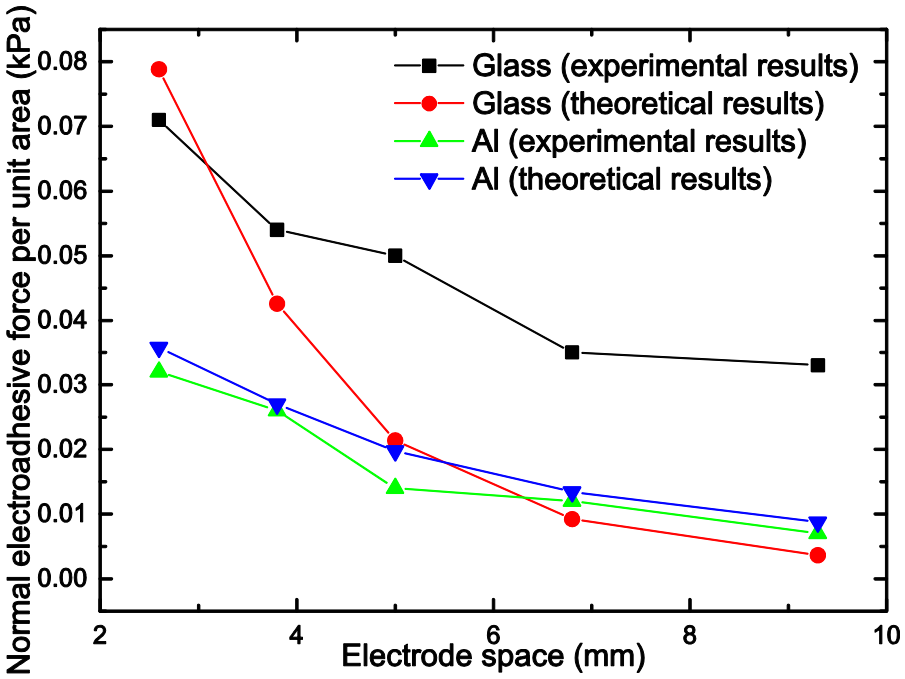

Figure 4-38 Comparison between the theoretical and experimental results on forces vs spaces between electrodes

Empirical modelling, based on the employment of the Taguchi method for design of experiments to less the number of experiments, is maybe a promising way to produce an accurate model that can predict the performance of the electroadhesive pad, such as the relationship between the applied voltage and the electroadhesive force. This is because it will be challenging to both simulation and theoretical modelling of the high voltage based dynamic polarisation and de-polarisation process. In order to achieve an accurate empirical model, a highly controlled and confident pad testing platform and procedure is definitely needed to minimise the errors/noises.

For academic researchers who want to study electroadhesion, the results highlight that it is important to have a controlled and confident pad testing platform and procedure to validate the models. Also, the need for advanced modelling of the electroadhesion phenomenon is identified.

For industrialists who want to commercialise electroadhesive products, the result has identified the need for the investigation into environmentally stable

electroadhesives by careful dielectric material design and selection. Environmentally stable and optimised electroadhesives will greatly promote the commercial electroadhesive applications. Ceramic materials may help with the implementation of environmentally stable electroadhesives.

4.7 Summary

This Chapter has presented the development of a simplified and novel theoretical optimisation modelling of coplanar interdigitated electroadhesives and its experimental verification. This is the first experimentally validated theoretical model on electroadhesion in terms of the trend, especially that there is an optimum electrode width, when the space between electrodes is fixed, for interdigital coplanar electroadhesives. The following conclusions can be made:

● The results demonstrated in Figure 4-34 not only highlight the importance of controlling the environment when testing the pads to validate the models but also identifies the need for the investigation of environmentally stable electroadhesives.

● The proposed simplified and computationally easier theoretical optimisation modelling of coplanar interdigitated electroadhesives is promising to predict the performance of interdigitated electroadhesive pads. This was validated by the experimental results both on conductive substrates, such as the Al plate, and on non-conductive substrates, such as the glass. For both conductive substrates, and non-conductive substrates, the smaller the space between electrodes, the larger the electroadhesive forces obtainable. This agrees with all the theoretical and simulation results have been reported. On the Al plate, the larger the electrode width, the larger the effective pad area, thus the larger the forces obtainable. This means, for conductive substrates, the electrode width should be as large as possible to achieve larger effective pad area thus larger force per unit area. On the glass plate, however, there is an optimum electrode width of approximately 1.9 mm when the space between the electrodes as fixed at 1 mm.

● The proposed 2D electrostatic simulation results showed that the wall thickness and air gap have a large bearing on the optimum widths achievable. The consideration of only the interfacial electric fields and the electric fields within the whole substrate generated different results. If one only considers the interfacial electric fields, the smaller the electrode width, the larger the forces obtainable regardless of the effect of the wall thickness. If one considers the electric fields within the whole substrate, an optimum electrode width can always be found. This may be the reason why the existing simulation results have difference conclusions.

It has been identified that the surface texture play an important role in accurate modelling of electroadhesion. This is further investigated in Chapter 5.

5 Investigation of the Relationship between the Electroadhesive Force and Surface Texture

5.1 Introduction

Surface texture plays an important role in the electroadhesive forces obtainable [20][63][72]. In Chapter 5 the need for a systematic investigation into the relationship between the electroadhesive forces obtainable and different surface textures is identified. A novel and recognised research methodology for the systematic investigation is then provided. After this, an advanced electroadhesive force measurement platform and procedure, together with a recognised areal-based non-contact surface texture measurement platform and procedure have been used to conduct the investigation and obtain the relationship.

5.2 The research need

Understanding the surface textures of contacting surfaces is of great importance to any contact phenomenon such as the contact between an electroadhesive pad and a substrate. Both the pad and substrate surface textures may influence the effective contact area, air gap and air pressure between the pad and substrate. This will, as aforementioned in section 3.8, influence the electroadhesive forces obtainable. As such, it is necessary to take surface texture information into consideration.

The seminal work considering surface texture (surface roughness) as an influencing factor on the obtainable electroadhesive forces between an electroadhesive pad and a wall substrate can be found in the work completed by Krape [1], where a randomly scratched and gouged circular electrode plate was employed and a 44.4 % decrease in shear forces, compared with a smooth substrate surface, was obtained in ambient temperature and pressure. However, no quantification of surface roughness parameters were reported and only two

substrates were used. The profile parameter, arithmetic average of the roughness profile, *Ra*, was employed by Téllez et al. to quantify different substrate materials by using a surface profilometer [63]. However, the same substrate material with different surface textures is required to systematically investigate the relationship between interfacial electroadhesive forces and surface textures as the substrate material itself will greatly influence the obtainable electroadhesive forces. Therefore, *Ra* may not be good enough to represent the full contacting surfaces. The most recent work by Ruffatto et al. selected 14 different tiles with different surface textures to exhibit the improved performance of their proposed hybrid electroadhesive pad on rough surfaces [72]. However, no distinctive conclusions were made for the relationship between obtainable electroadhesive forces with different surface textures alone. Additionally, only some of the possible surface profiles obtained by a profilometer were applied [72]. Further inspection by Ruffatto et al. found that a single profile value was difficult to characterise the surface texture fully [72]. Although the work published by Koh et al. [20] stated the importance of surface roughness in the electroadhesive forces obtainable, only a profilometer and average *Ra* of five profiles were used to characterise the substrate surfaces and no result concerning how surface texture influences the electroadhesive forces was reported.

A systematic research methodology, investigation platform and procedure are therefore needed to understand the relationship between the electroadhesive forces obtainable and different surface textures. This will enable new insights into understanding electroadhesion and for more advanced and accurate electroadhesion modelling in the future.

5.3 Research methodology

The aim of this chapter is to identify how substrate surface textures will influence the electroadhesive forces generated on those substrates. To this end, four major

stages have been addressed, as identified in Figure 5-1.

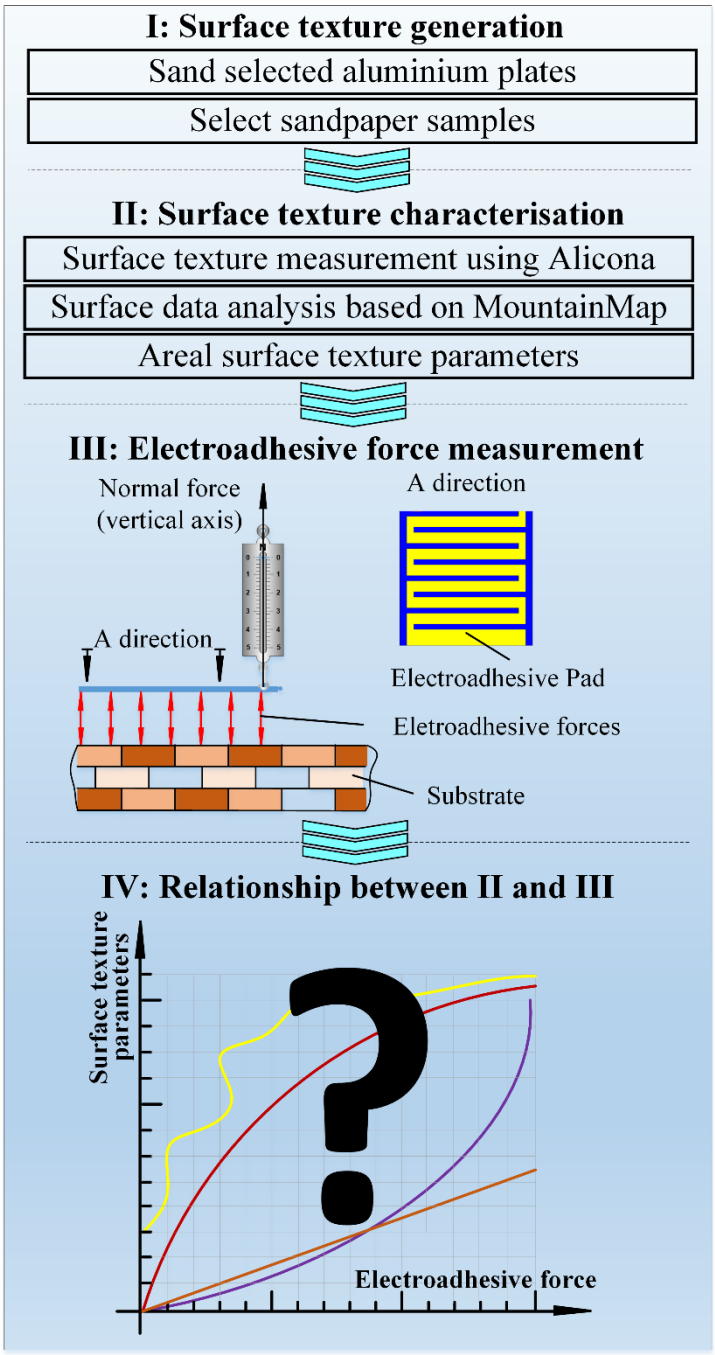

Figure 5-1 Research procedure for the investigation of the relationship between the electroadhesive force and surface texture

The first stage of this research was to generate a range of different surface textures by sanding Al plates (type: grade 1050) and using silicon carbide sandpaper samples with grit designations of P120, P400 and P1200 directly. Following this, surface texture measurements and quantification of those

surfaces were conducted using Alicona InfiniteFocus and DigitalSurf MountainMap (v5) respectively. The areal surface texture parameter, *Sq*, root mean square height of the surface, will be used in this chapter to quantify the surface texture. Alicona is a non-contact surface texture measurement platform based on focus variation [141] and MountainMap is a common commercial surface texture data analysis software widely used in research and industries [142]. Once the characterisation of the surfaces was completed, the electroadhesive forces were measured using the advanced electroadhesive force measurement platform and procedure as described in section 5.4.5. Finally, the correlation between electroadhesive forces and surface textures was identified and is presented in section 5.5.

5.4 Relationship between the electroadhesive force and surface texture

5.4.1 Substrate preparation of the different surface textures

As sandpaper samples can bring a large range of different surface roughnesses, three A4 size silicon carbide sandpaper samples were selected, with grit designations of P120, P400 and P1200. Four similar smooth circular Al plates, with a thickness of 1 mm and a diameter of 275 mm, were selected to act as the conductive substrate and to further investigate the effect of the direction of surface textures on the electroadhesive forces obtainable. The initial selection of the four plates was based on the fact that the variation of *Sq* values between them was within 0.2 μm. One plate was maintained without sanding, the other three were sanded by a 60 grit aluminium oxide sanding disc to generate different surface texture directions, uni-directional, bi-directional, and multi-directional, as shown in Figure 5-2, where the circular shape denotes the Al plates that the pad can be attached onto. Different surface texture directions were achieved by rotating the plate with uni-directional scratches to the desired angle without needing to sand additional substrates.

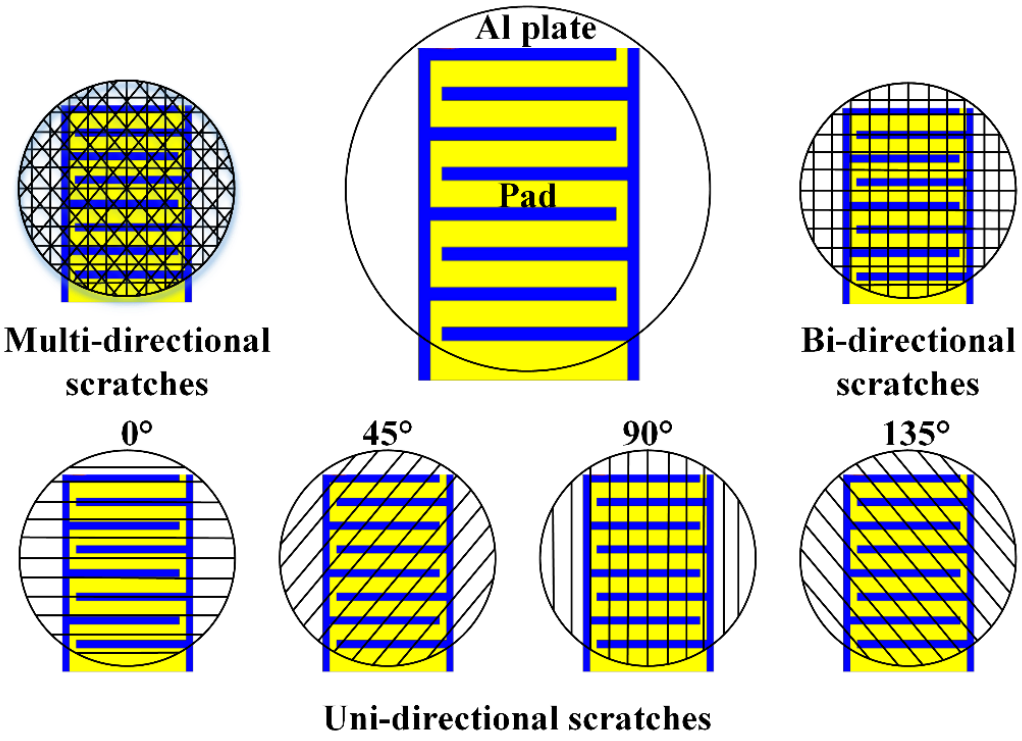

Figure 5-2 Aluminium plates with different scratch directions after sanding

5.4.2 Surface texture measurement

Alicona was then used to measure all the prepared substrate surfaces. Alicona, as mentioned above, is based on focus variation where height or depth information is gathered about a measured surface by applying optics with limited depth of field (DoF) and vertical scanning [143]. The use of limited DoF optics is to emphasise a small region in the measured surface so that each region can be sharply focused. Variation of focus, a function of height information of the measured surface, can be detected by a light sensitive charge-coupled device (CCD) sensor during the vertical scanning. Also, colour information of the measured surface can be obtained as the optic system uses a white light source. The optical principle of the Alicona Infinite Focus is schematically demonstrated in Figure 5-3, where 1 denotes the surface being measured, 2 denotes the objective, 3 denotes the white light source, 4 denotes the collimation optics, 5 denotes the light beam, 6 denotes the beam splitter, 7 denotes the CCD camera, and 8 denotes the vertical scan.

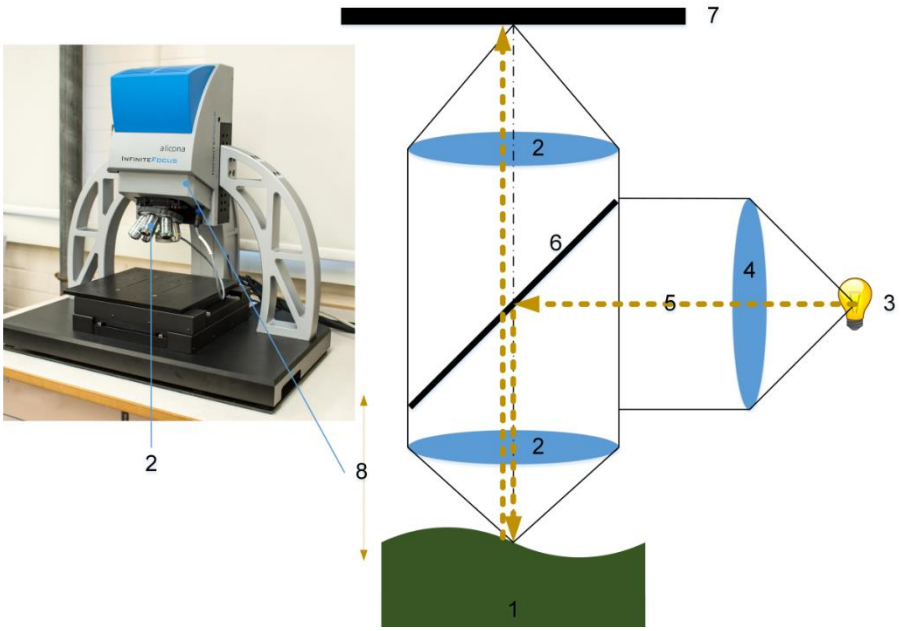

Figure 5-3 Optical principle of the Alicona [143]

The light beam from the white LED coaxial light is focused/collimated via the lens, and then transmitted through the semi-transparent beam splitter and focused on the surface being measured through the objective lens with limited DoF. The light reflected from the measured surface is then collected by the objective lens and transmitted though the beam splitter and finally focused on the CCD sensor. During the vertical movement of the optic system, the degree of focus of the selected region from the measured surface varies, usually from low to high and back to low again. This focus variation can be detected by the light sensitive CCD sensor in terms of a contrast variation. For every pixel point (with lateral position (x, y)) in the CCD sensor, a small region around it is selected to measure its contrast in the image. The optimum focus position (related to the height information, z(x, y)) can be obtained by analysing and calculating the changing contrast (searching for the sharpest image) from the stack of images obtained during the vertical scanning. The height or depth information of the whole measured area can then be obtained after conducting the highest contrast detection of all the detectable lateral positions [143].

For the sandpaper samples, a random area of 7.86 mm x 5.78 mm on each

sandpaper sample was measured. For the aluminium plates, ten carefully designated areas, each 1.43 mm x 1.09 mm, as shown in the experimental setup in Figure 5-4, were measured from each plate. The ten areas were evenly located in the middle part of the plates with a radius of 40 mm. The coordinates of each area was designated in the green boxes.

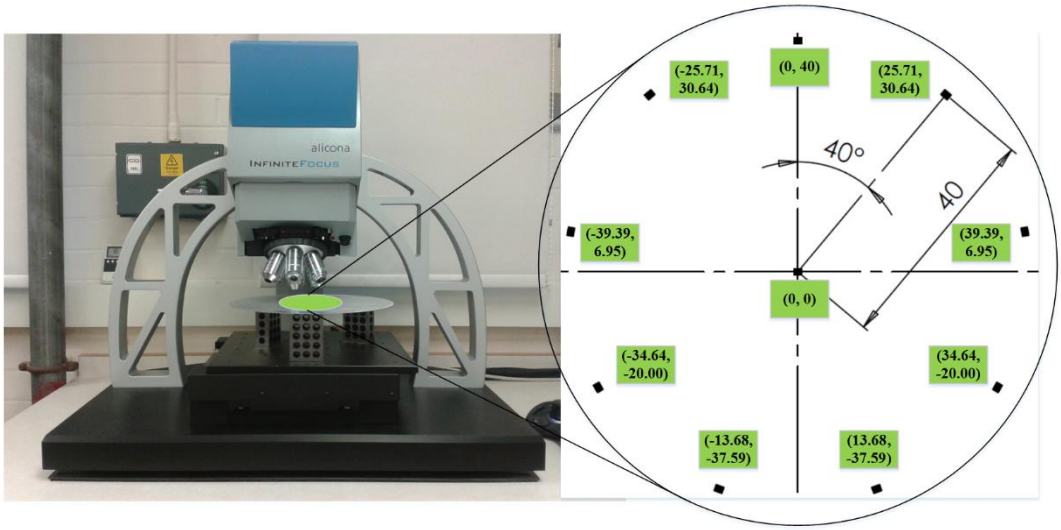

Figure 5-4 Experimental setup for surface texture measurement

The surface texture information of the selected area of the three sandpaper samples in three dimensions can be seen in Figure 5-5, where (a) is for P1200, (b) is for P400, and (c) is for P120. The surface texture information of a measured area of each aluminium plate can be seen in Figure 5-6, where (a) is the original smooth plate, (b) is the plate with uni-directional scratches, (c) is the plate with bi-directional scratches, and (d) is the plate with multi-directional scratches. For all the sandpaper samples and aluminium plates, the IFG4 10X objective was used. This objective has a working distance of 17.5 mm and a field of view of 1.43 mm x 1.09 mm. For the aluminium plates, a lateral resolution of 3.91 µm and vertical resolution of 0.5 µm were used, whereas for the sandpaper samples, a lateral resolution of 7.82 µm and vertical resolution of 1.26 µm were used. The rougher resolution used on the sandpaper samples was due to more steep slopes being observed in the sandpaper surfaces where a finer resolution resulted in a large amount of void data being observed.

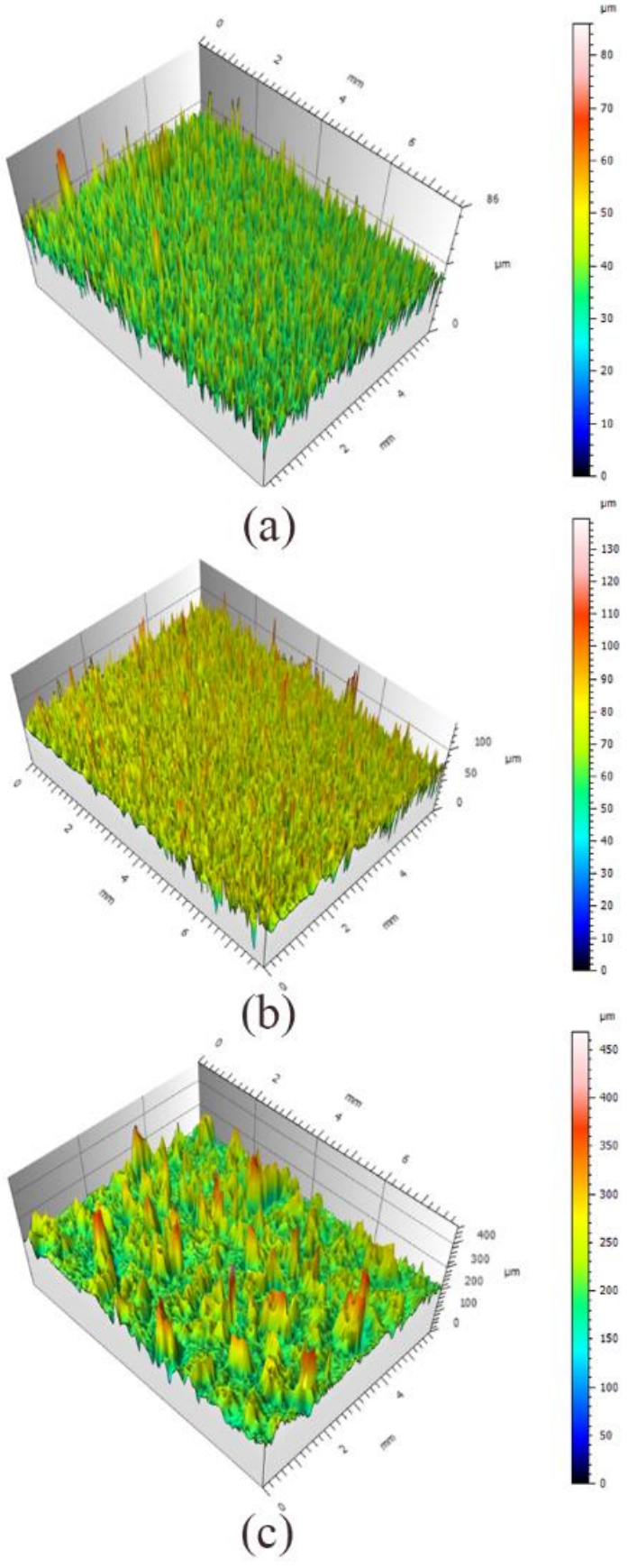

Figure 5-5 Surface texture information of the sandpaper samples

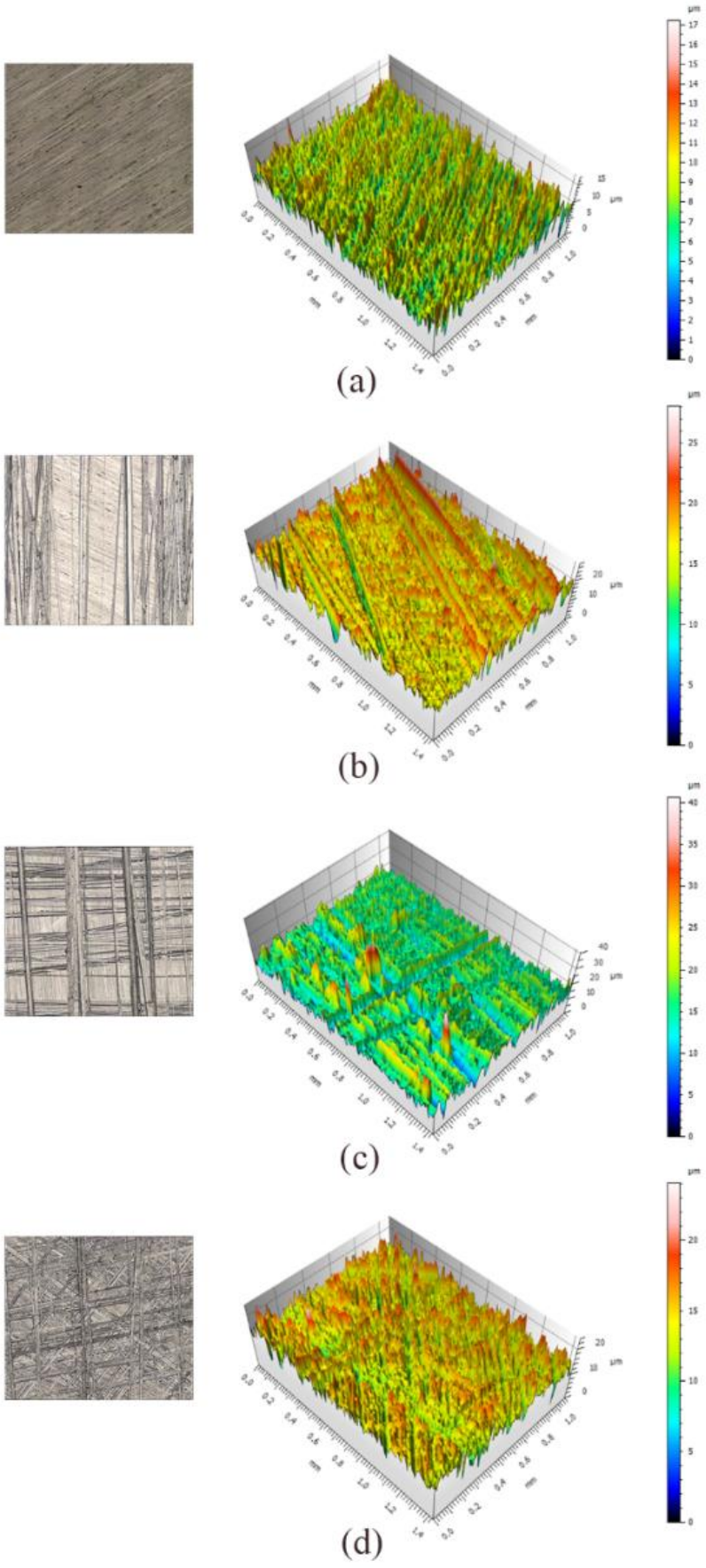

Figure 5-6 Surface texture information of the aluminium plates

5.4.3 Surface texture data analysis

The same data analysis procedure was carried out for all the measured data using the MountainMap. This procedure started with uploading raw data into the MountainMap and any non-measured data was filled in based on an embedded average algorithm (the average values of neighbouring points) in the software. Filtrations were then conducted, including removing the surface form/slope by the default polynomial surface fitting method and removing waviness by the Gaussian filter, before the quantification of each measured data was completed using areal parameters. A template containing the full data analysis procedures of any measured area was used to save time for the data analysis otherwise the same procedure should be conducted manually for each measured area. Applying the template requires that all the other data should be in a folder. The software will automatically analyse all the data located in a designated folder using the same data analysis procedure applied in the template file. There is no need to manually conduct the same analysis process for all measured areas as the quantification results will be located in the same folder.

For both the sandpapers and the aluminium plates, the standard cut-off length of 0.8 mm [143] was used, so surface wavelengths shorter than this had their amplitude transmitted as surface roughness. The standard areal Gaussian filter was employed as it is a zero-phase low pass filter. This is useful for avoiding phase distortions. Also, it is symmetric and separable. This is useful for simplifying its implementation and bringing computational efficiency. In addition, it has a gradual fall-off. It can be therefore used for avoiding ringing effects associated with sharp cut-offs [144]. The Gaussian filter was applied after removing the surface form. This is because the surface profile after filtration will not follow the surface form if the surface form is not removed [145]. A second order polynomial surface fit was conducted to remove the surface form using the MountainMap. Since boundary distortions occur after applying the Gaussian filter, half the cut-off length on both sides of the surface data was removed before

quantification, as per [145]. These two limitations regarding the Gaussian filter can be seen from the red line in Figure 5-7. For an already small area of the surface data, discarding one cut-off length however is an unacceptable solution. The end effects were therefore managed using the MountainMap software so that the filtered surfaces were the same size as the source surface. As can be seen from Figure 5-7, robust Gaussian filters, were used for managing the end effects brought out by the traditional Gaussian filter.

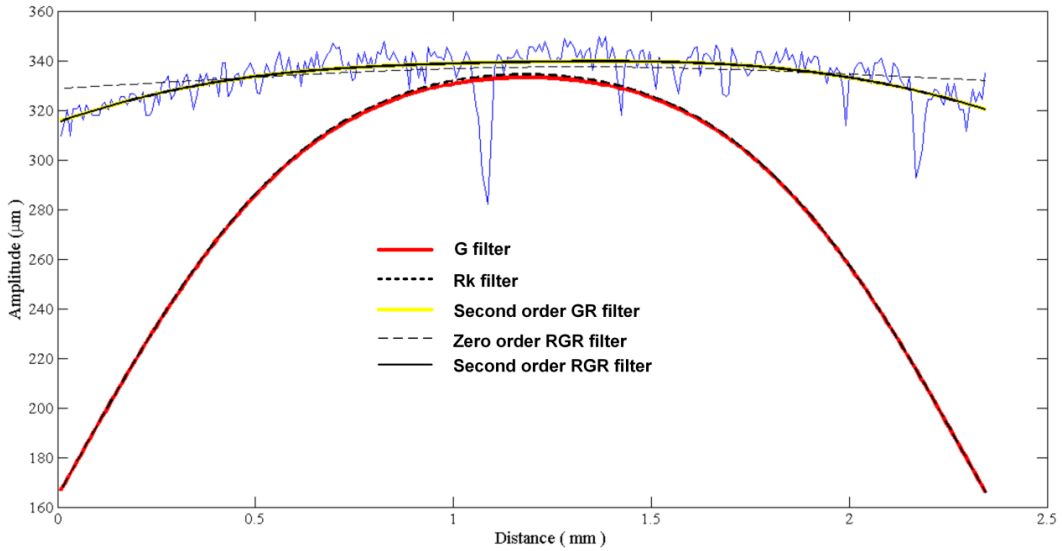

Figure 5-7 Comparison of different Gaussian-based filters

The comparison of the different Gaussian-based filters (shown in Figure 5-7) was based on the data of a sanded wood surface profile, which is the blue line in Figure 5-7. This was measured by the Heliotis H3, a parallel optical coherence tomography (pOCT) based non-contact surface texture measurement device which has better measurement repeatability and quicker data acquisition speed [146]. Although an automatic surface texture data analysis algorithm was generated using MATLAB for the sanded wood surfaces, this chapter will not introduce them in detail as the focus of this chapter is on the relationship between the electroadhesive forces and surface textures. The algorithm is, however, presented in detail in the Appendix.

After this quantification process, the *Sq* values of the prepared surfaces were

obtained. The *Sq* of the sandpaper samples was *Sq* = 4.8 μm for P1200, *Sq* = 10.7 μm for P400 and *Sq* = 31.5 μm for P120. The average *Sq* of the 10 selected areas of each plate was *Sq* = 1.5 μm for the original smooth plate, *Sq* = 2.8 μm for the uni-directional sanded plate, *Sq* = 3.1 μm for the bi-directional sanded plate and *Sq* = 2.8 μm for the multi-directional sanded plate. As the aluminium plates were carefully sanded, the standard deviation of the three plates was all within 10%.

5.4.4 Electroadhesive pad design and manufacturing

Since the comb or interdigitated electroadhesive pad geometry is the one of the most widely used pad geometries, a comb shape pad was designed using Solidworks. It was professionally spray etched to remove the unwanted copper areas after dry film lamination and laser direct imaging and then coated using a polyurethane (PUC) conformal spray coating. Degassing and curing of the coated PUC were conducted in a vacuum oven at 80 °C for 90 minutes. The electroadhesive pad design and manufacturing process shown in Figure 5-8, which is similar to the pad manufacture process described in section 4.6.1. The copper area outside of the interdigitated pattern was for supporting the pad flat enough during the coverlaying process. Only the interdigitated pattern part of the design was used for the electroadhesive force testing. The effective pad area is 190 mm x 230 mm. The space between electrodes, electrode width, and thickness are 2 mm, 2mm, and 40 μm respectively. The base dielectric material covering the electrode is a 25 μm thick Polyimide (PI) with a 13 μm thick Polyacrylates adhesive. The professional manufactured pads cannot bear 6 kV on sandpaper samples. A self-coating method was therefore used is to enable the pad to endure 6 kV.

The Alicona cannot measure the polyimide surface of the pad, therefore the Zygo Newview 5000 was used to measure the pad. The reason why the Alicona could not be used to measure the PI pad surface was because that the surface of the

PI used in this research was quite shiny and transparent. Plenty of missing data were found when using the Alicona to measure the PI surface. Zygo is also a non-contact surface texture measurement platform based on coherence scanning interferometry [143], where the superposition property of the light waves that indicate the surface height information of the part being measured is adopted.

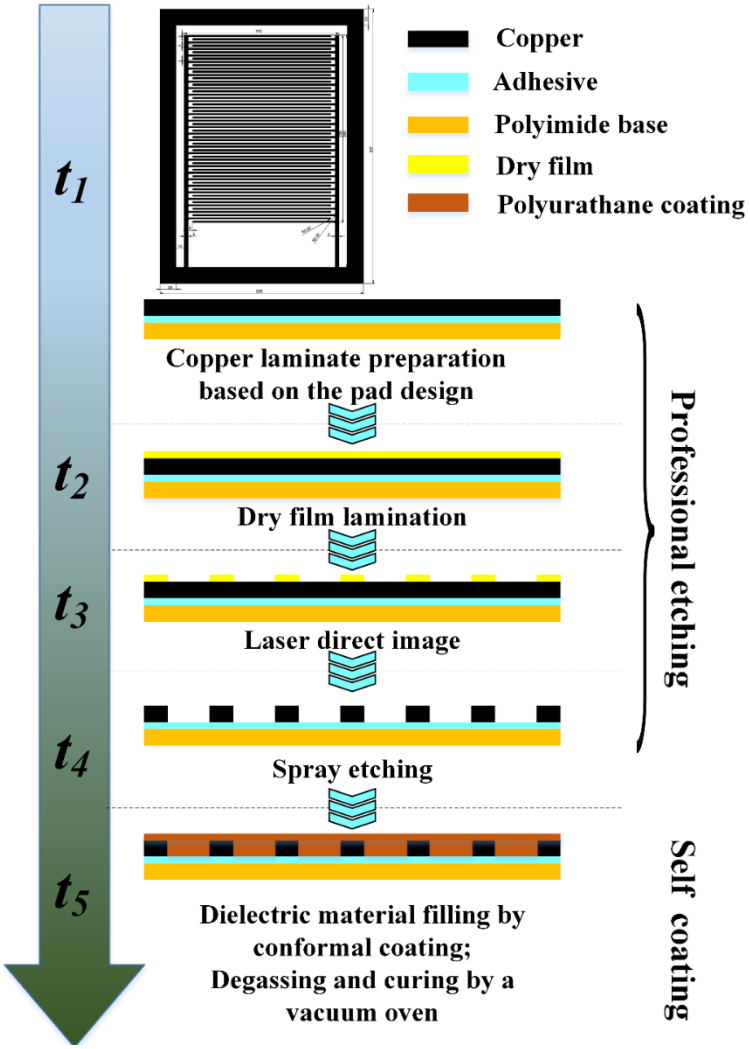

Figure 5-8 Pad design and manufacturing process for Chapter 5

The optical principle of the Zygo Newview 5000, mounted with a Mirau 10X objective, is schematically demonstrated in Figure 5-9, where 1 denotes the surface being measured, 2 denotes the lower beam splitter, 3 denotes the reference mirror, 4 denotes the Mirau objective, 5 denotes the white light halogen

source, 6 denotes the beam splitter, 7 denotes the upper beam splitter, 8 denotes the camera optics, 9 denotes the CCD sensor and 10 denotes the vertical movement using a piezo drive system.

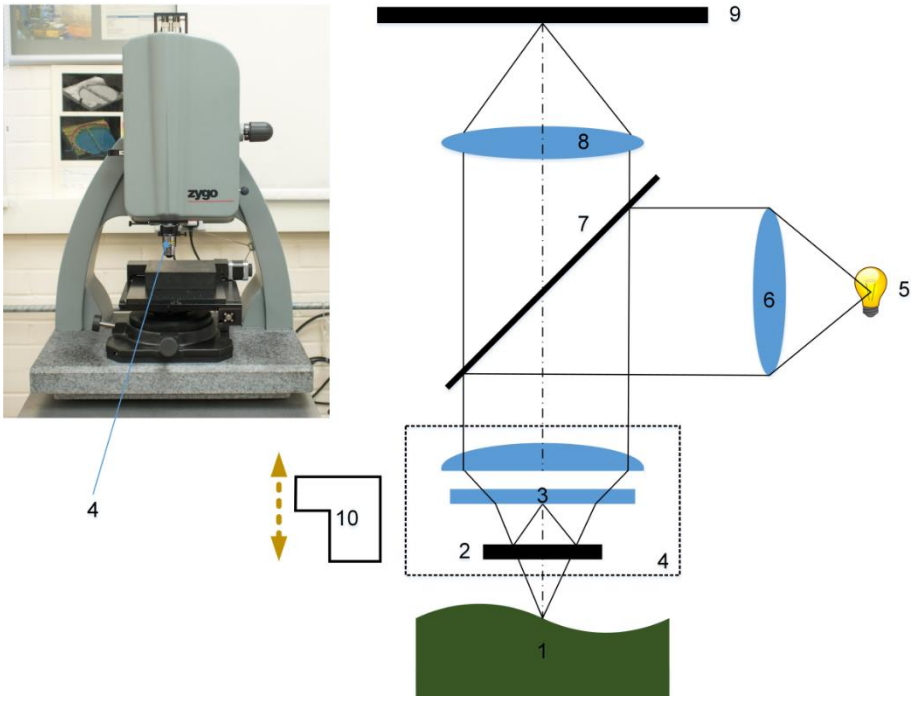

Figure 5-9 Optical principle of the Zygo Newview 5000 [143]

The white light source is directed towards the Mirau objective by the upper beam splitter. The lower beam splitter then splits the light into two beams: one goes to the sample and the other is directed towards the reference mirror. The two beams are recombined with constructive and destructive interference, leading to a set of dark and light bands, which can be seen from the monitor, and detected by the CCD sensor. The CCD sensor then converts the light intensity signals as a function of scan positions into electric signals that can be processed to obtain the surface profile or areal parameters. The Zygo is not good at measuring surfaces with large slopes, it was therefore not used to measure the sandpaper and aluminium plate due to a large amount of surface slopes being observed on those surfaces.

The pad with its polyimide base side in the front can be seen in Figure 5-10 (a). The 3D surface texture information of a random area of the polyimide base side

can be seen in Figure 5-10 (b). The working distance of the Mirau 10X objective is 7.6 mm and a vertical resolution of 3 nm and lateral resolution of 1.18 μm were employed. The recognised standard Gaussian filter and a cut-off length of 0.8 mm were applied as per the sandpaper and Al samples, and the end effects were managed during the data analysis process in the MountainMap software. As a result, the *Sq* of the surface of the polyimide (PI) base is 0.2 μm. The reason why this value was bigger than expected was due to dust and grease on the PI surface.

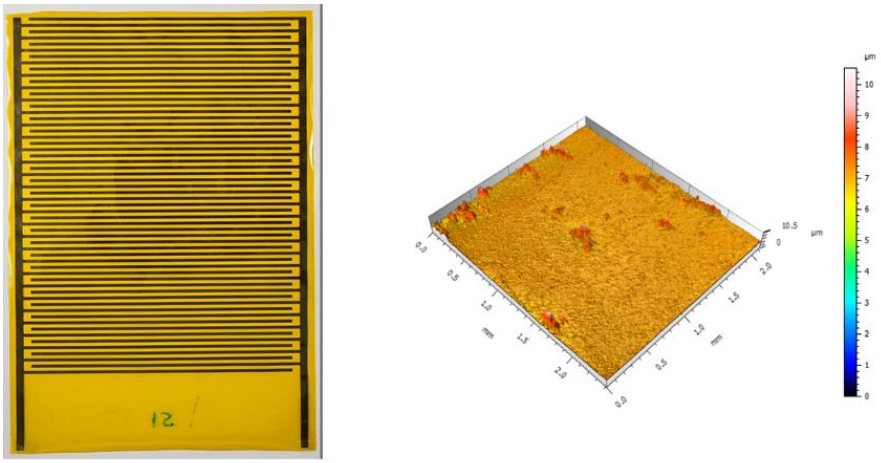

(a) (b)

Figure 5-10 The pad used for Chapter 5

5.4.5 Electroadhesive force measurement

The electroadhesive force measurement platform used to obtain the interfacial vertical electroadhesive forces between the pad and substrates was the same with the one described in section 4.6.2. Only the test rig orientation is new. The system diagram can be seen in Figure 5-11, where 1 is the test rig base, 2 is the toughened glass, 3 is the pad, 4 is the pad holder, 5 is the ATI F/T sensor, 6 is the pad holder supporter, 7 is the linear rail, 8 is the servo motor, and 9 is the rail supporter. The physical setup can be seen in Figure 5-11 (b).

In order to investigate the relationship between the electroadhesive forces and substrate surface textures, only the substrate surface texture was varied whilst keeping all other influencing variables constant based on the control variable

method. Since the obtainable electroadhesive forces may change during the day and between days, the experiments were conducted when less variation in room temperature, humidity, and air pressure was observed, as shown in Table 5-1.

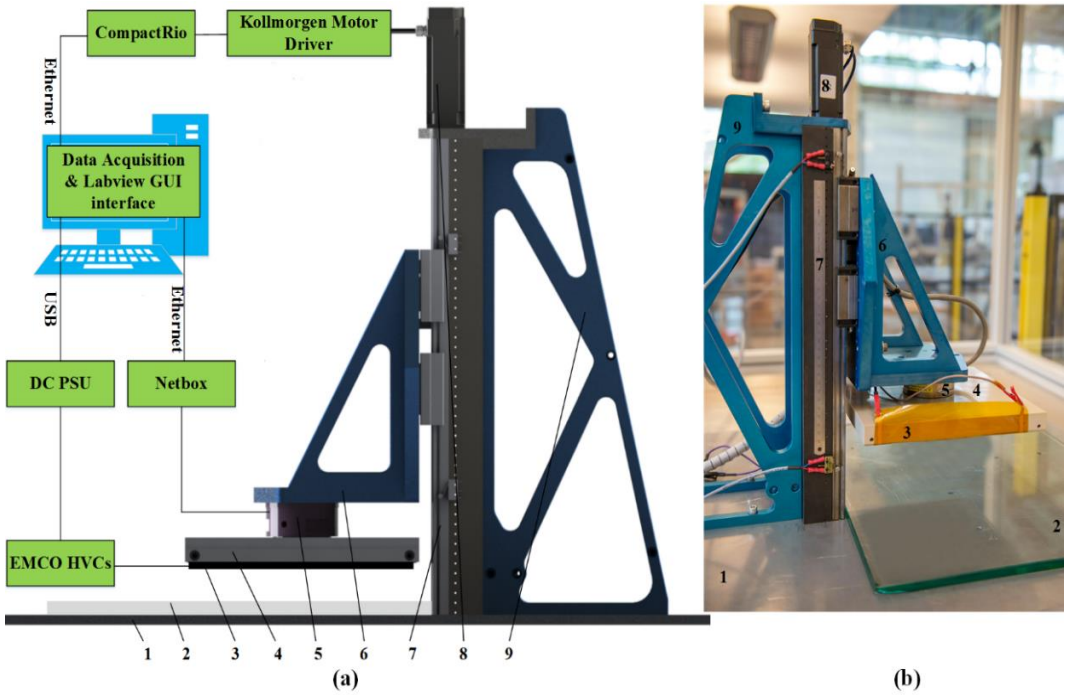

Figure 5-11 Electroadhesive force measurement platform

Table 5-1 Controlled parameters for the force measurement

Controlled parameters	Sandpaper samples	Aluminium plates
Applied voltage (kV)	2, 4.4 and 6	4.4
Polarity of applied voltage	Dual polarity	
Substrate material and thickness	1 mm sandpaper samples with 12 mm toughened glass	1 mm aluminium plates with 12 mm toughened glass
Substrate surface texture	**Varies**	
Dielectric material and thickness	25 μm PI and 13 μm adhesive	
Pad surface roughness (*Sq*, μm)	0.2	
Electrode pattern and area	Comb and an area of 190 mm x 230 mm	
Space between electrodes (mm)	2	
Electrode width (mm)	2	
Electrode thickness (μm)	40	
Electrode material	Copper	
Environment temperature (°C)	21.5 ± 0.1	
Environment humidity (%)	43 ± 1	
Environment pressure (hPa)	1003 ± 1	
Preload (air gap, N)	34 ±1	

For each selected substrate surface texture, the experiments were repeated 5 times. The electroadhesive force measurement procedures were similar to the contents presented in section 4.6.2, as shown in Figure 5-12, where the aforementioned dynamic changing of the obtainable electroadhesive forces are shown and can be seen in step 3: the pad charging phase after turning on the voltage. The measurement procedure started with the attachment of the substrates with different surface textures onto a 12 mm toughened glass. The substrates were fixed properly such that the position of the different substrates was guaranteed to be the same with respect to the pad. A 34 $\pm$ 1 N preload was then applied on all substrates. The charge time was 90 seconds and the dwell time was 510 seconds. During the residual charge dissipation process, the aluminium plate with uni-directional scratches was also grounded for 300 seconds each time before rotating it to a different angle to investigate the influence of surface texture directions on the electroadhesive forces obtainable.

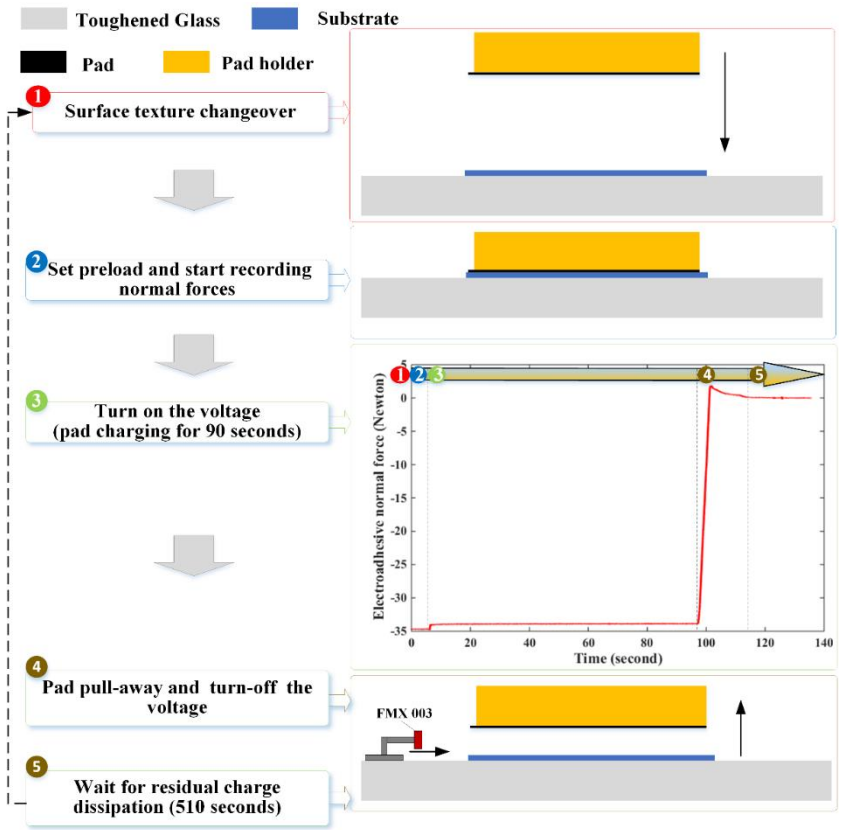

Figure 5-12 Electroadhesive force measurement procedures

5.5 Results and discussion

As aforementioned, the experimental data with regard to the electroadhesive forces were saved into txt files that require further filtrations to remove any noise in the data. The correlation between the obtainable interfacial electroadhesive forces and surface textures was then found after obtaining the surface texture parameter and filtering the electroadhesive force data.

5.5.1 Data analysis on the electroadhesive forces

Various data smoothing filters have been investigated and compared for the filtration of the force data, including the Gaussian filter, the Savitzky-Golay filter, the Loess and Robust Loess filter, the Lowess and Robust Lowess filter, the Smoothing Spline filter and the Butterworth filter. The Gaussian filters are sensitive to spikes. The Savitzky-Golay filters are usually used to retain the high frequency component of the data rather than removing it. The Loess and Lowess filters are also sensitive to spikes whereas the Robust Loess and Lowess filters are robust against spikes but computational intensive. The smoothing spline filters will bring edge distortions. In contrast, the Butterworth filters are relatively quick and good at removing the high frequency or noisy component of the data. The inbuilt MATLAB function, ‘butter()’, was used to smooth the raw data extracted from Labview (see Figure 5-13).

It is demonstrated in Figure 5-13 that the second order Butterworth filter is not good enough to follow the actual trend of the raw data which contains a large amount of noise and the fourth order may bring over-fit problems. The third order was therefore employed. The normal electroadhesive forces for each test were then recorded as the maximum value of the data after the third order Butterworth filtration.

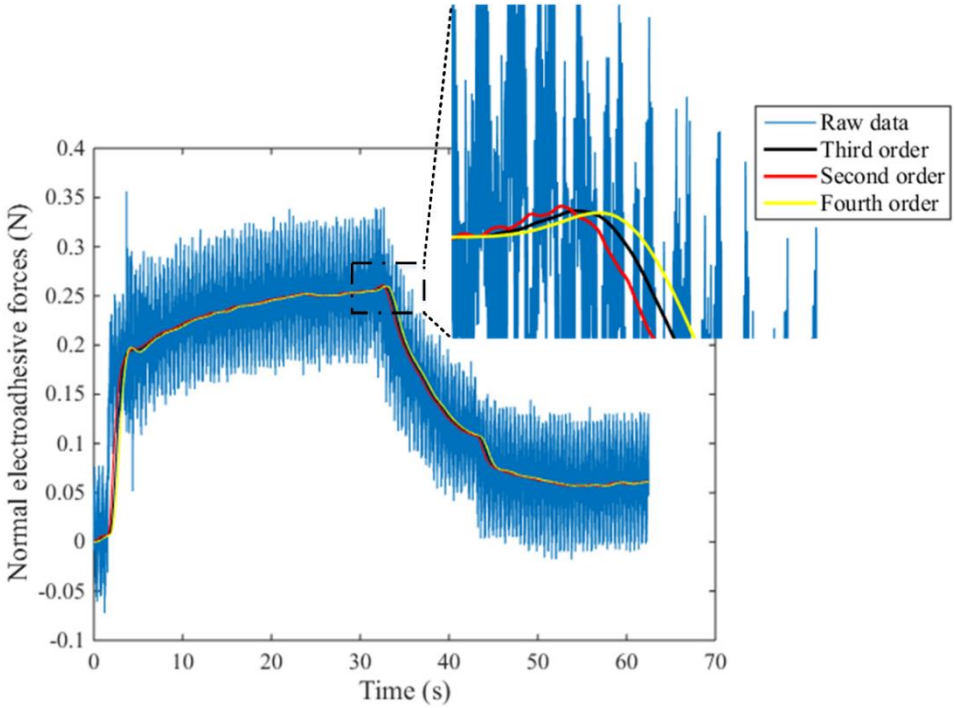

Figure 5-13 Comparison of different orders of the Butterworth filter

5.5.2 Results on the sandpaper samples

The mean normal electroadhesive forces and their standard deviations (the error bars) over five repeated measurements for each test on the sandpapers are plotted in Figure 5-14.

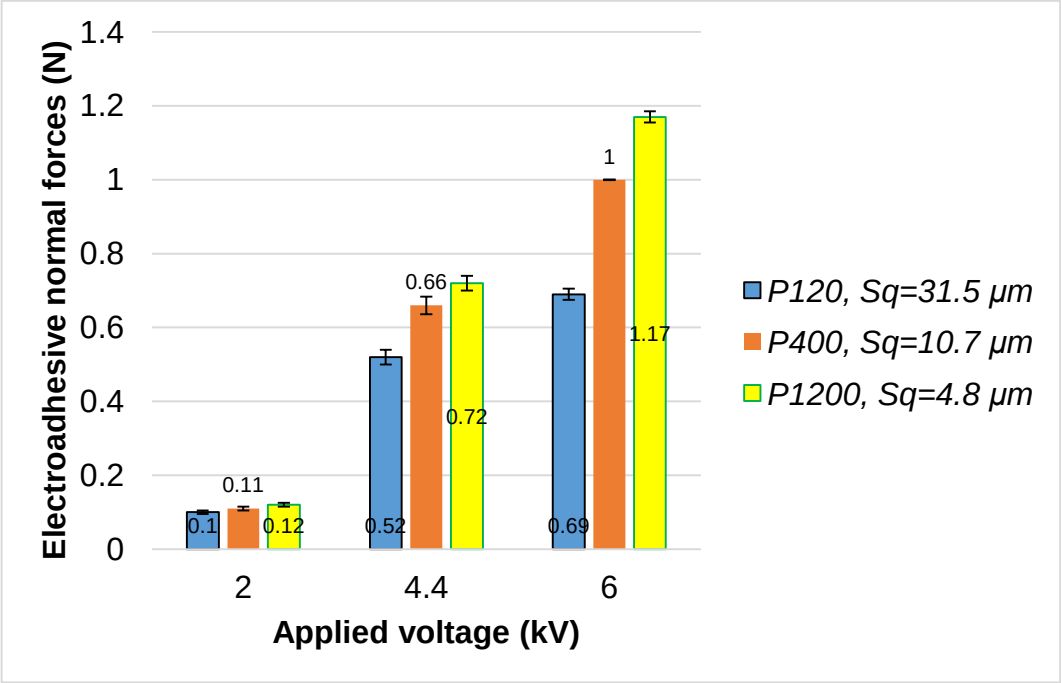

Figure 5-14 Electroadhesive forces on sandpaper samples

It can be seen from the figure that the obtained interfacial electroadhesive forces increase with decreasing *Sq* values. This may be due to the fact that the larger the *Sq* value, the less the air gap and therefore more contact area between the pad and the substrate. Also, the higher the voltage applied, the larger the relative increase in the electroadhesive forces was observed. Between the sandpaper samples P120 and P400, for instance, a relative increase of 9.1 % was achieved at 2 kV, but 21.2 % at 4.4 kV and 31 % at 6 kV. The stated voltage supplied was based the voltage difference between the positive electrodes and negative electrodes. The reason why the 4.4 kV was selected rather than 4 kV was because the voltage output of the power supply unit was not stable at 4 kV. The electroadhesive force measurements on voltages greater than 6 kV were not conducted due to possible electric discharge and dielectric breakdown of the pad.

5.5.3 Results on the Al plates

The mean normal electroadhesive forces and their standard deviations over five repeated measurements for each test on the Al plates are plotted in Figure 5-15.

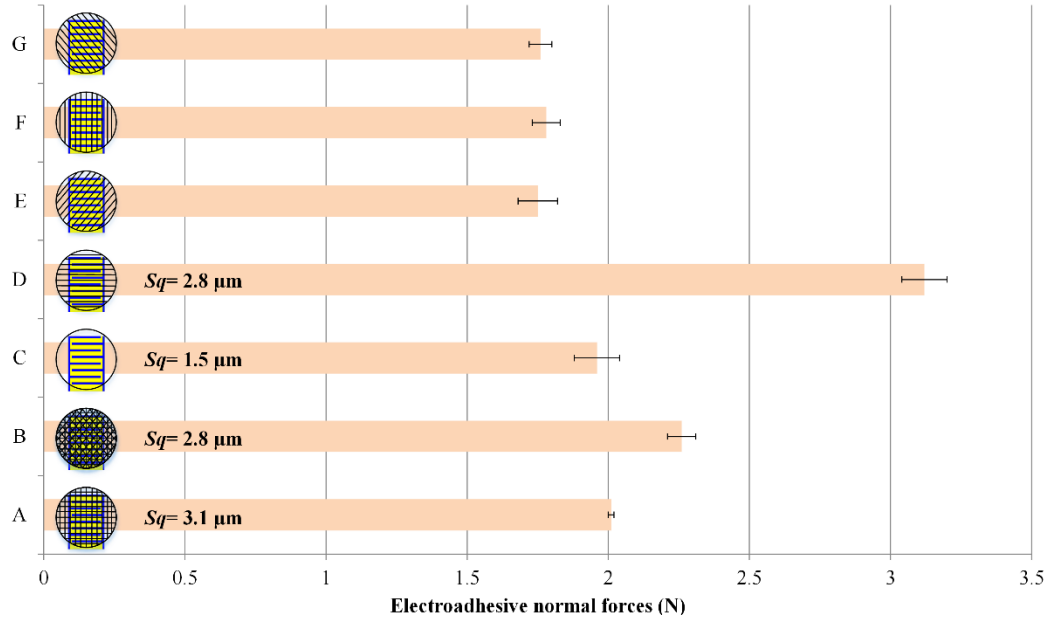

Figure 5-15 Electroadhesive forces on aluminium plates

In Figure 5-15, A denotes the sanded surface with bi-directional scratches, B denotes the sanded surface with multi-directional scratches, C denotes the

original plate surface, D denotes the sanded surface with horizontal scratches, E denotes the sanded surface with 45° scratches, F denotes the sanded surface with vertical scratches and G denotes the sanded surface with 135° scratches. **Note that only four Al plates were tested. Plates D, E, F and G were based on the same plate. Different scratch orientations were obtained by rotating the plate.**

As can be seen from the results obtained for plates B and D, it can be concluded that the obtainable electroadhesive forces are not necessarily the same even when the *Sq* values of the two substrate surfaces are the same. This may also suggest that a single *Sq* cannot be used to represent the effective air gap between the pad and the substrate. In addition, the sanded Al surface with horizontal scratches has a relative increase of 38.1 % more electroadhesive forces than the surface with multi-directional scratches. This is maybe due to charge trapping in those corners of those multi-directional scratches.

Based on the results for plates A, B and C, when the difference of the *Sq* values between different substrate surfaces is within 2 μm, the obtained interfacial electroadhesive forces do not necessarily increase with decreasing *Sq* values as observed with the sandpaper samples. This may due to the fact that, based on the data shown from plate C to G, the directions of surface texture on substrate surfaces play an important role in achieving the electroadhesive forces. Compared with the original Al plate (C), the Al surface with approximately 45° (E), 90° (F) and 135° (G) scratches all have obtained slightly less forces (around 10 %). The Al surface with approximately horizontal scratches, however, has a 59.2 % increase in the obtained electroadhesive forces. This is maybe due to the reason that a perpendicular relationship between the electric field and scratch direction is helpful.

5.5.4 Discussion

Although some interesting results have been obtained, the reason leads to these

results requires further investigation. This may be due to charge trapping in the scratches. This may also be due to interactions between the electric fields and scratch directions.

As only ten small areas (each 1.43 mm x 1.09 mm) were measured from a radius of 275 mm, the surface texture parameter value may still not fully representative. Larger areas are therefore required to be measured. Also, the use of the only single *Sq* value is not well-representative of the surface texture. The conclusion was based on a limited number of substrate samples and limited variations of the surface texture. More consistent surface textures are therefore necessitated be generated to gain a further understanding of this contacting phenomenon. The results may be different under 2 μm and between 2 μm to 5 μm.

For academic researchers who want to study electroadhesion, the results highlight that it is necessary to have similar surface texture of substrate surfaces (control the surface texture) when investigating the relationship between the obtainable electroadhesive forces and other influencing factors on electroadhesion such as the substrate material. Only in this way can we gain a confident understanding of the electroadhesion phenomenon. Also, it will be interesting to investigate how varying electrode widths and spaces between electrodes affect this relationship.

For industrialists who want to commercialise electroadhesive products, the result has identified the need for the generation of substrate surface texture adaptive electroadhesives to enable the electroadhesive pad to deal with different surface conditions. A layer of soft foam backing to the pad may be helpful for the pad to conform to rough surfaces. In addition, it will be interesting to vary different pad geometries whilst maintaining the same surface texture of the dielectric layer and the substrate to investigate the relationship between the interfacial electroadhesive force and pad geometries. Furthermore, it will be useful to vary different surface textures of the dielectric layer facing the substrate whilst keeping

the surface texture of the substrate the same to investigate the obtainable interfacial electroadhesive forces.

5.6 Summary

This is the first systematic and novel investigation into the relationship between the interfacial vertical electroadhesive forces obtainable and different substrate surface textures. The key findings from this work are:

● The obtained interfacial electroadhesive forces increase with decreasing the *Sq* values of the substrate surfaces provided that the difference in *Sq* between different substrates is greater than 5 μm.

● The higher the applied voltage, the larger the relative increase in the obtainable electroadhesive forces. For instance, when the voltage was increased from 2 kV to 6 kV, the relative increase in forces between P400 and P120 was increased from 9.1% to 31%.

● When the difference in *Sq* between different substrate surfaces is within 2 μm, the obtained interfacial electroadhesive forces do not necessarily increase with decreasing the *Sq* values. Also, the electroadhesive forces are not the same when the *Sq* value of two substrate surfaces are the same due to the fact that the direction of the surface texture plays an important role in achieving electroadhesive forces.

The spiral/concentric pattern would be independent of the scratch directions. The investigation into the relationship between the electroadhesive force and pad geometry is described in Chapter 6.

6 Investigation of the Relationship between the Electroadhesive force and Pad Geometry

6.1 Introduction

Various attempts have been made to investigate the performance of different pad geometries for electroadhesive applications [63][74][77]. In chapter 6 the need for a systematic investigation into the relationship between the electroadhesive forces obtainable and different pad geometries is identified. The proposed research method for the investigation is then demonstrated. In section 6.4, a 3D electrostatic simulation of the selected pad geometries and a customised mechatronic electroadhesive grasping platform have been used to conduct the investigation, before the initial results on experimental validation are presented.

6.2 The research need

Both the simulation and experimental results have shown that the pad geometry design is essential to achieve both the maximum electroadhesive force [63][73] and fastest clamp/unclamp characteristics [15][41]. New and novel pad geometries are still desirable for different electroadhesive applications as there lacks an extensive research on electroadhesive pad geometric optimisation. Also, there lacks a comprehensive comparison of some major pad designs stated in the literature review. It is therefore still necessary to continue answering the following two questions:

● which pad geometry can produce the maximum electroadhesive force on conductive substrates, non-conductive substrates, and both ?

● which pad geometry can achieve the fastest clamping and unclamping speed, especially on non-conductive substrates ?

This Chapter has been focusing on solving the first proposed question.

6.3 Research methodology

The aim of this Chapter is to identify the relationship between the electroadhesive forces obtainable and different pad geometries. To this end, four major stages have been addressed, as identified in Figure 6-1.

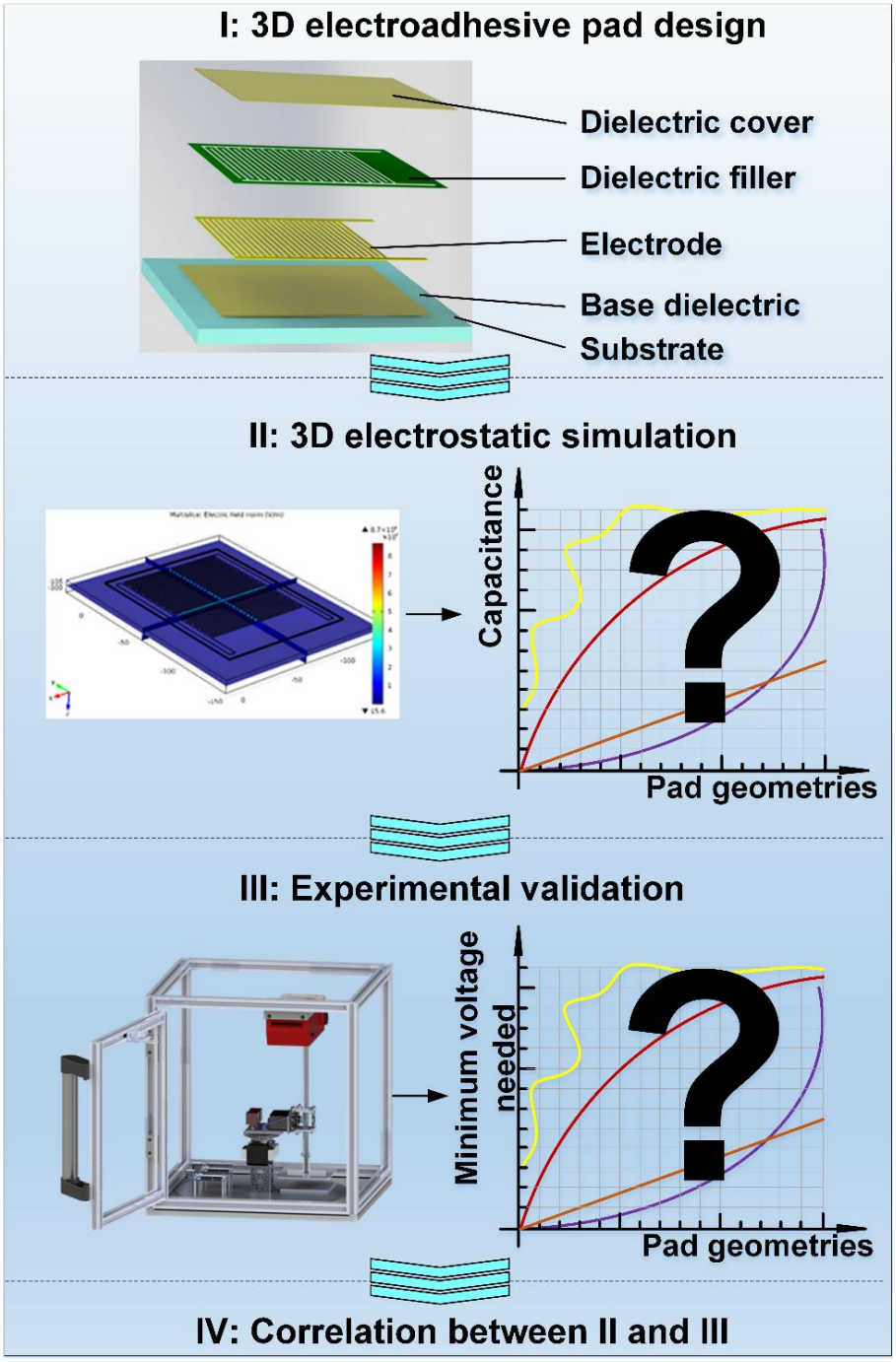

Figure 6-1 Research procedure for the investigation of the relationship between the electroadhesive force and pad geometry

The first stage of this research was to design the pad geometries in 3D using the SOLIDWORKS and assemble the designed pads with the substrates into electroadhesive systems. Following this, the 3D electrostatic simulation was conducted using the COMSOL Multiphysics 5.0 to obtain to the overall capacitance of each pad design for comparison. Then, experimental validation using the customised mechatronic electroadhesive grasping platform was conducted. A known weight was picked up by all the selected pads, and the minimum voltage to pick up the weight for each pad was recorded. Finally, a correlation between the simulation results and the experimental results was performed.

6.4 3D electrostatic simulation using COMSOL

3D electrostatic simulation is useful as it can provide the 3D electric field distribution and field strength of each pad geometry and inform the author about which pad geometry can output the largest capacitance with no pad manufacturing and testing, thus less cost and time is spent.

6.4.1 Selected pad designs

Although various pad designs have already been investigated, as shown in section 2.2.2 in Chapter 2, only 9 pad designs, including two novel pad designs, were selected for comparison in this Chapter. These pad designs can be seen in Figure 6-2, where (a) is the interdigitated or comb shape, (b) is the snake-electrode shape [64], (c) is the serpentine-electrode shape [108], (d) is the curve-comb shape, (e) is the worm-comb shape, (f) is tooth-comb shape, (g) is the concentric shape [73], (h) is the spiral shape [41] and (i) is the double-electrode shape [41]. All the pads (except design g) have the same pad area of 110 mm x 140 mm and effective pad area of 100 mm x 100 mm, electrode width of 2 mm, and space between electrodes of 2 mm. Please note that a smaller pad area, compared with those A4 size pads mentioned in Chapter 4 and 5, was used in this Chapter as the best geometry design produced by this chapter will be used

for implementing an electroadhesive legged climbing robot in the future and also to simplify the simulation model. Also, for the concentric design, the radius was 50 mm, the effective area was therefore 21.5% smaller.

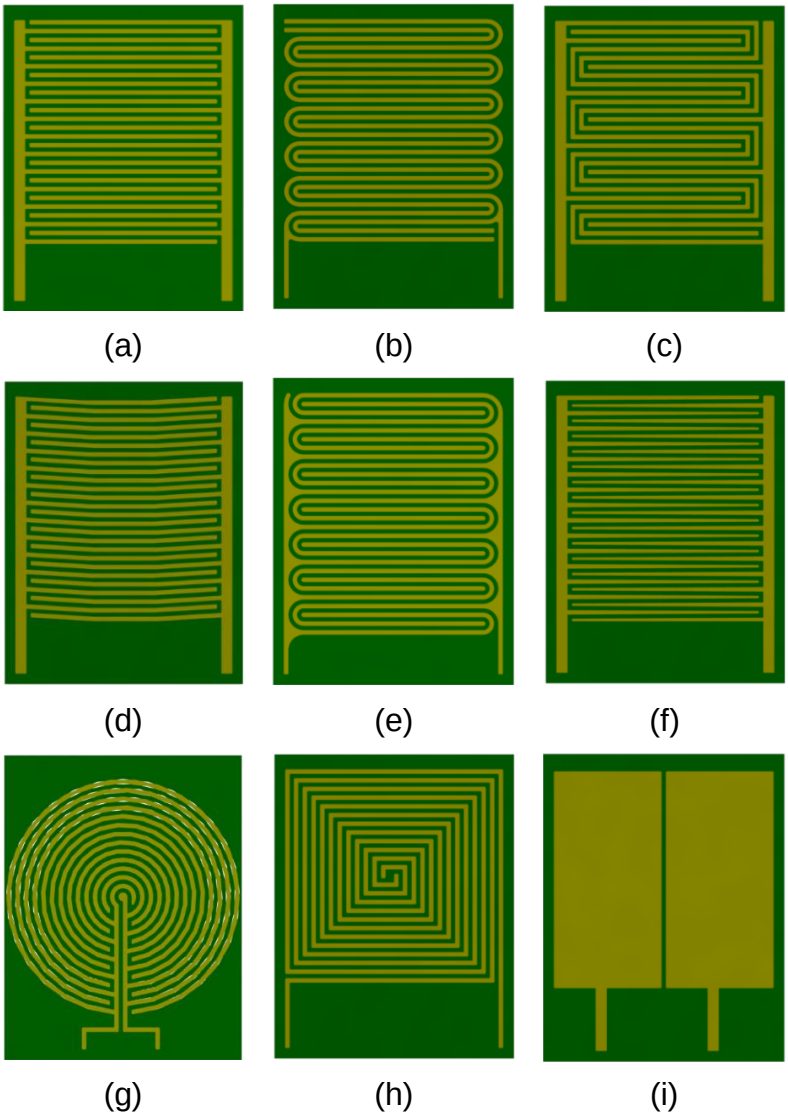

Figure 6-2 Selected pad geometries for Chapter 6

6.4.2 3D electrostatic simulation procedures

A 3D electroadhesive system, including the pad and the substrate assembly together, should be created before the 3D electrostatic simulation is carried out. In order to only vary the pad geometry, the same substrate, with dimensions of 10 mm (substrate thickness) x 150 mm x 180 mm, was used. Also, the same base dielectric, dielectric filler and cover were used to ease the process of material addition.

The 3D electrostatic simulation procedures can be seen in Figure 6-3. The 3D component should be added before adding the assembled electroadhesive system from SOLIDWORKS using the LiveLink function in COMSOL. Then the material of each part of the assembled electroadhesive system should be added. For the copper electrodes, the dielectric constant was set as 10000; for the glass substrate (quartz), the dielectric constant was set as the default value 4.2; for the dielectric material, polyimide, Kapton H was selected and 3.5 was set as its dielectric constant.

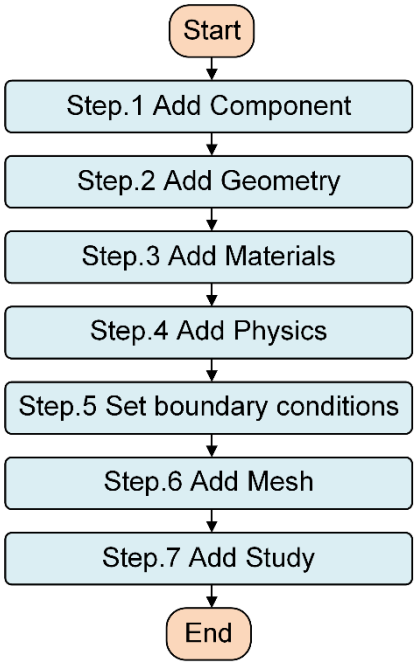

Figure 6-3 3D electrostatic simulation procedures

Electrostatics was then selected when adding physics into the model. After this, boundary conditions of the model can be set. For all the pad designs the left electrode was set with an electric potential of 3000 V, the right electrode was set with an electric potential of -3000 V, and the bottom face of the glass substrate was set with an electric potential of 0 V. The mesh part is the most difficult part of this study to obtain the value as close as the true value. This is because the real electrode thickness is about 0.04 mm and the thickness of the dielectric cover and base dielectric are 0.05 mm, but the overall dimension of the simulated system is 10 mm x 150 mm x 180 mm. It is therefore impossible to obtain true

results if no special meshing technique (such as the local meshing refinement method [147]) is adopted.

After the mesh, a stationary study was added. The results were then obtained after the computation and data post-process. The 3D electric field distribution of the selected pad geometries on the glass in COMSOL is presented from Figure *6-4* to Figure 6-12.

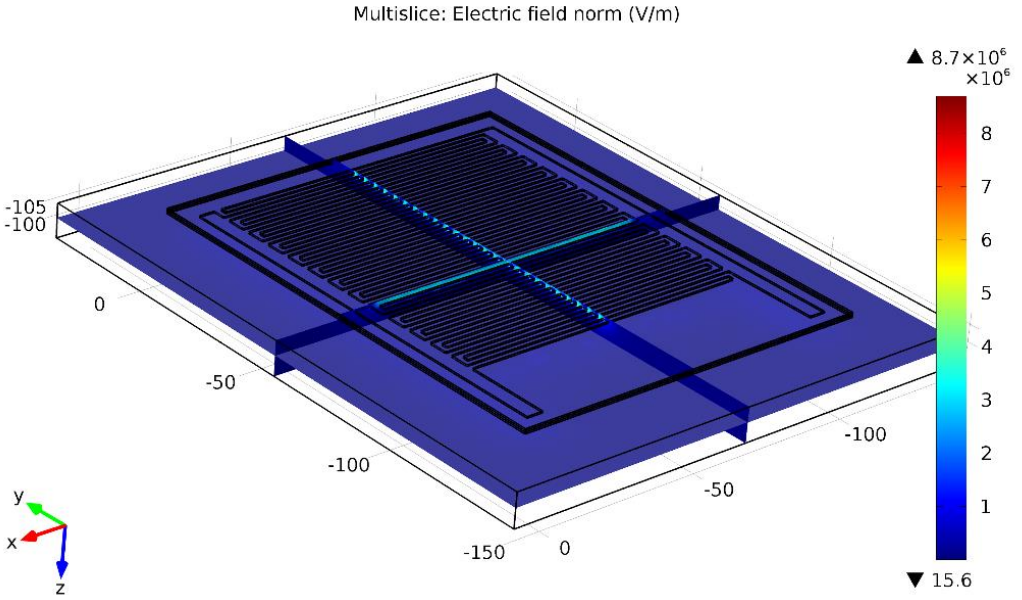

Figure 6-4 3D electric field distribution of the design (a) in COMSOL

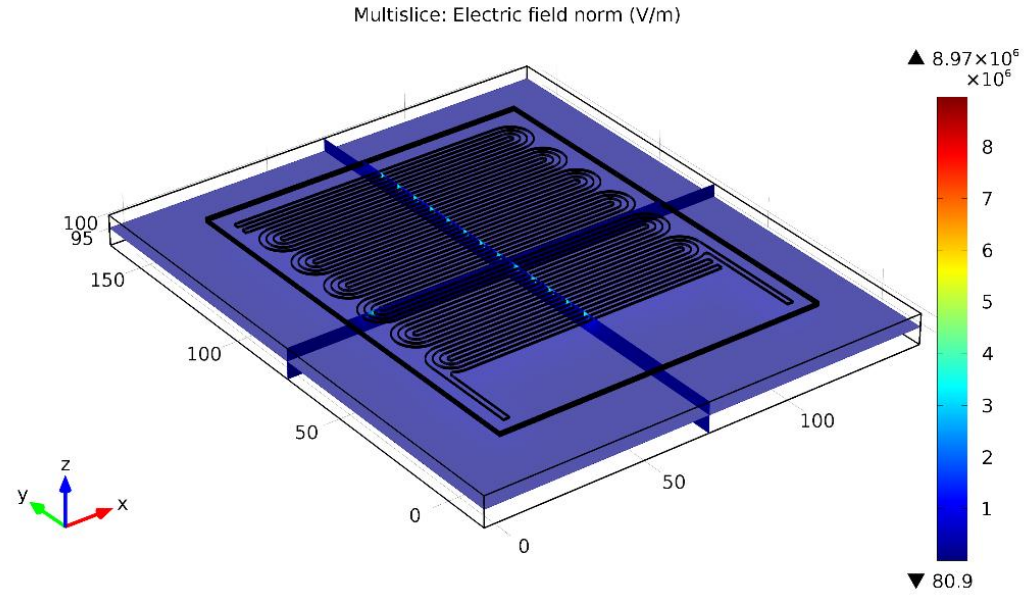

Figure 6-5 3D electric field distribution of the design (b) in COMSOL

As stated in section 3.3.3 in Chapter 3, there is nearly no difference in the electroadhesive forces obtainable when varying the electrode thickness. Therefore, in order to quickly have a successful mesh, the electrode thickness and thickness of the base dielectric and dielectric cover were all set as 0.5 mm. Finer mesh values produced similar results, within 1% difference, which agreed with the results of the work completed by Ruffatto et al. [73].

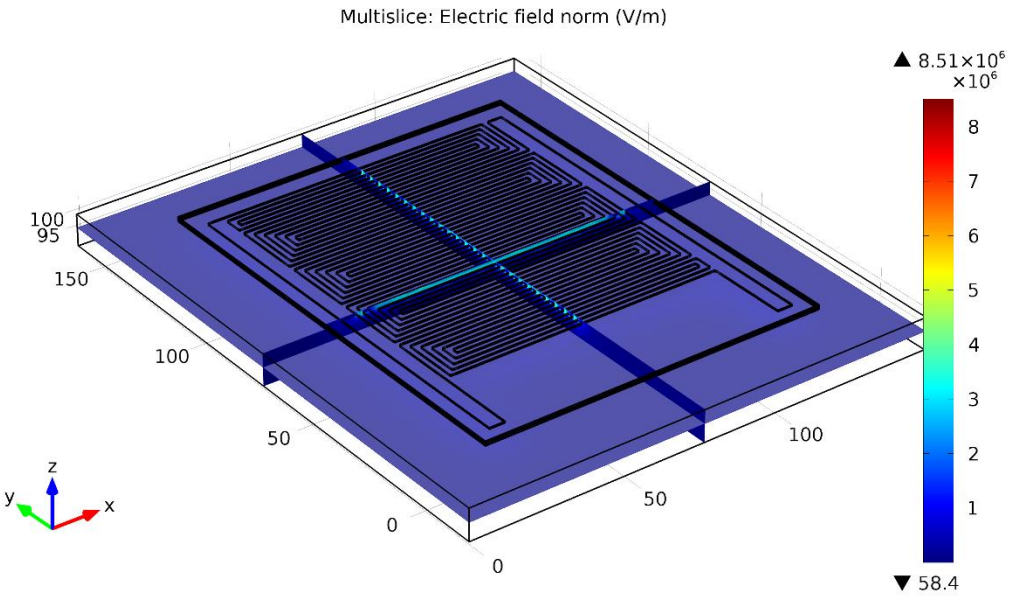

Figure 6-6 3D electric field distribution of the design (c) in COMSOL

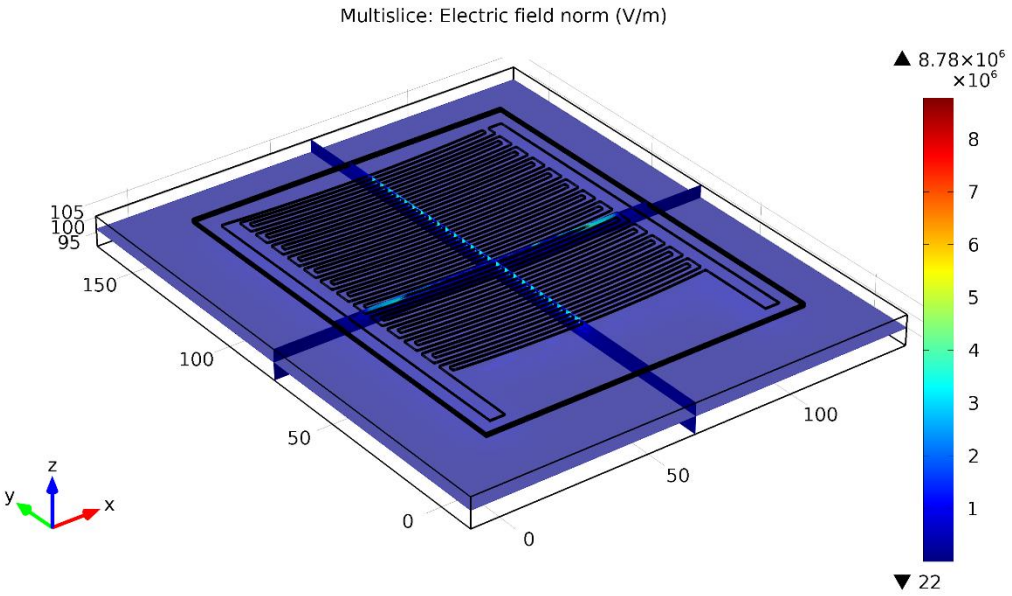

Figure 6-7 3D electric field distribution of the design (d) in COMSOL

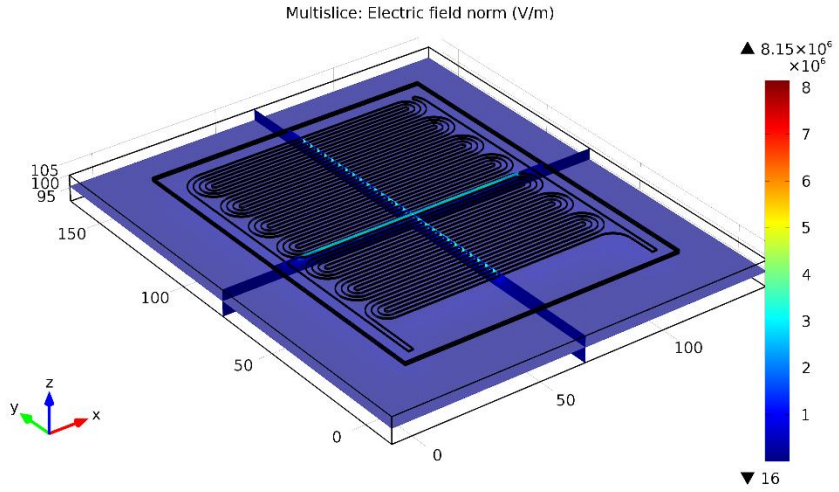

Figure 6-8 3D electric field distribution of the design (e) in COMSOL

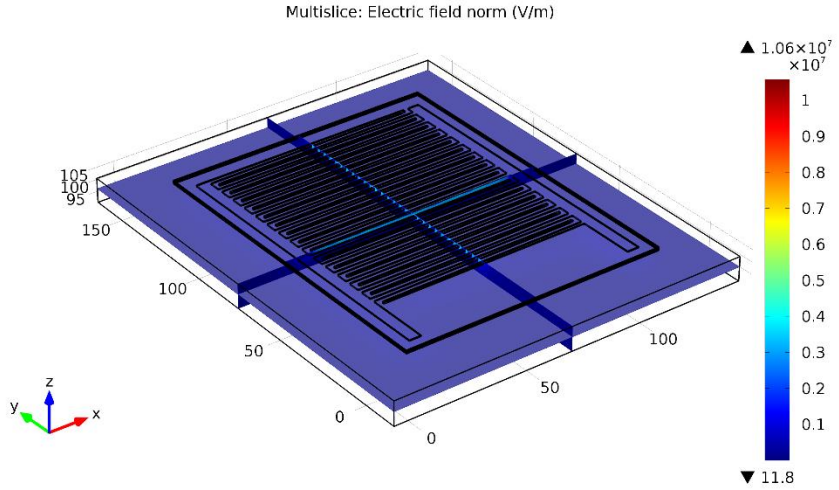

Figure 6-9 3D electric field distribution of the design (f) in COMSOL

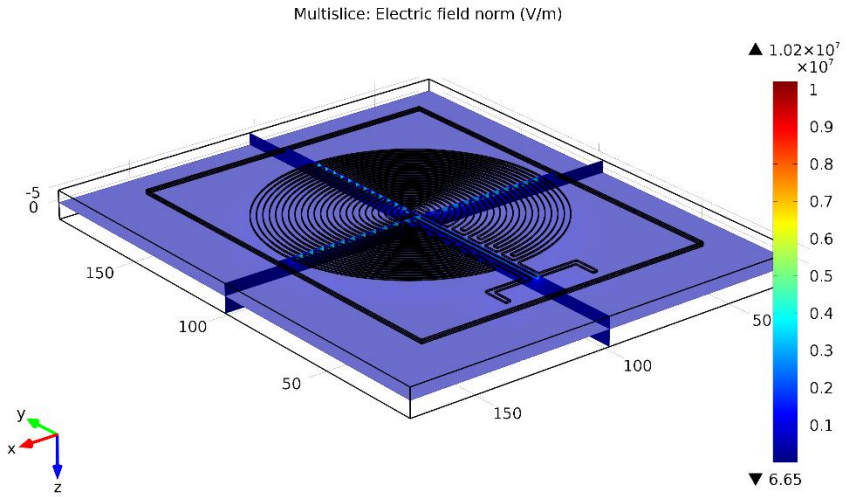

Figure 6-10 3D electric field distribution of the design (g) in COMSOL

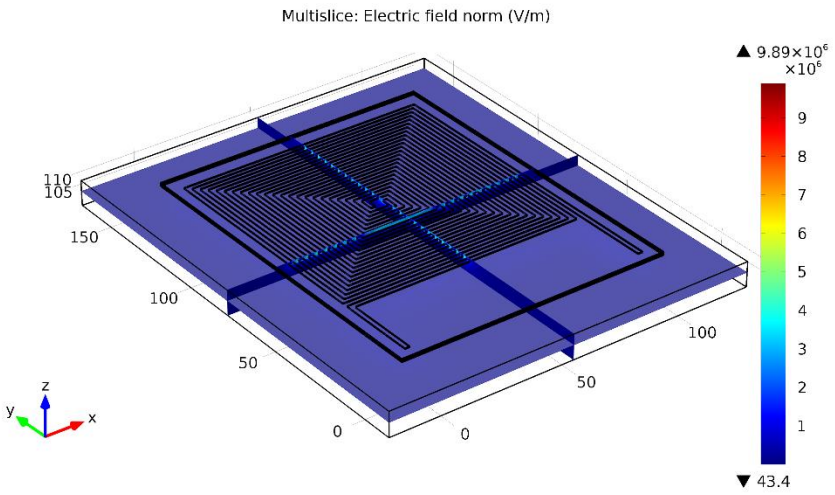

Figure 6-11 3D electric field distribution of the design (h) in COMSOL

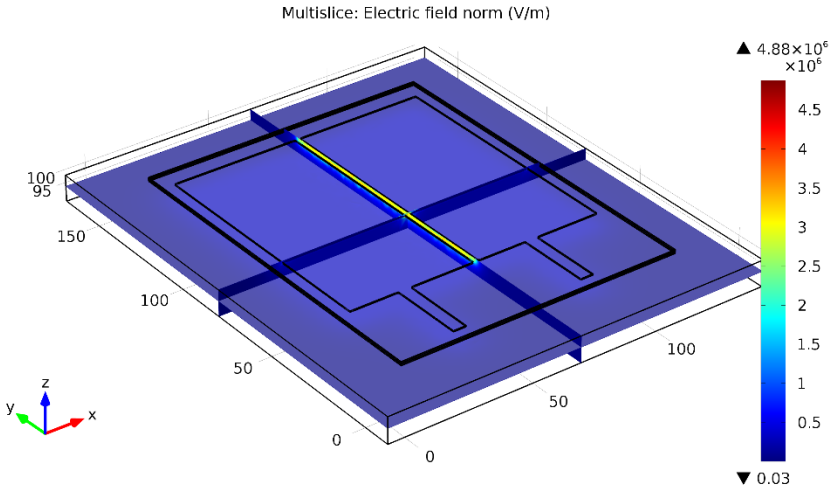

Figure 6-12 3D electric field distribution of the design (i) in COMSOL

6.4.3 3D electrostatic simulation results and discussion

Although the electrode and dielectric thicknesses were not the same as their physical dimensions, in terms of comparing only the pad geometry, the simulation results, i.e., the total capacitance obtainable for each pad geometry, are still helpful. In COMSOL, the total capacitance can be derived from the following expression:

$$C = \frac{2W_e}{V^2} \quad (6\text{-}1)$$

where W_e is the total electric energy of the electroadhesive system and V is

the voltage applied across the electrodes.

The total capacitance generated by each pad geometry on the glass substrate is presented in Figure 6-13, where a is the interdigitated or comb shape, b is the snake-electrode shape, c is the serpentine-electrode shape, d is the curve-comb shape, e is the worm-comb shape, f is tooth-comb shape, g is the concentric shape, h is the spiral shape, and i is the double-electrode shape. As aforesaid in Chapter 4, the larger the total capacitance, the larger the electroadhesive forces can be generated by the pad.

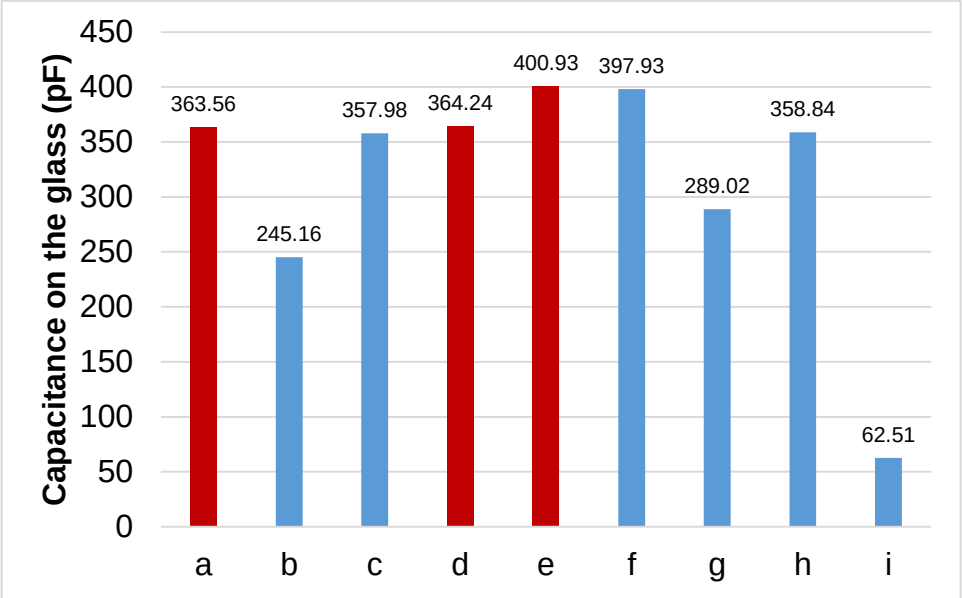

Figure 6-13 Capacitance of the electroadhesion systems on the glass

From the results in Figure 6-13, the novel worm-comb shape (design e) has the largest total capacitance on the glass plate, whereas the double-electrode shape (design i) has the lowest total capacitance on the glass plate. There is a 540% relative increase between the double-electrode shape and the novel worm-comb shape. This means that the pad geometry does cause a significant difference to the electroadhesive forces obtainable on non-conductive substrates such as the glass. Based on the literature review in Chapter 3, to order to achieve the maximum forces, it is preferable to have as many electrode pairs as possible. For the double-electrode design, as there is only one electrode pair, it is

reasonable to have smaller capacitance and thus smaller force.

Also, it is interesting to note that among the five comb shapes, i.e. the geometry a, c, d, e and f, only a 10% relative difference can be seen. The geometry b generates a lower total capacitance on the glass than the comb shapes. This is similar to the results obtained by Savioli et al. [64]. It seems that the concentric shape is not necessarily superior to the comb shapes, which is different from the results obtained by Ruffatto et al. [73]. This may be because varying electrode widths [73] were not adopted here. Also, the effective electrode area is smaller. This requires a further and systematic experimental validation.

In COMSOL, the force generated on the whole substrate can be produced as well. The electromagnetic force derived in COMSOL is based on the Maxwell stress tensor method based on the equation (2-20). The force per unit area (as shown in Figure 6-14) can be derived by the following expression:

$$f_z = \frac{F_z}{S} \quad (6\text{-}2)$$

where F_z is the force on the substrate and S is the effective pad area.

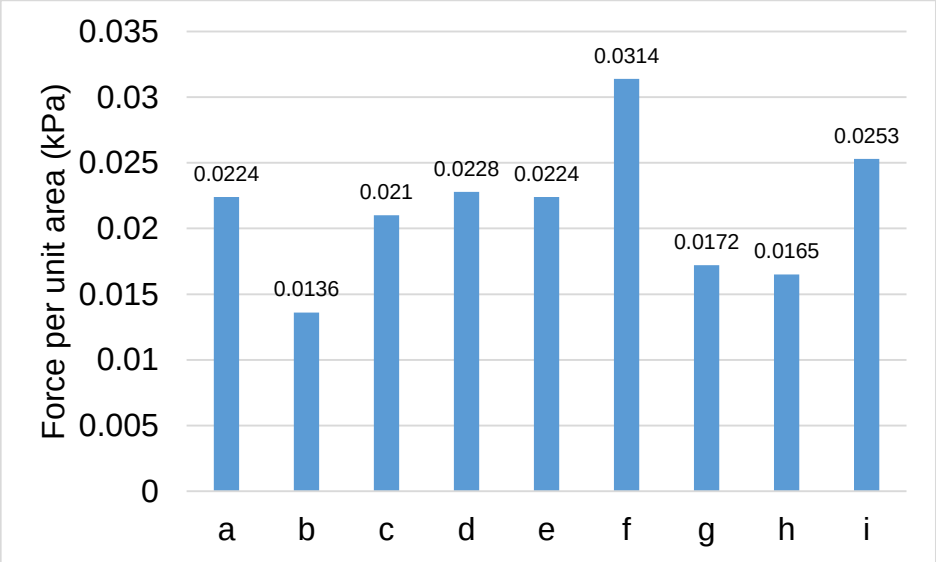

Figure 6-14 Force per unit area of the electroadhesion systems on the glass

The trend shown in Figure 6-14 is different from Figure 6-13. Based on the literature review, the result shown in Figure 6-14 is doubtful and requires further validation. The total capacitance generated by each pad geometry on the Al substrate is presented in Figure 6-15, where a to i denotes the pad geometry mentioned in Figure 6-2. The Al substrate is the default Al material in the COMSOL material library. The dielectric constant of this material was set as 10000. It is demonstrated in Figure 6-15 that all the pad geometries have larger total capacitance obtained from the glass substrate. This is due to the fact that the Al is grounded at the bottom. The larger forces are expected as depicted in section 2.2.1. The novel worm-comb shape (design e) has the largest total capacitance on the Al plate, whereas the concentric shape (design g) has the lowest total capacitance on the glass plate. This is due to the fact that the pathe effective electrode area of design g is smaller.

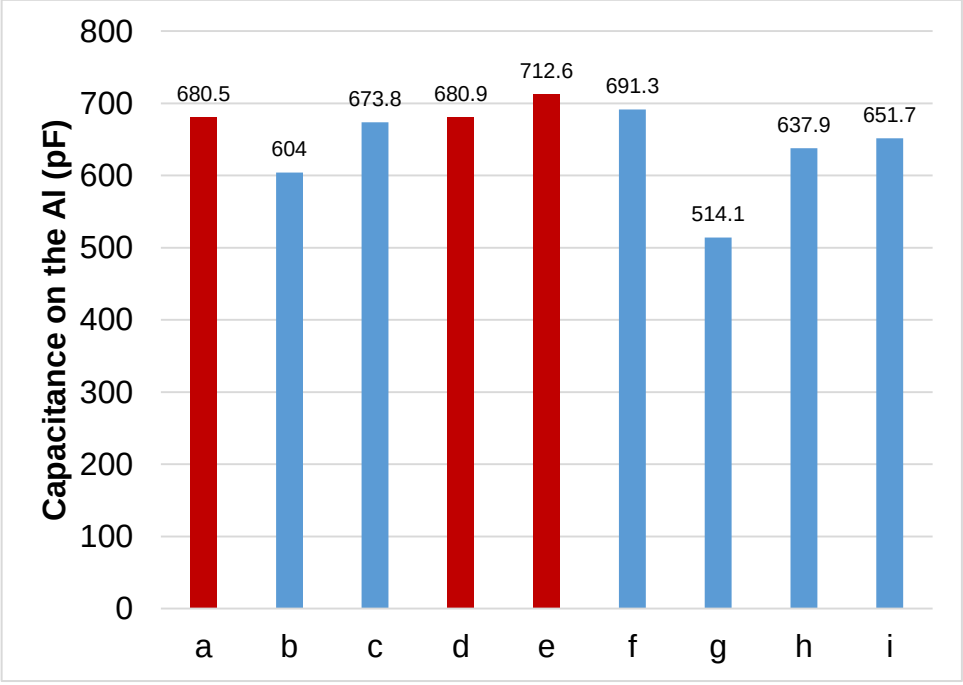

Figure 6-15 Capacitance of the electroadhesion systems on the Al

Again, the trend shown in Figure 6-16 is different from Figure 6-15, which requires further validation. The larger results shown in Figure 6-16 is due to the fact that the Al was earthed.

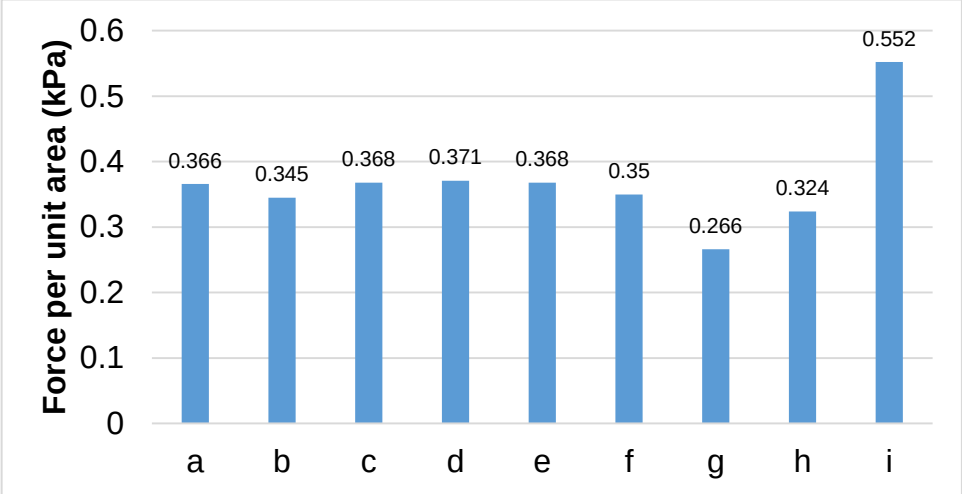

Figure 6-16 Force per unit area of the electroadhesion systems on the Al

6.5 Design of a custom setup for the experimental validation

Experimental validation should be conducted to check whether the simulation results are accurate and can bring enough confidence. It is desirable that the experimental results agree with the simulation results as this will result in less pad manufacturing and experimental testing, thus a more cost-effective and efficient process being achieved in the future of novel pad geometry investigation.

The DC PSU (Instek GPD3303) used in Chapter 4 and 5 can only output a 0.1 V resolution, which means the resolution of the EMCO HVC output is as low as 200 V. In order to validate the simulation results, where only a slight difference between some pads such as (c) and (d) in Figure 6-2 is seen, a better voltage output resolution should be used. In this Chapter, an Arduino based electroadhesive grasping platform was designed and is used here. This platform was adapted from the platform that has been presented in detail in Chapter 7. Only the vertical movement part of the platform was used. The pad was attached to the pad holder of the linear rail to pick up a plasterboard tile, with dimensions of 80 mm x 80 mm x 2 mm (thickness). Plasterboard tile has good electroadhesion properties and is easy to procure. The minimum voltage needed for each pad geometry to pick-up the plasterboard tile was recorded and

compared. This information is also useful for the adaptive electroadhesive gripper design that has been introduced in Chapter 7.

6.5.1 Design of an UNO based electroadhesive grasping platform

In order to use the Arduino to control the actuators via inputs from sensors or inputs from the Arduino, the open-source Arduino integrated development environment (IDE) was installed and used to write, compile, debug and upload programs (also called sketches). The Arduino IDE is a simplified and intuitive programming environment with numerous premade examples and tutorials already in existence. The Arduino can then communicate with a computer over a USB connected between the Arduino and the computer. The communication between the Arduino IDE and the Arduino is not straightforward as it involves several steps after programming in sketch and clicking the upload button. The first step involves a compilation that translates the code into machine code, the binary language that the Arduino is able to understand and execute. If successful, the binary code is then uploaded via the USB connection to the bootloader on the Arduino and stored in the flash program memory. The binary code can then be used by the central processing unit (CPU) of the microcontroller to control the sensors connected with the I/O ports on the Arduino [148].

In this Chapter, an Arduino UNO, based on the ATmega328 microcontroller, has been used as it is the most popular and easy-to-use version of the Arduino family. The Atmega16U2, a USB-to-serial converter on the Arduino UNO, enables the Arduino to communicate with the computer. The introduction, schematic and specifications of the Arduino UNO will not be presented in detail here. The system diagram of the Arduino UNO based electroadhesive grasping platform can be seen in Figure 6-17.

As shown in Figure 6-17, MATLAB GUI was created using the graphical user interface development environment (GUIDE) in MATLAB where a set of tools for creating interactive GUIs is provided. Creating a GUI such as the slider shown in

the figure was helpful as it was possible to control the output voltage of the electroadhesive pads. Also, there was less code as required and the results from the I/O ports could be seen immediately without the need to complete the 'program-compile-upload-execute' circle in the Arduino IDE each time. In order to interface between the Arduino UNO and MATLAB, the MATLAB support package for Arduino hardware [149] was installed.

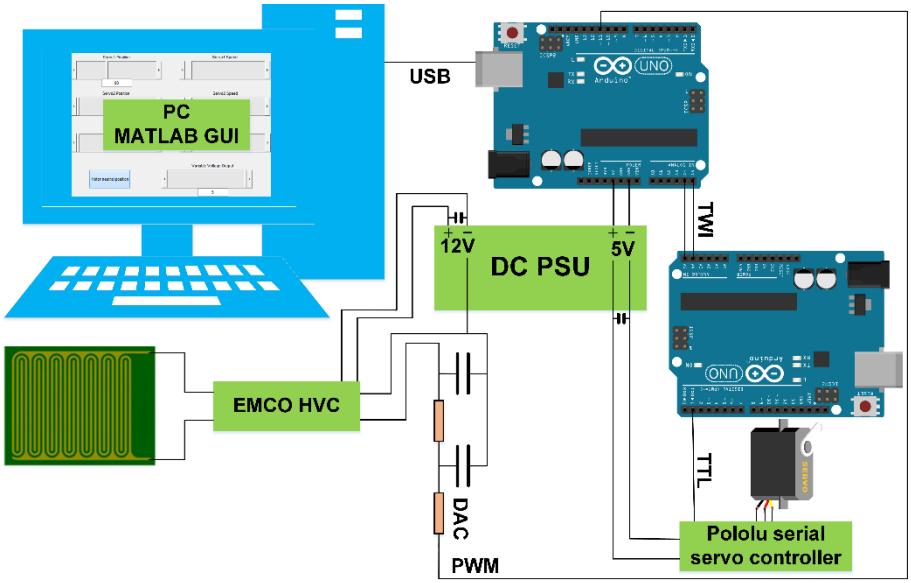

Figure 6-17 System diagram of the Arduino UNO based electroadhesive grasping platform

Since servos draw considerable power, an external servo controller is necessary to free the Arduino UNO from onerous servo control. The Pololu micro serial servo controller is the smallest serial servo controller with individual smooth speed and position control of eight servos. In order to interface between the UNO with the Pololu micro serial servo controller, so that the UNO can control the servo movement, the digital pin 1 on the UNO has to be used. However, the communication between the UNO and the computer is also a serial communication. Therefore, when the serial communication between the computer and the UNO is in use, it is impossible to use digital pin 1 for anything else such as controlling the servo controller. Fortunately, controlling the servo directly using the MATLAB is feasible if two UNOs are used. The communication between the UNO and the Pololu servo controller is via TTL whereas the

communication between the UNO master and the UNO slave is via a two wire interface (TWI) or inter-integrated circuit (I2C).

The pulse width modulation (PWM) pins on the UNO are capable of producing analog outputs with digital means. Analog voltage outputs (0-5 V for HVC inputs) can be achieved by using a low-pass filter such as an RC circuit. In this chapter, a second order RC circuit, was used to output an analog voltage. The resistance was selected as 2.2 kΩ and the capacitance was 10 μF. To generate different analog levels, i.e. different input analog voltages for the HVCs, the duty cycles and thereby the pulse widths of the digital signal was changed accordingly.

Please note that there are three ways (see Figure 6-18) for the interactive communication between MATLAB GUI and Arduino controlled Polou servo controller. Two MEGAs, as shown in Figure 6-18 (a), can also be used instead of two UNOs mentioned above. As the MEGA has four serial ports, a USB-TTL adapter can be used such that only one Arduino board is used. If one prefers to program himself/herself (no Arduino Support from MATLAB) and simply the setup such that the PC can control the Pololu directly using only one Arduino board, functions such as ‘serial()’ and ‘fwrite()’ can be used. The reason of adopting the (a) solution was because the plan to use this setup control a two-module based electroadhesive climbing robot that employs 24 servos (see future work). In Figure 6-18, (a) and (c) have been investigated and completed the proof-of-concept. However, this is an ongoing investigation and is not yet fully completed.

The CAD design for the customised Arduino UNO based electroadhesive grasping platform can be seen in Figure 6-19, where the HVCs are the same ones used in Chapter 4 and 5. The vertical movement part is adapted from the 785 gear rack kit where the continuous rotation servo for the linear movement is HS-785HB, the metal servo gear has 16 teeth and it has the same pitch (32 pitch) with the beam gear rack [150]. Please note that the platform shown in

Figure 6-19 was designed to test the professionally manufactured pads mentioned in section 6.4.1. It is not the test platform for the experimental validation presented in section 6.6 as the time and fund are limited for this PhD.

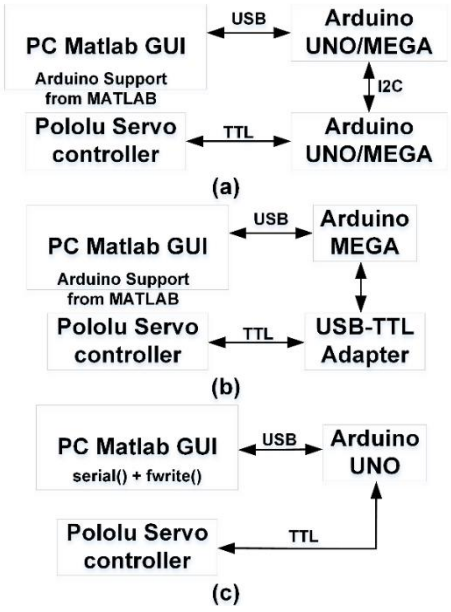

Figure 6-18 Solutions for the interactive communication between MATLAB and the Pololu

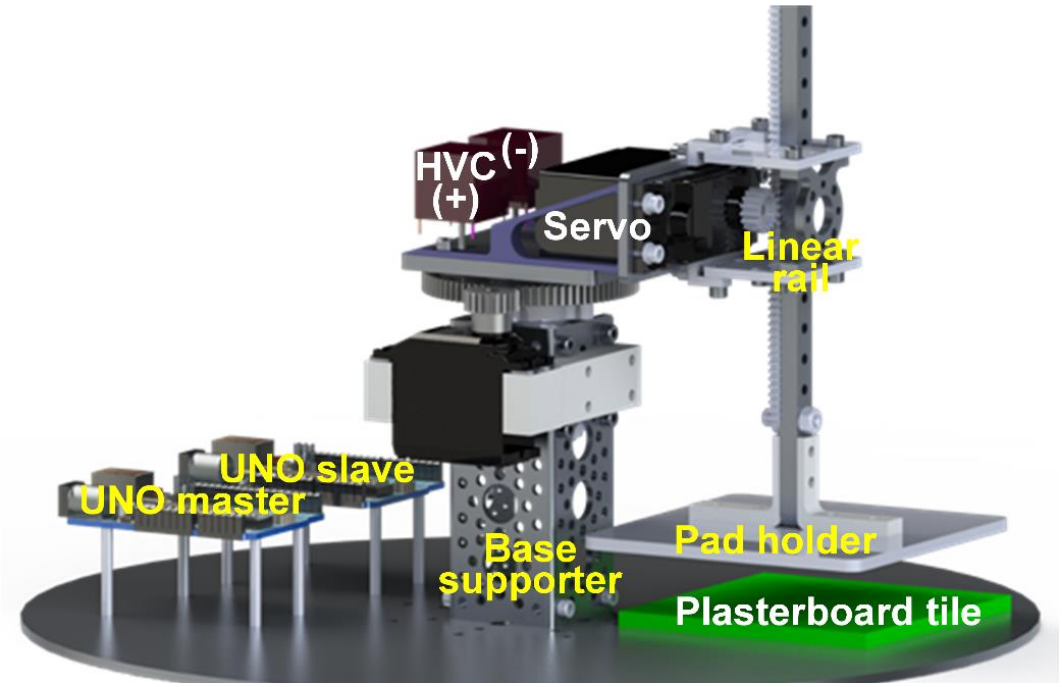

Figure 6-19 CAD for the UNO based electroadhesive grasping platform

A proof of concept of the design was accomplished. The schematic diagram of the proof of concept setup can be seen in Figure 6-20, where three BMS-620MG

servos were used.

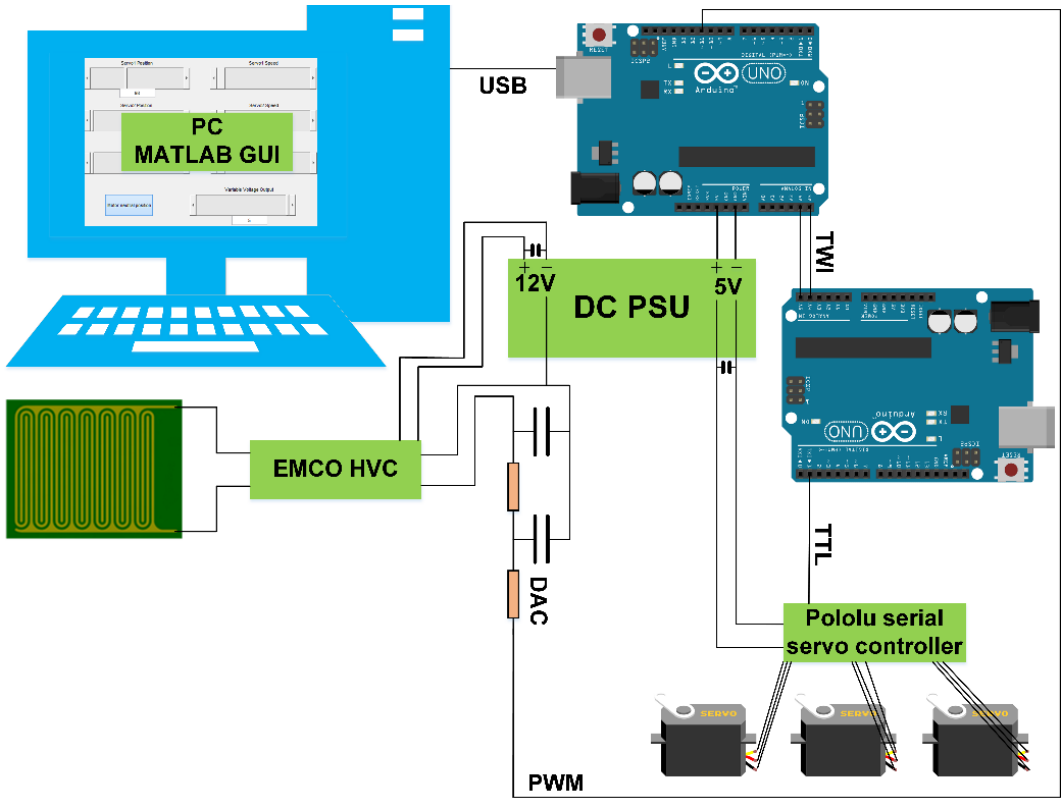

Figure 6-20 Schematic diagram of the setup for proof-of-concept of the customised Arduino UNO based electroadhesive grasping platform

6.5.2 Design of experiments based on the custom test setup

As aforementioned and can be seen from Figure 6-19, the known weight, a plasterboard tile, with dimension of 80 mm x 80 mm x 2 mm (thickness), was chosen to be the substrate to be picked up by the selected pads. The Arduino UNO based electroadhesive grasping platform was used to obtain the minimum voltage needed to pick up the known weight. To this end, the experimental procedure was designed as shown in Figure 6-21.

The pad is first attached to the pad holder and then the linear rail is driven by the continuous rotation servo will move the pad down to the substrate. The linear rail is located to the same designated position for each pad and holds that position for 30 seconds. A voltage is then applied to charge the pad for 300 seconds,

which is long enough to reach the maximum electroadhesive forces between the pads and the substrate. After this, the pad is pulled away. If the substrate is successfully picked up, the substrate will be unclamped and grounded for 600 seconds, which is long enough to dissipate the residual charges. The applied voltage was then decreased by a set value, 20 V, and the pad was moved down to the same position again to pick up the same known weight. This procedure was repeated until the pad could no longer pick up the weight. The minimum voltage needed was therefore categorised as the value before this. If the substrate could not be successfully picked up, it was still grounded for 600 seconds for residual charge dissipation. The applied voltage was then increased by the same set value, 20 V, and the pad was moved back down into position again to pick up the known weight. This procedure would be repeated until the pad could once again pick up the weight. The minimum voltage needed was recorded to be the value before this.

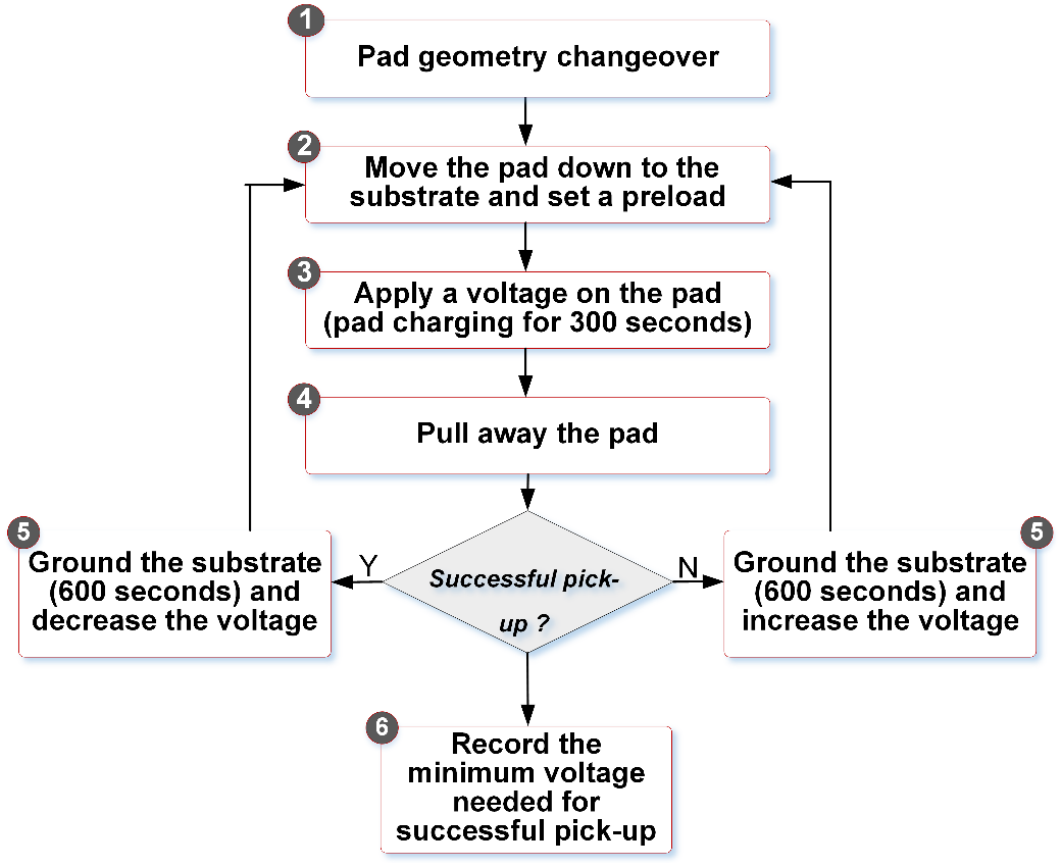

Figure 6-21 Testing procedures for the experimental validation

6.6 Experimental validation of the 3D electrostatic model

An initial experimental validation was conducted to compare the two novel designs, the curve-comb shape (design d) and the worm-comb shape (design e), with the normal comb shape (design a). This initial validation was based on an in-house pad manufacturing process and the same experimental setup used in Chapter 4. Please note that this is due to the limited time and fund for the implementation of the test-rig and high quality pads for comparison.

6.6.1 Electroadhesive pad design and manufacturing for the experimental validation of the 3D electrostatic model

The pads were manufactured using the steps shown in Figure 6-22, where the low-cost in house pad manufacturing method based on the solid ink printing technique was employed. This pad manufacturing method was adopted because it is an economic and efficient approach for the initial experimental validation, although the printer can only print electrode width as small as 0.5 mm. The steps for the pad design and manufacture are presented as follows [140]:

Step 1: Copper laminate preparation

The roll of copper laminate was cut by a cutter into A4 sized pads. The edges of the A4 pads were smoothed with sand paper to remove any burrs or jagged edges to prevent catching within the printer. The pads were then cleaned using Iso-Propyl Alcohol (IPA) and acetone to remove any contaminants to ensure a clean surface for the wax to adhere to. The copper laminate was made of a 20 μm copper adhered on a 23 μm Polyester (PET, dielectric strength: 310 $kVmm^{-1}$, dielectric constant: 3.2)

Step 2: Electroadhesive pad geometry design

All the pads were designed in Solidworks. The effective electrode area of the pad was designed to be 176 mm x 228 mm. The electrode width and space between electrodes were designed to be 1.8 mm and 4 mm respectively.

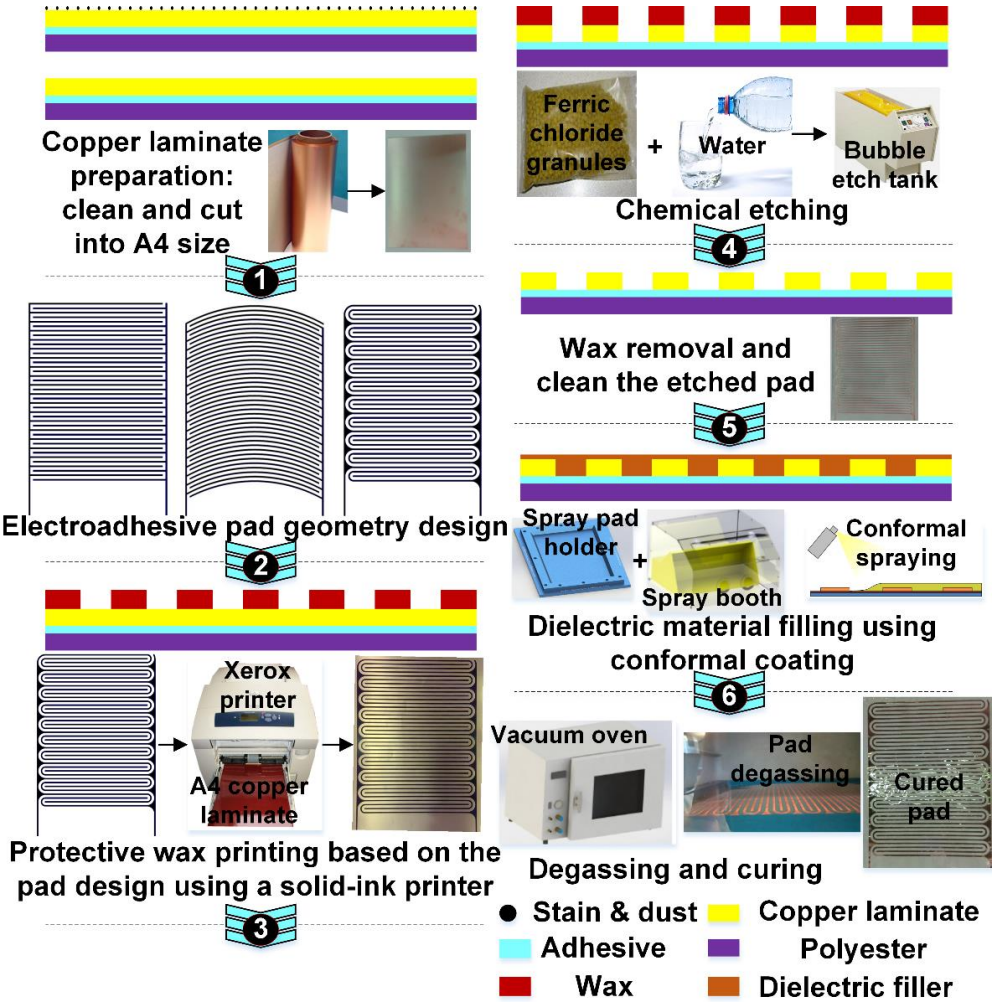

Figure 6-22 Pad manufacturing procedures for the initial experimental validation of the two novel comb pad designs

Step 3: Protective wax printing based on the pad design using a solid-ink printer

The dried A4 pad was loaded into a Xerox solid-ink printer. A protective layer of wax was then printed on the copper side of the copper laminate based on the pad design.

Step 4: Chemical etching

The pad was then placed into a heated bubble etching tank where ferric chloride granules dissolved in water removed the unprotected copper areas leaving the protected wax regions behind.

Step 5: Wax removal and cleaning the etched pad

Once the etching was completed any excess chemical acid was washed off using a water bath. The wax was then removed by applying a label removal. After this, the pad was cleaned using IPA and acetone again

Step 6: Dielectric material filling using conformal coating

After drying the pad, the pad was held flat using a spray pad holder. The conformal spraying of an aerosol of Polyurethane (PUC, dielectric strength: 60 $kVmm^{-1}$, dielectric constant: 3.6) was carried out in a spray booth.

Step 7: Degassing and curing

Once an even coat was applied to the surface of the pad, the pad was placed into a vacuum oven. Once inside, the vacuum was applied to pull out any air bubbles that were within the dielectric. As soon as bubbles were no longer appearing on the surface of the dielectric the oven was turned on and set to 80 ^{o}C and the pad left to cure inside for 90 minutes.

Once the dielectric was cured, the pad was taken out of the oven. The quality of the dielectric covering was then inspected for contaminants, distribution evenness, and areas that were not covered by any dielectric. The cured pad was then left to cool down overnight to ensure that there was no tackiness to the dielectric which would cause it to adhere to the pad holder or substrate.

6.6.2 Electroadhesive force testing and results

The same experimental setup and procedure used in Chapter 4 was adopted in this investigation. During the tests, the pads were properly clamped on the pad holder using double-sided tape, and the PET side of the pads was used to face the toughened glass and the Al substrates used in Chapter 4. The pads were all charged by applying 3.2 kV for 60 seconds before pulling away the pad from the substrate (60 seconds are enough to achieve the maximum forces). The

experiments were conducted when the relative humidity was 40 ± 1 %, room temperature was maintained at 25 ± 0.2 °C by an air conditioning unit, and the preload was set to 32 ± 1 N. The results of the electroadhesive forces obtained by normal comb shape, the curve-comb shape and the worm-comb shape pad on the glass and Al substrates can be seen in Figure 6-23.

On the glass substrate, a relative increase of 1 % and 28 % in the electroadhesive forces obtainable can be seen in the curve-comb pad and the worm-comb pad respectively. On the Al substrate, a relative increase of 5 % and 12 % in the electroadhesive forces obtainable can be seen in the curve-comb pad and the worm-comb pad respectively. These results are both close to the simulation results presented in section 6.4.3, in terms of relative increase in forces. This means that the 3D electrostatic simulation based on COMSOL is a promising method for the pad geometric investigation and optimisation. However, more in-depth simulation and comprehensive experimental validation of all the presented designs are required.

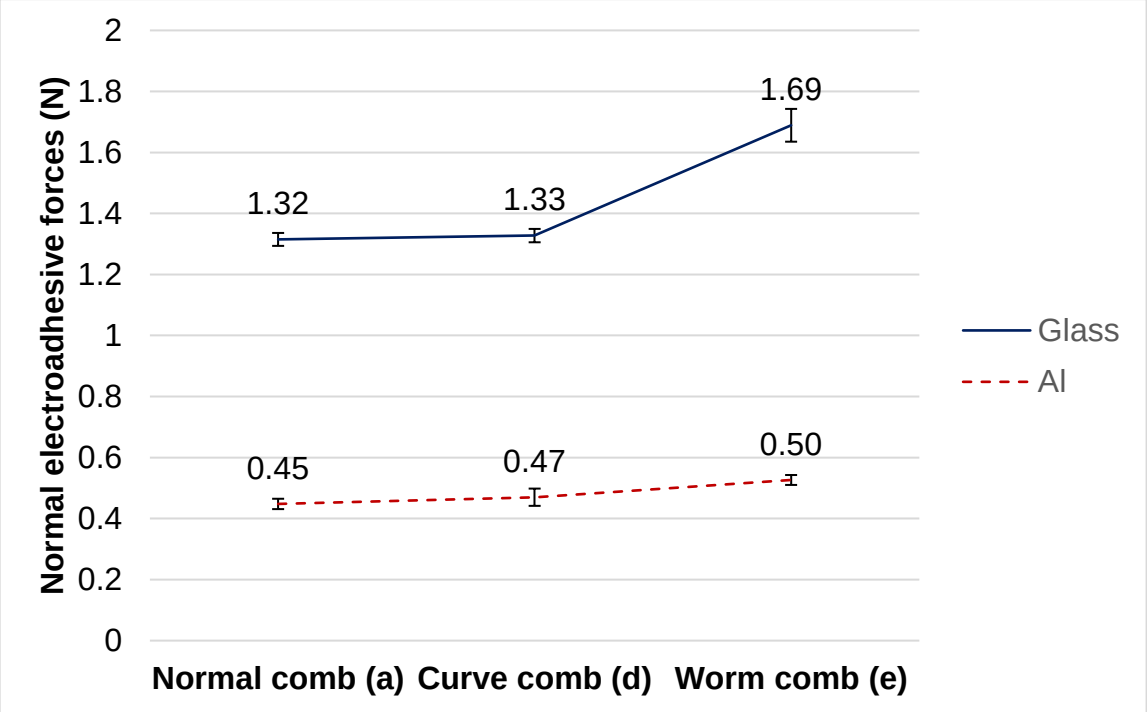

Figure 6-23 Comparison of the normal comb (a), the curve-comb (d), and the worm-comb pad (e) on the glass and Al substrate

6.7 Investigation of the relationship between the double-sided electroadhesive and the electroadhesive force obtainable

The pad designs mentioned in section 6.4.1 are all based on coplanar electrodes. It was presented by Prahlad et al. [151] that double-sided pad designs are better at bearing higher voltages. Although Tong et al. [93] were first to implement the double-sided comb electroadhesive on their climbing robot, no 3D electrostatic simulation and experimental validation has been published to ascertain whether the double-sided pad design is better or not.

6.7.1 3D electrostatic simulation of the worm-comb double-side electroadhesive

The worm comb pad design was selected to compare the coplanar and double-sided designs. The 3D electric field distribution of the double-sided worm-comb pad in COMSOL can be seen in Figure 6-24 (a). The exploded view of the double-sided worm-comb electroadhesive system can be seen in Figure *6-24* (b).

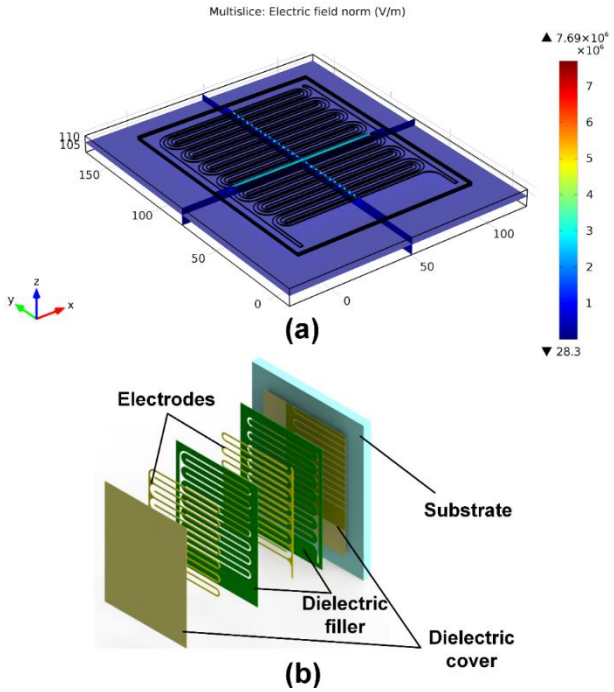

Figure 6-24 Double-sided worm-comb pad: (a) 3D electric field distribution and (b) 3D exploded view of the system

All the geometric dimensions and materials used and the magnitude of the

voltage applied for the double-sided worm-comb design were the same with the aforementioned coplanar design, (e), as mentioned in section 6.4.1. It can be seen in Figure 6-25 that, the double-sided worm-comb design has a 3.2% relative increase in capacitance on the glass compared with the coplanar design. The simulation result manifests that the double-sided design can bring a slightly larger electroadhesive forces than the coplanar design on non-conductive substrates.

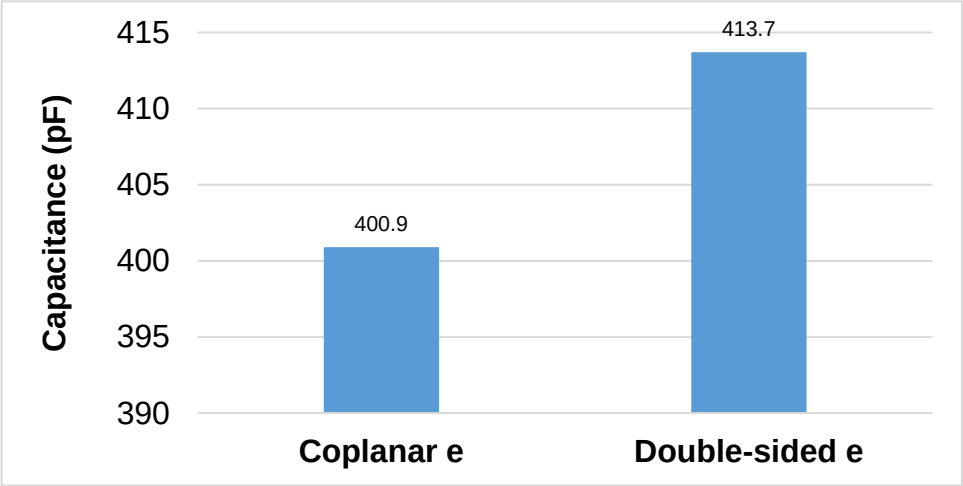

Figure 6-25 Capacitance of the coplanar and double-sided e design on the Al

6.7.2 Experimental comparison between the coplanar pad design and double-side pad design

Experimental validation has been conducted to compare the coplanar comb design with the double-sided comb design based on the same experimental setup used in Chapter 4. Both the double-sided comb pad and the coplanar comb for comparison were professionally manufactured as mentioned in section 4.6.1. The manufacturing steps for the double-sided pads can be seen in Figure 6-26. The geometric specifications of the pads were set as: electrode width: 2 mm, space between electrodes: 2 mm, copper electrode thickness: 38 μm, effective pad area: 190 mm x 230 mm, and PI coverlay thickness: 12.5 μm.

The same experimental setup and similar procedure used in Chapter 4 was adopted in this investigation. The only difference was that the pads were charged

by applying 6/8 kV for 120 seconds before pulling the pad away from the substrate. During the tests, the PI coverlay side of the pads was used to face a plasterboard tile. 6 kV was applied on the coplanar comb pad. 6 kV and 8 kV were applied on the double-sided comb pad. The experiments were conducted when the relative humidity was 44 % ± 1 %, room temperature was 23.6 °C ± 0.1 °C, and the preload was set to 33 N ± 1 N. The initial results, the mean normal electroadhesive forces and their standard deviations (the error bars) for each test, are plotted in Figure 6-27.

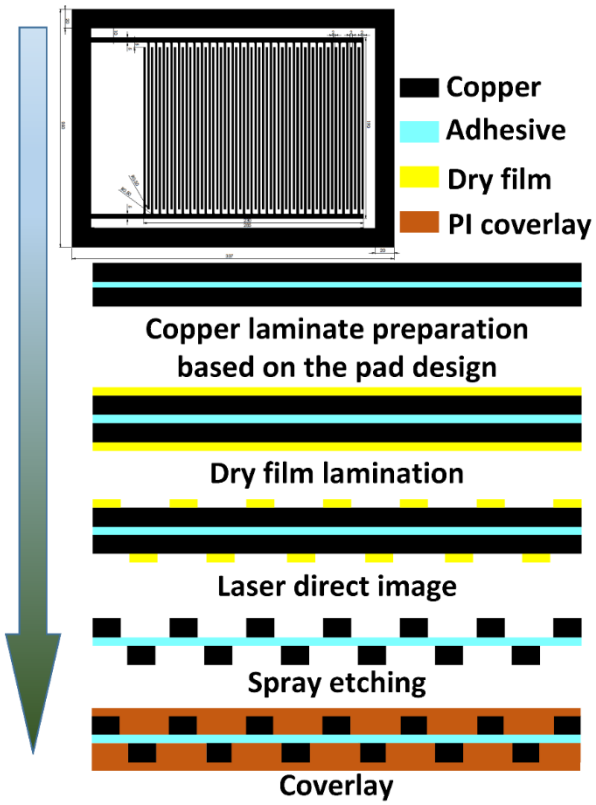

Figure 6-26 Manufacturing process for the double-sided pads

On the tile, the coplanar comb pad failed due to the dielectric breakdown or corona discharge after three times of testing at 6 kV. The result presented in Figure 6-27 for the coplanar comb pad was therefore only based on three experiments. The double-sided comb pad still worked properly up to 8 kV. This indicates that double sided can cope with higher voltages. Also, the double-sided comb pad has a relative increase of 8 % in the electroadhesive forces obtainable

on the tile compared with the coplanar one at 6 kV. Experiments over 8 kV on the double-sided pad were aborted due to potential damage to the pad.

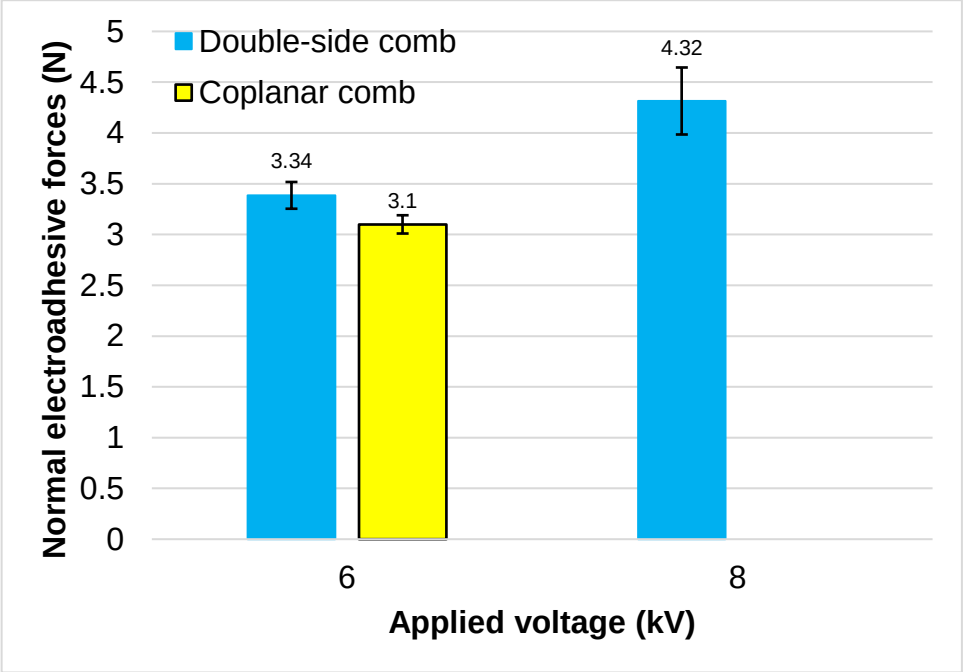

Figure 6-27 Experimental comparison between the coplanar and double-sided comb pad

The reason why the double-sided design can cope with higher voltages is maybe due to the insulating layer between the two layers of the electrodes as shown in Figure 6-27. Further investigation into why larger forces can be obtained using the double-sided design is required.

6.8 Discussion

In order to validate that the proposed 3D electrostatic simulation method is useful for pad design and performance checking prior to pad manufacture and testing, the simulation results from Figure 6-13 and Figure 6-15 and experiment results from Figure 6-23 were compared and demonstrated in Figure 6-28. Clearly, the trend is similar, manifesting that the method is promising for evaluating the pad design before spending time and money on pad manufacture and testing.

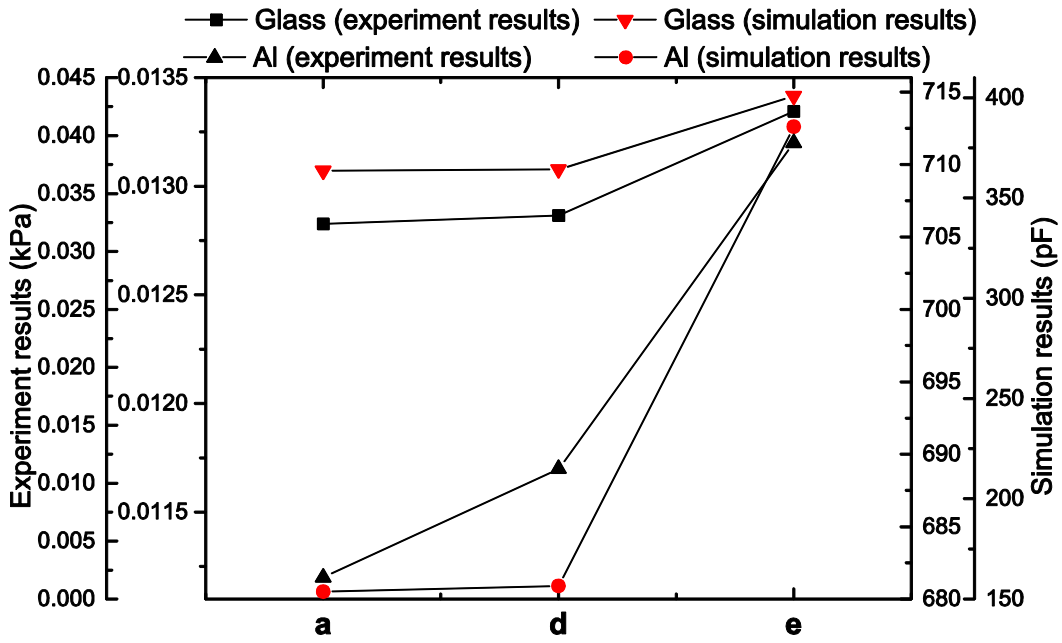

Figure 6-28 Trend comparison between the simulation results and the experiment results

This research is an ongoing investigation and is not yet fully completed. The major continuation work, which has already been designed and planned, is to use the customised test rig to tests the pads mentioned in section 6.4.1 based on the design of experiments described in section 6.5.2. A comprehensive experimental comparison of all the 9 pad designs should be conducted support or revise the simulation model. Also, it has to be noted that the electric field distribution of normal comb designs is not uniform. It is therefore useful for the investigation into novel pad designs such as novel electrode configurations [152] that can output uniform electroadhesive forces across the pad area.

6.9 Summary

The contents presented in this Chapter are, to the best of the author's knowledge, the most comprehensive investigation into the relationship between the electroadhesive forces obtainable and different pad geometries based on 3D electrostatic simulation using COMSOL Multiphysics and experimental validation based on the novel and customised mechatronic electroadhesive grasping platform.

The key findings from this work are:

● Different pad geometries do bring different total capacitances of the electroadhesive systems thus the electroadhesive forces obtainable.

● The novel curve-comb shape and worm-comb shape perform better in the electroadhesive forces obtainable than the normal comb shape based on the results both from simulation and experiments.

● The double-sided pad designs can not only result in larger electroadhesive forces than the coplanar designs but also perform better at higher voltages on non-conductive substrates.

All the summarisations and findings from Chapter 2 to Chapter 6 suggest that it is necessary to enhance the level of adaptability and intelligence of the electroadhesion system. This is discussed in detail in Chapter 7.

7 General Discussion

7.1 Introduction

As previously stated, electroadhesion, as an advanced adhesion mechanism, has a distinctive advantage, enhanced adaptability, over other adhesion mechanisms [13]. In Chapter 7 the need for adaptive and intelligent electroadhesion based on reviewing other researchers' work and evidences obtained in this research is identified. Based on this, a new and detailed definition of adaptive and intelligent electroadhesion is proposed. Possible solutions towards the proposed concept are also discussed. After this, a mobile and autonomous electroadhesive grasping platform based on the Arduino MEGA is designed after a feasibility study and for future proof of concept demonstration.

7.2 Need for adaptive and intelligent electroadhesion and solutions

Electroadhesion can be adaptable to different surfaces, however, the level of its adaptability is limited to flat and smooth surfaces if only a flat and rigid electroadhesive pad is used. Different methods can be applied to enhance the level of adaptability of the electroadhesion system. Desirable solutions to adaptive and intelligent electroadhesion can be substrate surface texture adaptive, substrate shape adaptive, environmentally adaptive and substrate surface material adaptive with quick clamp/unclamp speed, lower power consumption, longer life cycles, and greater safety. This leads to the proposed adaptive and intelligent electroadhesion concept that has not been described in the literature.

An adaptive and intelligent electroadhesion system is an electrostatic adhesion system that is substrate surface texture adaptive, substrate shape adaptive, environmentally stable and adaptive, and substrate surface material adaptive with quick clamp/unclamp speed, lower power

consumption, longer life cycles, and greater safety.

It has been concluded from Chapter 5 that the electroadhesive force would vary significantly from the same substrate material with different surface textures. Higher voltages or mechanisms that enable the electroadhesive pad to conform to rough surfaces are therefore required to maintain the forces on different surface conditions. Researchers have employed compliant dielectrics into electroadhesion for adapting to rough surfaces such as dry adhesives made of Vytaflex [72] and PDMS [61][97], fluid dielectrics, a layer of elastic foam [49], and inductive fibres [42]. However, the Vytaflex attracts dust and hardens over several weeks of use. The film enclosing the fluid dielectrics become damaged easily. The polymeric electrostatic inductive fibres and delicate dry adhesives are difficult and expensive to manufacture. Investigating economic dry adhesive (similar to the gecko feet, with self-cleaning capabilities) manufacturing methods and combining the dry adhesive with electroadhesion may be an appropriate method going forwards. If this is feasible, the electroadhesive gripper may be able to adhere to a wider range of rough substrate surfaces, thus reducing the need for a priori identification of those surfaces. The **best solution** at the present time would be to employ an optimised electroadhesive geometry that is not sensitive to surface texture directions with a layer of elastic foam and a higher voltage if required.

Elelctroadhesive pads are able to conform to curved surfaces to some extent if compliant dielectric materials are used [14], however, in order to grasp uncooperative objects/surfaces, substrate shape adaptive methods are more preferable. Morphing electroadhesive mechanism [64], i.e. electrodes embedded into shape memory polymers, curved surface gripper mechanism [80][120], i.e. electroadhesive pads attached onto a two-finger end effector, and vacuum augmented electroadhesive [153] have been therefore applied. For the existing solutions to enhance the adaptability of the electroadhesive pad to adhere to

different substrate shapes, curved electroadhesive surface gripper mechanism may not grasp complex freeform objects. The vacuum augmented electroadhesive design may help grasp complicated surface shapes but an extra pump is required and it cannot be used in vacuum environments. The resistive-electroadhesive mechanism is a promising solution although it is inefficient at the moment due to the long time required for the cooling phase. The **best solution** at the present time would be to combine the economic memory foam approach with the electroadhesive pad.

It has been concluded from Chapter 3 that environmental factors significantly influence the electroadhesive forces obtainable. Designing and implementing an electroadhesive system that can output repeatable and reliable electroadhesive forces in changing ambient environments where significant temperature/humidity/pressure variations may be observed is also highly desirable. From the extensive literature undertaken as part of this thesis, the author has not found any publication detailing a method for creating an environmentally stable and adaptive electroadhesive system. One possible solution is to embed the electrodes into a dielectric material that is less sensitive to environmental changes. A novel environmental adaptive electroadhesive pad manufacturing is plasma sputtering or conformal spraying of environmental stable dielectrics such as ceramic materials on top of etched or plasma sputtered conductive electrodes, be it copper, aluminium, or gold.

Electroadhesion itself can be adaptable to different substrate materials, although potentially not on some plastics [14]. If the substrate materials to be grasped (such as an aluminium plate, a glass plate, and a polycarbonate sheet) have the same weights, the polycarbonate sheet will need a higher voltage. If a higher voltage is used for all substrates then the power consumption will increase and the number of life cycles of the electroadhesive pads will decrease because higher voltages than required are applied. Also, adhesion failure may occur when

changing from grasping the polycarbonate sheet to the aluminium plate as the high voltage used to grasp the polycarbonate sheets could result in a dielectric breakdown of the electroadhesive pad or instant ionisation of the air between the pad and the aluminium plate. This will bring potential safety issues to operators working nearby. It is therefore desirable to have electroadhesive systems that can produce large enough forces for grasping different substrate materials by applying lower voltages thus greater safety, minimum power consumption, and longer life cycles can be achieved. **The solution to this will greatly enhance the adaptability and robustness level of the electroadhesive system to grasp different substrate materials.** As an example, this Chapter has been focusing on offering solutions to this.

The solution proposed here is based on embedding the electroadhesive systems with intelligence so that the minimum voltage can be applied on the end effector: the electroadhesive pad, when grasping different substrate materials. In order to inform the electroadhesive systems with regard to varying the voltages to be applied on the pad when grasping different materials, some feedback or signal such as force or voltage should be extracted from the end effector. The feedback signal should enable the pad to have the intelligence it needs so that an adaptive voltage can be applied. Two possible designs have been conceptualised based on the fact that the electroadhesive forces obtainable are different when grasping different substrate materials, even when the same voltage is applied. One is the force feedback design where the forces obtained can be used for identification. The other is the voltage feedback design where the output voltages can be used for material identification. For the moment, these solutions are based on the assumption that a prior knowledge with regard to the weight and dimension of the substrate to be picked up is known. The minimum voltages needed to pick up the specified substrates are also known.

There are several possible solutions to the force feedback design. One solution

is to use the commercially available 9.1 grams Nano171 ATI F/T sensor (17 mm in diameter). However, this solution is expensive will cost at least £4000 and the integration between the Nano171 with the Arduino is not straightforward. Another solution inspired by Nano171 is to customise a compression and extension force sensor based on four TML strain gauges from Tokyo Sokki Kenkyujo Co., Ltd. Two of these strain gauges could be installed in the radial direction. The other two could be installed in the circumferential direction. The four gauges can then be connected as a Wheatstone bridge so that temperature can be compensated for. A data type that can be read by the Arduino based on the 4-wire SPI communication interface could be transformed from the strain data via a 24-bit ADC, such as PmodAD5™ (Digilent). However, careful installation and calibration of the strain gauges are required for this customised design. A final design are compression and extension springs connected in series used together with distance sensors such as an infrared sensor or ultrasonic sensor to provide the force feedback. For this solution, high resolution is a necessity for the distance sensors to record the movement of the springs that correspond to the force changes.

For all the solutions to the force feedback design detailed above, a 5-step procedure, as shown in Figure 7-1, is needed to fulfil the proposed adaptive electroadhesion design. The force-time curve can be seen in Figure 7-1 (a) and the implementation procedures can be seen in Figure 7-1 (b). The system starts with approaching the substrate with a pre-defined preload such as 10 N. The pad is then pulled away after applying a lower voltage such as 1000 V, for a predefined period of time such 30 seconds. The maximum force is then recorded and saved to a look-up table (LUT) that links the minimum required voltages for different substrates with the forces obtained based on the same lower voltage applied. The pad then approaches the substrate again with the same preload. The substrate can be finally picked up based on the minimum voltage required specified in the LUT.

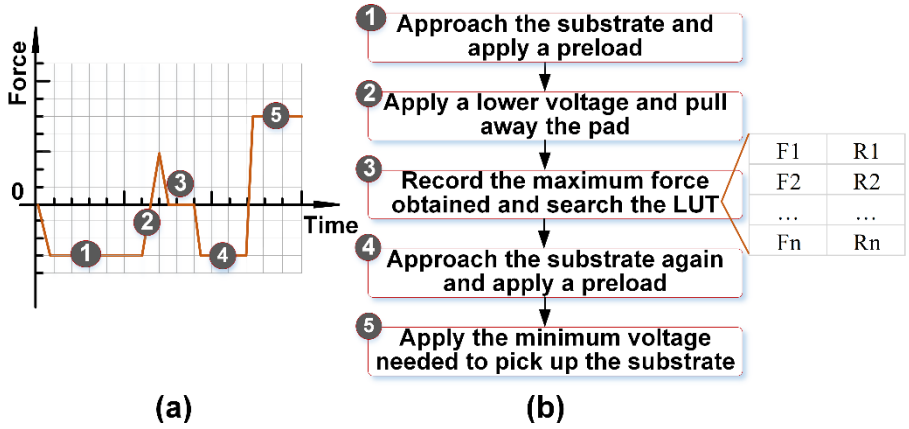

Figure 7-1 Implementation steps for the force feedback design

For the voltage feedback design, an analog capacitive sensor such as BCW M18B4M1-ICM80C-DV02 (Balluff) could be used. The capacitive sensor can be used for material identification. A LUT can then be generated, linking the relationship between substrate materials with known weights and the minimum voltage for grasping them. The analog capacitive sensor can be eliminated, however, due to the fact that the electroadhesive pads can be capacitive sensors themselves. This is an advanced adaptive electroadhesion solution. For instance, one electrode of the pad can be connected with sine pulse excitation, and another electrode can be connected with a charge amplifier that will output different voltages when facing different substrates. An intelligent switch should then be adopted that can enable the pad to switch from the high voltage input mode to the low voltage sine pulse excitation mode needed for material identification. An attempt, as shown in Figure 7-2, has been conducted to prove the concept. One electrode of the electroadhesive pad was connected with an oscillating circuit that can output 12 V AC voltage with frequency of 2 kHz. The other electrode was connected with an oscilloscope. The initial result can be seen in Figure 7-3, annotated by a yellow arrow.

For all the solutions to the voltage feedback design, only a 3-step procedure, as shown in Figure 7-4, is needed to fulfil the proposed adaptive electroadhesion. The force-time curve can be seen in Figure 7-4 (a) and the implementation

procedures can be seen in Figure 7-4 (b).

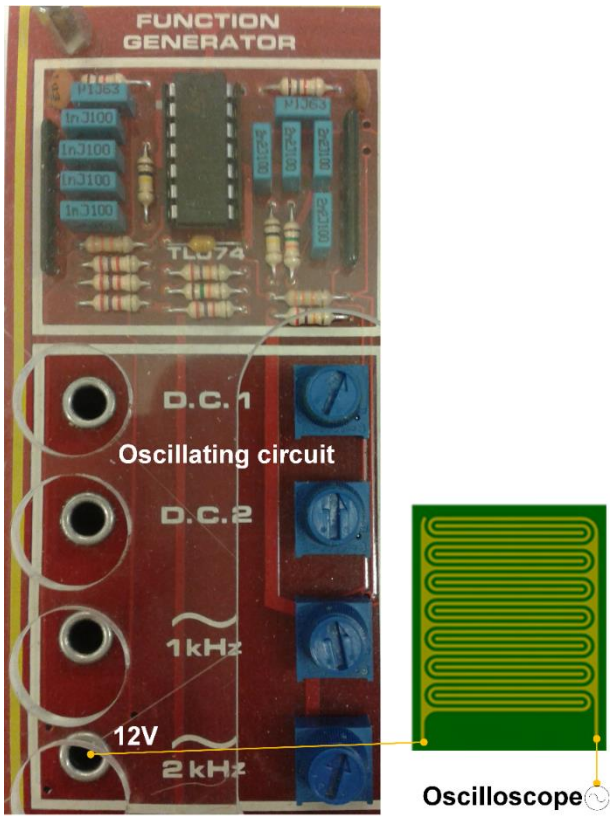

Figure 7-2 Proof-of-concept setup for the advanced adaptive electroadhesion solution

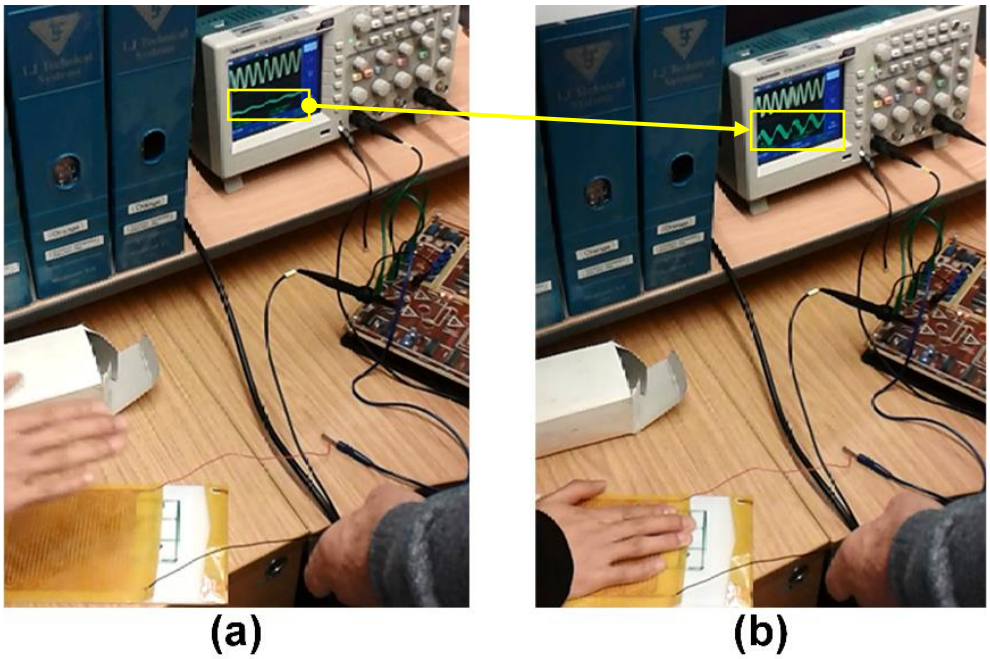

Figure 7-3 Initial results of the advanced adaptive electroadhesion solution: (a) the hand was not touching and (b) was touching the pad

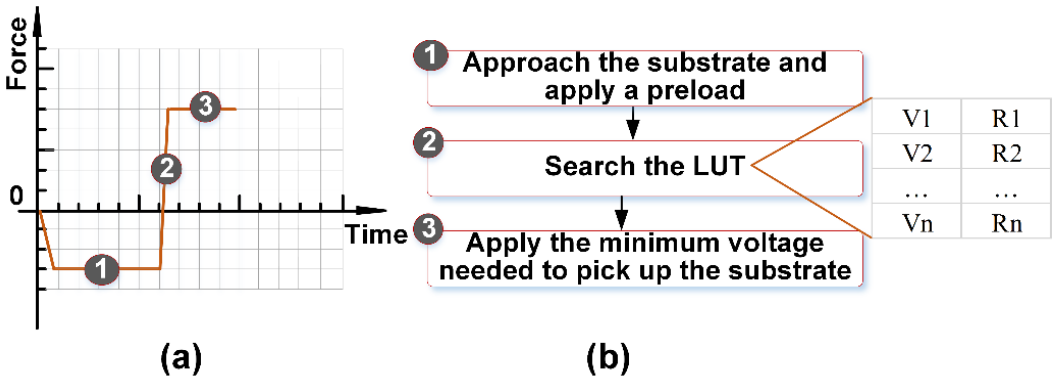

Figure 7-4 Implementation procedures for the voltage feedback design

In step one, the pad is driving down to approach the substrate and a pre-defined preload is applied (10 N). In step two, the analog capacitive sensor is then energised for material identification. After this step, the output voltages for different substrates can be recorded and saved to the LUT that links the minimum required voltages for different substrates with the output voltages based on the same applied preload. Finally, in step three, the substrate can be picked up based on the minimum voltage required, as specified in the LUT. The **best solution** at the present time is to combine the Balluff analog capacitive sensor with the electroadhesive pad, to create a proof of concept for substrate surface material adaptability with lower power consumption, longer life cycles, and greater safety.

7.3 Design and implementation of the proposed concept

The platform for the proof of concept was designed to be as simple as possible. Only two degrees of freedom (DOF) were therefore used. One DOF was for the linear vertical movement to clamp and unclamp the substrates. The other DOF was for the rotational movement for grasping different substrates. The linear movement part, the 785 Gear Rack Kit [154], is commercially available from ServoCity. The rotational movement part was adapted from the Gear Drive Pan Kit [155] from ServoCity.

7.3.1 Feasibility study of the capacitive sensor

Before the final design of the platform for the proof of concept, the Balluff analog capacitive sensor was integrated with an UNO to validate its capability of material identification. A schematic diagram can be seen in Figure 7-5. A 250 Ω resistor was used because the maximum current output of the analog capacitive sensor is 20 mA when the sensor is out of its effective sensing distance. The maximum resolution can therefore be output and read by the analog port on the Arduino. It should be noted that a special calibration (refer to the application note [156]) is needed in order to maintain the full output signal range when performing measurements on objects with a low dielectric constant below 10. This is because the delivered part is calibrated on a metal target [156]. The physical setup for the feasibility study of the analog capacitive sensor can be seen in Figure 7-6.

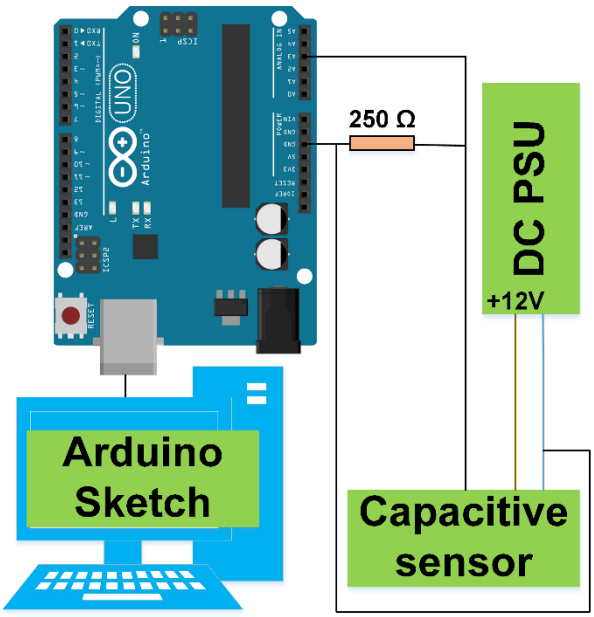

Figure 7-5 Schematic diagram for the feasibility study of the analog capacitive sensor

The capacitive sensor was tested on the same four aluminum plates and three sandpaper samples used in Chapter 5 to investigate the influence of surface roughness to the result. For all aluminium plates, the results were the same, 0.85 V. For the P1200 and P400 sandpaper samples, the result was 1.35V. For the P120 sandpaper sample, however, the result was 1.5V. This may indicate

that the sensor is insensitive to surfaces (based on the same material) if the surface roughness difference is small. Also, the sensor was tested on other different dielectric substrates: wax, MDF, and acrylic. It is clear from Figure 7-7 that the sensor is feasible to differentiate different substrate materials, where the measured voltages are displayed and summarised in Table 7-1.

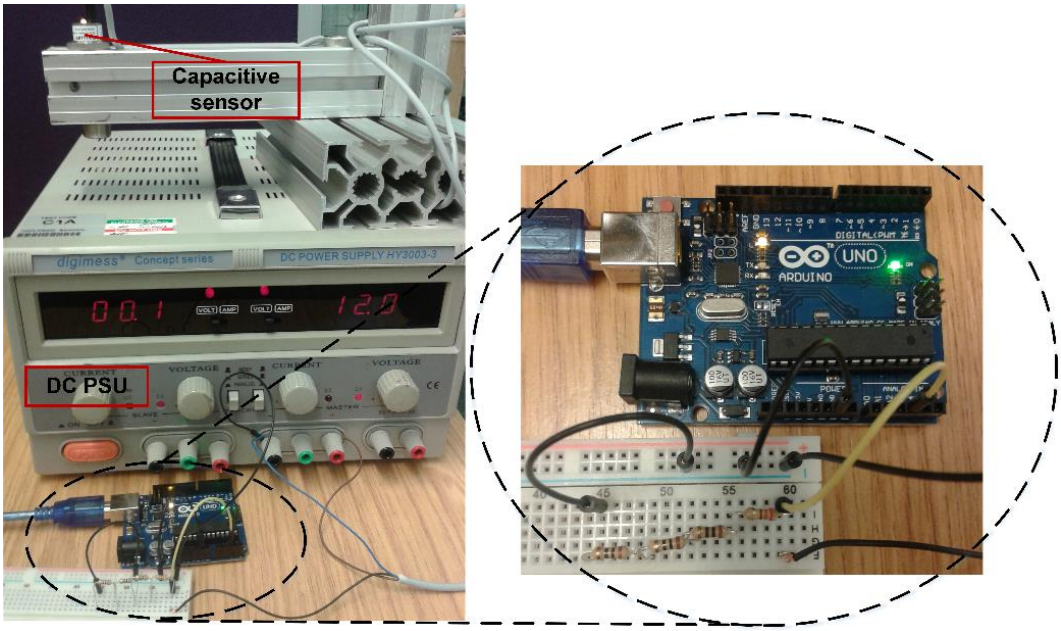

Figure 7-6 Physical setup for the feasibility study of the analog sensor

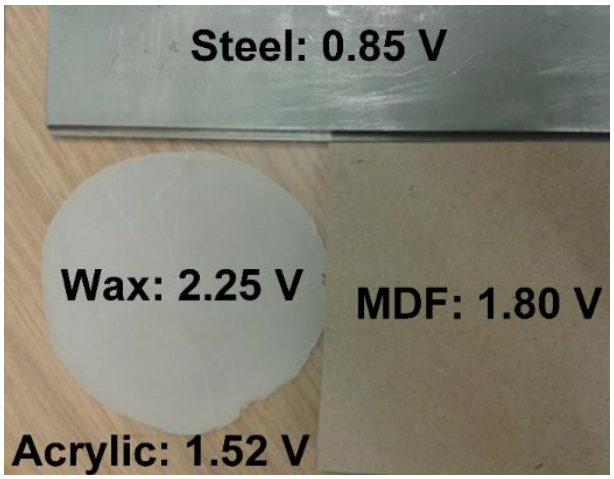

Figure 7-7 Experimental testing of the analog capacitive sensor on different substrate materials

Whether there is any interference between the energised pad and the capacitive sensor was also checked. Little difference was found on the voltage output when the pad (the same pad used in Figure 7-2) was not energised and energised at

4 kV. This manifests that it is feasible to integrate the capacitive sensor with the electroadhesive system, which agrees with the results found by Daviet et al. [157].

Table 7-1 Measured voltages for different dielectric materials

Materials	Measured voltage (V)
Steel	0.85
Acrylic	1.52
MDF	1.80
Wax	2.25

7.3.2 Design of a MEGA based autonomous electroadhesive grasping platform

The platform used in this Chapter is the same one used in Chapter 6. However, the rotational movement part is used in this chapter to grasp the other two substrates. Furthermore, the capacitive sensor is integrated and the Arduino MEGA 2560 R3 is used instead of the UNO. The CAD model for the platform can be seen in Figure 7-8 and the schematic diagram of the platform for the proof of concept can be seen in Figure 7-9.

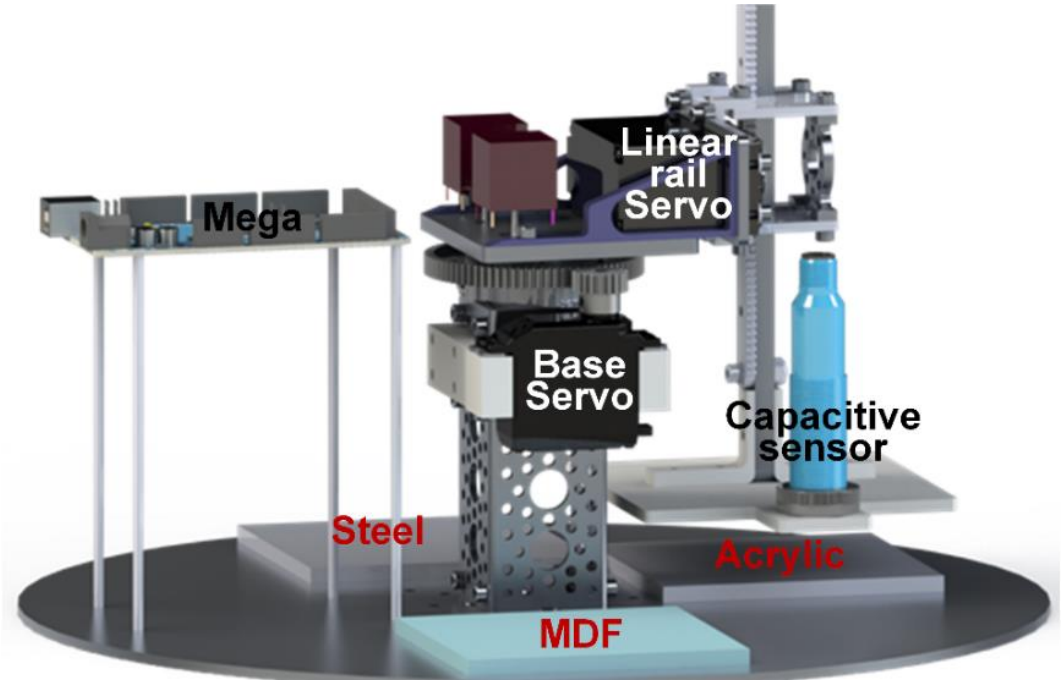

Figure 7-8 CAD for the MEGA based electroadhesive grasping platform

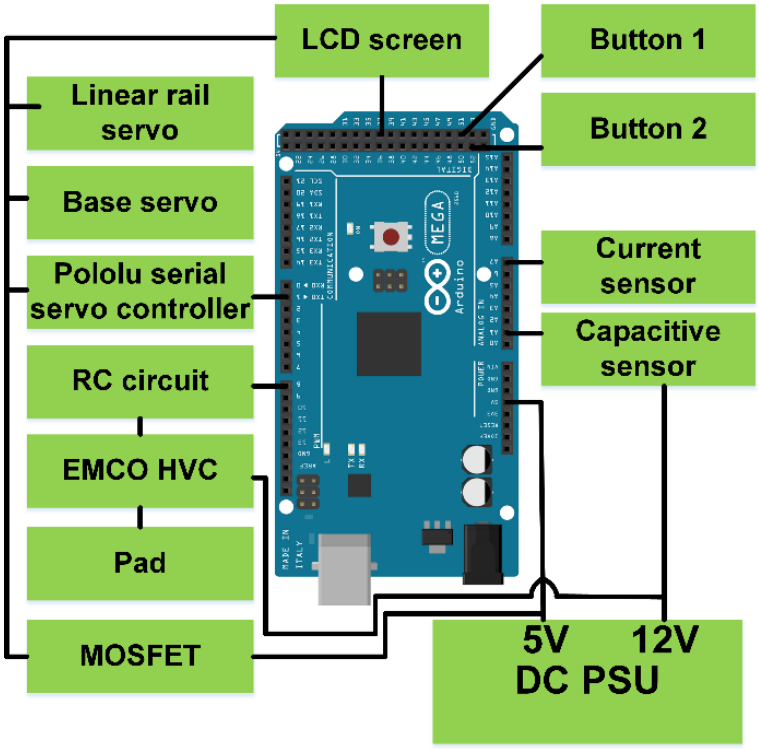

Figure 7-9 Schematic diagram of the platform for the proof of concept

The designed operational procedure of this platform demonstrating the proposed concept is:

● Switch on button 1 (the base servo will rotate from MDF to Acrylic and then to Steel);

● The linear servo moves down to the MDF and stops until the value detected by the arduino voltage and current sensor surpasses a designated value;

● The linear servo then maintains the same level for a pre-determined period of time and conducts a material identification based on the reading from the sensor;

● The result of the material identification is then displayed on the LCD;

● The linear servo then moves up to pick the substrate up after applying a voltage that is smaller than the required voltage at first to show the importance of adaptive electroadhesion and then applying the required voltage;

● The linear servo moves down to place the substrate;

● Switch on button 2 to turn off the voltage after the demonstration.

One of the limitations with regard to the analog capacitive sensor is that the sensor is not able to differentiate between metals as the output for different metals such as steel, copper, and aluminum plate is the same. An analog inductive sensor is therefore necessitated to be integrated into the system to differentiate different metals.

Considering the potential safety issues mentioned in section 4.6.1, the designed platform must be in an enclosed environment, forming a mobile autonomous electroadhesive grasping platform. The CAD design of this demonstration system can be seen in Figure 7-10, where the mobile base is set on B48-50 casters and A01-1 50 x 50 Kanya base extrusions and the enclosure with the safety interlock system is based on D01-5 20 x 20 Kanya base extrusions.

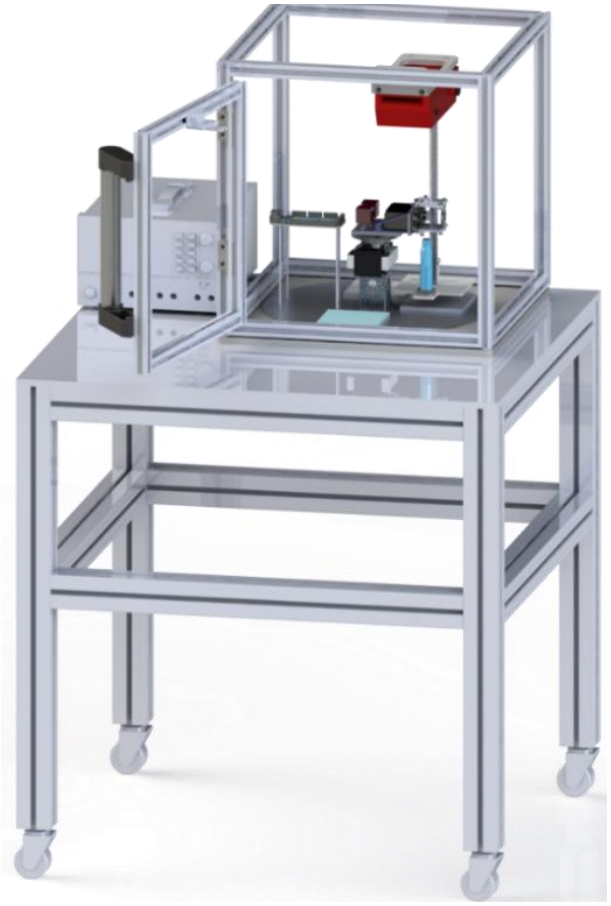

Figure 7-10 The mobile autonomous electroadhesive grasping demonstration system

7.4 Summary

In this Chapter, the need for adaptive electroadhesion has been illustrated based on the extensive literature review and evidences presented from Chapter 3 to Chapter 6. A new and detailed definition of adaptive and intelligent electroadhesion has been proposed. The feasibility study of the proposed solution to the concept has showed that it is promising to implement the designed mobile autonomous electroadhesive grasping platform to demonstrate the proposed concept.

8 Conclusions and Future Work

8.1 Introduction

In order to understand electroadhesion starting from the scratch comprehensively and provide research directions for future researchers, various work and challenges require to be addressed. This is due to the fact that electroadhesion is a multidisciplinary research phenomenon in nature. Conclusions for this thesis are summarised in terms of literature review, modelling of electroadhesion, pad design, manufacture, and testing. Future work for this thesis are summarised in terms of modelling of electroadhesion, pad design, manufacture, testing, and electroadhesive application.

8.2 Conclusions

With reference to the aim and objectives identified in Chapter 1, key conclusions based on this work are summarised as follows.

8.2.1 On literature review

This work has comprehensively conducted a literature review on electroadhesion technologies including fundamentals on electroadhesion, electroadhesive pad design, manufacturing and testing, modelling of electroadhesion, and electroadhesive applications. The findings indicate that:

● Optimised dielectric selection for different electroadhesive applications is the key for better electroadhesion properties.

● The failure of the electroadhesion phenomenon can be aroused by air gaps between the electrodes, sharp edges along the electrode surface, electrical aging, electrical discharges, and electrical breakdown in solids.

● The electroadhesion phenomenon can be both contact and contactless based. For conductive substrates, the electroadhesive forces are principally generated by electrostatic induction. For insulating substrates, the electroadhesive forces

are generated by polarisation. The contact based electroadhesion is mostly due to the orientational polarisation and interfacial polarisation whereas the contactless electroadhesion is due to, mostly, the atomic and electric polarisation.

● It is inappropriate to derive the normal electroadhesive forces, by the division of the measured shear forces and friction coefficients. The measured normal forces are therefore only useful for validating the models.

● Electroadhesive pad design involves the design of electrode configurations, electrode materials and dielectric materials. Pads can be manufactured in-house or professionally, involving the manufacture of both electrodes and dielectric materials. Electroadhesive pad performance characterisation can be conducted through normal force measurement methods and shear force measurement methods.

● Modelling of electroadhesion is important for understanding and designing electroadhesives. Empirical modelling is maybe a potential way to derive a model that can accurately predict the force obtainable. However, it takes a large amount of time and money to achieve enough confident experimental results to derive an empirical model.

● Material handling and robotic climbing are the two main electroadhesive applications.

8.2.2 On modelling of electroadhesion

This work has proposed a simplified optimisation modelling of coplanar interdigital electroadhesives. The theoretical model has been supported by an example of a 2D electrostatic simulation and experimental validation. The findings include:

● The results not only have highlighted the importance of controlling the environment when testing the pads to validate the models but also identified the need for the investigation of environmentally stable electroadhesives.

● The proposed simplified and computationally easier theoretical optimisation modelling of coplanar interdigitated electroadhesives is promising to predict the performance of interdigitated electroadhesive pads.

● The proposed 2D electrostatic simulation results showed that the wall thickness and air gap have a large bearing on the optimum widths achievable.

8.2.3 On pad design, manufacture, and testing

This work has proposed a systematic research methodology to investigate the relationship between different surface textures and the electroadhesive forces, based on an advanced electroadhesive force measurement platform and procedure, together with a recognised areal-based non-contact surface texture measurement platform and procedure. The key findings are:

● The obtained interfacial electroadhesive forces increase with decreasing the *Sq* values of the substrate surfaces provided that the difference in *Sq* between different substrates is greater than 5 μm.

● The higher the applied voltage, the larger the relative increase in the obtainable electroadhesive forces.

● When the difference in *Sq* between different substrate surfaces is within 2 μm, the obtained interfacial electroadhesive forces do not necessarily increase with decreasing the *Sq* values.

● The obtainable electroadhesive forces are not the same when the *Sq* value of two substrate surfaces are the same due to the fact that the direction of the surface texture plays an important role in achieving electroadhesive forces.

This work has also proposed a systematic research methodology to investigate the relationship between different pad geometries and the electroadhesive forces, based on a 3D electrostatic simulation using COMSOL Multiphysics, a cost-effective electroadhesive pad design and manufacturing process based on solid-

ink printing, chemical etching, conformal coating, and an advanced electroadhesive force testing platform and procedure. The key findings are:

● Different pad geometries do bring different total capacitances of the electroadhesive systems thus the electroadhesive forces obtainable.

● The novel curve-comb shape and worm-comb shape perform better in the electroadhesive forces obtainable than the normal comb shape based on the results both from simulation and experiments.

● The double-sided pad designs can not only result in larger electroadhesive forces than the coplanar designs but also perform better at higher voltages on non-conductive substrates.

In addition, this work has proposed a novel concept, adaptive and intelligent electroadhesion. The proof of concept has been implemented based on integrating the analog capacitive sensor with the electroadhesive system controlled by the Arduino MEGA. The feasibility study of the proposed solution to the concept has showed that it is promising to implement the designed mobile autonomous electroadhesive grasping platform to demonstrate the proposed concept.

8.3 Future work

The understanding of electroadhesion is still incomplete. Future work are therefore needed to gain a more in-depth understanding.

8.3.1 On modelling of electroadhesion

All the theoretical, electrostatic simulation, and empirical models fail to accurately derive the electroadhesive force between the pad and the substrate. Future work on advanced modelling of electroadhesion includes:

● Comparison of the existed theoretical models.

● Dynamic theoretical modelling of electroadhesives considering the dynamic

polarisation and de-polarisation process and the un-uniform electric field distribution in nature.

● Advanced theorectial modelling considering the surface texture information of the pad and the substrate and environmental factors. In the future, more consistent and structured surface textures/scratches thus even small variations should be generated using more advanced techniques.

● Theoretical modelling of the non-coplanar interdigital electroadhesives.

● Advanced dynamic simulation modelling considering the dynamic polarisation and de-polarisation process, and the surface texture information of the pad and the substrate, various material properties of the pad and substrate, and environmental factors.

● Investigation of an accurate empirical model that can predicts the relationship between the applied voltage and the electroadhesive force based on the employment of the Taguchi method for design of experiments to less the needed number of experiments.

8.3.2 On pad design, manufacture, and testing

Novel pad designs are needed for different electroadhesive applications. Future work to implement adaptive and intelligent electroadhesives includes:

● A comprehensive experimental comparison of all the pad designs mentioned in Chapter 6 to support or revise the simulation model.

● Investigation of novel pad designs that can output uniform electroadhesive force across the pad area. The electric field distribution of normal comb designs is not uniform. Novel electrode configurations [152] can help produce uniform electric field distribution and therefore uniform electroadhesive force.

● Investigation of novel pad geometries that can produce the maximum electroadhesive force on conductive substrates, non-conductive substrates, and

both, and can achieve the fastest clamping and unclamping speed, especially on non-conductive substrates. It is interesting to investigate how electrode width and the space between electrodes affect the clamp and unclamp speed by checking the residual charge dissipation.

● Varying different pad geometries such as spiral and concentric patterns whilst maintaining the same surface texture of the dielectric layer and the substrate to investigate the relationship between the interfacial electroadhesive force and pad geometries. The spiral/concentric pattern would be independent of the scratch directions. Also, different electrode widths and spaces of the same pad geometry will be used to investigate how these two variables influence the relationship.

● A comprehensive experimental comparison of various electrode materials mentioned in Chapter 2.

● Investigation of novel electrode materials that can produce the maximum electroadhesive force and support the implementation of intelligent and adaptive electroadhesion.

● Investigation of novel dielectric materials that can produce the maximum electroadhesive force and help achieve the fastest clamping and unclamping speed, especially on non-conductive substrates, and environmentally stable electroadhesives.

● Investigation of using a layer of soft foam backing to the pad to conform to rough surfaces.

● Varying different surface textures of the dielectric layer facing the substrate whilst keeping the surface texture of the substrate the same to investigate the obtainable interfacial electroadhesive forces.

● A comprehensive experimental comparison of various pad manufacture methods mentioned in Chapter 2.

● Investigation of novel pad manufacturing methods such as plasma sputtering.

● Employment of an advanced vacuum chamber enclosing the rig and investigation of robust methods of controlling the temperature, humidity, and air pressure in the test rig independently.

● Investigation of novel techniques for assessing (such as measurement of the dielectric constant) the electroadhesion properties of the electroadhesive pad and substrate.

8.3.3 On electroadhesive application

Future work on electroadhesion applications mainly includes the implementation of the mobile autonomous electroadhesive grasping platform, as described in section 7.3.2, to demonstrate the proposed concept, adaptive and intelligent electroahesion, a possible paradigm shift towards promising electroadhesive based material handling applications. In addition, the investigation into contactless based electroadhesion systems for handling delicate objects is useful. Furthermore, it is interesting to implement the designed two-module based electroadhesive climbing robot [13].

References

[1] R. P. Krape, “Application studies of electroadhesive devices,” Springfield (National Aeronautics and Space Administration), 1968.

[2] R. W. Warning, “Electrostatic force employed to hold work-pieces,” in *La Physique des Forces Electrostatiques et leurs Applications*, 1960, pp. 117–127.

[3] G. P. Beasley and W. W. Hankins, “Development of electroadhesive devices for zero-g intraextravehicular activities,” in *AIAA*, 1971, pp. 71–853(6pp).

[4] B. C. Leung, L. A. Miller, N. R. Goeser, and S. Gonzalez, “Validation of electroadhesion as a docking method for spacecraft and satellite servicing,” in *2015 IEEE Aerospace Conference*, 2015, no. 1, pp. 1–8.

[5] G. A. Wardly, “Electrostatic wafer chuck for electron beam microfabrication,” *Rev. Sci. Instrum.*, vol. 44, no. 10, pp. 1506–1509, 1973.

[6] G. J. Monkman, P. M. Taylor, and G. J. Farnworth, “Principles of electroadhesion in clothing robotics,” *Int. J. Cloth. Sci. Technol.*, vol. 1, no. 3, pp. 14–20, 1989.

[7] G. J. Monkman, “Robot grippers for use with fibrous materials,” *Int. J. Rob. Res.*, vol. 14, no. 2, pp. 144–151, 1995.

[8] Z. Zhang, J. a Chestney, and M. Sarhadi, “Characterizing an electrostatic gripping device for the automated handling of non-rigid materials,” *Proc. Inst. Mech. Eng. Part B J. Eng. Manuf.*, vol. 215, no. 1, pp. 21–36, 2001.

[9] B. F. Seitz, B. Goldberg, N. Doshi, O. Ozcan, D. L. Christensen, E. W. Hawkes, M. R. Cutkosky, and R. J. Wood, “Bio-inspired mechanisms for inclined locomotion in a legged insect-scale robot,” in *2014 IEEE International Conference on Robotics and Biomimetics (ROBIO)*, 2014, pp. 791–796.

[10] A. Yamamoto, T. Nakashima, and T. Higuchi, “Wall climbing mechanisms using electrostatic attraction generated by flexible electrodes,” in *2007 International Symposium on Micro-NanoMechatronics and Human Science*, 2007, pp. 389–394.

[11] H. Prahlad, R. Pelrine, S. Stanford, J. Marlow, and R. Kornbluh, “Electroadhesive robots-wall climbing robots enabled by a novel, robust, and electrically controllable adhesion technology,” in *2008 IEEE International Conference on Robotics and Automation*, 2008, pp. 3028–3033.

[12] Grabit, “Revolutionizing Material Handling with Electroadhesion.” [Online]. Available: http://grabitinc.com/. [Accessed: 03-Dec-2015].

[13] J. L. Guo, L. Justham, M. Jackson, and R. Parkin, “A concept selection

method for designing climbing robots," *Key Eng. Mater.*, vol. 649, pp. 22–29, 2015.

[14] D. Ruffatto, J. Shah, and M. Spenko, "Increasing the adhesion force of electrostatic adhesives using optimized electrode geometry and a novel manufacturing process," *J. Electrostat.*, vol. 72, no. 2, pp. 147–155, 2014.

[15] K. Yatsuzuka, F. Hatakeyama, K. Asano, and S. Aonuma, "Fundamental characteristics of electrostatic wafer chuck with insulating sealant," *IEEE Trans. Ind. Appl.*, vol. 36, no. 2, pp. 510–516, 2000.

[16] J. U. Jeon and T. Higuchi, "Electrostatic suspension of dielectrics," *IEEE Trans. Ind. Electron.*, vol. 45, no. 6, pp. 938–946, 1998.

[17] G. J. Monkman, "Electrostatic techniques for fabric handling," The University of Hull, 1987.

[18] M. A. Graule, P. Chirarattananon, S. B. Fuller, N. T. Jafferis, K. Y. Ma, M. Spenko, R. Kornbluh, and R. J. Wood, "Perching and takeoff of a robotic insect on overhangs using switchable electrostatic adhesion," *Science (80-.).*, vol. 352, no. 6288, pp. 978–982, 2014.

[19] A. Chestney and M. Sarhadi, "Dielectric selection for a robotic electrostatic gripping device," in *Seventh International Conference on Dielectric Materials, Measurements and Applications*, 1996, no. 430, pp. 23–26.

[20] K. H. Koh, M. Sreekumar, and S. G. Ponnambalam, "Experimental investigation of the effect of the driving voltage of an electroadhesion actuator," *Materials (Basel).*, vol. 7, no. 7, pp. 4963–4981, 2014.

[21] J. Guo, M. Tailor, T. Bamber, M. Chamberlain, L. Justham, and M. Jackson, "Investigation of relationship between interfacial electroadhesive force and surface texture," *J. Phys. D. Appl. Phys.*, vol. 49, no. 3, p. 35303(9pp), 2016.

[22] M. Gacanovic, "Electrostatic application principles," in *International PhD Seminar on Computational electromagnetics and optimization in electrical engineering*, 2010, pp. 63–97.

[23] J. M. Crowley, "Electrostatic fundamentals," in *Handbook of electrostatic processes*, no. 1, 1995, pp. 1–5.

[24] K.-C. Kao, *Dielectric phenomena in solids: with emphasis on physical concepts of electronic processes*. 2004.

[25] J. M. Crowley, "Electric fields with known voltages," in *Fundamentals of applied electrostatics*, 1st ed., Laplacian Press, 1999, pp. 18–22.

[26] Z. Ahmad, "Polymeric dielectric materials," in *Dielectric Material*, M. A. Silaghi, Ed. InTech, 2012, pp. 3–26.

[27] K. Nagasawa, M. Honjoh, T. Takada, H. Miyake, and Y. Tanaka, "Electric charge accumulation in polar and non-polar polymers under electron beam

irradiation," *IEEJ Trans. Fundam. Mater.*, vol. 130, no. 12, pp. 1105–1112, 2010.

[28] Wikipedia, "Electrostatic induction." [Online]. Available: https://en.wikipedia.org/wiki/Electrostatic_induction. [Accessed: 08-Jun-2016].

[29] G. J. Monkman, S. Hesse, R. Steinmann, and H. Schunk, *Robot grippers*. WILEY-VCH, 2007.

[30] S. J. Woo and T. Higuchi, "Electric field and force modeling for electrostatic levitation of lossy dielectric plates," *J. Appl. Phys.*, vol. 108, no. 10, p. 104906(10pp), 2010.

[31] G. J. Monkman, "An analysis of astrictive prehension," *Int. J. Robot.*, vol. 16, no. 1, pp. 1–10, 1997.

[32] T. Yu, "ESC (Electricity Static Chuck) Fabric Chucking," 2014. [Online]. Available: https://www.youtube.com/watch?v=tuqrZWcqj50.

[33] J. Jin, T. Higuchi, and M. Kanemoto, "Electrostatic levitator for hard disk media," *IEEE Trans. Ind. Electron.*, vol. 42, no. 5, pp. 467–473, 1995.

[34] J. Berengueres, M. Urago, S. Saito, K. Tadakuma, and H. Meguro, "Gecko inspired electrostatic chuck," in *Proceedings of the 2006 IEEE International Conference on Robotics and Biomimetics*, 2006, pp. 1018–1023.

[35] G. I. Shim and H. Sugai, "Dechuck operation of Coulomb type and Johnsen-Rahbek type of electrostatic chuck used in plasma processing," *Plasma Fusion Res.*, vol. 3, p. 051(4pp), 2008.

[36] R. Atkinson, "A simple theory of the Johnsen-Rahbek effect," *J. Phys. D. Appl. Phys.*, vol. 2, no. 3, pp. 325–332, 1969.

[37] M. R. Sogard, A. R. Mikkelson, V. Ramaswamy, and R. L. Engelstad, "Analysis of Coulomb and Johnsen-Rahbek electrostatic chuck performance in the presence of particles for extreme ultraviolet lithography," *J. Micro/Nanolithography, MEMS, MOEMS*, vol. 8, no. 4, p. 041506(9pp), 2009.

[38] S. Qin and A. McTeer, "Wafer dependence of Johnsen-Rahbek type electrostatic chuck for semiconductor processes," *J. Appl. Phys.*, vol. 104, no. 9, p. 064901(4pp), 2007.

[39] C. Balakrishnan, "Johnsen-Rahbek Effect with an Electronic Semi-Conductor," *Br. J. Appl. Phys.*, vol. 1, no. 8, pp. 211–213, 1950.

[40] T. Bryan, T. Macleod, L. Gagliano, S. Williams, and B. McCoy, "Innovative electrostatic adhesion technologies," in *Advanced Maui Optical and Space Surveillance Technologies Conference*, 2015, p. 8.

[41] K. Asano, F. Hatakeyama, and K. Yatsuzuka, "Fundamental study of an electrostatic chuck for silicon wafer handling," *IEEE Trans. Ind. Appl.*, vol.

38, no. 3, pp. 840–845, May 2002.

[42] R. Dhelika, K. Sawai, K. Takahashi, W. Takarada, T. Kikutani, and S. Saito, “Electrostatic chuck consisting of polymeric electrostatic inductive fibers for handling of objects with rough surfaces,” *Smart Mater. Struct.*, vol. 22, no. 9, p. 095010(9pp), 2013.

[43] S. Saito, F. Soda, R. Dhelika, K. Takahashi, W. Takarada, and T. Kikutani, “Compliant electrostatic chuck based on hairy microstructure,” *Smart Mater. Struct.*, vol. 22, no. 1, p. 015019(6pp), 2013.

[44] T. Watanabe, T. Kitabayashi, and C. Nakayama, “Electrostatic force and absorption current of alumina electrostatic chuck,” *Japanese J. Appl. Physics, Part 1 Regul. Pap. Short Notes Rev. Pap.*, vol. 31, no. 7, pp. 2145–2150, 1992.

[45] J. Yoo, J.-S. Choi, S.-J. Hong, T.-H. Kim, and S. J. Lee, “Finite element analysis of the attractive force on a coulomb type electrostatic chuck,” in *Proceeding of International Conference on Electrical Machines and Systems 2007*, 2007, pp. 1371–1375.

[46] F. Industries, “Hybrid ESC With Interdigitated Electrode Design.” [Online]. Available: http://www.fmindustries.com/hybrid-esc-interdigitated-electrode-design.html.

[47] SEMCO, “Wafer Handling.” [Online]. Available: http://www.thesemcogroup.com/wafer-handling.

[48] Y. Sun, J. Cheng, Y. Lu, Y. Hou, and L. Ji, “Design space of electrostatic chuck in etching chamber,” *J. Semicond.*, vol. 36, no. 8, p. 084004, 2015.

[49] G. J. Monkman, “Compliant robotic devices, and electroadhesion,” *Robotica*, vol. 10, no. 2, pp. 183–185, 1992.

[50] G. Monkman, “Workpiece retention during machine processing,” *Assem. Autom.*, vol. 21, no. 1, p. 61, 2001.

[51] X. Q. Chen and M. Sarhadi, “Investigation of electrostatic force for robotic lay-up of composite fabrics,” *Mechatronics*, vol. 2, no. 4, pp. 363–373, 1992.

[52] Z. Zhang, “Modeling and analysis of electrostatic force for robot handling of fabric materials,” *IEEE/ASME Trans. Mechatronics*, vol. 4, no. 1, pp. 39–49, 1999.

[53] A. Yamamoto, “Selected Publications.” [Online]. Available: http://am.t.u-tokyo.ac.jp/publication_e.html. [Accessed: 22-Jan-2016].

[54] M. E. Karagozler, J. D. Campbell, G. K. Fedder, S. C. Goldstein, M. P. Weller, and B. W. Yoon, “Electrostatic latching for inter-module adhesion, power transfer, and communication in modular robots,” in *IEEE International Conference on Intelligent Robots and Systems*, 2007, pp. 2779–2786.

[55] W. Thiel and A. Heinz, “Electroadhesion gripper for retaining workpieces,” US20150124369A1, 2015.

[56] S. S. Sangari, K. S. Willden, J. M. Cobb, G. M. Buckus, C. Crespo, and S. F. Pedigo, “Automated ply layup system and method of laying up,” US20120330453A1, 2012.

[57] T. Eisele and A. Defranceski, “Gripper apparatus,” US20150298320A1, 2015.

[58] ElectroGrip, “Advanced Electrostatic Gripping Solutions.” [Online]. Available: http://electrogrip.com/Egrip2013Products/chucks/Egrip2013ElectrostaticChucks1.htm. [Accessed: 23-Jan-2016].

[59] C. Brecher, M. Emonts, B. Ozolin, and R. Schares, “Handling of preforms and prepregs for mass production of composites,” in *The 19th international conference on composite materials*, 2013, pp. 1296–1305.

[60] J. Krahn and C. Menon, “Electro-dry-adhesion,” *Langmuir*, vol. 28, no. 12, pp. 5438–5443, 2012.

[61] J. M. Krahn, A. G. Pattantyus-Abraham, and C. Menon, “Polymeric electro-dry-adhesives for use on conducting surfaces,” *Proc. Inst. Mech. Eng. Part L J. Mater. Des. Appl.*, vol. 228, no. 2, pp. 109–114, 2014.

[62] J. Krahn, A. Pattantyus-Abraham, and C. Menon, “Polymeric electro-dry-adhesives for use on conducting surfaces,” *Proc. Inst. Mech. Eng. Part L J. Mater. Des. Appl.*, vol. 228, no. 2, pp. 109–114, 2014.

[63] J. P. D. Téllez, J. Krahn, and C. Menon, “Characterization of electro-adhesives for robotic applications,” in *IEEE International Conference on Robotics and Biomimetics (ROBIO)*, 2011, pp. 1867–1872.

[64] L. Savioli, G. Sguotti, A. Francesconi, F. Branz, J. Krahn, and C. Menon, “Morphing electroadhesive interface to manipulate uncooperative objects,” in *Sensors and Smart Structures Technologies for Civil, Mechanical, and Aerospace Systems 2014*, 2014, vol. 9061, p. 906129(13pp).

[65] K. H. Koh, M. Sreekumar, and S. G. Ponnambalam, “Electrostatic devices for material handling,” *Int. J. Adv. Electron. Electr. Eng.*, vol. 3, no. 3, pp. 38–42, 2014.

[66] K. H. Koh, M. Sreekumar, and S. G. Ponnambalam, “Hybrid electrostatic and elastomer adhesion mechanism for wall climbing robot,” *Mechatronics*, vol. 35, pp. 122–135, 2016.

[67] K. H. Koh, K. C. Ramanathan, and S. G. Ponnambalam, “Modeling and simulation of electrostatic adhesion for robotic devices,” in *2012 International Conference on Electronics, Information and Communication Engineering*, 2012, vol. 11, pp. 208–216.

[68] K. H. Koh, K. C. Ramanathan, and S. G. Ponnambalam, “Modeling and

simulation of electrostatic adhesion for wall climbing robot," in *2011 IEEE International Conference on Robotics and Biomimetics*, 2011, pp. 2031–2036.

[69] K. H. Koh, M. Sreekumar, and S. G. Ponnambalam, "Feasibility study for applying electrostatic adhesion on wall climbing robots," in *International Conference on Advances in Mechanical, Aeronautical and Production Techniques - MAPT*, 2014, pp. 31–36.

[70] G. Griffiths and S. Matthew, "Wall climbing robots using electro-adhesion technology," in *Proceedings of CLAWAR 2011: the 14th International Conference on Climbing and Walking Robots and the Support Technologies for Mobile Machines*, 2011, pp. 377–383.

[71] C. J. C. Heath, I. P. Bond, and K. D. Potter, "Integrating electrostatic adhesion to composite structures," in *Proc. SPIE 9433, Industrial and Commercial Applications of Smart Structures Technologies*, 2015, vol. 9433, p. 94330D(10pp).

[72] D. Ruffatto, A. Parness, and M. Spenko, "Improving controllable adhesion on both rough and smooth surfaces with a hybrid electrostatic/gecko-like adhesive," *J. R. Soc. Interface*, vol. 11, no. 93, p. 20131089(10pp), 2014.

[73] D. Ruffatto, J. Shah, and M. Spenko, "Optimization of electrostatic adhesives for robotic climbing and manipulation," in *Proceedings of the ASME 2012 International Design Engineering Technical Conferences & Computers and Information in Engineering Conference*, 2012, pp. 1–10.

[74] D. Ruffatto, J. Shah, and M. Spenko, "Optimization and experimental validation of electrostatic adhesive geometry," in *2013 IEEE Aerospace Conference*, 2013, pp. 1–8.

[75] D. Ruffatto, D. Beganovic, A. Parness, and M. Spenko, "Experimental evaluation of adhesive technologies for robotic grippers on micro-rough surfaces," in *2014 IEEE International Conference on Robotics and Automation (ICRA)*, 2014, pp. 6150–6155.

[76] D. Ruffatto, D. Beganovic, A. Parness, and M. Spenko, "Experimental results of a controllable electrostatic/gecko-like adhesive on space materials," in *IEEE Aerospace Conference Proceedings*, 2014, pp. 1–7.

[77] J. Germann, M. Dommer, R. Pericet-Camara, and D. Floreano, "Active connection mechanism for soft modular robots," *Adv. Robot.*, vol. 26, no. 7, pp. 785–798, 2012.

[78] J. Shintake, S. Rosset, B. Schubert, D. Floreano, and H. Shea, "Versatile soft grippers with intrinsic electroadhesion based on multifunctional polymer actuators," *Adv. Funct. Mater.*, pp. 1–28, 2015.

[79] B. Schubert and D. Floreano, "Stretchable electroadhesion for soft robots," in *2014 IEEE/RSJ International Conference on Intelligent Robots and*

Systems (IROS), 2014, pp. 3933–3938.

[80] J. Shintake, S. Rosset, B. Schubert, S. Mintchev, D. Floreano, and H. R. Shea, “DEA for soft robotics: 1-gram actuator picks up a 60-gram egg,” in *Electroactive Polymer Actuators and Devices (EAPAD)*, 2015, vol. 9430, p. 94301S(6pp).

[81] R. Liu, R. Chen, H. Shen, and R. Zhang, “Wall climbing robot using electrostatic adhesion force generated by flexible interdigital electrodes,” *Int. J. Adv. Robot. Syst.*, vol. 10, no. 36, pp. 1–9, 2012.

[82] H. Shen, R. Liu, R. Chen, and J. He, “Modeling of attraction force generated by interdigital electrodes for electroadhesive robots,” in *2012 10th IEEE International Conference on Industrial Informatics (INDIN)*, 2012, pp. 678–681.

[83] R. Chen, R. Liu, and H. Shen, “Modeling and analysis of electric field and electrostatic adhesion force generated by interdigital electrodes for wall climbing robots,” in *IEEE International Conference on Intelligent Robots and Systems*, 2013, pp. 2327–2332.

[84] R. Chen, R. Liu, J. Chen, and Z. Jin, “A gecko inspired wall-climbing robot based on electrostatic adhesion mechanism,” in *IEEE International Conference on Robotics and Biomimetics (ROBIO)*, 2013, pp. 396–401.

[85] R. Chen, R. Liu, and H. Shen, “Design of a double-tracked wall climbing robot based on electrostatic adhesion mechanism,” in *2013 IEEE Workshop on Advanced Robotics and its Social Impacts (ARSO)*, 2013, no. 2012, pp. 212–216.

[86] J. C. Guo, G. H. Dai, and G. C. Cui, “A wall climbing robot based on the improved electro adhesion technology,” *Appl. Mech. Mater.*, vol. 328, pp. 56–61, 2013.

[87] J. Guo, D. Chu, and G. Cui, “Analogous vacuum electrostatic adsorption technology based on the electrode array optimization,” *J. Zhengzhou Univ. Light Ind. Sci. Ed.*, vol. 30, no. 1, pp. 85–89, 2015.

[88] J. Guo, G. Cui, X. Chen, and Y. Gao, “Model construction and optimization of wall climbing robot oriented electro-adhesion array,” *J. Mech. Eng.*, vol. 51, no. 9, pp. 51–57, 2015.

[89] J. Guo, D. Chu, G. Cui, and D. Yan, “Research and building of a new type of electrode array model,” *J. Comput. Theor. Nanosci.*, vol. 12, no. 7, pp. 1330–1335, 2015.

[90] G. Cui, K. Liang, J. Guo, H. Li, and D. Gu, “Design of a climbing robot based on electrically controllable adhesion technology,” in *2012 International Conference on Solid State and Materials*, 2012, pp. 90–95.

[91] R. Etkins, “Characterization of electroadhesion technologies for use in wall-climbing robots,” 2013. .

[92] A. Kiran and H. Lipson, “Electroadhesion Based Pick-and-Place Device.” [Online]. Available: http://www.ctl.cornell.edu/events/celebration13/Kiran.pdf. [Accessed: 11-Dec-2015].

[93] W. Tong, C. S. Chin, and W. Lin, “Design of a miniature tri-axis vertical wall structure climbing robot using electroadhesion,” in *2014 9th IEEE Conference on Industrial Electronics and Applications*, 2014, pp. 473–477.

[94] J.-B. Mao, L. Qin, W.-X. Zhang, L. Xie, and Y. Wang, “Modeling and analysis of electrostatic adhesion force for climbing robot on dielectric wall materials,” *Eur. Phys. J. Appl. Phys.*, vol. 69, no. 1, p. 11003(11p), 2015.

[95] J. Mao, L. Qin, and W. Zhang, “Modelling and simulation of electrostatic adhesion force in concentric ring electrode structures of multi-layer dielectrics,” *J. Adhes.*, vol. 8464, 2015.

[96] J. Mao, L. Qin, Y. Wang, J. Liu, and L. Xue, “Modeling and simulation of electrostatic attraction force for climbing robots on the conductive wall material,” in *2014 IEEE International Conference on Mechatronics and Automation (ICMA)*, 2014, pp. 987–992.

[97] A. Takada, S. Nakamura, Y. Yamanishi, S. Hashimura, S. Nagasawa, T. Kogure, and S. Maeda, “Design of electrostatic adhesion device using the flexible electrodes,” in *2014 International Symposium on Micro-NanoMechatronics and Human Science (MHS)*, 2014, pp. 1–4.

[98] C. Cao, X. Sun, Y. Fang, Q.-H. Qin, A. Yu, and X.-Q. Feng, “Theoretical model and design of electroadhesive pad with interdigitated electrodes,” *Mater. Des.*, vol. 89, pp. 485–491, 2016.

[99] T. Kubo and Y. Kakinuma, “Basic performance evaluation of electro-adhesive film with micro mesh sheet,” *Key Eng. Mater.*, vol. 516, pp. 222–227, 2012.

[100] V. Sabermand, Y. Hojjat, and H. M. Hasanzadeh, “Study of parameters affecting the electrostatic attractions force,” *Int. J. Electr. Comput. Electron. Commun. Eng.*, vol. 8, no. 11, pp. 1628–1631, 2014.

[101] S. Panich and C. Priyanka, “Control of wall climbing robots using mobile phone through dual tone multi frequency,” in *Proceedings of 24th IRF International Conference*, 2015, pp. 44–48.

[102] M. I. Yehya, S. Hussain, A. Wasim, M. Jahanzaib, and H. Abdalla, “A cost effective and light weight unipolar electroadhesion pad technology for adhesion mechanism of wall climbing robot,” *Int. J. Robot. Mechatronics*, vol. 2, no. 1, pp. 1–10, 2015.

[103] Z. Huang, P. Wang, M. Li, L. Sun, and L. Li, “Study on wall-climbing robot based on flexible electrostatic attraction technique,” *Mach. Des. & Manuf.*, no. 6, pp. 166–168, 2010.

[104] H. E. University, “Electroadhesive climbing robot.” [Online]. Available: http://v.youku.com/v_show/id_XMTAxNDQ3NDc2.html. [Accessed: 22-Jan-2016].

[105] L.-M. Wang and Q.-C. Hu, “Design of a double track wall climbing robot based on electrostatic adsorption mechanism,” *J. Mach. Des.*, vol. 29, no. 4, pp. 4–7, 2012.

[106] Electrogrip, “Electrostatic chucks,” 2006. [Online]. Available: http://www.electrogrip.com/Egrip2013Support/faq2006no1.pdf. [Accessed: 30-Nov-2015].

[107] H. Allison, R. K. Fricker, and M. C. Smit, “Electro adhesion device,” US6791817, 2001.

[108] A. Rivadeneyra, J. Fernández-Salmerón, J. Banqueri, J. a. López-Villanueva, L. F. Capitan-Vallvey, and A. J. Palma, “A novel electrode structure compared with interdigitated electrodes as capacitive sensor,” *Sensors Actuators B Chem.*, vol. 204, pp. 552–560, 2014.

[109] M. a. Rosa, S. Dimitrijev, and H. B. Harrison, “Improved operation of micromechanical comb-drive actuators through the use of a new angled comb finger design,” *J. Intell. Mater. Syst. Struct.*, vol. 9, no. 4, pp. 283–290, 1998.

[110] B. D. Jensen, S. Mutlu, S. Miller, K. Kurabayashi, and J. J. Allen, “Shaped comb fingers for tailored electromechanical restoring force,” *J. Microelectromechanical Syst.*, vol. 12, no. 3, pp. 373–383, 2003.

[111] I. P. F. Harouche and C. Shafai, “Simulation of shaped comb drive as a stepped actuator for microtweezers application,” *Sensors Actuators, A Phys.*, vol. 123–124, pp. 540–546, 2005.

[112] H. E. Prahlad, R. E. Pelrine, A. Wong-Foy, R. D. Kornbluh, and B. K. McCoy, “Materials for electroadhesion and electrolaminates,” US20130010398A1, 2013.

[113] R. Barbucha, M. Kocik, J. Mizeraczyk, G. Kozioł, and J. Borecki, “Laser direct imaging of tracks on PCB covered with laser photoresist,” *Bull. Polish Acad. Sci. - Tech. Sci.*, vol. 56, no. 1, pp. 17–20, 2008.

[114] Clacktronics-uk, “Etching PCBs with Press’n'Peel.” [Online]. Available: http://www.instructables.com/id/Etching-PCBs-with-PressnPeel/. [Accessed: 22-Jan-2016].

[115] A. V. Mamishev, K. Sundara-Rajan, F. Yang, Y. Du, and M. Zahn, “Interdigital sensors and transducers,” *Proc. IEEE*, vol. 92, no. 5, pp. 808–844, 2004.

[116] G. Cummins and M. P. Y. Desmulliez, “Inkjet printing of conductive materials: a review,” *Circuit World*, vol. 38, no. 4, pp. 193–213, 2012.

[117] E. project Design, “Conformal Coating Of Printed Circuit Board Assembly.”

[Online]. Available: http://www.electronics-project-design.com/ConformalCoating.html. [Accessed: 22-Jan-2016].

[118] AgIC Inc., “Paper circuits created with markers and printers.” [Online]. Available: http://agic.cc/en. [Accessed: 08-Dec-2015].

[119] J. Lessing, A. C. Glavan, S. B. Walker, C. Keplinger, J. a. Lewis, and G. M. Whitesides, “Inkjet printing of conductive inks with high lateral resolution on omniphobic ‘R F Paper’ for paper-based electronics and MEMS,” *Adv. Mater.*, vol. 26, no. 27, pp. 4677–4682, 2014.

[120] S. a. Suresh, D. L. Christensen, E. W. Hawkes, and M. Cutkosky, “Surface and shape deposition manufacturing for the fabrication of a curved surface gripper,” *J. Mech. Robot.*, vol. 7, no. 2, p. 021005, 2015.

[121] M. M. Tazetdinov, “Electrostatic fixtures,” *Mach. Tool.*, vol. 40, no. 8, pp. 49–50, 1969.

[122] Y. Kyoko, T. Junichi, and K. Asano, “Electrostatic chuck with a thin ceramic insulation layer for wafer holding,” in *2001 IEEE Industry Applications Conference Thirty-sixth IAS Annual Meeting*, 2001, vol. 00, no. C, pp. 399–403.

[123] A. Parness, T. Hilgendorf, P. Daniel, M. Frost, V. White, and B. Kennedy, “Controllable on-off adhesion for earth orbit grappling applications,” in *2013 IEEE Aerospace Conference*, 2013, pp. 1–11.

[124] A. R. M. Syaifudin, S. C. Mukhopadhyay, and P. L. Yu, “Modelling and fabrication of optimum structure of novel interdigital sensors for food inspection,” *Int. J. Numer. Model.*, vol. 25, pp. 64–81, 2012.

[125] M. Ibrahim, J. Claudel, D. Kourtiche, and M. Nadi, “Geometric parameters optimization of planar interdigitated electrodes for bioimpedance spectroscopy,” *J. Electr. Bioimpedance*, vol. 4, no. 1, pp. 13–22, 2013.

[126] T. Watanabe, T. Kitabayashi, and C. Nakayama, “Relationship between electrical resistivity and electrostatic force of alumina electrostatic chuck,” *Japanese J. Appl. Physics, Part 1 Regul. Pap. Short Notes Rev. Pap.*, vol. 32, no. 2, pp. 864–871, 1993.

[127] Fraunhofer IPT, “Composites Europe 2012 – Electrostatic gripper automates handling of carbon fiber materials.” .

[128] D. Longo, G. Muscato, and G. Tarantello, “Performance evaluation of electrostatic adhesion for climbing robots,” in *Proceedings of the 13th International Conference on Climbing and Walking Robots and the Support Technologies for Mobile Machines*, 2010, pp. 1029–1036.

[129] “Justick.” [Online]. Available: http://justick.com/. [Accessed: 22-Jan-2016].

[130] “Mylar® polyester film.” [Online]. Available: http://usa.dupontteijinfilms.com/informationcenter/downloads/Electrical_Properties.pdf. [Accessed: 28-Jan-2016].

[131] P. M. Taylor, G. J. Monkman, and G. E. Taylor, “Electrostatic grippers for fabric handling,” in *1988 IEEE International Conference on Robotics and Automation*, 1988, pp. 431–433.

[132] X. Wang, J. Cheng, K. Wang, Y. Yang, Y. Sun, M. Cao, and L. Ji, “Finite element analysis on factors influencing the clamping force in an electrostatic chuck,” *J. Semicond.*, vol. 35, no. 9, p. 094011(5pp), 2014.

[133] R. Igreja and C. J. Dias, “Extension to the analytical model of the interdigital electrodes capacitance for a multi-layered structure,” *Sensors Actuators, A Phys.*, vol. 172, no. 2, pp. 392–399, 2011.

[134] T. Sun, H. Morgan, and N. G. Green, “Analytical solutions of ac electrokinetics in interdigitated electrode arrays: Electric field, dielectrophoretic and traveling-wave dielectrophoretic forces,” *Phys. Rev. E - Stat. Nonlinear, Soft Matter Phys.*, vol. 76, no. 4, pp. 1–18, 2007.

[135] S. S. Gevorgian, T. Martinsson, P. L. J. Linn??r, and E. L. Kollberg, “CAD models for multilayered substrate interdigital capacitors,” *IEEE Trans. Microw. Theory Tech.*, vol. 44, no. 6, pp. 896–904, 1996.

[136] E. Carlsson, S. Member, S. Gevorgian, and S. Member, “Conformal mapping of the field and charge distributions in multilayered substrate CPW’s,” *IEEE Trans. Microw. Theory Tech.*, vol. 47, no. 8, pp. 1544–1552, 1999.

[137] M. W. den Otter, “Approximate expressions for the capacitance and electrostatic potential of interdigitated electrodes,” *Sensors Actuators A Phys.*, vol. 96, no. 2–3, pp. 140–144, 2002.

[138] J. Z. Chen, A. a. Darhuber, S. M. Troian, and S. Wagner, “Capacitive sensing of droplets for microfluidic devices based on thermocapillary actuation,” *Lab Chip*, vol. 4, no. 5, pp. 473–480, 2004.

[139] S. Schaur and B. Jakoby, “A numerically efficient method of modeling interdigitated electrodes for capacitive film sensing,” *Procedia Eng.*, vol. 25, pp. 431–434, 2011.

[140] T. Bamber, J. Guo, M. Chamberlain, L. Justham, and M. Jackson, “A simplified, inexpensive, electrostatic adhesion manufacturing process and an advanced experimental platform,” *J. Electrostat.*, p. under review.

[141] R. Danzl, F. Helmli, and S. Scherer, “Focus variation - a robust technology for high resolution optical 3D surface metrology,” *J. Mech. Eng.*, vol. 57, no. 3, pp. 245–256, 2011.

[142] DigitalSurf, “DigitalSurf MountainMap.” [Online]. Available: http://www.digitalsurf.com/en/mntproducts.html. [Accessed: 14-Aug-2015].

[143] L. Richard, *Optical measurement of surface topography*. Springer Berlin Heidelberg, 2011.

[144] Y. Liao, “Extraction of 3D machined surface features and applications,” The

University of Michigan, 2010.

[145] W. Zeng, X. Jiang, and P. J. Scott, “Fast algorithm of the robust Gaussian regression filter for areal surface analysis,” *Meas. Sci. Technol.*, vol. 21, no. 5, p. 055108(9pp), 2010.

[146] M. J. Tailor, “Automatic surface defect quantification in 3D,” Loughborough University, 2013.

[147] X. K. Wang, J. Cheng, K. S. Wang, Y. Y. Yang, Y. C. Sun, M. L. Cao, C. K. Han, and L. H. Ji, “Modeling of electrostatic chuck and simulation of electrostatic force,” *Appl. Mech. Mater.*, vol. 511–512, pp. 588–594, 2014.

[148] S. Monk, *Programming Arduino: getting started with sketches*. 2011.

[149] “Arduino Support from MATLAB.” [Online]. Available: http://uk.mathworks.com/hardware-support/arduino-matlab.html. [Accessed: 13-Sep-2015].

[150] “785 Gear Rack Kit (637170).” [Online]. Available: https://www.servocity.com/html/785_gear_rack_kit__637170_.html#.VfVF67Eitas. [Accessed: 13-Sep-2015].

[151] R. E. Pelrine, H. Prahlad, J. S. Eckerle, R. D. Kornbluh, and S. E. Stanford, “Electroadhesive devices,” 2014.

[152] M. S. Abdul Rahman, S. C. Mukhopadhyay, and P.-L. Yu, “Novel planar interdigitatal sensors,” in *Novel Sensors for Food Inspection: Modelling, Fabrication and Experimentation*, vol. 10, 2014.

[153] H. Prahlad, T. P. Low, and R. E. Pelrine, “Vacuum augmented electroadhesive device,” 2014.

[154] ServoCity, “785 Gear Rack Kit (637170).” [Online]. Available: https://www.servocity.com/html/785_gear_rack_kit__637170_.html#.Vg7JT7Eitas. [Accessed: 03-Oct-2015].

[155] ServoCity, “Gear Drive Pan Kit (637168).” [Online]. Available: https://www.servocity.com/html/gear_drive_pan_kit_a__637168_.html#.Vg6sFLEitav.

[156] Balluff, “Capacitive Sensors.” [Online]. Available: http://www.audin.fr/pdf/documentations/balluff/capteurs-capacitifs/SIE-catalogue_K08K13.pdf. [Accessed: 03-Oct-2015].

[157] J. F. Daviet, L. Peccoud, and F. Mondon, “Electrostatic clamping applied to semiconductor plasma processing II.experimental results,” *J. Electrochem. Soc.*, vol. 140, no. 11, pp. 3256–3261, 1993.

Appendix A: Wood surface texture measurement and characterisation

A.1 Data acquisition by the Heliotis H3

The Heliotis H3 is a non-contact optical surface texture measurement device based on pOCT using super-luminescent light emitting diodes. The optical principle of the Heliotis H3 can be seen in Figure A-1. The technical specifications of the device are: 1) stand-off distance: 22.7 mm, 2) field of view (approximately): 2.3 mm x 2.3 mm, vertical resolution: 1 µm, 4) lateral resolution: 8 µm, 5) scan range: 80 mm, and 6) data acquisition time: 1 to 2 seconds.

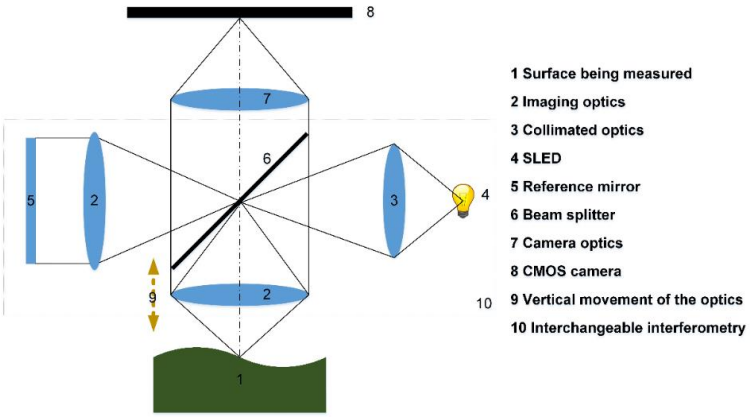

Figure A-1 The optical principle of the Heliotis H3

The measurement setup and raw data from the Heliotis H3 can be seen in Figure A-2 (a) and (b) respectively.

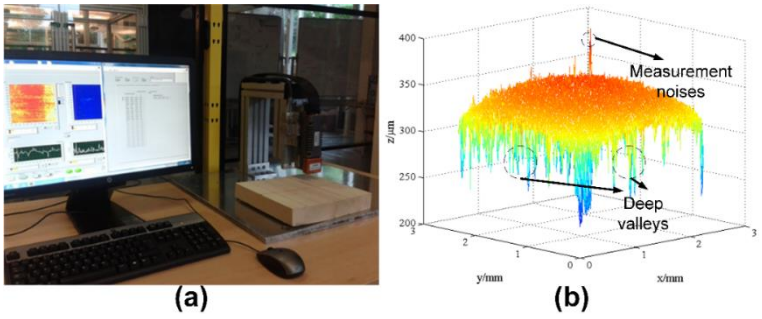

Figure A-2 The measurement setup and raw data from the Heliotis H3

A.2 Automatic surface texture data analysis algorithm

An automatic surface texture data analysis algorithm for stratified surfaces has been generated in MATLAB. The data analysis procedure can be seen in Figure A-3. The first step was to remove the surface form by surface fitting. A robust surface fitting algorithm was generated as can be seen in Figure A-4.

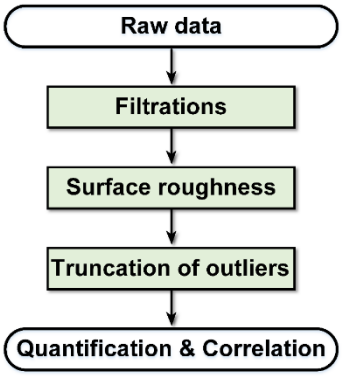

Figure A-3 The automatic surface texture data analysis procedure

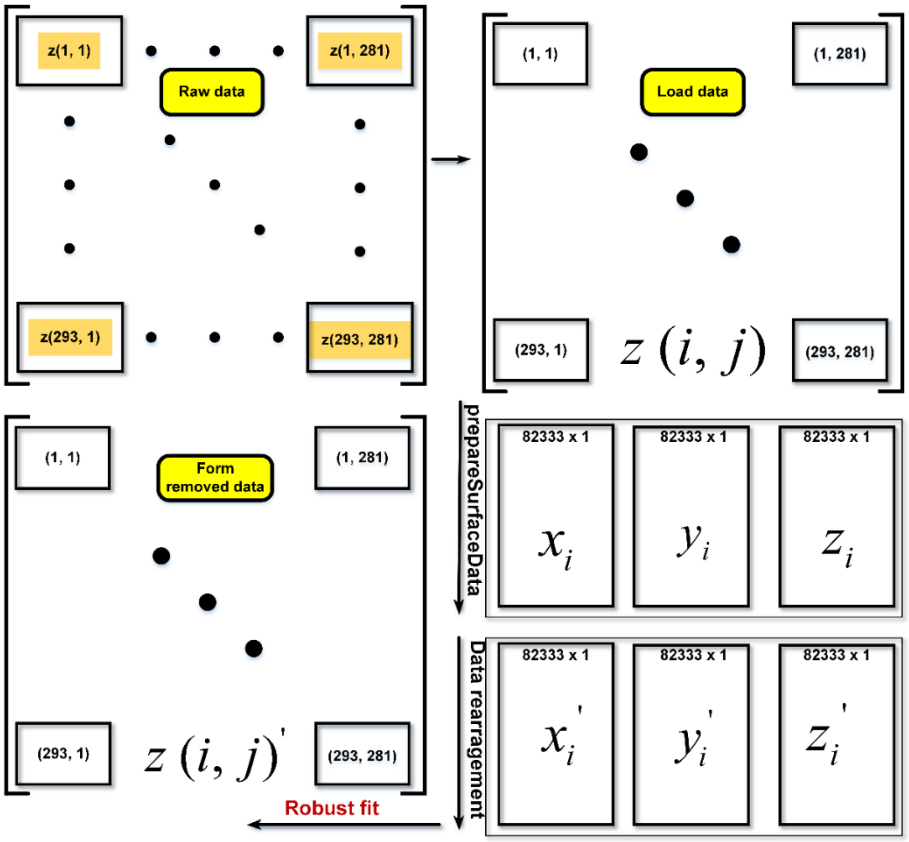

Figure A-4 The robust surface fitting procedure

Then an areal zero-order robust Gaussian regression filter was applied to obtain the surface roughness (Figure A-5 (a)). Edge noises were trimmed as can been seen in Figure A-5 (b).

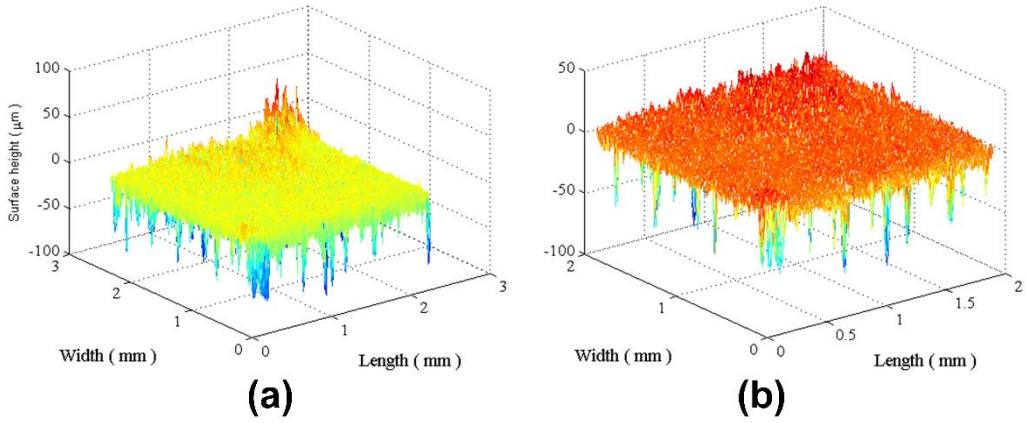

Figure A-5 Surface roughness of the sanded wood surface

Since the wood anatomy varies significantly in nature, the surface roughness obtained by traditional filtrations may contain deep valleys or outliers that will greatly influence the results (such as roughness parameters). This will result in inaccurate estimations of the relationship between wood surface roughness and sanding processes. Reducing or excluding these surface features is, therefore, necessary to provide a more precise relationship between surface roughness and sanding process. Based on the surface roughness data in Figure A-5 (b), a deep valley trunction method based on searching the standard lower valley limit (ISO 13565-3:2000) plane. The lower valley limit plane was found based on the algorithm shown in Figure A-6 (a). The data beyond the lower valley limit plane, as shown in Figure A-6 (b), was deleted before the quantification, as shown in Figure A-6 (c). The results show that the outlier truncation is necessary to obtain a reasonable relationship between sandpaper grit sizes and surface texture parameters.

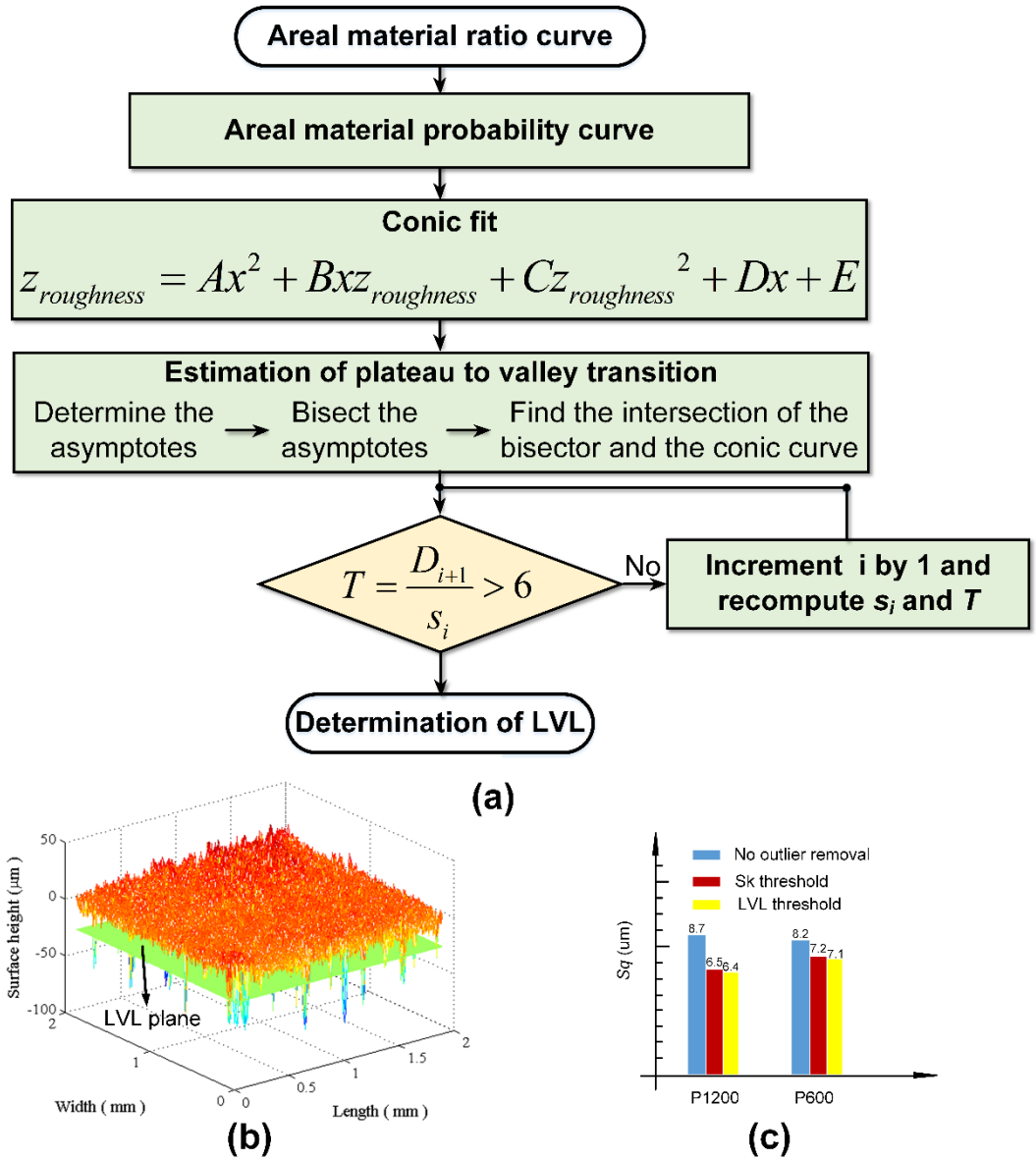

Figure A-6 Deep valley truncation of the wood surface roughness data

Appendix B: List of Figures

Appendix C: List of Tables

Appendix D: Nomenclature

D.1 List of Units

m metre

cm centimetre (=10^{-2} m)

mm millimetre (=10^{-3} m)

µm micrometre (=10^{-6} m)

s second

rev revolution

W watt

mW milliwatt (=10^{-3} W)

µW microwatt (=10^{-6} W)

V volt

kV kilovolt (=1000 V)

A ampere

mA milliampere

µA microampere

Hz hertz

Ω ohm

kΩ kilohm

N newton

F farad

°C degree in Celsius

Pa pascal

kPa kilopascal (=10^3 Pa)

Torr 133.3 Pa

hPa hectoPascal (=10^2 Pa, the reading from the weather station)

D.2 List of Symbols

m^2 square metre

cm^3 cubic centimetre

$revs^{-2}$ revolution per second square (acceleration)

mms^{-1} millimeter per second (speed)

Vmm^{-1} volt per millimeter (dielectric strength)

$kVmm^{-1}$ kilovolt per millimeter ($=10^3$ Vmm^{-1})

Ω-cm ohm x centemeter

Nmm^{-2} newton per square millimeters

Fm^{-1} farad per meter

pFm^{-1} picofarad per meter ($=10^{-12}$ Fm^{-1})

Sq root mean square height of the surface

Ra arithmetic average of the roughness profile

D.3 List of Abbreviations

3D three dimensional

ADC analog to digital converter

AC alternating current

B.C.E before common era

CAD computer aided design

CCD charge-coupled device

DC direct current

DOF degrees of freedom

DoF depth of field

FEA finite element analysis

F/T force and torque

HVC high voltage converter

I2C inter-integrated circuit

TTL transistor-transistor logic

TWI two wire interface

SPI serial peripheral interface

USB universal serial bus

IDE integrated development environment

GUI graphic user interface

LUT look-up table

MDF Medium-density fibreboard

PCB printed circuit board

FPCB flexible printed circuit board

IPA Iso-Propyl alcohol

PI Polyimide

PDMS poly(dimethylsiloxane)

cPDMS PDMS filled with carbon

PC polycarbonate

PE polyethylene

PEN polyethylene-naphthalate

PET polyester

PMMA polymethylmethacrylate

PP polypropylene

PS polystyrene

PTFE polytetrafluoroethylene

PUC polyurethane

PVC polyvinylchloride

D.3 List of Terminologies

Accuracy: how close a result is to its real value

Repeatability: a measure of how closely a result can be reproduced under controlled conditions (usually quantified using standard deviation)

Crystallinity: the degree of structural order in a solid (has a large bearing on material hardness, density, transparency, and diffusion)

Dielectric strength: a measure of the electrical strength of a material as an insulator (the maximum voltage required to produce a dielectric breakdown through the material)

Dissipation factor: a measure of loss-rate of energy of a mode of oscillation (mechanical, electrical, or electromechanical) in a dissipative system

Electronegativity: a measure of the tendency of an atom to attract a bonding pair of electrons (electropositivity is opposite to electronegativity)

Linear dielectric: materials in which the dielectric polarisation is linearly related to the electric field and the dielectric constant is not dependent on the electric field

Molecular structure: the 3D arrangement of the atoms that constitute a molecule (determines several properties of a substance including its reactivity, polarity, phase of matter, color, magnetism, and biological activity)

Molecular weight: the mass of one mole of a substance

Permittivity: a measure of how an electric field affects, and is affected by, a dielectric medium (the dielectric's ability to store electric energy)

Polarisability: the ability to form instantaneous dipoles (the dynamical response of a bound system to external fields, and provides insight into the internal structure of molecule)

Resistivity: an intrinsic property that quantifies how strongly a given material opposes the flow of electric current

Surface texture: the nature of a surface as defined by the 3 characteristics of lay, surface roughness, and waviness (also known as surface topography